Forschungszentrum Jülich

Höchstleistungsrechenzentrum

Microscopic dynamics of granular materials

Sabine Dippel

JÜL-3510

Microscopic dynamics of granular materials

Sabine Dippel

Berichte des Forschungszentrums Jülich ; 3510
ISSN 0944-2952
Höchstleistungsrechenzentrum Jül-3510
D464 (Diss. Universität-GH-Duisburg)

Zu beziehen durch: Forschungszentrum Jülich GmbH · Zentralbibliothek
D-52425 Jülich · Bundesrepublik Deutschland
☎ 02461/61-6102 · Telefax: 02461/61-6103 · e-mail: zb-publikation@fz-juelich.de

Microscopic dynamics of granular media

Abstract

In the present dissertation, the motion of inelastic spheres on a rough inclined plane is investigated by means of numerical simulations. In a special case, a theoretical model for the motion is presented as well.

After an overview of the physics of granular media and a brief outline of existing theoretical models and their limits, the simulation methods used in the present work are explained, where the focus is on time-step driven and event driven molecular dynamics. Advantages and disadvantages are discussed, as well as possible artifacts. In time-step driven molecular dynamics simulations the contact forces acting between particles have to be specified. Since there is no generally accepted force model available for granular materials, a number of common force models is investigated by simulations of simple sample systems. These simulations are compared with experiments (binary collision of spheres) and analytical results (a cylinder pushed along a plane by a block). It is shown that some force laws exhibit unphysical behaviour. In some, though not all, of these cases, possibilities to evite these problems by simple physically motivated modifications are presented.

The central part of this work deals with the motion of a sphere on a rough inclined plane. By means of molecular dynamics simulations the mechanisms leading to a steady state and its limits are investigated. It turns out that this mechanism leads to independence of the mean steady state velocity of material parameters like the normal restitution coefficient and the coefficient of friction. Based on this observation, a simplified and analytically solvable model for the motion in two dimensions is presented which approximates the steady state velocity and the lower limit of the steady state very well. In the 3-dimensional case very similar characteristics of the motion are present, but the 2-dimensional model could not be extended to this case. In the 3-dimensional case, also the fluctuations of the motion are investigated and compared to experimental results.

Finally it is checked in how far the results obtained for the single particle are valid for the flow of many particles on the inclined plane. Here, simulations are restricted to a 2-dimensional system. After a general discussion of previous experimental, numerical and theoretical results on this particular system it is shown for the first time, that for a very broad range of coefficients of restitution the flow profiles of most quantities characterizing the flow do not depend on this coefficient. Particularly the density and velocity profiles are independent of the coefficient of restitution. The coefficient of friction, however, strongly influences the motion, since it strongly increases the dissipation in the system.

Abstract

In der vorliegenden Dissertationsschrift wird die Bewegung inelastischer Kugeln auf einer rauhen schiefen Ebene mit Hilfe von Computersimulationen untersucht und in einem Spezialfall ein theoretisches Modell zu ihrer Beschreibung vorgestellt.

Nach einem Überblick über die Physik granularer Medien und einem kurzen Abriß existierender theoretischer Modelle und der Grenzen, an welche diese Modelle stoßen, werden die in der Arbeit verwendeten Simulationsmethoden, insbesondere zeitschrittgetriebene und ereignisgetriebene Molekulardynamik, erläutert. Vor- und Nachteile werden diskutiert, insbesondere auch auftretende Artefakte. In zeitschrittgetriebenen Molekulardynamiksimulation müssen die zwischen den Teilchen wirkenden Kontaktkräfte spezifiziert werden. Da es hierfür kein allgemein akzeptiertes Modell gibt, wird anhand der Simulation einfacher Beispielsysteme eine große Anzahl allgemein üblicher Kraftgesetze untersucht. Diese werden mit Experimenten (Stoß zweier Kugeln) bzw. analytischen Ergebnissen (ein von einem Block über eine Ebene geschobener Zylinder) verglichen. Es wird gezeigt, daß einige Kraftgesetze unphysikalisches Verhalten zeigen. In einigen, wenn auch nicht allen, dieser Fälle werden Möglichkeiten aufgezeigt, diese Probleme durch einfache physikalisch motivierte Modifikationen zu umgehen.

Der zentrale Teil der Arbeit befaßt sich mit dem Verhalten einer Kugel auf einer rauhen schiefen Ebene. Durch Molekulardynamiksimulationen wird untersucht, wie sich in diesem System ein stationärer Zustand einstellt, und wo dessen Grenzen liegen. Anhand der Details der Bewegung wird geklärt, durch welchen Mechanismus der stationäre Zustand aufrechterhalten wird. Es zeigt sich, daß dieser Mechanismus zu einer Unabhängigkeit der mittleren Geschwindigkeit im stationären Zustand von Materialparametern wie dem normalen Restitutionskoeffizienten und dem Reibungskoeffizienten führt. Aufgrund dieser Beobachtung wird für den 2-dimensionalen Fall ein einfaches analytisch lösbares Modell für die Bewegung der Kugel aufgestellt, das die Geschwindigkeit im stationären Zustand und dessen untere Grenzen gut annähert. Im 3-dimensionalen Fall zeigen sich sehr ähnliche Charakteristika der Bewegung, allerdings konnte das 2-dimensionale Modell nicht auf diesen Fall erweitert werden. Im 3-dimensionalen Fall wurden außerdem die Fluktuationen der Bewegung untersucht und ein Vergleich mit Experimenten vorgenommen.

Schließlich wird untersucht, inwiefern sich die am Beispiel des einzelnen Teilchens gewonnenen Erkenntnisse auf Fluß vieler Teilchen auf einer schiefen Ebene anwenden lassen. Hier beschränken sich die Simulationen auf ein 2-dimensionales Beispielsystem. Nach einer allgemeinen Diskussion bisheriger experimenteller, numerischer und theoretischer Ergebnisse zu diesem Thema wird erstmals gezeigt, daß in einem sehr breiten Bereich von Restitutionskoeffizienten die Profile der meisten den Fluß charakterisierenden Größen nicht von diesem abhängen. Insbesondere sind Dichte- und Geschwindigkeitsprofil unabhängig vom Restitutionskoeffizienten. Der Reibungskoeffizient indessen hat starken Einfluß auf die Bewegung, da er die Dissipation im System deutlich erhöht.

Contents

Introduction

> *Je n'ai fait celle-ci plus longue que parce que je n'ai pas eu le loisir de la faire plus courte.*
> — Blaise Pascal, Lettres Provinciales, xvi (1657)

Granular materials like sand, flour, coffee, pills, gravel, sugar, or coal are commonplace in our daily lives. Any solid that has to be transported or processed has to be ground into small entities to be manageable. Therefore, a huge amount of materials handled in industrial applications is in granular form.[1] However, efficiency in powder processing is quite low. Ennis *et al.* [1] estimate that facilities processing powders operate at only 63 % of their design capacity. The economic interest in a better understanding of the properties of granular materials is thus obvious.

Granular materials are as important in nature as in industry. Rockfalls, snow avalanches, dunes and erosion of soils are only a few examples which are of great consequence to daily life – predicting and understanding the behaviour of granular flows in a laboratory setting might facilitate predictions of the reach of avalanches or allow more efficient transport. E. g. it is still not understood why avalanches seem to have a smaller effective friction angle the larger their volume, i.e. the larger an avalanche or rockfall, the farther they will move down the slope [2].

Besides this practical importance, granular materials are inherently interesting for physicists. The fact that so little is known about their behaviour indicates that a theoretical description is far from simple or straightforward. The main complication arises from the dissipative nature of particle contacts. Without external agitation, an assembly of grains always comes to rest, though very often only in a local equilibrium, which may be far from global equilibrium. If motion is to be sustained, energy has to be fed into the system continuously. Granular materials thus represent a driven dissipative system far from thermodynamic equilibrium. Many of their properties cannot be described well solely by considering mean quantities, since fluctuations are very often of the same magnitude as the mean values, or even exist on all length and time scales. Often structures form on mesoscopic length scales, a fact that complicates continuum descriptions and hinders averaging.

Though in many real situations, the interstitial fluid (e.g. air, water) can affect the motion,

[1] In chemical industry in the US, 75% of the raw materials and 50% of the final products are estimated to be granular materials [1].

its influence will be neglected here. Besides, the material is assumed to be non-cohesive, which for grains larger than 1 μm and not too soft is a good assumption.

Here, the focus is on a particular granular system, namely the flow of granular materials (in this case spheres or discs) on a rough inclined plane. This system is a very common one - examples are the motion of grains or rocks on natural slopes as well as the transport in industrial applications via inclined chutes and channels or their storage in heaps. Despite its apparent simplicity, this particular flow geometry gives rise to a number of complications. Since the system is open at the top, the material may dilate if enough energy is fed into the system. Since the number of collisions and thus the dissipation strongly depends on the volume fraction of the material, this has an enormous influence on the stability of the motion. On an inclined plane, the material can get stuck when the inclination is too small, but it can as well accelerate without ever reaching a steady state if the inclination is too large.[2]

This dissertation discusses simulations of flow on an inclined plane, as well as a simple model for the motion of a single particle on a rough incline, which was motivated by simulation results. After a detailed examination of commonly used models for the interaction of soft particles and comparison with experimental results on the binary collision of spheres, I focus on the motion of a single particle on a rough inclined plane. Already this simple problem shows surprisingly rich behaviour, which gives important insights into the way global dissipation in a granular system arises from the inelasticity of the grain-grain interaction. The analysis then turns to the flow of many particles on an inclined plane, where special attention is drawn to the influence of material parameters like the coefficient of restitution and the coefficient of friction on the flow properties.

[2] If energy losses only occur through collisions – in nature there is always the braking influence of the air resistance, which at some point will stop the flow from accelerating.

Chapter 1

Properties of granular materials

> *Researchers have already cast much darkness on the subject, and if they continue their investigations, we shall soon know nothing about it.*
> — Mark Twain

Granular materials have been described as constituting "an additional state of matter in its own rights" [3]. Considering that they consist simply of a large number of classical solid particles, this may seem far-fetched, but indeed they exhibit very complex behaviour that cannot be described with existing theories pertaining to solids, liquids or gases. In this chapter, the peculiar properties of granular materials are discussed, as well as some corresponding attempts to describe them in a theoretical framework. This discussion is by no means complete, even though it touches many aspects of granular materials not directly related to the topic of the present work. However, since many aspects of the physics of granular materials still pose a lot of open questions, a summary of the most important problems, as well as theoretical approaches to them, seems to be appropriate at this point.

A simple sand dune may serve as an example for the number of different states a granular material can exhibit. Bagnold[1] describes some of these very vividly (p. 236 of [5]):

> "No one who has travelled in dune country can have failed to be struck by the sudden and often very disconcerting changes in the supporting properties of the material, whether underfoot or under the wheels of a car. A heavily loaded vehicle can often be driven for long distances over the rounded tops of dunes without disturbing the surface to a greater depth than that of the ripple trough – a matter of a centimetre or so. The underlying substance is exceedingly resistant to normally applied pressures. A scraping movement of the fingers will, however, prove at once that the firmness cannot be explained by cohesion or cementing between the grains. The grains are quite loose, but

[1] R. A. Bagnold (1896-1990) worked for the British army as a land surveyor in the years 1929-1938. During this time, he performed large scale measurements and some field experiments on the formation and structure of dunes, out of which the books *Lybian Sands* and *The Physics of Blown Sand and Desert Dunes* emerged. The latter of the two was the standard work on dunes for nearly 40 years. Only recently, a modern textbook on dunes was published [4].

> are packed together in a peculiar way.
>
> Then, without any warning being given by a change in the appearance of the surface, the wheels drop suddenly into a soft yielding mass through which a six-foot rod can be thrust with one hand without effort. Sometimes these dry quicksands are so unstable that by bringing the weight of one's body to bear sharply by a small jump, a real circular wave can be made to radiate outwards for several metres. Yet no difference is perceptible between the appearance of samples taken from these quicksands and from the firm ground nearby."

Even though the dune is a very solid structure (it does not flow away on its own), parts of it may be unable to sustain an additional load and behave like a liquid under external pressure. This example illustrates the most striking feature of a granular material. Depending on outer circumstances, it may behave liquid-like or solid-like – but it is not easy to quantify what these circumstances are. In the above example, it is the way in which the packing was obtained. While on the luv side of a dune, particles are usually very densely packed due to the "bombardment" by sand particles, on the lee side they can be very loosely packed, since here sand accumulates by avalanches, which deposit sand in a very random manner. Changing wind conditions over longer periods of time can result in very unpredictable arrangement of such densely and loosely packed parts of a dune.

In this chapter, the different states of granular matter are characterized and the conditions under which transitions between them take place are discussed. In addition, theoretical approaches for the description of these states will be briefly summarized. Still, this separation is slightly arbitrary, and the transitions are far from well-defined compared e.g. to "real" liquid-solid transitions. Even though this work deals mainly with granular flow in a very special geometry – on an inclined plane – a general discussion of the properties of granular materials may serve to illustrate the intrinsic problems encountered in dealing with granular media.

1.1 Granular materials at rest

1.1.1 Dilatancy

As described above, the properties of a granular material at rest can depend strongly on the packing (or rather the density of the packing). This is related to the concept of *dilatancy*, introduced by Reynolds in 1885 [6]. If a granular packing is sheared, it will generally expand, since particles have to "make room" for others to move around. This is illustrated in Fig. 1.1. From this figure it is clear as well that packings exist where shearing can lead to a *contraction* of the packing as also remarked by Reynolds. If due to outer constraints, the volume of the packing is fixed, it cannot be deformed in general. The expansion of a granular material is accompanied by an increase of the pore volume, i.e. the volume fraction of grains decreases. Some everyday examples and illustration experiments are the following:

- A packet of vacuum-sealed coffee is very hard to deform, because one has to counteract the atmospheric pressure to achieve a volume change and thus a deformation

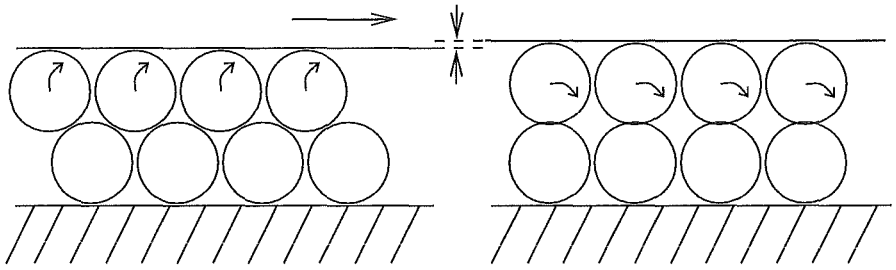

Figure 1.1: *Illustration of the dilation of a granular material under shear. The material must expand to allow particles in a dense packing to move.*

of the packet. If the atmospheric pressure is removed by perforating the packet, it can be deformed quite easily.

- A stick stuck into a beaker, which is then filled with sand, can easily be pulled out. If, however, the sand is compacted by lightly tapping the walls of the beaker, the attempt to pull out the stick results in lifting the whole assembly. A similar phenomenon was first reported by Jenkin [7], who tried to conceive a setup to reproducibly measure the coefficient of friction of various granular materials. Recent measurements show that increasing compaction by a few percent increases the force on the stick by two orders of magnitude [8].

- When walking on a wet beach, the area around the footprints and, when the foot is lifted, the footprint itself looks drier than the surroundings, because, due to the pressure exerted by the foot, the material around it expands and the additional pore volume fills with water. After a while, this water spills back into the footprint.

- A rubber bag, e.g. a balloon, is filled with sand, a small pipe pushed into it and the balloon closed, with the pipe sticking out at the top. Water is filled into the bag through this pipe. If now the bag is squeezed, the water level in the pipe sinks instead of rising. This experiment was first described by Reynolds [6] to illustrate the effects of dilatancy.

The density of a packing is quantified by the volume or area fraction of the material η =(volume of the grains)/(total volume). The upper and lower limits for random packings of spheres are referred to as random close packed (RCP) and random loose packed (RLP), but they are hard to define. RLP can be defined as the lowest packing fraction for which a continuous stable network of touching spheres exists, i.e. as the rigidity-percolation threshold. Scott and Kilgour [9] determined the value for the random loose packing of monodisperse spheres to be $\eta_{\mathrm{RLP}} = 0.60 \pm 0.02$ by pouring ball bearings into a container. For neutrally buoyant glass spheres in a liquid (i.e. for $g \to 0$), Onoda and Liniger [10] found $\eta_{\mathrm{RLP}} = 0.550 \pm 0.005$. They showed experimentally that this corresponds to the packing fraction below which no dilation of the sheared material occurs. This means that no stable packing can be sheared without dilation. For discs, I could find no value for η_{RLP} in the literature.

The RCP limit is defined as the densest packing of uniform spheres having a random structure, the difficulty here being to define when the structure ceases to be random (for

a discussion of this problem see [11]). Scott and Liniger [9] found $\eta_{\mathrm{RCP}} = 0.6366 \pm 0.0004$, which is consistent with values obtained later in various works [10]. For discs, the corresponding value is $\eta_{\mathrm{RCP}} = 0.82 \pm 0.02$ [11]. The closest *ordered packing* of monodisperse spheres is the hexagonal close packing with $\eta_{\mathrm{hcp}} = 0.74$, for discs it is the triangular lattice with $\eta_{\mathrm{tl}} = 0.91$. Clearly, for multidisperse spheres or nonspherical particles different limits apply, which depend on the size ratio, composition of the mixture and shape of the particles. The small difference between the respective RLP and RCP values (even the values for regular packings are quite close to those) shows how little variation is possible in the density of a sandpile, though this variation can cause strong changes in the behaviour of the material, due to steric constraints.

So far, the influence of friction on the properties of a granular packing was not discussed, though of the above mentioned examples the one referring to lifting a beaker with the help of a stick would not work without friction. In addition, a pile of sand on a smooth surface would not be stable without static friction. However, friction is of crucial importance to many problems arising in the description of stresses in granular packings, which will be discussed in the following subsection.

1.1.2 Stresses in granular packings

Due to the presence of friction between grains, a granular packing is able to withstand a certain amount of shear stress before it starts to flow. According to Coulomb's law of friction[2] [14,15] the shear force F_s in a contact is related to the normal force F_n by

$$F_s \leq \mu_s F_n \quad \text{for static friction } (v_s = 0), \tag{1.1}$$

$$F_s = \mu_d F_n \quad \text{for dynamic friction } (v_s \neq 0). \tag{1.2}$$

The static friction force is a reaction force and adjusts to the value necessary to maintain zero shear velocity v_s at the contact surface. Since usually the static friction coefficient μ_s has a larger value than the dynamic friction coefficient μ_d, the exact value of the friction force depends on the history of the contact. In a pile of granular material, where particles have a number of frictional contacts, the distribution of forces depends on the way the packing was prepared. Thus, a calculation attempting to describe a static packing would have to take into account the way in which the packing was obtained, i.e. the static state is only defined through the dynamics of the system. In an experimental set-up this is given by the way the pile was built.[3]

[2] C. A. Coulomb (1736-1806) was the first to distinguish between static and kinetic friction. He showed that the static and kinetic friction coefficients differ for most materials and that the sliding friction force is independent of the sliding velocity [12]. The fact that the friction force only depends on the applied normal force, but not on the apparent contact surface, was already remarked by Leonardo da Vinci (1452-1519) and rediscovered by G. Amontons (1663-1705) (for a brief account of the history of tribology up to the present see [13]).

[3] Since the history of a system very often is not known, in soil mechanics a similar constant as the static friction coefficient is defined for granular packings. If the normal stress in the direction of one principal stress axis σ_{xx} is known, the stress σ_{yy} corresponding to the other principal stress axis is related to σ_{xx} by $\sigma_{xx} = K\sigma_{yy}$, where the value of the proportionality factor K may be anywhere between the so-called active or passive coefficient of earth pressure K_A and K_P. $K_P\sigma_{yy}$ corresponds to the stress where a material pushed together by the walls will yield, $K_A\sigma_{yy}$ to the stress when a material pressing walls outside will yield. K_P and K_A can be obtained by a Mohr-Coulomb criterion (for details see [16]).

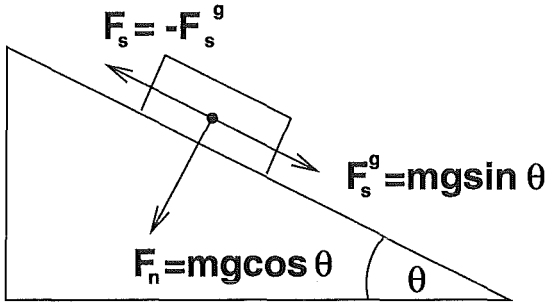

Figure 1.2: *Definition of the shear and normal forces in eq. (1.1) and (1.2). For a block resting on an inclined plane, F_s is the reaction force corresponding to the shear component of gravity F_s^g. The block starts to slide when* $\tan\theta > \mu_s$.

The measurement of stresses in granular materials is a difficult task. The force network inside a granular material is extremely sensitive to small perturbations [17], thus measurements should be non-invasive. The reason for this sensitivity is the strong localization of forces in a granular material along force lines. A tiny perturbation may completely change these stress paths if it affects a particle inside such a path. If only mean stresses on a small area are of interest, strain gauges or pressure cells can be used [18], but to access the fluctuations on the scale of the particle size, and even to measure the forces on single particles, different methods have to be employed. One way to visualize the stress path inside a granular material is to use a material that rotates the direction of polarization of light, like plexiglass, and to view the packing through crossed polarizers [19–22]. However, the measurement of intensities is not very exact, and such systems are hard to gauge. Besides, reliable data can only be obtained from quasi two dimensional systems. Another technique to measure forces on single particles is the carbon paper technique [21]. The radius of the imprint made by a sphere on carbon paper is proportional to the normal load on the particle. Though the packing has to be prepared very carefully (as not to leave marks on the carbon paper while piling up the material), with careful gauging this technique gives quite a good resolution.

Since measurement of stresses in granular materials on the particle scale is so difficult, recently computer simulations have been performed on such systems, as these allow to access all interesting quantities even in the interior of the packing [23]. The latter is especially important since it is not perfectly clear a priori if the distribution of stresses exerted on the bottom plate by the material is identical to the distribution of stresses inside the packing. It was shown [23–25] that the forces larger than the mean value decay exponentially, while those smaller than the mean value decay algebraically. These findings are in accordance with experimental results for the normal forces on the bottom and walls of a container [21,26]. Moreover, the simulations provide additional information, since the tangential stresses and other details, e.g. correlations of forces inside the system, can be extracted.

Recently, there has been considerable activity devoted to the study of stresses in a particular geometry. The system in question is a conical sandpile built by pouring particles from a point source. Surprisingly, measurement of the pressure on the bottom plate showed a local minimum for the pressure under the apex of the pile [27]. A number of possible

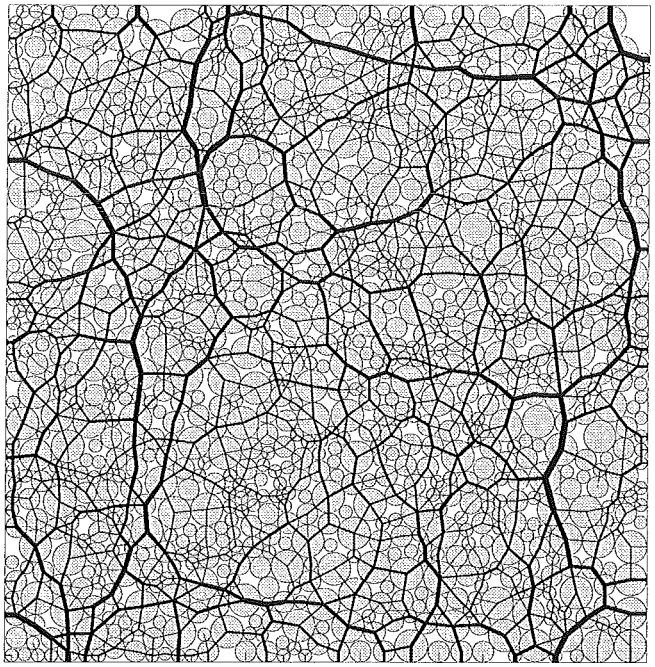

Figure 1.3: *Example for the force chains in a 2d packing of discs as obtained in numerical simulations, where pressure is applied from the top (from [25]). The thickness of the lines codes the absolute value of the normal force in contacts.*

explanations for this phenomenon were proposed [18], however, all were based on the assumption that this stress minimum resulted from arches inside the material directing the pressure away from the apex. Arches in granular materials are stress chains stable enough to support the weight above them, directing the pressure away towards the sides, like the walls of a container, similar to arches in buildings. When material is flowing, especially in a geometry with vertical walls, such arches are continually formed and destroyed [28]. Since the peak pressure for such dynamic arches can be much higher than in the static case [29] and is hard to predict, this complicates the construction of containers for granular materials, like silos, immensely.[4]

Though it seems to be clear that arches are indeed the reason for the stress minimum that may occur under the apex of the pile, it has to be pointed out that whether there is at all a stress minimum under a pile depends on many factors, like the preparation of the pile, the elasticity of the bottom plate, etc. The occurrence of this minimum is by no means a generic feature of sand piles, and there are as many experiments exhibiting the by now famous "pressure dip" as there are experiments showing no such feature in the pressure on the bottom plate [18]. In the experiment of Smid and Novosad [27] generally quoted on this subject, the arches in the system (and thus the pressure minimum) probably built up due to a relatively soft bottom plate, which sagged slightly in the middle and thus induced the arches.

[4]Indeed, silos collapse 100 to 1000 times more often than other industrial structures [30].

1.1.3 Theoretical approaches

Owing to the problem of history dependence and to the presence of large fluctuations, a theoretical description of stresses in granular packings is a difficult task. Traditional theoretical approaches to the description of granular packings have, however, put aside these problems. Besides, they often reduce the problem to two dimensions, either by considering two dimensional geometries or geometries with appropriate symmetries (like a conical pile). The system is then described as a continuum and an equation relating the principal stress axes is postulated (see [16, 18] and references therein). This is the traditional approach in the engineering community.

The first analysis of such a problem was performed by Janssen [31] in 1895, who modeled the forces acting on the bottom of a silo. The main assumptions in his analysis are that the stresses are uniform across any horizontal section of the material, and that the vertical and horizontal stresses are principal stresses, as would be expected from the symmetry of the system (though, as discussed above, this is usually not the case due to the formation of arches). Janssen calculates the force balance on a small horizontal slice of granular material, and assumes that the vertical normal stress σ_{zz} is related to the horizontal normal stress σ_{xx} by a constant factor K, such that $\sigma_{xx} = K\sigma_{zz}$. He assumes likewise that the wall shear stress τ_w is related to the horizontal stress σ_{xx} in the same way through the friction coefficient μ_w. That way, it can be shown that the force on the bottom plate exponentially approaches a constant value. The fact that the pressure on the bottom plate in a granular material hardly depends on the amount of material above it (and thus the flow velocity out of a hole at the bottom of a container is constant during outflow) was already remarked by Hagen [32], who measured the outflow rate from a hole at the bottom of a container. The fact that the flow rate is independent of the height of the material above the hole has been used for centuries in the guise of a simple hourglass.

The problem of all continuum approaches is that they have to make assumptions relating stress and strain, i.e. to formulate constitutive relations, because the equations arising from continuity considerations are incomplete if the material is considered perfectly rigid or plastic [16,18]. Recently, Wittmer *et al.* [33] proposed a model which they claimed takes the history of the system into account. Their FPA (fixed principal axis) assumption simply states that the stress on a volume element remains fixed as soon as this volume element is buried in the pile. For a sand pile built by pouring material from above the apex, this means that the angle of repose of the material provides the missing relation between the principal stresses. However, this model is only a special case of a more general model already introduced 40 years ago [34], and mainly gives a physical motivation for the choice of a free parameter in this model. Though the FPA assumption yields a local minimum in the stress under a conical pile, and gives reasonable agreement with the experimental data by Smid and Novosad, other models do so as well [18], so it is not obvious if the FPA assumption is in any way superior to previous continuum models.

To capture the force *fluctuations* in the system as well, the analysis has to go back to the scale of single grains, since by definition continuum approaches discussed above describe only mean quantities and provide no equation for the fluctuations. Approaches from the single particle scale have recently been explored by the statistical physics community to obtain statistics for force distributions. Common to all these stochastic models is that the

stresses at the base of a packing are calculated by randomly distributing the weight of the particles between the particles they rest on, thus constructing the force distribution by moving through the pile from top to bottom [35–37]. They differ mainly in the detailed way in which the weight of a particle is distributed between the particles below.

In the so-called q-model by Coppersmith *et al.* [35] particles are placed on a lattice and the weight of each particle plus the weight already resting on it is randomly distributed between its lower nearest neighbors. This sequential model computes the pressure in the system by moving from top to bottom and is accessible to an analytical treatment. It reproduces the exponential decay of the large forces for a number of probability distributions for the redistribution of weight. Claudin and Bouchaud [36] extend the q-model by allowing some bonds to "break", i.e. some sites chosen randomly will not support weight from a particle above them. Hemmingsson [37] uses a very similar model, but incorporates the fact that the weight is a vector.

These stochastic models show the stress minimum under the apex of a pile if some bonds are randomly broken, i.e. if there are some particles which have to put all their weight onto a single particle below. Since all these models are defined on triangular lattices, this directly introduces arches in the system which direct the weight away from the center of the pile. The same effect was seen in molecular dynamics simulations of regular pilings if some particles were removed randomly, or where a reasonably large distribution of particle sizes was introduced, even without friction [38]. Arching can also be tuned by the boundary conditions, and is connected to specific structures in the contact network.

The objective of this discussion of static packings, though this thesis is concerned with granular flow, is to illustrate the problems we face in dealing with granular materials, especially as recent interest of physicists has focused more and more on static or quasi-static problems. All models, be they of the continuum or stochastic kind, rely heavily on assumptions about the particular geometry in question, and always have to be supplied with experimental data on some global properties of this particular system. None of them can simply be supplied with details from the particle level, like the shape and size distribution of the particles or their friction coefficient. However, this is probably to be expected in such systems, which are extremely sensitive and history dependent. The whole discussion of the by now famous "pressure dip" shows the dilemma. Whenever arching is built into a model, no matter by what means, this pressure minimum appears. So we can be reasonably sure that arching is indeed the reason for its occurrence. But why these arches appear in some heaps, and are absent in others, is not explained by any of the theories, and can probably only be explained by taking the history into account in a more detailed way than in the model of Wittmer *et al.*

1.2 Liquid-solid transition

Since a granular material consists of many single particles, it may flow if enough energy is supplied to them. However, the energies required to achieve motion are much higher than for molecules, so the thermal energy can be neglected for grains. Due to the inelasticity of grain-grain interactions, the flow will cease again if the supply of energy is stopped or diminished too much. Energy loss is mainly due to two mechanisms: friction and loss of

relative velocity in head-on collisions. The precise nature of the dissipative grain-grain interactions will be discussed at the end of this chapter.

As discussed in the previous section, a granular material yields when the shear stress exceeds a certain limit. A typical example for this yielding is an avalanche on a pile of sand. When a sandpile is built by dropping particles onto it, these particles will, due to dissipation in collisions and due to friction, come to rest on the surface of the pile. However, when a certain limiting angle is exceeded (the so-called *angle of marginal stability* θ_m), the surface becomes unstable (the shear stress imposed on the upper layer by gravity exceeds the yield criterion) and a small layer of grains flows down the surface. The surface is thus eroded until a smaller angle (the *angle of repose* θ_r) is reached which is stable. Grains added to the pile at this angle of inclination will again stop on the pile.

Bak *et al.* [39] used the sand pile as a simple example to illustrate the concept of self organized criticality (SOC). They state that slowly driven systems with many degrees of freedom under certain conditions will self-organize into a critical state which is an attractor of the dynamics. They claim that the return to this critical state, when the system is driven out of it by the dynamics, happens without a characteristic time or length scale, i.e. the corresponding dynamics shows algebraically decaying power spectra. In the case of the sand pile, this means that at the critical point there are avalanches of all sizes up to the size of the system. Though this holds for the toy model of a sand pile Bak *et al.* propose, this toy model does not behave like a real sand pile. The only common property is that real sand piles may exhibit avalanche statistics with power law size distributions (but they do not necessarily do so, see [40] and references therein).

Recent experiments on rice piles show a strong dependence of avalanche statistics on the aspect ratio of the particles [41], i.e. for rice with a large aspect ratio the avalanche size distribution obeyed a power law, while for a small aspect ratio a stretched exponential was found. A possible explanation, which is supported by recent computer simulations on avalanches in bidisperse mixtures of discs in a rotating drum [42], is that the rice grains with a large aspect ratio form a more irregular surface, which exhibits niches that are able to accomodate small particles, thus helping to build up enough mass for a large avalanche. For the bidisperse mixture in the rotating drum, a power law was found for the avalanches of small particles (which can be accommodated in small niches on the surface), but a stretched exponential for the large particles (which cannot be stopped so easily), which supports this conjecture.

Aside from being used as a model for SOC, the sandpile illustrates two far more important features of granular materials. The first is again (just as described for granular packings) the history dependence of the system. Any angle θ with $\theta_r < \theta < \theta_m$ may be stable or unstable, depending on whether it was achieved by adding grains to the system or by taking grains away by means of an avalanche. A similar hysteresis is seen in rotating drums [43]. Depending on the rotation frequency, the surface of the material can exhibit either continuous flow or discrete avalanches. The transition between these two regimes occurs at different frequencies, depending on whether the frequency was increased or reduced.

Jaeger *et al.* proposed a simple phenomenological model for the hysteresis related to the angle of repose θ_r and the angle of marginal stability θ_m of a pile of grains [44]. They

argue that the faster a grain moves, the less it will probe the holes in the rough surface it passes, and the less energy it will lose. On the contrary, a relatively slow grain will fall into all these holes, and will additionally lose part of the potential energy gained in this fall. The particle thus experiences a velocity-weakening friction force at low shear rates (though at higher shear rates, when the holes become unimportant, it experiences the usual friction force quadratic in the shear rate), which can account for the hysteresis observed.

Another important point that has to be mentioned in describing the "liquid-solid transition" is the strong localization of the flow. When granular material yields and starts to flow, this flow is often localized in a small shear zone – just like the avalanche on the granular pile. Shear zones in granular materials are often only 5 to 10 particle diameters wide [45–48]. Thus, in flowing granular materials very often liquid and solid parts coexist [49], which complicates their description even more.

1.3 Flowing granular materials

When energy is fed into a granular material, e. g. via shearing, shaking, or simply by the action of gravity, it can start to flow. If there is very strong energy input, the material can reach so dilute a state that it resembles a gas. However, there are marked differences between a classical and a "granular" fluid or gas. Due to the dissipation in general, energy must continually be supplied to keep the material in this agitated state. Thus, a non-trivial steady state can only exist if there is continuous energy input to the system. Generally, one can distinguish three types of granular flow, though again the boundaries between them are diffuse. According to Savage [50], they can be classified in the following way:

- Quasi-static regime. In this regime, shear rates are very low, the density is very high and the particles are in mutual contact. The behaviour is quite insensitive of the shear rate, and rather determined by the shear stress. This is characteristic of friction dominated systems.
- Grain-inertia regime. Here, due to high shear rates and low to intermediate density, the shear rate dominates the behaviour, since particle collisions dominate the motion. Transmission of stresses and momentum transport takes place either by collisions (at intermediate density), or by particle transport (at low density). Most kinetic theories apply to this regime at intermediate densities.
- Transition regime. In situations where regions of high and low density coexist, parts of the system may be classified as quasi-static, others as in the grain-inertia regime. Both friction and collisions contribute to the dissipation. This is probably both the most common regime and the one most difficult to describe theoretically.

An important quantity in the description of the "liquid" or "gaseous" state of granular materials is the so-called *granular temperature*, analogous to the temperature in real liquids or gases.[5] However, the granular temperature is not defined as the mean kinetic energy of

[5]The thermal agitation of grains that would arise e.g. at room temperature is so small that it can be neglected for grains of the size considered here.

the particles, but rather related to the mean deviation of the individual particle velocities from the mean velocity, i.e.

$$T_g = \langle \vec{v}^{\,2} \rangle - \langle \vec{v} \rangle^2, \tag{1.3}$$

where $\langle . \rangle$ denotes the ensemble average. The concept of granular temperature was introduced by Ogawa [51, 52], who recognized the importance of fluctuations in the system. It has to be noted that, just as for the fluctuations in stresses for static granular materials, the velocity fluctuations $\sqrt{T_g}$ in the system are usually of the same order of magnitude as the mean velocity of the particles, and thus cannot simply be neglected. These fluctuations have a strong influence on both the dissipation and the momentum transport in the system.

1.3.1 Instabilities

The transition regime provides a good example for the instabilities occurring in granular flow. Due to the dissipative nature of collisions, the system can partially reorganize itself on intermediate length scales. The reason for this reorganization is the attenuating effect of dissipative collisions on density fluctuations. Assume that in a particular flow situation there is a region with slightly higher particle density than in its surroundings. In such a region, the collision frequency is also higher than in the surroundings, and thus more energy is dissipated in such a region, so that the particles are hampered from leaving it again. The surrounding material "feels" the pressure drop in this dense region and moves towards it as well. As a result, the dense regions get denser, and the dilute regions more dilute. This phenomenon is referred to as "clustering." It can be shown [53–55] that the typical size L of these clusters at the beginning of their formation is related to the mean free path s and the coefficient of restitution e_n (which describes the velocity loss in head-on collisions, see Section 1.5) by

$$L = \frac{s}{\sqrt{1 - e_n^2}}. \tag{1.4}$$

However, once this cluster formation has started, the size of the clusters will grow with time.

This clustering in granular flow or granular "gases" has important consequences in a number of flow situations or geometries [56]. A granular "gas" may cool down more slowly than would be expected for a homogeneous density [57]. In computer simulations of the cooling of granular gases with periodic boundaries the development of long range correlations was observed, leading to curious instabilities, like the development of a shearing mode [54, 58] or even eddies [58] in a previously random system. In a flowing granular material, this clustering may lead to density waves in flow through vertical pipes [59–61], in Couette geometries [62, 63] as well as in inclined chutes [64].

To rule out the emergence of such mesoscopic length scales in the system, the system size has to be smaller than L, which can be achieved either by small system sizes or by using very elastic material with a coefficient of restitution close to unity. This implies that there are systems which cannot be described by theories that cannot deal with the evolution of this microstructure. Systems that are too inelastic may have a typical length L only

a few particle diameters large, so in such cases clustering cannot be avoided if physically meaningful systems are investigated.[6]

1.3.2 Theoretical description of granular flow

Theories for the description of granular flow apply mostly to the quasi-static and the grain-inertia regime, i.e. either to slow deformations of materials ruled by frictional contact of the particles [16], or to rapid deformations involving mainly collisions [53, 65–69]. So far, there is no theory for systems in which both collisions and persistent contacts coexist, i.e. there is no theoretical description of the transitional regime.

The description of quasi-static flow is very similar to the modeling of forces in static granular materials as described in Section 1.1.3 [16]. While there, constitutive relations have to be formulated to relate stress and strain, in quasi-static flow the strain rate has to be related to the stress. Though these models work quite well, they rely heavily on phenomenological relations obtained from experiments, i.e. suffer the same problems as continuum theories for the statics of granular materials – including the inability to describe fluctuations, which have been shown to be quite large in recent shear cell measurements [70].

The first theoretical description of the grain-inertia regime is due to Bagnold [65]. He performed shear cell experiments of a suspension of neutrally buoyant wax spheres immersed in a fluid [65, 71]. His theoretical modeling was motivated by the observation that in shear flow, particles move in layers over one another, constantly colliding with particles from the adjacent layers. Since it is reasonable to assume that the collision frequency is proportional to the velocity difference between the layers, i.e. the velocity gradient, and since the velocity loss in a single collision is proportional to the relative velocity of the particles themselves, this yields for the shear (τ_{xy}) and normal (τ_{yy}) stresses

$$\tau_{xy} = \tau_{yy} \tan\alpha = \sigma\lambda^2 d^2 a_i \sin\alpha \left|\frac{\partial v_x}{\partial y}\right| \frac{\partial v_x}{\partial y}, \tag{1.5}$$

with $\lambda = d/s$, where d is the diameter of the grains and s their spacing, σ their specific weight, v_x the velocity in the direction of shear, and $a_i \sin\alpha$ a geometrical factor describing the transfer of v_x to v_y in an average collision. This relation between shear and normal stress has been confirmed in a number of shear cell experiments [72–74].

However, for granular material flowing in a vertical pipe, the same argument leading to eq. (1.5) would give $(\partial v_x/\partial y)^2 = \text{const.}$[7] Since in equilibrium,

$$\frac{\partial \tau_{yx}}{\partial x} + \frac{\partial \tau_{yy}}{\partial y} = 0 \tag{1.6}$$

should be fulfilled, this yields, according to eq. (1.5), $\partial\tau_{xy}/\partial x = \text{const.}$ and therefore $(\partial v_x/\partial y)^2 = \text{const.}$ For symmetry reasons, $\partial v_x/\partial y = 0$ in the middle of the pipe, and thus $\partial v_x/\partial y \equiv 0$ over the whole width of the pipe. The ingredients missing in Bagnold's

[6] Note that many naturally occurring materials like sand, rocks, soils, etc. are very inelastic, and therefore fall into this category.

[7] It has to be remembered, though, that Bagnold's theory does not attempt to describe such a system.

description of the motion to describe this system correctly are the velocity fluctuations. These are taken into account in *kinetic theories* for granular materials, which were developed approximately 30 years after Bagnolds analysis [53, 65–69].

Kinetic theories usually apply to nearly elastic particles, since they follow the kinetic theory of gases [75]. Most of these theories apply to relatively dense systems ($s \ll d$), where momentum transport occurs mainly through collisions, and the contribution of particle transport can be neglected. For smooth, nearly elastic spheres, balance equations for three mean quantities are derived, namely the mean mass density ρ, mean velocity $\vec{u} = \langle \vec{v} \rangle$, and the granular temperature T_g. Just like in the case of classical fluids, these balance equations are obtained from mass conservation, momentum conservation, and energy balance. The fact that one has to write energy *balance* instead of *conservation* complicates things enormously and is the point where kinetic theories for granular materials deviate from those of gases. The mass and momentum conservation equations are the same as for liquids, i.e.

$$\frac{\partial \rho}{\partial t} + \nabla \cdot (\rho \vec{u}) = 0 \tag{1.7}$$

for the mass conservation and

$$\frac{D\vec{u}}{Dt} = \nabla \cdot \overleftrightarrow{\tau} + n\vec{F} \tag{1.8}$$

for momentum conservation, where $D\vec{u}/Dt$ denotes the time derivative following the mean motion, i.e. $D\vec{u}/Dt = \partial \vec{u}/\partial t + (\vec{u} \cdot \nabla)\vec{u}$, $\overleftrightarrow{\tau}$ is the symmetric stress tensor, n the number of particles per unit volume, and $\vec{F}$ the sum of all body forces acting on the particles (in granular flow usually gravity or electromagnetic interactions). By contrast, the energy balance contains an additional term, the collisional energy loss γ, i.e.

$$\frac{3}{2}\rho \frac{DT_g}{Dt} = -\nabla \cdot \vec{Q} + \mathrm{tr}(\overleftrightarrow{\tau} \cdot \nabla \vec{u}) - \gamma. \tag{1.9}$$

Here, $\vec{Q}$ is the flux of translational energy, and (tr) denotes the trace of a tensor. The problem lies in specifying appropriate pair distribution functions to calculate the quantities γ, $\vec{Q}$ and $\overleftrightarrow{\tau}$ [50, 67], and, maybe even more important, to specify the right boundary conditions for $\vec{u}$ and T_g [76–80]. Unlike for fluids, there is no no-slip boundary condition, but the amount of slip at the walls depends on a number of properties of the system (microscopic and macroscopic roughness of the walls, coefficient of restitution, even the granular temperature of the flow itself).

Another problem arising in kinetic theories of granular materials is that the averaging usually takes place only over a relatively small number of particles, since the flow is often only a few particle diameters wide. The applicability of continuum approaches in the description of a granular material is therefore quite limited. Besides, very often the flow is not stable, i.e. evolves into the transition regime, due to the formation of the inelastic microstructure discussed in the previous subsection [56].

An alternative approach to kinetic theories, where it is tried to derive mean velocities, temperature profiles, etc. from first principles is to derive rate equations for these fields from phenomenological considerations [61]. This certainly can work only for relatively simple geometries, where it is easy to make reasonable assumptions about the flow geometry, symmetries etc. However, where applicable, such continuum models can lead to a simpler description of granular flow than kinetic theories. Besides, even in kinetic theories

one has to make some phenomenological assumptions, though at a different level, i.e. for particle distribution functions etc.

1.3.3 Flow in simple geometries

The simplest geometries that may be imagined for granular flow are certainly a vertical pipe, shear flow between two parallel plates, and flow on an inclined plane, although the latter is far more complicated than the other two, due to the open boundary at the top. In such simple geometries the differences between fluid flow and granular flow become clear.

In a vertical pipe, the flow behaviour depends strongly on both the volume fraction of grains in the pipe and on the width of the pipe with respect to the particle diameter. In very wide pipes, a plug may form in the middle with essentially no shear taking place inside the plug, but only in a narrow strip between this plug and the pipe wall [61, 73]. In a vertical pipe, the material comes in contact with the walls only through fluctuations.[8] Therefore, the material actually flows faster with decreasing coefficient of restitution, since the fast damping of fluctuations helps in the formation of such a plug [61]. In addition, density waves occur for relatively small coefficients of restitution [59–61] due to the cluster instability.[9]

Shear flow between two parallel plates shows the most predictable behaviour. A number of experiments with annular shear cells (which can, to some extent, be viewed as a good approximation to this geometry) have confirmed Bagnold's result of a constant relation of shear to normal stress [72–74], and numerical simulations [82–85] have shown nearly linear velocity profiles, accompanied by nearly constant density profiles, though sometimes with obvious shear zones at the wall [82, 85]. If one wall shearing the material is not forced to move at constant velocity, but is fixed to a spring that is pulled with constant velocity, as is usual in friction measurements, stick-slip motion can be observed [86, 87], with large fluctuations in the normal stress [87].

For flow in inclined chutes or on inclined planes, the problem is far more complicated. Since this is an important geometry both in nature and in industry, many studies have been performed on this system. So far, there are a number of experiments [88–104] and simulations [105–109] which seem partly contradictory at first sight. Many of these discrepancies are probably due to small differences in the details of the experimental set-up or the simulations, especially as far as the preparation of the bottom of the chute is concerned (e.g. flat and frictional, flat and smooth, bumpy). The details of all these experiments and simulations will be discussed in Chapter 5. Here it should only be mentioned that the main controversy evolves around the question of the density and temperature profiles. Kinetic theories predict a density minimum and temperature maximum at the bottom of the chute [110] for certain parameters. So far this has not been observed in experiments, and only very seldom in simulations [105, 107, 109]. In any case, the flow properties depend strongly on the boundary conditions at the bottom of the chute. Therefore, in this thesis a careful study of the interaction of particles with the chute bottom will be performed,

[8] As we have seen, Bagnold's theory, which neglects fluctuations, would give zero shear rate for a material flowing in a vertical pipe.

[9] In real systems, very often air flow can be the reason for density waves [81]. However, here no effects arising from the influence of the interstitial fluid will be discussed.

both in the case of a single particle moving down a rough incline, as well as in the case of many-particle flow in a two dimensional geometry.

1.4 Vibrated granular materials

Besides using simply the influence of gravity or shearing a granular material to set it in motion, there is another possibilty of liquefying a granular packing. The simplest way to supply energy to the system continuously is to vibrate a box containing grains.[10] This system shows extremely rich behaviour [112], which here can only be briefly summed up. All results described in the following relate to vertical shaking. Recently, the study of horizontal shaking has been taken up as well [113,114], however, the results are so far too inconsistent to draw any conclusions from them.

Compaction

Vibrating a system only slightly can result in small relative motion of the particles, which allows the material to compact, due to rare events leading to the reorganization of large parts of the structure. The dynamics is logarithmically slow, and the maximum density which can be reached in the end depends on the vibration amplitude and frequency [115]. There have been a number of phenomenological models to explain this time dependence, as relating it to a parking problem [116], random walk models [117], modeling it by a discrete map for the density [118] or using a spin glass like model [119, 120]. All of these models give the logarithmically slow decay of the height of the free surface, however, none can relate the vibration intensity and the compaction dynamics directly, i.e. their predictive power is quite limited.

Convection

If the system is shaken a bit more violently, and the walls and particles are sufficiently rough, the material may self-organize to form a small heap [121,122], which is sustained by a convective flow transporting material up to the top of the heap, which then avalanches down on the sides. Such heaping patterns were already observed by Faraday [123], who used very fine powder and showed that in this case, the heaping is due to air flow. Though air flow can be the motor for this phenomenon for very fine powder [124, 125], it persists also for heavier and larger particles, which should not be influenced by air flow [121, 122]. In the case where air flow can be neglected, the walls drive the convective motion [112].

If the acceleration of the system increases even further, the heap is destroyed again, but convection still persists [122]. The extension of the convection rolls, which are first localized near the top surface, grows with increasing acceleration, until they extend down to the

[10] Some care has to be taken here. As McNamara and Barrat point out [111], most commonly used waveforms both supply and take away kinetic energy, depending on what phase the vibration is in when the material hits the bottom of the container. Therefore, even though vibration *on average* supplies kinetic energy, this supply is not continuous for all waveforms.

bottom of the container. These convective patterns have been observed both in two dimensional [122] and three dimensional [126, 127] geometries. While in two dimensions the convective patterns can simply be observed with the help of high-speed cameras [122], in three dimensions NMR (Nuclear Magnetic Resonance) was used to visualize the flow patterns [126, 128, 129].

Convection, if it is not induced by the interstitial fluid, like air, obviously comes about by the shearing induced by the walls of the container, along with the dilation of the material due to the energy input at the bottom plate.[11] Usually, the material moves downwards at the wall and upwards in the middle of the container. This direction can be reversed by using a container with walls slightly inclined towards the outside [133, 134]. The wall angle for which the direction of the rolls is reversed depends on the roughness of the walls [133], but even for relatively smooth walls, this reversal is observed [134].[12] Obviously, the net downward drag exerted on the particles by vertical walls can be overpowered by the upward impulse imparted to the material by the upward moving inclined walls.

Pattern formation

When a relatively shallow bed of particles is shaken, completely different patterns emerge. In two dimensional systems, surface waves are observed [136–138], in three dimensional systems, these waves form even more complicated patterns like stripes, squares, hexagons or strongly localized patterns (the by now famous "oscillon") [139–142]. However, only a tentative explanation for these patterns has been given so far. As Shinbrot points out [142], the patterns are sustained by a competition between randomizing collisions of the particles when hit by the bottom plate and dissipation in inelastic collisions during the free flight phase. Based on these assumptions, he is able to give reasons for the symmetry of the patterns emerging. This simple model also explains why these patterns have a periodicity of twice the driving frequency. However, just as for the other effects described above for shaken granular materials, there is so far no theoretical description relating the number of layers in the system and the dissipative properties to the patterns observed at a specified driving amplitude and frequency.

Fluidization

If the vibrated material is very smooth and elastic (e.g. polished steel spheres) and in a container with smooth walls (or even periodic boundaries, i.e. in a quasi two dimensional experiment contained between two concentric cylindrical walls), no convection rolls appear, but the material reaches a fluidized state [143–148]. The fluidization usually starts at the top of the container, i.e. it is possible that only the upper layers are fluidized, while the lower layers behave like a solid block [145].

[11] Convection in numerical simulations can also be induced by the use of too soft particles [130, 131]. This is related to the "detachment-effect," which will be discussed briefly in Section 2.1.2. If this effect occurs, convection may even be observed in systems with periodic boundary conditions, but without the influence of air flow [132].

[12] A similar roll reversal could even be observed by solving the Navier-Stokes equations for a vibrated liquid, but only if a "negative slip" boundary condition was imposed at the walls. For the regular no-slip boundary condition the flow was always upwards at the side walls [135].

Kinetic theories [148, 149] predict the potential energy of the fluidized system, i.e. the height h of the center of mass, to scale with the maximum velocity of the bottom plate v_M as $h \propto v_M^2$, independently of the dimensionality of the system. However, experiments in two dimensional systems gave scaling exponents between 1.3 and 1.4 [148], close to the results 1.5 found in simulations of two dimensional [146, 150] and three dimensional [151] systems. Only in a one dimensional system the exponent 2 could be recovered [143, 152]. Obviously, the kinetic theories underestimate the dissipation in the system. Since in 1D, the exponent predicted by the kinetic theories is found, the deviation is probably due to increased dissipation due to fluctuations in the transverse directions. However, in this case, one would expect even stronger deviation of the exponent from 2 in three dimensions, which could not be confirmed by simulations so far [151].

1.5 Segregation

Another important aspect of the dynamics of granular materials is the phenomenon of segregation. Contrary to liquids, in granular materials components of different properties (size, shape, surface finish, density, etc.) separate when they are agitated, i.e. stirred, shaken,[13] or when they flow [153]. This property is very annoying in industrial applications, making the perfect mixing of granular materials a difficult task [154]. Recently, some progress has been made in the understanding of the mechanisms behind certain forms of segregation, though mainly on a qualitative basis. Therefore, here I will briefly sum up what is known so far about the most common forms of segregation.

Segregation due to vibration

If a box containing particles of different sizes is shaken, the material separates into the components of different size, with the largest particles accumulating at the top of the box, the smallest particles at the bottom [155–165]. This segregation takes place even if the large particles have a higher specific weight than the small ones (Ahmad and Smalley [155] performed experiments with lead spheres and sand), and is not a collective effect of the larger particles tending to collect together. Already a single particle of different size than the other particles in the system may move to the top or bottom of the container, depending on its relative size [155, 156, 159–165].

By now, two different mechanisms of size segregation have been identified:

- Segregation due to geometrical constraints. When the material is shaken, the pore volume of the system expands when the material lifts off from the bottom plate. Very small particles may then percolate through these small holes while the material is falling down again. When the material is compressed again by hitting the bottom plate, these small holes are more likely to be filled by smaller particles, which thus sneak into small spaces created below the large particles. The segregation velocity obtained with this mechanism depends strongly on the relative size of the particles

[13] The perfect way to mix oil and vinegar for a vinaigrette, namely to put both in a jar and shake it violently, thus does not work for granular materials.

[159, 160, 163, 165] and is of the order of thousands of vibration periods for a rise of a few particle diameters.

- Segregation due to convection. If the container is shaken violently enough to produce convection rolls, it is possible that large particles are carried to the top by the broad convection stream in the middle of the container, but then stay at the top because they are too large to reenter the narrow downward convection streams near the walls [161–163, 165]. In this type of segregation, the ascent velocity is independent of the particle size, i.e. the large particles rise at the same speed as the smaller bulk particles. The speed of upwards motion may be much larger than in the above case. Large particles can even be forced to go down in this regime by reversing the direction of the convection rolls, e.g. by inclining the container walls [133, 161].

Usually, both mechanisms are at work in a shaken granular material, and it only depends on the intensity of shaking which of the two mechanisms will dominate. However, even though qualitatively the mechanisms for size segregation due to vibration are clear now, there are so far no quantitative predictions on the segregation velocity as a function of vibration amplitude or frequency.

Segregation in flowing granular materials

Whenever a granular material flows, void spaces open up as well, just as described for vibrated granular materials. Under the influence of gravity, similar geometrical causes for size segregation as in a vibrated bed are at work. In granular surface flow, this leads to the rise of large particles to the top of the flow. This segregation was termed *inverse grading* by geologists, since in deposits of rocks etc. the larger particles are usually found on top, contrary to what is observed in sediments in lakes or river beds, where the smaller particles are found on top, due to their slower sedimentation velocity [166–168]. Besides, in avalanches, the large particles are usually found in the front part of the avalanche, i.e. move farther as well. The reason is that the large particles that reach the top of the pile flow towards the front faster than the small particles, and when buried again by the advancing pile, segregate upwards again faster than the small particles [167]. This kind of segregation is by now recognized to be the reason for the fingering instability observed in slow surface flow [169].[14]

Related to this segregation in surface flow is the phenomenon of stratification. If a mixture of grains of different size and shape is poured in the narrow gap between two parallel plates, the material deposits in stripes of the different materials [170]. For this segregation mechanism it seems to be important that the smaller particles have a smaller angle of repose than the larger ones, so that the material will deposit in stripes with the smaller species below and the larger species on top. However, this stratification seems to disappear when the plate separation is increased [171].

[14] As a matter of fact, the mechanism is slightly more complicated than suggested here. The large particles also have to be quite irregular, to be easily trapped by the rough surface and thus for a while stop the flow behind them.

Segregation in rotating drums

A mixture of particles of different sizes or specific weight in a rotating drum "mixer" segregates as well. There are in fact two different types of segregation observed in this situation, which take place on different time scales.

- Radial segregation. This type of segregation happens both in quasi two dimensional [172–174] and three dimensional systems [175, 176] and is very efficient and fast. It was observed especially for quite low rotation frequencies (of the order of 0.02 - 0.15 Hz) [172]. In the two dimensional system, already after one revolution of the drum, a core of small particles has formed at the center of the drum. The reason for this type of segregation is that when avalanches move down the free surface of the material in the drum, smaller particles will move to the bottom of the avalanches, where they are more likely to be stuck, since there the velocity is smaller, and they see a more pronounced roughness than the large particles. In a two dimensional numerical simulation, mass segregation was observed as well for particles of equal size, but different specific weight [177]. There, the heavier particles, just like the smaller particles in the case of size segregation, move towards the bottom of the avalanche zone, where they are more likely to get stuck.
- Axial segregation. This type of segregation is very slow, taking minutes to hours of revolution at rotation frequencies of the order of 1 Hz [175,178–181]. Here, particles of different size and/or form arrange themselves in stripe patterns along the rotation axis of the cylinder. It is even possible to get the material to separate completely in only two stripes. This can be achieved either by rotating the material for a very long time [181] or by using a drum in the form of a screw [178]. Axial segregation seems to come about either by local fluctuations in the density [178], or by the influence of the lateral walls of the drum [180]. However, it is not completely understood what the size ratio of the different particle species has to be to promote axial segregation [180]. Contrary to radial segregation, axial segregation can be made to disappear again by reducing the rotation frequency of the cylinder [180].

Common to all the segregation mechanisms described here is the fact that even though in the last decade it has become clear what drives segregation *qualitatively*, hardly any quantitative predictions can be made. For the case of segregation in surface flow, it is hoped that the study of the motion of a single particle on a rough inclined plane, which will be taken up in this work, provides more quantitative information about this problem.

1.6 Collisions

So far, nothing has been said about the exact nature of dissipation in collisions. It has only been mentioned that dissipation arises both from velocity loss in head-on collisions, and from frictional losses. In principle, contact mechanics should provide expressions for the frictional and collisional losses in the collision of two spheres, but the problem of two touching bodies under general conditions is very complicated (see, e.g., [182] and references therein). Even the oblique impact of two perfectly elastic spheres cannot be described in

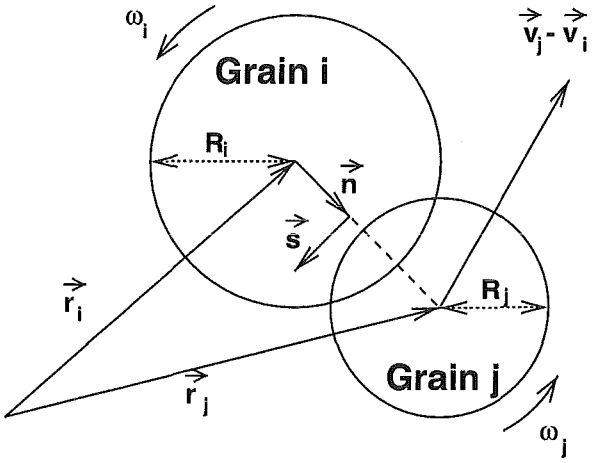

Figure 1.4: *Sketch of the impact geometry in 2D.*

a simple way, since its outcome depends on the history of the collision. When dissipation enters the picture, the situation becomes even more complicated, since the dissipation mechanisms are not known exactly. Figure 1.4 shows the geometry of the impact of two spheres. The collision of two spheres always reduces to a two dimensional problem (see the more detailed discussion in section 2.1.1). In the following, the physics of a binary collision of spheres will be discussed.

The collision of two spheres of radii R_i, R_j with velocities v_i, v_j can be described in a local coordinate system defined by the positions $\vec{r_i}$ and $\vec{r_j}$ of the particles with the unit vectors $\vec{n}$ and $\vec{s}$

$$\vec{n} = \frac{\vec{r_j} - \vec{r_i}}{|\vec{r_j} - \vec{r_i}|} = (n_x, n_y) \tag{1.10}$$

$$\vec{s} = (n_y, -n_x). \tag{1.11}$$

Since the particles in general also may have rotational velocities ω_i and ω_j, the relative velocity $\vec{v}$ at the contact point is given by

$$\vec{v} = \vec{v}_j - \vec{v}_i + (R_i\omega_i + R_j\omega_j)\vec{s}. \tag{1.12}$$

The relative normal velocity v_n and relative shear velocity v_s are thus given by

$$v_n = (\vec{v}_j - \vec{v}_i) \cdot \vec{n} \tag{1.13}$$

$$v_s = (\vec{v}_j - \vec{v}_i) \cdot \vec{s} + \omega_i R_i + \omega_j R_j. \tag{1.14}$$

In the following, the quantities before the impact will be denoted by the superscript i (initial), after the impact by a superscript f (final).

If the shear velocity component $v_s = 0$ at the beginning of a contact, the impact is head on or *normal*, otherwise it is shearing or *oblique*. There are various measures for the obliqueness of the impact, e.g. the impact angle

$$\vartheta = \arccos\left(\frac{(\vec{v}_j^{\,i} - \vec{v}_i^{\,i}) \cdot \vec{n}}{\left|\vec{v}_j^{\,i} - \vec{v}_i^{\,i}\right|}\right), \tag{1.15}$$

or the dimensionless initial tangential velocity,

$$\psi^i = v_s^i / v_n^i, \tag{1.16}$$

which is related to ϑ by $\tan\vartheta = \psi^i$. In the following, normal and oblique impacts will be discussed separately.

1.6.1 Normal impacts

1.6.1.1 Elastic collisions

Hertz was the first to derive the expression for the repulsive force acting in the normal contact of two perfectly elastic spheres [182–184]. He found that the normal force F_n acting on the particles in contact varies with the relative normal displacement ξ

$$\xi = \max\left(0,\, R_i + R_j - |\vec{r}_j - \vec{r}_i|\right) \tag{1.17}$$

as

$$F_n = -k_n\, \xi^{3/2}. \tag{1.18}$$

The spring constant k_n is related to the size of the particles and the elastic material constants by

$$k_n = \frac{4}{3}\sqrt{R_{\text{eff}}}\, E_{\text{eff}}, \tag{1.19}$$

where $R_{\text{eff}} = R_i R_j/(R_i + R_j)$ is the effective radius of the sphere and E_{eff} an effective elastic modulus that can be computed from the elastic moduli E_i and E_j and the Poisson numbers ν_i and ν_j by $E_{\text{eff}} = E_i E_j/(E_j(1-\nu_i^2) + E_i(1-\nu_j^2))$.

The proportionality $F_n \propto \xi^{3/2}$ can also be derived from a simple dimensional argument [182]. It is assumed that the deformation δ of the contact region (see Fig. 1.5) can be approximated by the deformation at the outer limit of the contact. Assuming that the deformation is small, i.e. that $\delta \ll a$, $\xi \ll a$ and $a \ll R$, so that terms quadratic in ξ and δ can be neglected with respect to a and R, from geometrical considerations it follows that

$$a^2 \approx 2\delta R \tag{1.20}$$

and

$$a^2 \approx R\xi. \tag{1.21}$$

If we assume a linear stress-strain relation (i.e. Hooke's law), it follows that the local pressure p is proportional to the relative deformation δ/a, so that according to eq. (1.20)

$$p \propto a/R, \tag{1.22}$$

so that

$$F_n \propto a^3/R, \tag{1.23}$$

which, according to eq. (1.21), yields

$$F_n \propto \xi^{3/2}\sqrt{R}. \tag{1.24}$$

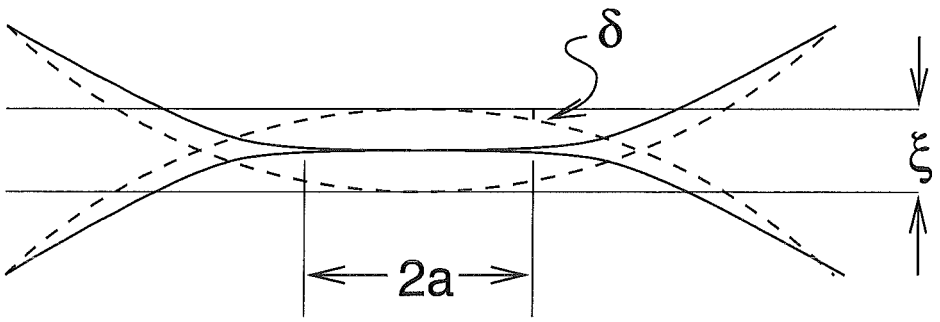

Figure 1.5: *Illustration of a Hertzian contact of two spheres of radius R. The dashed lines illustrate the virtual overlap of the undeformed spheres, the solid lines the deformed surfaces.*

The contact duration can also be derived from eq. (1.18). The maximum penetration depth ξ_0 can be calculated from the energy balance. Energy conservation yields

$$\frac{1}{2} m_{\text{eff}} \dot{\xi}^2 + \frac{2}{5} k_n \xi^{5/2} = \frac{1}{2} m_{\text{eff}} {v_n^i}^2, \tag{1.25}$$

where $m_{\text{eff}} = m_i m_j/(m_i + m_j)$ is the reduced mass of the particles. The maximum penetration of the spheres is reached when $\dot{\xi} = 0$, i.e. for

$$\xi_0 = \left(\frac{5}{4}\frac{m_{\text{eff}}}{k_n}\right)^{2/5} {v_n^i}^{4/5}. \tag{1.26}$$

The duration t_n of the collision is thus

$$t_n = 2 \int_0^{\xi_0} \frac{d\xi}{\sqrt{{v_n^i}^2 - \frac{4}{5}\frac{k_n}{m_{\text{eff}}}\xi^{5/2}}}, \tag{1.27}$$

which yields, after integration,

$$t_n = \frac{4\sqrt{\pi}\Gamma(2/5)}{5\Gamma(9/10)} \left(\frac{4}{5}\right)^{2/5} \left(\frac{m_{\text{eff}}^2}{k_n^2 v_n^i}\right)^{1/5} = 3.21 \left(\frac{m_{\text{eff}}}{k_n}\right)^{2/5} {v_n^i}^{-1/5}. \tag{1.28}$$

This expression for the duration of a collision has been confirmed in experiments on impact of spheres of different materials with a flat plate [185, 186]. If the spheres are neither too soft nor too small,[15] adhesion forces arising either from a gain in surface energy [187] or from van der Waals forces can be neglected, and the Hertz law eq. (1.18) describes the elastic normal contact of spheres well.

1.6.1.2 Inelastic collisions

In general, two colliding spheres undergo a deformation which will be somewhere between the extremes of perfectly inelastic and perfectly elastic. Possible mechanisms for dissipation (i.e., transformation of kinetic energy into other forms of energy which ultimately

[15] This is fulfilled for particles of diameter of the order of 1 mm and larger, and for the elastic moduli used in this work.

transform into heat) are plastic deformation, viscoelasticity of the material, and also elastic waves excited by the impact [182]. The latter are always present – they make the noise – but carry so little energy that one can generally neglect them as source of dissipation. Recently, some theories have been proposed where only these elastic waves contribute to the energy loss [188], but where it is assumed that the degree of excitation of the internal degrees of freedom of the particles is a stochastic quantity. Phenomenologically, the elasticity of the impact is described by the coefficient of normal restitution e_n,

$$e_n = -v_n^f / v_n^i \in [0, 1]. \tag{1.29}$$

According to Johnson [182], the critical yield velocity necessary to cause plastic deformation is given by

$$v_{\text{yield}}^2 \approx 107 \frac{R_{\text{eff}}^3}{m_{\text{eff}}} \frac{Y^5}{E_{\text{eff}}^4} \tag{1.30}$$

where $m_{\text{eff}} = (m_1 m_2)/(m_1 + m_2)$ and $R_{\text{eff}} = (R_1 R_2)/(R_1 + R_2)$ are the reduced mass and radius, Y is the yield strength of the softer of the spheres, and E_{eff} is related to Young's modulus E and Poisson's ratio ν of both spheres through $1/E_{\text{eff}} = (1 - \nu_1^2)/E_1 + (1 - \nu_2^2)/E_2$. If $v_n^i < v_{\text{yield}}$, no plastic deformation may occur during the impact, and all energy loss must be due to other effects like viscoelasticity or sound waves excited by the impact. If $v_n^i > v_{\text{yield}}$, on the other hand, the energy loss due to plastic deformation should dominate over the energy loss due to viscoelasticity. Most materials have a critical yield velocity that is quite small (e.g. $v_{\text{yield}} \approx 0.14$ m/s for cellulose acetate, $v_{\text{yield}} \approx 0.02$ m/s for steel). There are even indications that plastic deformation of surface asperities contributes to quite a large part of the energy loss. Experiments performed with steel spheres showed that simply by polishing the surface, e_n can be varied between 0.82 and 0.95 [186].

For the case of plastic deformation of the sphere as a whole, a simple theory [182] predicts e_n to fall off like ${v_n^i}^{-1/4}$ with increasing impact velocity. For the case of purely viscoelastic losses, Kuwabara and Kono [189] obtain a coefficient of normal restitution e_n that also decreases with increasing v_n^i; for e_n close to one, $(1 - e_n) \propto {v_n^i}^{1/5}$. Experimental studies by Goldsmith and others [185], Bridges *et al.* [190], Kuwabara and Kono [189] and Sondergaard *et al.* [191] for spheres made of a large class of different materials all show a slight monotonic decrease of e_n with increasing v_n^i which is compatible with a ${v_n^i}^{-1/4}$ power law over several orders of magnitude of v_n^i. Lifshitz and Kolsky [186], however, find in their experiments with highly polished steel spheres a coefficient of restitution $e_n = 0.95$ which is constant for all velocities below v_{yield}, and then a strong decay (without commenting on what law might be fitted to this decay). On the other hand, measurements by Drake and Shreve [192] and Foerster *et al.* [193] on cellulose acetate spheres show no systematic dependence of e_n on v_n^i for the range of impact velocities used, which in both cases was rather narrow (Foerster *et al.* measured $e_n \approx 0.87$ in a velocity range 0.29 m/s $\leq v_n^i \leq$ 1.2 m/s).

Obviously, so far there is no generally accepted theory that would describe the energy loss in a normal collision adequately. Though there are strong indications that the coefficient of restitution e_n depends on the impact velocity, this dependence is weak enough that for the typical range of relative velocities occurring in a specific flow situation, a constant coefficient of restitution seems to be a good approximation.

1.6.2 Oblique impacts and frictional contacts

In general, the shear force is connected to the normal force by the Coulomb laws of friction [eqs. (1.1) and (1.2)]. In the contact area of two colliding convex bodies, a *local* version of eqs. (1.1) and (1.2) holds that relates normal and shear stresses along the contact. For elastically similar bodies, the shear stresses do not influence the normal stress distribution over the contact area [182], so that the results of Hertz theory can still be used for the normal stresses. Then, in the outer regions of the contact area, where the normal stresses are small because the strains are small, one must in general expect the condition for dynamic friction to be fulfilled, whereas in the central regions, where one has large normal strains and stresses, static friction may occur. This leads to the development of an *annulus of microslip* surrounding an inner *region of sticking* in the contact area. Because the friction laws are strongly nonlinear, the size and form of the annulus of microslip depends on the loading–unloading history of the contact, making the prediction of tangential deformation and friction forces in a given situation complicated [194].

Mindlin and Deresiewicz [195] have discussed the tangential friction forces between two elastic spheres for the case of several distinct loading-unloading histories and assuming the Hertz theory to hold. Maw *et al.* [196,197] and Walton [198] performed such an analysis for the case of the oblique impact of spheres. One interesting result is that due to the ability of the sticking contact to store and restore "tangential" kinetic energy, there may be a reversion of tangential velocity v_s under certain circumstances, a fact that has been confirmed experimentally for discs [197] and spheres [185,193].

One may introduce a tangential coefficient of restitution, e_s, analogous to the normal coefficient of restitution e_n, but allowing it to become both positive or negative, i.e.

$$e_s = v_s^f / v_s^i. \tag{1.31}$$

The possible reversal of the shear velocity (i.e. the possibility of negative e_s) can be understood by taking into account the tangential elasticity of the material. In a sticking contact, the material deforms in the tangential as well as in the normal direction. The energy stored in this tangential deformation of the sphere can be regained if the contact remains sticking during the whole collision. How much of this energy can be regained depends on the relative sizes of the central region of sticking at the beginning and the end of the collision.

One way to characterize an oblique collision independently of the normal velocity was introduced by Maw *et al* [196]. They plot the dimensionless initial tangential velocity,

$$\psi^i = v_s^i / v_n^i, \tag{1.32}$$

as a function of the dimensionless final tangential velocity,

$$\psi^f = v_s^f / v_n^i. \tag{1.33}$$

In such a MBF diagram (short for Maw, Barber and Fawcett), e_s can be directly read off as $e_s = \psi^f / \psi^i$. Maw *et al.* point out that in principle, three distinct situations can occur in oblique impact:

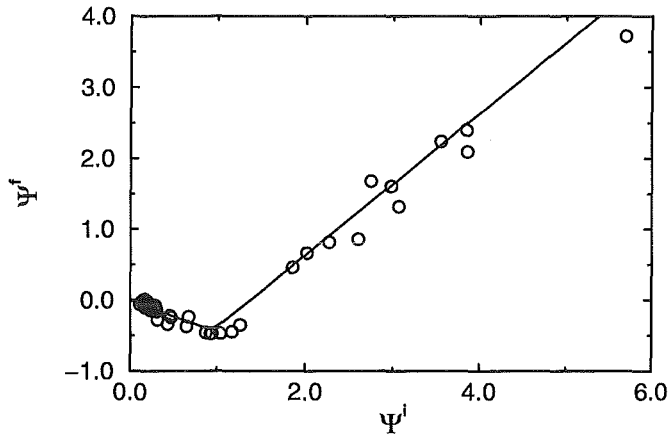

Figure 1.6: *MBF diagram corresponding to cellulose acetate spheres (data from [193]). The solid line corresponds to Waltons collision model with* $e_n = 0.89$, $\mu = 0.21$ *and* $\beta = 0.39$.

- The shear velocity is so high throughout the whole collision that only dynamic friction occurs. In this case $e_s > 0$, and there is no reversal of the tangential velocity. This case corresponds to large ψ^i, i.e. grazing collisions.
- Initially, there is sliding friction in the contact, but this friction force is strong enough to reduce v_s to zero during the collision. The outcome of the collision depends on the point in time when sticking starts, and when it ends again. Such a collision may lead to positive or negative e_s. This is the case for intermediate ψ^i.
- The contact is sticking during the whole contact duration. In this case the value of e_s depends on the relative duration of the normal and tangential oscillation, t_n/t_s. Again, e_s may be positive or negative, depending on which direction the tangential oscillation has when the contact opens. This case corresponds to small ψ^i, i.e. to nearly head-on collisions.

Figure 1.6 shows the MBF diagram as obtained from measurements of collisions of cellulose acetate sphere by Foerster *et al.* The solid lines illustrate a simplified collision model introduced by Walton [199]. He assumed a negative constant coefficient of tangential restitution $e_s = -\beta$ in sticking collisions, and neglects the intermediate regime. This model will be explained in more detail in section 2.1.3, when the collision operator used in event driven simulations will be discussed. The parameters used in Fig. 1.6 were derived from a fit of this model to the experimental data.

Obviously, the correct description of the general dissipative collision of two spheres is a complicated task, which still has not been achieved. All theoretical descriptions mentioned here for the description of oblique impacts neglect dissipation in the normal direction, i.e. they assume that the normal and tangential motion can be decoupled. As far as normal impacts are concerned, no correct model for the dissipation exists so far, since it is unclear what exactly the dissipation mechanisms are. To model granular materials via computer simulations, some assumptions have to be made about the nature of the contact forces or the collisions. In Chapter 3, such models will be discussed in more detail with

respect to experimental results on the binary collision of spheres.

1.7 Concluding remarks

In the last decade, significant progress has been made in understanding in detail a number of phenomena observed in granular flows. Nevertheless, even though in many cases the reasons for their behaviour have become clear in a qualitative way, theoretical predictions are still lacking.

One big problem is the formulation of appropriate constitutive relations for continuum theories both for the prediction of stresses in granular media and for flowing granular media, especially in the case of slow deformations. The inherent instability of granular flows complicates their description in the framework of kinetic theories, where another great problem is the formulation of appropriate boundary conditions for velocity and granular temperature. Due to the presence of large fluctuations, the description of granular materials by means of such continuum theories is problematic anyway. So far, no quantitative predictions for the description of the collective effects in granular materials, like segregation, convection, heaping, or surface waves exist. In the case of vibrated granular materials, kinetic theories only give quantitative predictions for the fluidization of the material, but these are quite far off from experimental and simulation results. Even the seemingly simple problem of the binary collision of two spheres is not resolved.

Therefore, in this thesis, instead of tackling the investigation of collective effects in granular materials right away, I take an alternative route. I will study a very simple problem, namely the motion of a single sphere on a rough inclined plane. The hope in the detailed investigation of such a simple problem is to get a deeper understanding of the subject. Particular attention is also paid to the influence of the simulation methods used in this investigation. As it turns out, a number of results obtained for the single particle are valid in dense flows of granular material on an inclined plane as well, and can be understood in a similar way as the motion of the single particle.

Chapter 2

Simulation methods

"No machine can lie," said Father Brown; "nor can it tell the truth."
— G. K. Chesterton, "The mistake of the machine"

Various methods are commonly used in the simulation of granular materials [200]. They can essentially be divided into two subclasses. In the first class, one tries to model the particle interactions as realistically as possible, and the trajectory of each particle is computed numerically. These simulations can be seen as "numerical experiments," in the sense that they intend to duplicate or substitute physical experiments, and allow for easy measurement of many quantities which are difficult to access or are inaccessible in experiments. However, since even these simulations introduce simplifications, they are also not perfect models of the "real" world. Simulation techniques of this category include hard-sphere and soft-sphere molecular dynamics simulations and contact dynamics simulations.

In the second class of simulations, one tries to simplify the interactions, i.e. only the essential features of the interactions are retained. *What* exactly is considered to be an essential feature of the interaction or the motion varies from method to method. Some of these methods (like cellular automata or Monte Carlo methods) are already used with success in other fields and were adapted to granular materials, others, like the BTR (Bottom-To-Top-Restructuring) model involved significant extensions of previous methods (Random Sequential Absorption model [201]) to apply to the simulation of granular materials. In this chapter, molecular dynamics simulations are discussed in some detail, since these will be used here to model granular materials. Other methods, such as Contact Dynamics or indirect methods, will be explained very briefly.

2.1 Molecular dynamics

Molecular dynamics (MD) simulations were developed for the simulation of liquids and gases on the basis of individual particle motion [202].[1] There are essentially two types of

[1] If applied to granular materials (the molecules being replaced by grains), they are sometimes referred to as "granular dynamics" simulations.

MD simulation methods: time-step driven MD (here labeled TD) and event driven MD (here labeled ED). In both cases, all particle trajectories are computed explicity. The two methods differ mainly in their treatment of particle-particle interactions. While in TD simulations, a potential acts between the particles (repulsive when they overlap and zero otherwise in the case of grains), in ED the particles are assumed to be hard, and to interact via instantaneous collisions. Thus in TD simulations, the equations of motion for all particles are integrated numerically, with a specified constant time-step (hence "time-step driven"), while in ED simulations, the trajectories between collisions (events) are computed analytically if the outer forces acting on the particles allow it, and the simulation advances from collision to collision (hence "event driven"). The two methodes will be described seperately here, as well as some problems that can arise in each of them.

2.1.1 Time-step driven MD

The application of time-step driven MD to the simulation of granular materials was introduced by Cundall and Strack [203]. Especially with the increasing computer power that has become available in the last decade, it is probably the most popular simulation method for granular materials, and has been used in numerous studies (see e.g. [49, 87, 106, 130, 131, 144, 204–209]).

The equations governing the system are Newtons equations of motion

$$\vec{F}_i = m_i \ddot{\vec{r}}_i \quad (i = 1, N), \tag{2.1}$$

where N is the number of grains, $\vec{r}_i$ their position and $\vec{F}_i$ the force acting on grain i. If there are also rotational degrees of freedom, the equations

$$\vec{M}_i = I_i \dot{\vec{\omega}}_i \quad (i = 1, N), \tag{2.2}$$

where $\vec{M}_i$ is the torque of the particles, I_i the moment of inertia, and $\dot{\vec{\omega}}_i$ the rotational velocity of the particles, have to be added.

Two grains i and j are considered to interact only when they are in contact, i.e. their "virtual overlap" ξ,

$$\xi = \max\,(0,\, R_i + R_j - |\vec{r}_j - \vec{r}_i|), \tag{2.3}$$

is larger than zero. If $\xi = 0$, the grains move freely under the action of gravity, i.e. $\vec{F}_i = m_i \vec{g}$ and $\vec{M}_i = 0$. A general contact between two grains of radii R_i, R_j, positions $\vec{r}_i$, $\vec{r}_j$ velocities $\vec{v}_i$, $\vec{v}_j$, and angular velocities $\vec{\omega}_i$, $\vec{\omega}_j$ is sketched in Fig. 1.4 for a two dimensional geometry. Though the binary collision of spheres can always be reduced to a two dimensional problem, in the following the impact geometry is taken as arbitrary in a three dimensional system, since this is how it is handled in a 3D simulation.

To reduce the general three dimensional geometry to the two dimensional impact geometry, two unit vectors $\vec{n}$ and $\vec{s}$ are used to decompose the forces and velocities into normal and shear components:

$$\vec{n} = \frac{\vec{r}_j - \vec{r}_i}{|\vec{r}_j - \vec{r}_i|} \tag{2.4}$$

$$\vec{s} = \frac{\vec{v}_j - \vec{v}_i - [(\vec{v}_j - \vec{v}_i)\cdot\vec{n}]\,\vec{n} + \vec{n}\times(R_j\,\vec{\omega}_j - R_i\,\vec{\omega}_i)}{|\vec{v}_j - \vec{v}_i - [(\vec{v}_j - \vec{v}_i)\cdot\vec{n}]\,\vec{n} + \vec{n}\times(R_j\,\vec{\omega}_j - R_i\,\vec{\omega}_i)|}. \tag{2.5}$$

In a 2D system, this reduces to eqs. (1.10) and (1.11). Thus, the relative normal velocity v_n and relative shear velocity v_s are given by

$$v_n = (\vec{v}_j - \vec{v}_i) \cdot \vec{n} \tag{2.6}$$

$$v_s = (\vec{v}_j - \vec{v}_i + \vec{n} \times (R_j \vec{\omega}_j - R_i \vec{\omega}_i)) \cdot \vec{s}, \tag{2.7}$$

or, in 2D, by eqs. (1.13) and (1.14).

So far, none of the forces have been specified. Since, as already discussed briefly in Section 1.5, the exact law governing a collision or a lasting contact is not known, various approximations are employed to model the contact forces. Their properties will be discussed in detail in Chapter 3, here only two out of these (one for the normal, one for the tangential direction) will be used to elucidate some points of the TD simulation method.

The simplest repulsive dissipative normal force that can be used is a linear spring with linear damping,[2]

$$F_n = -k_n \xi - \gamma_n \dot{\xi}. \tag{2.8}$$

The duration of the collision is then half of one oscillation period,

$$t_n = \pi \left(\frac{k_n}{m_{\text{eff}}} - \left(\frac{\gamma_n}{2m_{\text{eff}}} \right)^2 \right)^{-1/2}. \tag{2.9}$$

This duration of a collision is the most important time scale in the simulation. It fixes the time step for the integration of the equations of motion, and thus the real time that can be simulated. To get good integration of the collision, the time step δt in the simulation should be at least $\delta t = t_n/50$ [202]. But t_n is not merely a technical parameter – a real collision has a certain duration, as discussed in Section 1.6 ($\approx 10^{-5}$ seconds for steel balls with a diameter of 1 cm), and, as will be shown in the next subsection, this has an influence on the dissipation in dense systems. Since computation time increases with decreasing t_n, which is related to increasing k_n, i.e. the stiffness on the particle, a compromise has to be found between realistic stiffnesses and reasonable computation time.

A common tangential force is

$$F_s = -\min(|\gamma_s v_s|, |\mu F_n|) \cdot \text{sign}(v_s), \tag{2.10}$$

which is the Coulomb friction law for sliding friction, regularized for $v_s \to 0$. If the particle in question is in contact with a number of particles, the contributions to the total force by each particle are simply added up, and this total force is fed into the equations of motion (2.1).

Now, knowing the forces that enter into eqns. (2.1) and (2.2), these can be integrated numerically. There are a number of methods available for numerical integration [202, 210], here only the predictor corrector method will be discussed, since it is the only one used in the simulations presented here. The method is straightforward. Assuming that at time t all positions $\vec{r}_i(t)$, velocities $\vec{v}_i(t)$, accelerations $\vec{a}_i(t)$ and even higher order time-derivatives

[2]The extension of the Hertz normal force (1.18) discussed in Section 1.6.1.1 has some unphysical properties, as we will see in Chapter 3, which is why it is not used in this discussion. Besides, for this force the duration of a collision depends on v_n^i, which also would complicate the discussion which follows.

(as in the example shown here $\vec{b}_i(t) = \dot{\vec{a}}_i(t)$ and $\vec{c}_i(t) = \dot{\vec{b}}_i(t)$) of the position are known, the quantities at the later time $t+\delta t$ can be approximated by the Taylor expansion about the time t

$$\begin{aligned}
\vec{r}_i^{\,p}(t+\delta t) &= \vec{r}_i(t) + \delta t\,\vec{v}_i(t) + \frac{1}{2}\delta t^2\,\vec{a}_i(t) + \frac{1}{6}\delta t^3\,\vec{b}_i(t) + \frac{1}{24}\delta t^4\,\vec{c}_i(t) + \ldots \\
\vec{v}_i^{\,p}(t+\delta t) &= \vec{v}_i(t) + \delta t\,\vec{a}_i(t) + \frac{1}{2}\delta\, t^2\vec{b}_i(t) + \frac{1}{6}\delta t^3\,\vec{c}_i(t) + \ldots \\
\vec{a}_i^{\,p}(t+\delta t) &= \vec{a}_i(t) + \delta t\,\vec{b}_i(t) + \frac{1}{2}\delta t^2\,\vec{c}_i(t) + \ldots \\
\vec{b}_i^{\,p}(t+\delta t) &= \vec{b}_i(t) + \delta t\,\vec{c}_i(t) + \ldots \\
\vec{c}_i^{\,p}(t+\delta t) &= \vec{c}_i(t) + \ldots
\end{aligned} \tag{2.11}$$

This is the predictor step, i.e. the variables at the next time step are predicted on the basis of their values at the present time step. However, so far the forces have not been used – they are needed to correct this prediction. From the new positions and velocities the corresponding forces $\vec{F}_i(t+\delta t)$ are predicted, and from these the corresponding acceleration $\vec{a}_i^{\,c}(t+\delta t) = \vec{F}_i(t+\delta t)/m_i$ is calculated. This gives an estimate for the error made in the calculation of the predicted quantities,

$$\Delta\vec{a}_i = \vec{a}_i^{\,c}(t+\delta t) - \vec{a}_i^{\,p}(t+\delta t). \tag{2.12}$$

This error can now, with appropriate weights c_i, be used to correct the predicted values:

$$\begin{aligned}
\vec{r}_i^{\,c}(t+\delta t) &= \vec{r}_i^{\,p}(t+\delta t) + c_1\Delta\vec{a}_i \\
\vec{v}_i^{\,c}(t+\delta t) &= \vec{v}_i^{\,p}(t+\delta t) + c_2\Delta\vec{a}_i \\
\vec{a}_i^{\,c}(t+\delta t) &= \vec{a}_i^{\,p}(t+\delta t) + c_3\Delta\vec{a}_i \\
\vec{b}_i^{\,c}(t+\delta t) &= \vec{b}_i^{\,p}(t+\delta t) + c_4\Delta\vec{a}_i \\
\vec{c}_i^{\,c}(t+\delta t) &= \vec{c}_i^{\,p}(t+\delta t) + c_5\Delta\vec{a}_i.
\end{aligned} \tag{2.13}$$

In principle, this process can be iterated and converges to the exact result, but since each iteration requires the calculation of the forces acting on all particles, which is the most time-consuming part of the simulations, in MD simulations usually only one iteration is taken into account. The weights c_i are chosen to optimize the approximation; the optimal values depend on the number of derivatives taken into account and on the order of the differential equation. For forces of the form $\vec{F} = f(\vec{r}, \vec{v})$, and expansion up to fifth order [as in eqns. (2.11) and (2.13)], as used here, the optimal choice is [202]

$$(c_o, c_1, c_2, c_3, c_4) = \left(\frac{19}{90}, \frac{3}{4}, 1, \frac{1}{2}, \frac{1}{12}\right). \tag{2.14}$$

With this integration scheme, eqns. (2.1) and (2.2) can now be integrated.

2.1.2 Generic problems of TD simulations

Though very straightforward, TD simulations of inelastic bodies have some inherent problems, which were overlooked for a long time, since it was not obvious at first sight what

additional complications might arise when dissipation is introduced.[3] These complications are caused by the fact that normal collisions have a finite duration t_n that decreases with increasing stiffness. Two effects are connected with this finite duration of contacts when dissipation is present.

First consider a one-dimensional column of N grains of same size and material, all a distance s_0 apart and having a velocity v_0 along the common axis. Let this column hit a wall, wait until all grains move away from the wall and each other, and measure the restitution coefficient of the whole column,

$$e_{\text{tot}} = -\frac{\sum_{i=1}^{N} v_i^f}{\sum_{i=1}^{N} v_i^i} = \frac{-1}{Nv_0} \sum_{i=1}^{N} v_i^f . \tag{2.15}$$

As Luding *et al.* discussed [143, 211], e_{tot} depends on t_0/t_n, where $t_0 = s_0/v_0$ is the time that a grain needs to catch up with the grain in front of it when the latter is suddenly stopped (e.g. by impact on a wall). In the limiting case $t_0/t_n \gg 1$, the column's hitting the wall leads to a large number of binary collisions between the grains, namely N^2. The total restitution coefficient thus is considerably smaller than the coefficient of restitution for a binary impact, e_n. On the other hand, in the limiting case $t_0/t_n \ll 1/N$, the column's hitting the wall leads all grains into mutual contact at the same time, and the grains interact with the wall as a chain of coupled damped oscillators rather than as N distinct grains. The total restitution coefficient is close to one in this case, the column disperses. Therefore, this regime was called the *detachment regime* [211].

This example illustrates that it is very important to choose realistic collision times, i.e. realistic stiffness, especially when dense systems are considered. However, this effect is not wholly an artefact of too soft particles. To some extent, it is always present if there is a finite contact duration. But, even though collisions *do* have a finite collision time, no signs of the detachment effect have been observed in experimental systems so far. One reason might be that the way in which multiple contacts are treated in TD simulations, namely by adding up the contributions of the individual contacts to the forces on a single grain, is not appropriate. This relates directly to the fact that the mechanism of energy dissipation in collisions is unclear as mentioned in Section 1.5.

The second effect is related to contact times in oblique impact and was described by Schäfer and Wolf [212]. Consider two grains hitting each other with relative velocity $v^i = |\vec{v}_{\text{rel}}^{\,i}|$ under an impact angle ϑ as sketched in Fig. 2.1. The duration of the contact, t_{cont}, now can depend on ϑ. Of course, for normal impacts ($\sin\vartheta = 0$), $t_{\text{cont}} = t_n$, but for an oblique impact this is not necessarily so. One can distinguish two regimes: a hard-sphere regime, where the stiffness of the grains is so high that $t_{\text{cont}} = t_n$ still holds, and a soft-sphere regime, where the stiffness is so low that the grains essentially traverse each other unhinderedly. In this case, $t_{\text{cont}} = \lambda/v^i$, where $\lambda = 2R\cos\vartheta$ is the length of the chord between initial and final contact point as drawn in Fig. 2.1.

Introducing a cartesian coordinate system with the x-axis in the direction of $\vec{v}_{\text{rel}}^{\,i}$, the question is now how $\Delta v_x = v_x^f - v_x^i$ depends on the initial velocity v^i in the two limiting regimes. In the hard-sphere limit, the collision follows approximately the law of reflection,

[3] In molecular systems, for which these algorithms where initially invented, forces are conservative and usually also continuous.

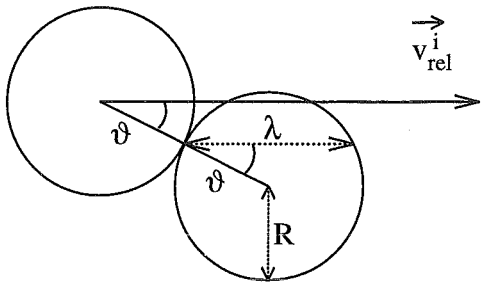

Figure 2.1: *Sketch to illustrate the brake failure effect.*

such that $\Delta v_x \propto v^i$. In the soft-sphere limit, one has

$$\Delta v_x \propto \int_{t_{\rm cont}} F_x(t)\,dt \approx \bar{F}_x\, t_{\rm cont}.$$

The mean x force during the impact, $\bar{F}_x$, is independent of v^i in this regime, while $t_{\rm cont} \propto 1/v^i$, so that $\Delta v_x \propto 1/v^i$. The braking efficiency goes *down* with increasing v^i; therefore, this regime has been termed the *brake failure regime*. It is clear that in a given impact it depends on v^i, k_n, and ϑ which of the regimes applies. An estimate for the transition between the regimes is provided by equating $t_n \approx \pi\sqrt{m_{\rm eff}/k_n} = \lambda/v^i$; solving for v^i gives the critical velocity for brake failure

$$v_{\rm bf} = \frac{2R}{\pi}\cos\vartheta\sqrt{k_n/m_{\rm eff}}. \tag{2.16}$$

This is illustrated in Fig. 2.2 for parameters of the cellulose acetate spheres whose collision properties are illustrated in Fig. 1.6 and $\vartheta = 87.4°$ ($\sin\vartheta = 0.999$). In the log-log plot of Fig. 2.2, the two regimes are clearly seen. The dotted curve corresponds to the usual $t_n = 1 \times 10^{-5}$s; here, the transition between the regimes takes place at about $v_{\rm bf} \approx 35$ m/s, in good agreement with the value predicted by Eqn. (2.16), $v_{\rm bf} \approx 27$ m/s. Increasing t_n by a factor of 10 (i.e., decreasing k_n by a factor of 100) leads to a decrease of $v_{\rm bf}$ by a factor of 10 (dashed line in Fig. 2.2). The corresponding $v_{\rm bf} \approx 3.5$ m/s is a speed typically obtained in experiments or simulations. The possible consequences of brake failure for simulated granular flow have been discussed by Schäfer and Wolf [212]. The most important consequence is the fact that the particle not only loses less normal velocity than it should, but also that it is reflected away from the wall less. As the particle accelerates and the brake failure effect increases, the particle starts to pass through a number of successive wall particles. Due to this (completely artificial) multiple collision dissipation increases again, which was termed the "emergency brake" by Schäfer and Wolf [212]. The reduction of reflection of the particle away from the wall, however, remains.

The detachment effect should exist in real systems – if it does not, this is an indication that our understanding of many-particle collisions might be wrong. By contrast, the brake failure effect is a real artefact of the constant collision time in TD simulations. It is due to the fact that the deformations of particles are modeled by overlaps of particles and not by real deformations. As the detachment effect, it can never be eliminated completely, its onset can only be shifted to higher relative velocities, at the cost of computational speed.

However, as long as these deficiencies of TD simulations are kept in mind, and parameters in the simulations are carefully chosen, TD simulations are a versatile tool for the simula-

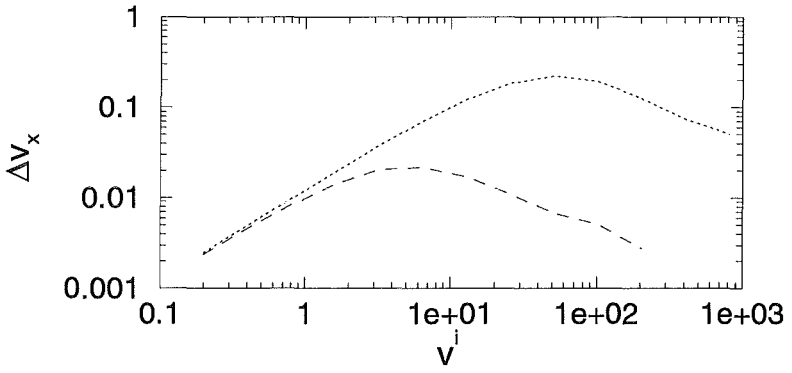

Figure 2.2: *Braking efficiency as a function of initial relative velocity for* $\vartheta = 87.4°$. *Dotted line:* $t_n = 1\times10^{-5}$ *s, dashed line:* $t_n = 1\times10^{-4}$ *s.*

tion of granular materials, especially to model flows where very dense and dilute regions coexist. Most of the results presented in this thesis were obtained with TD simulations. However, there are cases in the systems modeled, where ED simulations are more appropriate and safer than TD simulations, since brake failure cannot be ruled out. Thus, I will now discuss the concept of ED simulations.

2.1.3 Event driven MD

In event driven MD (ED), particles are treated as hard spheres, and collisions are assumed to be instantaneous, which rules out all problems of the constant time-step algorithm. Thus, instead of introducing a force acting between particles, a collision operator has to be defined which acts on the velocities of the particles in a collision. In the case of granular materials there are no long-range interactions between the particles, i.e. in the time between collisions the particles do not interact while moving under the action of gravity. This seems to make granular materials the perfect candidate for ED simulations, since this means that the determination of the next collision is very simple.

Consider two spheres with radii R_i and R_j at positions $\vec{r}_i$ and $\vec{r}_j$ with velocities $\vec{v}_i$ and $\vec{v}_j$ moving under the influence of gravity $\vec{g}$. These spheres collide at time t_{ij} if the equation

$$|\vec{r}_i(t+t_{ij}) - \vec{r}_j(t+t_{ij})| = R_i + R_j, \tag{2.17}$$

which in the case of two freely moving grains gives

$$|\vec{r}_i(t) + t_{ij}\vec{v}_i(t) - (\vec{r}_j(t) + t_{ij}\vec{v}_j(t))\,| = R_i + R_j, \tag{2.18}$$

has at least one real solution (usually there are two solutions - one for the first contact and one for the last contact if the particles would penetrate each other without interacting). The smallest positive real solution is then taken as the time of the next collision between these particles. t_{ij} is evaluated for all particle pairs, and the smallest value $t_{\min}$ obtained gives the time of the next collision in the system. The other particle positions and velocities

are simply advanced to this time by the equations

$$\vec{r}_i(t+t_{\min}) = \frac{1}{2}\vec{g}\,t_{\min}^2 + \vec{v}_i(t)\,t_{\min} + \vec{r}_i(t) \tag{2.19}$$

$$\vec{v}_i(t+t_{\min}) = \vec{g}\,t_{\min} + \vec{v}_i(t). \tag{2.20}$$

For the particles involved in the collision, a collision operator (which will be specified below) acts on the velocities. In the next evaluation of t_{ij} only the times corresponding to collisions with particles interacting with the ones involved in the previous collision have to be recalculated, for the other particle pairs the new time to the next collision is simply the one calculated previously minus $t_{\min}$. Unfortunately, for a particle i colliding with a particle j fixed at the wall, eq. (2.17) reads

$$|\vec{r}_i(t) - \vec{r}_j + t_{ij}\vec{v}_i(t) + \vec{g}\,t_{ij}^2| = R_i + R_j, \tag{2.21}$$

which yields a fourth-order polynomial for t_{ij}, the exact solution of which would be very cumbersome. Thus, numerical methods usually are employed to calculate t_{ij} in this case.

So far, nothing has been said about the treatment of the hard-sphere collision occurring at time t_{ij}. Here, I will discuss Walton's three-parameter model presented in Fig. 1.6. The three parameters included in the model are the coefficient of restitution e_n, the coefficient of friction μ for sliding collisions and the tangential coefficient of restitution $e_s = -\beta$ for sticking collisions. However, though for the normal velocity $v_n^f = -e_n\,v_n^i$, the shear velocities before and after the impact are not simply linked by $v_s^f = e_s\,v_s^i$ with a *constant* e_s. The relation for the shear velocities has to be derived from the impact geometry. In the following, I make a clear distinction between the general tangential coefficient of restitution $e_s = \psi^f/\psi^i$ which is defined for all collisions and the constant tangential coefficient of restitution β defined for sticking collisions in the Walton model.

Since in a collision momentum conservation holds, the impulse $\vec{J}$ exerted by sphere j on sphere i is related to the initial and final velocities by

$$\vec{J} = m_i(\vec{v}_i^{\,f} - \vec{v}_i^{\,i}) = -m_j(\vec{v}_j^{\,f} - \vec{v}_j^{\,i}) \tag{2.22}$$

and to the rotational velocities by

$$\frac{I_i}{R_i}(\omega_i^f - \omega_i^i) = \frac{I_j}{R_j}(\omega_j^f - \omega_j^i) = -\vec{n} \times \vec{J}. \tag{2.23}$$

Here, $I = \frac{2}{5}mR^2$ denotes the moment of inertia about the center of a homogeneous sphere. It follows from eqs. (2.22) and (2.23) that the relative velocities $\vec{v}$ defined in eq. (1.12) before and after the collision are related by

$$\vec{v}^{\,f} - \vec{v}^{\,i} = \frac{7}{2m_{\text{eff}}}\vec{J} - \frac{5}{2m_{\text{eff}}}\vec{n}(\vec{J}\cdot\vec{n}). \tag{2.24}$$

For frictionless particles, only the normal velocity changes according to $v_n^f = -e_n\,v_n^i$, i.e. there is only a normal component J_n for the impulse,

$$J_n = -m_{\text{eff}}(1+e_n)v_n^i. \tag{2.25}$$

For frictional particles, the outcome of the collision depends on whether it involved sliding or not. In a purely sliding contact, $|J_s| = \mu|J_n|$, since tangential and normal force during an impact are related by $|F_s| = \mu|F_n|$. Therefore,

$$J_s^{(sl)} = \mu(1+e_n)m_{\text{eff}}\, v_n^i \frac{v_s}{|v_s|}, \tag{2.26}$$

i.e. $J_s^{(sl)}$ depends on v_n. In terms of the dimensionless tangential velocity ψ^i defined in Section 1.6.2, this can be expressed as

$$J_s^{(sl)} = -\mu(1+e_n)m_{\text{eff}}\, v_s^i/|\psi^i|, \tag{2.27}$$

i.e. from eq. (2.24)

$$\psi^f = \psi^i - \frac{7}{2}\mu(1+e_n)\text{sgn}(v_s^i). \tag{2.28}$$

If the collision is sticking, a constant coefficient of tangential restitution is assumed, i.e. $v_s^f = -\beta\, v_s^i$. In this case, it follows from eq. (2.24) that

$$J_s^{(st)} = \frac{2}{7}m_{\text{eff}}(\beta-1)v_s^i, \tag{2.29}$$

or

$$\psi^f = -\beta\,\psi^i. \tag{2.30}$$

$J_s^{(st)}$ and $J_s^{(sl)}$ as a function of v_s^i intersect at

$$\psi_0^i = \frac{7}{2}\mu\frac{1+e_n}{1-\beta}, \tag{2.31}$$

i.e. for $\psi^i \le \psi_0^i$ eq. (2.30) has to be used and for $\psi^i > \psi_0^i$ eq. (2.28) describes the change in v_s. Note that this means that even in a collision classified as sliding, there may be a reversal of tangential velocity. As a matter of fact, the simple three parameter model thus even describes the intermediate regime of partly stick and partly slip during the collision explained in 1.6.2. The lines representing Walton's model in Fig. 1.6 correspond to Eqs. (2.28) and (2.30).

In comparison with MD simulations, ED simulations have the advantage of being much faster at low to intermediate densities, since no computing time is wasted integrating numerically the time of free flight, and also the treatment of collisions is faster. One disadvantage is that the algorithm is hard to parallelize, since in principle all particle-particle pairs have to be evaluated in each simulation step, a maybe more serious disadvantage is that extension to arbitrarily shaped particles is very problematic. Another problem of ED simulations is the fact that they cannot handle lasting contacts.

Inelastic collapse

Just as in the case of TD simulations, also in ED simulations complications can arise from the fact that collisions are dissipative; complications which are absent in simulations using elastic particles as in the simulation of liquids. The problem arises from the fact that an inelastic particle dropped on a flat plate with some initial velocity v_0 comes to

rest after an infinite number of collisions in finite time t_f. The reason is simply that the time t_k between successive collisions k and $k+1$ is given by $t_k = \sqrt{2v_k/g}$, which, since $v_k = e_n v_{k-1}$, leads to a geometric series for $t_f = \sum t_k$. For the algorithm described above, this constitutes a serious problem, since in such a case it would spend an infinite amount of time computing these collisions. Though described here in the context of a ball interacting with a plate under the action of gravity, this is also a problem in granular gases in the absence of gravity, since here particles can be pressed together in a cluster region strongly enough to encounter inelastic collapse.

Bernu and Mazighi [213] showed that a column of particles hitting a wall can collapse inelastically. The existence of inelastic collapse in granular gases, i.e. in the less directed motion of particles, was shown by McNamara and Young in 1D [214] and 2D [215]. Zhou and Kadanoff [216] showed by theoretical considerations that inelastic collapse in a granular gas is also possible in 3D, though for very low e_n, namely $0 \leq e_n < 7 - 4\sqrt{3} \approx 0.072$, i.e. only for very dissipative systems. However, it has to be kept in mind that under the influence of an external force driving the particles together, the value may be higher (as stated above, for a particle bouncing on a flat plate without energy input, collapse happens for all $e_n < 1$). If additionally the particles are frictional, collapse occurs even for higher e_n than for frictionless spheres [217].

There is, however, a way to avoid inelastic collapse in ED simulations, namely the use of a velocity dependent coefficient of restitution. Luding *et al.* use a coefficient of restitution $e_n(v_n) = 1 - e_n^0 \, (v_n/v_n^0)^\delta$ with $\delta = 1/5$ and v_n^0 a typical velocity [137,218]. This is consistent with the falling tendency of e_n with growing v_n discussed in Section 1.6.1.2 and models the velocity dependence of the viscoelastic Hertz-Kuwabara-Kono force Eq. (3.6) which will be discussed in more detail in Chapter 3. Luding also introduces a cut-off for the coefficient of restitution, i.e. if the time between two collisions falls below a specified contact time, the coefficient of restitution is set to $e_n = 1$ [218]. Therefore, the particle never comes to rest and keeps colliding, though without energy loss.

2.1.4 Hybrid methods

Besides TD and ED molecular dynamics simulations, there is also the possibility of combining features of both methods. E.g. Hopkins and Louge [62,219] use a constant time-step to integrate the equations of motion, but treat collisions instantaneously. To do so, they check in each time-step if an overlap occurred, and, in this case, they move the particles back to the point where the first contact would have been established. Then the collision is performed according to Walton's model presented above. In such an algorithm, collapse cannot occur, while the time-steps can be significantly larger than in soft-sphere simulations. Since a collision is not integrated, it suffices if the time-step is small enough to limit the overlap of the particles to a reasonable value.

2.2 Contact dynamics

As shown in the previous sections, both ED and TD simulations suffer from some drawbacks due to the introduction of dissipation to the system. While ED simulations are

not affected by the artifacts due to the constant timestep in TD simulations, they cannot handle lasting contacts, since by definition all particle contacts are instantaneous. Though long-lasting contacts are not a problem for TD simulations, even there no completely satisfactory implementation of static friction exists, as will be discussed in more detail in Chapter 3. The reason is that Coulombs law for static friction (1.1) is not a function, but a relation. Thus it cannot be directly implemented in TD simulations, since these require the forces to be a function of the displacement or velocity of the particle. Although, as we will see in Chapter 3, there exist tangential force laws which give quite a good approximation to Coulomb's law in the case $\mu_s = \mu_d$, TD simulations cannot handle different static and dynamic friction coefficients, which are one important reason for hysteresis and history dependence in granular systems.

However, there exists a simulation method that can handle Coulombs law directly, the so-called contact dynamics (CD) algorithm [25, 220]. Unlike MD simulations, CD was explicitly developed to simulate assemblies of rigid, inelastic, frictional particles. It is not a very common method, though, and literature on it is scarce. Here, I will give a brief account of the principles of this method, because this should facilitate the understanding of some of the results presented in Chapter 3.

In CD simulations, particles are considered to be undeformable, just like in ED simulations. Forces are computed from the constraints provided by the assumptions of non-interpenetration of particles and forces applied on the system from the outside. The normal forces are computed from the condition of non-interpenetrability of the particles. Coulombs law eqs. (1.1) and (1.2) is implemented in its exact form, i.e. the shear force F_s is computed as the reaction force to the other forces acting on the particle. As a matter of fact, Coulomb's law is not exact in the *kinematic* sense the way it is formulated in eqs. (1.1) and (1.2). The distinction between sticking and sliding contacts is in fact a kinematic definition of the state of a contact. If at a contact the relative tangent velocity v_s is zero but the relative tangent *acceleration* $\dot{v}_s$ is not, then the contact cannot stay sticking over whatever small time interval. The friction force at such a contact is necessarily fully mobilized, i.e. $F_s = -\mathrm{sgn}(\dot{v}_s)\mu_d F_n$. A contact is sticking in the *dynamic* sense only if both $v_s = 0$ and $\dot{v}_s = 0$. On the basis of this distinction between sticking and sliding contacts in the dynamic sense, Coulomb's law takes the following general form for a contact (ij) between two bodies i and j:

$$\begin{array}{lcl} v_s(ij) = 0 \text{ and } \left\{ \begin{array}{lcll} \dot{v}_s(ij) = 0 & \Rightarrow & F_s(ij) \in [-\mu_s F_n(ij), \mu_s F_n(ij)], \\ \dot{v}_s(ij) > 0 & \Rightarrow & F_s(ij) = -\mu_d F_n(ij), \\ \dot{v}_s(ij) < 0 & \Rightarrow & F_s(ij) = \mu_d F_n(ij), \end{array} \right. \\ v_s(ij) > 0 \Rightarrow \quad F_s(ij) = -\mu_d F_n(ij), \\ v_s(ij) < 0 \Rightarrow \quad F_s(ij) = \mu_d F_n(ij). \end{array} \tag{2.32}$$

This means that at each time step, all contacts have to be evaluated. The iteration procedure is as follows. In a given time step, all outer forces $\vec{F}_i^{\,a}$ acting on the particles and all velocitites $\vec{v}_i$ and angular velocities $\vec{\omega}_i$ (and therefore the relative shear and normal velocities $v_s(ij)$ and $v_n(ij)$) are known[4]. A preliminary choice for the application of Coulombs law (1.1) and (1.2) is made according to the relative shear velocities, i.e. for

[4]Note that non-interpenetrability of particles allows only normal velocities leading to separation of

$v_s(ij) \neq 0$ the tangential force in the contact is related to the normal force by (1.2), while in contacts with $v_s(ij) = 0$, the tangential force must be such that it balances all other force acting on the particle. These conditions give rise to the equation

$$\mathbf{M}\,\vec{x} = \vec{f}^{\,a} \tag{2.33}$$

where $\mathbf{M}$ is a matrix describing essentially the relations between the contact normals in the system, $\vec{x}$ is a $2m$-dimensional vector containing the $2m$ unknown normal and shear forces $F_n(ij)$ and $F_s(ij)$ in the m contacts in the system, and $\vec{f}^{\,a}$ is a $2m$-dimensional vector describing the outer forces acting on the contact. This equation for the shear forces is solved,[5] and from the dynamic equations relating forces and accelerations the corresponding accelerations are computed. It is then checked if the resulting forces and accelerations are in accordance with Coulombs law (2.32). For contacts where this is the case, essentially two situations forbidden by eq. (2.32) can occur, namely

$$|F_s(ij)| > \mu_s\, F_n(ij) \quad \text{while} \quad v_s(ij) = \dot{v}_s(ij) = 0 \tag{2.34}$$

$$|F_s(ij)| = \mu_d\, F_n(ij) \quad \text{while} \quad \dot{v}_s(ij) \cdot F_s(ij) > 0. \tag{2.35}$$

If such a situation occurs, the corresponding contact states have to be modified. If (2.34) is the case, $F_s(ij) = \pm\mu_s\, F_n(ij)$ is set; in the case of (2.35), $\dot{v}_s(ij) = 0$ is assumed. The matrix $\mathbf{M}$ is modified according to these changes, and the whole procedure repeated until a solution is found that is in agreement with Coulombs law. In a similar way, it is checked that the normal forces are consistent with the condition of non-interpenetrability.

This discussion gives only a brief description of the CD algorithm. In practice, it is not easy to implement, due to the number of alternatives that have to be tested. It is also not completely free from criticism, since in many cases deformation of particles can be important. Still, it is the only algorithm existing so far that can take the difference between static and dynamic friction into account. Since this difference is crucial to the very special behaviour of granular materials in many cases, CD is an important tool in helping us to understand the details of the dynamics underlying numerous phenomena.

2.3 Other methods

Aside from the *direct* methods described in this chapter so far, various approximate methods have been used to simulate granular materials. Such methods include Monte Carlo (MC) simulations, Direct Simulation Monte Carlo (DSMC), cellular automata and the Bottom-to-Top-Restructuring (BTR) model.

Monte Carlo simulations so far have only been used to simulate a nearly perfectly inelastic vibrated granular medium [156,160,222]. The influence of shaking is modeled by lifting all the material in the container and then randomly displacing the particles (with a preferential motion in the direction of gravity) allowing no overlap. Therefore, essentially sterical

particles. If nevertheless, due to the dynamics, a negative normal velocity occurs, a collision is performed according to some hard sphere collision law, like e.g. Waltons contact law discussed above.

[5] It is possible that the matrix $\mathbf{M}$ is singular, i.e. that there are a number of possible solutions. This is the case especially in very ordered system with a high degree of frustration of rotations of particles [221]. In such a case, a particular solution of eq. (2.33) has to be chosen to proceed with the iteration procedure.

constraints and the randomizing effect of collisions are taken into account. Extension of this method to other geometries and systems should not be too complicated, but has not been attempted so far.

Though DSMC might be viewed as an extension of this simple MC algorithm, it randomizes the system far more strongly. DSMC was first introduced to simulate the flow of dilute gases [223] and was extended by Müller *et al.* to include dissipation and excluded volume [112,151]. During one time step, the particles move only under the action of outer forces. Then the particles are sorted into small cells, and all particles in the same cell undergo collisions according to stochastic rules, where it is taken into account that only particles with suitable relative velocity can undergo a collision. The advantage of this model is that it can be used to simulate essentially any geometry and that it can be parallelized. However, it is not so easy to incorporate volume exclusion, so the model is most appropriate for dilute systems. Besides, correlations of particle motion due to inelastic collisions cannot occur, therefore probably none of the collective effects like convection, surface waves etc. can be modeled with this method.

Another model assuming completely inelastic particles and thus emphasizing geometrical constraints in the system is the BTR model. It has been used mainly to simulate size segregation in various geometries [42,158,224–227] like building of a sandpile [224], segregation by shaking [158,225,226] or in rotating drums [42,226,227]. In this model, particles are rearranged in each time step according to their height in the packing from bottom to top (without interacting with any particles higher in the packing than themselves). As a starting position, their lateral coordinates are retained, and each particle follows the path of steepest descent until it reaches a local minimum where its position is locally stable. Though the most intuitive interpretation of this algorithm is shaking of the particles, it can be applied to other systems as well. In a rotating drum, for example, the whole system is rotated by some angle before redeposition takes place.

Mehta and Barker [228] combine MC and BTR simulations to model shaking. In the first stage of shaking, the sytems expands uniformly, and then relaxes according to the MC procedure described above. However, when a certain packing density is reached, the final compaction is achieved by the BTR algorithm.

Aside from these methods emphasizing properties of the geometry of the packing, cellular automata were used as well especially in the simulation of granular flow [229,230]. There are also extensions to shaken granular materials or even to granular pilings, i.e. to coexistence of static and flowing material [231,232]. It was possible to reproduce the density waves observed in the discharge of a hopper [229] or of flow of granular material in a pipe [230,231]. However, in the case of flow in a pipe, an unphysical temperature profile is obtained in some cases [231] and, due to the use of integer velocities, momentum conservation can be violated [227]. Generally, the use of cellular automata in the simulation of granular materials is problematic, essentially because of the typical averaging problems in granular materials.

Chapter 3

Modeling of particle contacts

> *Es ist zum Erstaunen, wie wenig dasjenige oft, was wir für nützlich halten, und was auch leicht zu tun wäre, doch von uns getan wird. Die Begierde, geschwind viel wissen zu wollen, hindert oft an genauen Untersuchungen, allein es ist selbst dem Menschen, der dieses weiß, sehr schwer etwas genau zu prüfen, da er doch weiß, er kommt auch nicht zu seinem Endzwecke viel zu lernen, wenn er nicht prüft.*
> — G. Ch. Lichtenberg, "Sudelbücher"

As discussed in the previous chapter, the soft-particle MD method requires giving an explicit expression for the forces that act between grains. Many more or less strongly simplified force schemes have thus been suggested and employed in simulations (e.g., [49, 87,106,130,131,144,203–209]), often without a thorough discussion of their properties. In this chapter, I will discuss the most commonly used force laws and compare them, for the case of binary collisions, with experimental results for the binary impact of spheres. I will also briefly discuss the properties of some of these force laws in lasting contacts. Most of the results presented in this chapter are published in Ref. [233].

3.1 Collisions

As already mentioned in Section 1.5, very little is known about the mechanics of inelastic collisions of spheres.[1] Only recently, Foerster *et al.* performed careful measurements of the collision properties of spheres [193]. In the following, the properties of existing force schemes typically used in TD simulations will be compared critically to these experimental results and to some theoretical results on impact [185]. Example simulations are perfomed to illustrate the properties of the force laws with a constant-timestep fifth order predictor-corrector algorithm [202] as described in Section 2.1.1. Although it is in principle desirable to work with non-dimensional units, they are not always practical; for example, non-linear force laws do not define a unique timescale, as will be discussed later. Therefore, SI units

[1] Even less is known about collisions of non-spherical particles.

are used here, and all parameters tuned such as to mimick a specific granular material, namely the cellulose acetate spheres used in experiments by Drake [100, 101, 192] and Foerster *et al.* [193], of radius $R = 3$ mm and mass $m = 1.48 \times 10^{-4}$ kg. Thus, it is possible to compare the simulation results directly with experimental data.

3.1.1 Normal impacts

Modelling a force that leads to inelastic collisions requires at least two terms: repulsion and some sort of dissipation. The simplest force with the desired properties is the damped harmonic oscillator force

$$F_n = -k_n \xi - \gamma_n \dot{\xi}, \tag{3.1}$$

where γ_n is a damping constant and k_n is related to the stiffness of a spring whose elongation is ξ, the deformation of the grain. This model (also referred to as *linear spring-dashpot*) has the advantage that its analytic solution (with initial conditions $\xi(0) = 0$ and $\dot{\xi}(0) = v_n^i$) allows the calculation of important quantities. For instance, the coefficient of normal restitution is

$$e_n = \exp\left(-\frac{\gamma_n}{2m_{\text{eff}}} t_n\right), \tag{3.2}$$

where

$$t_n = \pi \left(\frac{k_n}{m_{\text{eff}}} - \left(\frac{\gamma_n}{2m_{\text{eff}}}\right)^2\right)^{-1/2} \tag{3.3}$$

denotes the duration of the collision.[2] The maximum overlap during a collision is

$$\xi_{\max} \leq v_n^i t_n / \pi, \tag{3.4}$$

where the equality holds for elastic grains ($e_n = 1$). In principle, force (3.1) has no free parameters, since k_n and γ_n can be set by adjusting e_n and t_n to the corresponding experimental values exhibited by a given material in a velocity range relevant for the simulations. Because of its advantages, it has been used in numerous works [49, 87, 131, 144, 204, 205, 212]. In Fig. 3.1, its behaviour is illustrated for $e_n = 0.87$ and $t_n = 1 \times 10^{-5}$ s ($\Leftrightarrow k_n = 7.32 \times 10^6$ N/m, $\gamma_n = 2.06$ kg/s).

In order to formulate a more refined force than (3.1), one can use the Hertz force (1.18) and add a damping term. The Hertz spring constant k_n can be computed from material properties according to Eq. (1.19) and gives for Drake's cellulose acetate spheres, $k_n = 9.0 \times 10^7$ Nm$^{-3/2}$. Since, according to Eq. (1.28), the duration of the collision depends on the impact velocity, there is no intrinsic timescale to collisions. The choice of the numerical time step Δt must depend on the maximum relative velocities expected during the simulation to ensure satisfactory numerical accuracy. In the simulations presented here, the maximum impact velocity is about 100 m/s, for which $t_n \approx 1.88 \times 10^{-5}$ s, and the time step is set to $\Delta t = t_n/100$.

In order to obtain a *dissipative* Hertz-type force, a viscous damping term was added to the Hertz force in an *ad hoc* fashion in some studies [60, 106, 206]:

$$F_n = -k_n \xi^{3/2} - \gamma_n \dot{\xi}. \tag{3.5}$$

[2] t_n is the time at which the virtual overlap ξ returns to zero. As will be shown in the following, this is not the time at which F_n returns to zero.

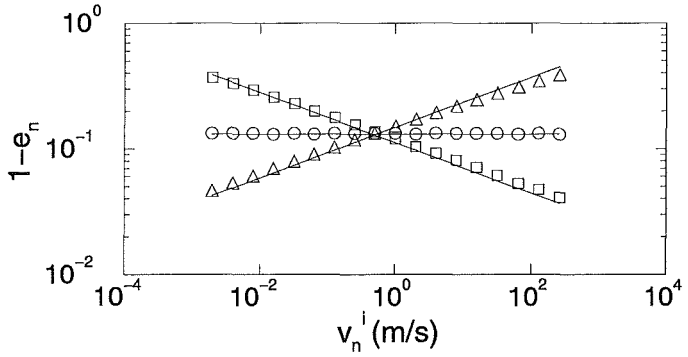

Figure 3.1: *Dependence of coefficient of normal restitution e_n on the impact velocity v_n^i for various normal forces. (○) Linear spring-dashpot (3.1), (□) Hertz law with linear damping (3.5), (◇) Hertz-Kuwabara-Kono force (3.6). The full lines correspond to a power law $(1 - e_n) \propto {v_n^i}^{\alpha}$ with $\alpha = 0$ (3.1), $\alpha = -1/5$ (3.5) and $\alpha = 1/5$ (3.6).*

However, as Taguchi [234] pointed out, this force leads to collisions that become more elastic as the impact velocity increases, contrary to the experimental evidence: $(1 - e_n) \propto {v_n^i}^{-1/5}$ [211]. For low impact velocities, where the Hertz results for elastic contacts should be regained, force (3.5) produces a coefficient of restitution that approaches zero. In Fig. 3.1, this behaviour is illustrated using $\gamma_n = 0.35$ kg/s, so that $e_n \approx 0.87$ in the velocity range covered by Foerster's measurements [193].

Besides its unrealistic dissipation properties, force (3.5) has another small disadvantage which it shares with the linear spring-dashpot force (3.1). At the beginning of the impact, the damping term is at its maximum (the velocity is at its maximum value with respect to the whole collision), while the elastic term is close to zero. Therefore, there is a discontinuity in the force which is the stronger the smaller the coefficient of restitution. Since the oscillation is damped, the points where ξ and F_n go to zero are not identical. This means that at the very end of the collision, there is even a small force pulling the particles together. Figure 3.2 shows this behaviour for both force (3.1) and (3.5). For small e_n, the jump in the force is considerable, and the maximum force can even be achieved right at the beginning of the contact.

Kuwabara and Kono [189] and Brilliantov *et al.* [235] extend the original Hertz approach assuming the material to be viscoelastic instead of elastic. They derive

$$F_n = -k_n \xi^{3/2} - \gamma_n \xi^{1/2} \dot{\xi}, \tag{3.6}$$

where k_n is identical to the k_n from Hertz theory and γ_n is connected to the radii of the spheres and the two coefficients of bulk viscosity. This force leads to a coefficient of normal restitution e_n that decreases with increasing v_n^i, in agreement with experimental results: $(1 - e_n) \propto {v_n^i}^{1/5}$ [189, 211]. In Fig. 3.1, this is illustrated using $\gamma_n = 190$ kg m$^{-1/2}$ s^{-1}. Besides giving a coefficient of restitution that slightly decreases with increasing impact velocity, force (3.6) goes smoothly to zero at the beginning and end of the contact.

An approach guided by the picture of plastic deformation was presented by Walton and Braun [83]. They assume that there are different spring constants, k_1 and k_2, for the

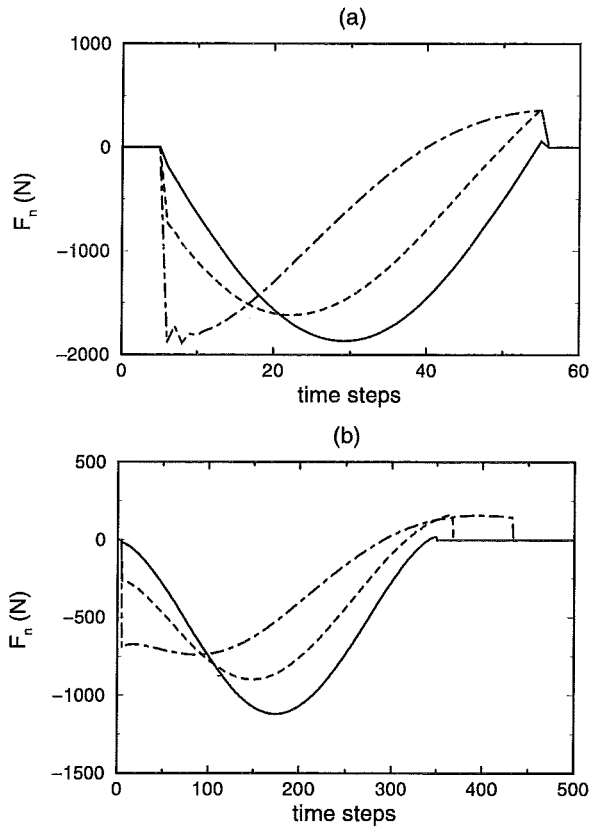

Figure 3.2: *Evolution of F_n during a normal collision for $v_n^i = 1$ m/s and (a) force (3.1) with $k_n = 7.32 \times 10^6$ N/m and $e_n = 0.95$ (full line), 0.6 (dashed line) and 0.2 (dot-dashed line); (b) force (3.5) with $k_n = 9.0 \times 10^7$ N/m and $\gamma_n = 42.8$ kg/s (full line), 528.4 kg/s (dashed line) and 1386.2 kg/s (dot-dashed line). The values for γ_n lead to the same e_n as in (a) for $v_n^i = 1$ m/s. The time step Δt has the same value as for the corresponding curve in (a).*

loading and unloading part of the contact:

$$F_n = \begin{cases} k_1 \xi & , \quad \dot{\xi} \geq 0 \quad \text{(loading)} \\ k_2(\xi - \xi_0) & , \quad \dot{\xi} < 0 \quad \text{(unloading)} \end{cases} \tag{3.7}$$

where ξ_0 is the value of ξ where the unloading curve intersects the abscissa under the given circumstances, or the permanent plastic deformation.[3] In this model, $e_n = \sqrt{k_1/k_2}$. By making k_2 a function of the maximum force $F_n^{\max}$ achieved during loading, $k_2 = k_1 + sF_n^{\max}$, e_n can be made a decreasing function of the impact velocity v_n^i,

$$e_n = (sv_n^i(m_{\text{eff}}/k_1)^{1/2} + 1)^{-1/2}. \tag{3.8}$$

In Fig. 3.3, this behaviour is illustrated with $k_1 = 7.32 \times 10^6$ N/m and $s = 2 \times 10^5$ m^{-1}.

Finally, I should comment briefly on the use of the reduced mass m_{eff} in the forces (omitted here for simplicity). In some studies, it is understood as an additional prefactor for the

[3]Note that after separation of the particles, i.e. when ξ has dropped to zero again, in the next contact this deformation has disappeared.

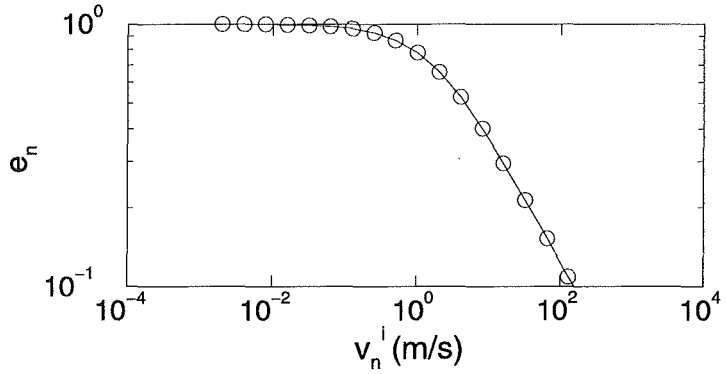

Figure 3.3: *Dependence of coefficient of normal restitution e_n on the impact velocity v_n^i for the hysteretic force (3.7) (∘). The full line is the result from Eq. (3.8).*

damping term [87, 106, 205–208, 212], leading to a coefficient of restitution that decreases with increasing m_{eff}. Other authors put it as prefactor in both the elastic and the dissipative term [49, 131, 234], such that the coefficient of restitution becomes independent of m_{eff}. If neither of the two terms is given a prefactor m_{eff} [144, 203, 204], e_n is an increasing function of m_{eff}. Unfortunately, there is no systematic experimental research on the mass dependence of e_n to my knowledge except some work dating from 1864, cited by Goldsmith [185], which indicates a slight decrease of e_n with increasing m_{eff} for spheres of equal size. This result suggests that the first of the possibilities described above might be most suited. It is definitely most desirable that more experimental work be done in order to settle this point. However, when the granular flow consists of particles without large mass differences, putting m_{eff} into the forces merely amounts to redefining the stiffness and/or damping constant.

3.1.2 Oblique impacts and frictional contacts

In oblique impacts, i.e. for $v_s^i \neq 0$, there is also a non-vanishing tangential component of the force, or shear force for short. Here, only *collisions* are discussed; the case of long-lasting contacts will be deferred to another section, since there, different aspects have to be considered.

To illustrate the properties of the shear force laws discussed in the following, they were implemented and test simulations of free binary impacts with varying obliqueness were carried out. The results are compared directly to the experimental results of [193]. The linear spring-dashpot force (3.1) was used as normal force in all cases, as it is simple and robust and, more importantly, makes the results of oblique impacts depend only on the obliqueness, not on the absolute value of the impact velocity v_n^i. Later in this section, the question of the influence of other force laws on obliqueness will be addressed. For comparison with experimental data on cellulose acetate spheres, the values $e_n = 0.87$ ($\Leftarrow k_n = 7.32 \times 10^6$ N/m, $\gamma_n = 2.06$ kg/s) and $\mu = 0.25$ were adopted for all example simulations except where explicitly stated otherwise.

In all impacts shown in the following, the initial particle spins are zero, so that $\psi^i =$

$\tan\vartheta$. Two quantities as a function of the impact obliqueness are measured, namely the dimensionless final tangential velocity ψ^f as a function of ψ^i (i.e. the MBF plot) and the coefficient of total restitution

$$e = \sqrt{\frac{E^f_{\text{kin}} + E^f_{\text{rot}}}{E^i_{\text{kin}} + E^i_{\text{rot}}}}, \tag{3.9}$$

measured in the center-of-mass system as a function of $\sin\vartheta$.

3.1.2.1 Oblique collisions with linear normal force

In Fig. 3.4, the simulation results are compared directly to the MBF plots measured by Foerster *et al.* for cellulose acetate spheres [193]. Recall that the tangential coefficient of restitution can be directly read off from these graphs as $e_s = \psi^f/\psi^i$. On the other hand, the form of e as a function of impact obliqueness plays a decisive role for the dissipation of granular temperature in the granular system and was not measured in experiments. In Fig. 3.5, $e(\sin\vartheta)$ is plotted for the force laws presented in the following.

The simplest shear force [205, 212] just applies the Coulomb law of dynamic friction, so that

$$F_s = -\mu \cdot |F_n| \cdot \text{sign}(v_s). \tag{3.10}$$

Obviously, this force cannot provide reversal of tangential velocity; it can only slow v_s down to zero. Note that (3.10) is discontinuous at $v_s = 0$. When $v_s \to 0$ (rolling regime), numerically one gets F_s jumping between positive and negative values instead of $F_s = 0$. However, this has no effect on the final velocity v_s^f, as the time average of F_s vanishes as it should, and the amplitude of the jumping goes to zero at the end of the contact if F_n goes to zero at the end of the contact (which, as said before, is not always the case). ψ^f vs. ψ^i as obtained with (3.10) is shown in Fig. 3.4a for $\mu = 0.15, 0.25, 0.35$. One distinguishes a regime of ψ^i where during the impact v_s was slowed down to zero (rolling) and a regime where v_s^i was too large, so that a finite v_s^f resulted. Both regimes are characterized by constant slope, and the transition between them is governed by the value of μ: the higher μ, the longer the rolling regime is sustained. The corresponding $e(\sin\vartheta)$ diagram is displayed in Fig. 3.5a. For normal impacts ($\sin\vartheta = 0$), $e = e_n$; for increasingly oblique impacts one sees a growing contribution of the shear force to the total dissipation, and grazing impacts approach $e = 1$, as physical intuition suggests.

Some authors [60, 130, 131, 144, 211] use a viscous friction force of the form

$$F_s = -\gamma_s v_s, \tag{3.11}$$

where γ_s is a shear damping constant without physical interpretation. Because here the deceleration is a linear function of the initial velocity, one obtains a constant $e_s > 0$ for all ψ^i (Fig. 3.4b) — the rolling case is never reached. On the other hand, the coefficient of total restitution e does not go smoothly to one for grazing impacts (Fig. 3.5b). This is due to the fact that (3.11) is not governed by the normal force F_n and hence does not vanish for grazing impacts. Thus, in the limits of nearly normal and nearly grazing impacts force (3.11) yields unphysical results.

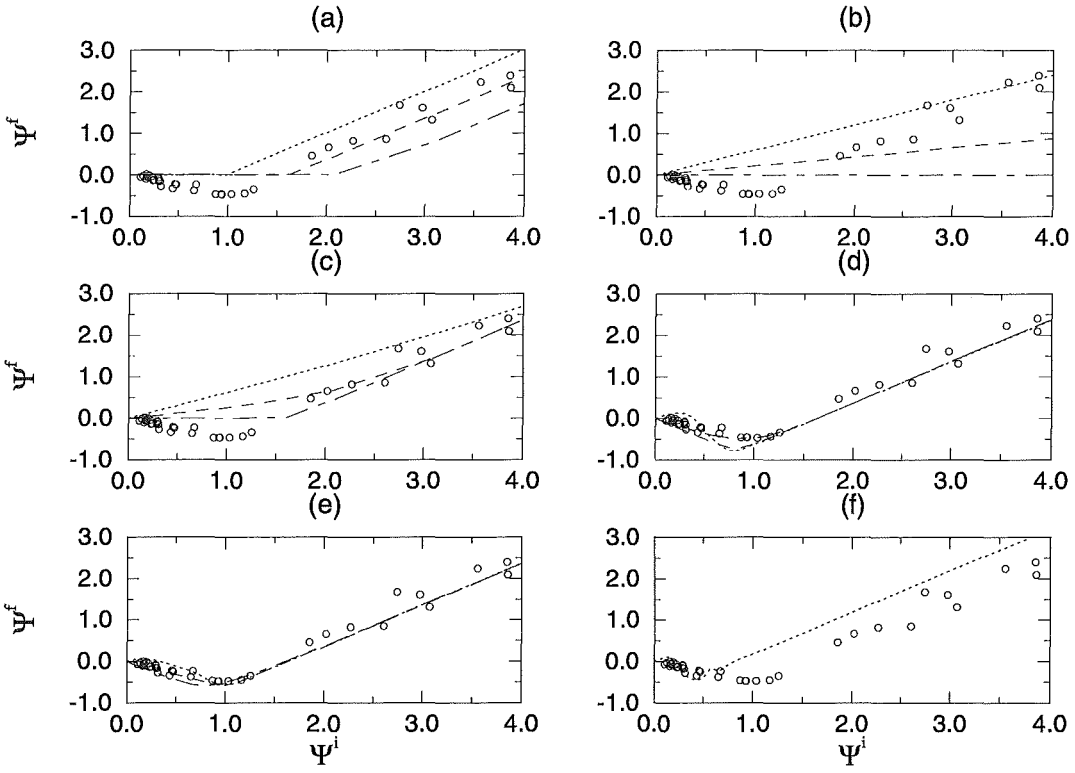

Figure 3.4: *ψ^f-ψ^i plots for various tangential forces combined with normal force (3.1). The circles denote the experimental data for the impact of acetate speres [193]. The dotted, dashed and dot-dashed lines denote respectively (a) Coulomb friction law (3.10) with $\mu = 0.15$, 0.25, 0.35 (b) viscous friction law (3.11) with $\gamma_s = 1$, 3, 20 kg/s (c) combination of (a) and (b) according to (3.12) with $\gamma_s = 1$, 3, 20 kg/s (d) linear tangential spring (3.13) with $k_s/k_n = 1$, 2/7, 1/5 (e) variable tangential spring (3.17) with $k_s^0/k_n = 1$, 2/3, 1/3 (f) stick-slip model (3.19) with $\zeta_0 = 10^{-8}$ (only dotted line).*

The discontinuity in (3.10) can be avoided by combining (3.10) with (3.11) [59, 87, 106, 162, 206, 209, 236],

$$F_s = -\min(|\gamma_s v_s|, |\mu F_n|) \cdot \mathrm{sign}(v_s). \tag{3.12}$$

Here, γ_s may be considered to be a technical parameter which should have a value high enough for collisional properties not to differ substantially from those of force (3.10). ψ^f vs. ψ^i for this force is shown in Fig. 3.4c. With increasing γ_s, force (3.12) approaches the behaviour of force (3.10).[4] The same trend is observed for $e(\sin\vartheta)$ (Fig. 3.5c). Apparently, a small γ_s changes mainly the properties of "moderately oblique" impacts, making them more elastic. Considering that the form of $e(\sin\vartheta)$ is decisive for the dissipation of granular

[4]This holds also for the details – if the sliding friction limit is reached for very samll v_s, the same jumping between the positive and negative branch of F_s can be observed, since it is possible that the numerical integration works in too large steps to find the correct point on the "static friction" part of eq. (3.12).

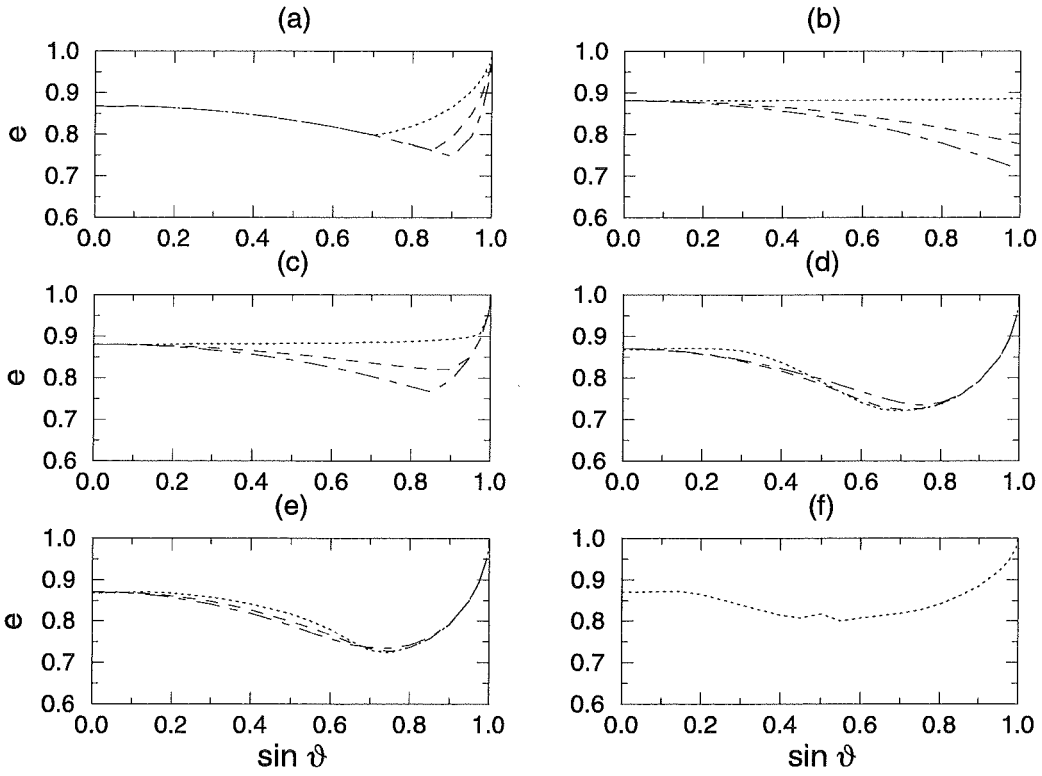

Figure 3.5: *Dependence of the coefficient of total restitution e on the impact offset* $\sin\vartheta$. *Forces, corresponding parameters and linestyles as in Fig. 3.4.*

temperature in an extended granular system, it seems very important that γ_s is given a high enough value.

All the force schemes presented so far do not account for tangential elasticity. Therefore, none of them shows a negative e_s in any part of the ψ^f vs. ψ^i diagram, contrary to the experimental data. There is a further disadvantage to them which is important in static or quasi-static systems: a pile made up of particles which interact through the force laws (3.10)–(3.12) is not stable. Stability would require that finite shear forces act between particles also at $v_s = 0$ in order to withstand gravitational force components in shear direction of the contacts.

Tangential elasticity was first introduced by Cundall and Strack [203] and used by many others [49, 60, 204, 207, 237] writing

$$F_s = -\min(|k_s\zeta|, |\mu F_n|) \cdot \mathrm{sign}(\zeta), \tag{3.13}$$

where k_s is some tangential stiffness and ζ denotes the displacement in the tangential direction that took place since the time t_0 when the contact was first established, i. e.

$$\zeta(t) = \int_{t_0}^{t} v_s(t')dt'. \tag{3.14}$$

It is essentially the ratio k_s/k_n that determines the results of an oblique impact, not the individual values of the stiffnesses. This can be understood considering that k_s determines a half period of tangential oscillation [238],

$$t_s = \pi \left(\frac{k_s}{m}(1 + mR^2/I) \right)^{-1/2} \tag{3.15}$$

just like k_n determines a half period of normal oscillation t_n (I is the moment of inertia). Thus the phase of the tangential oscillation at the moment when the contact ceases is determined by the ratio $t_s/t_n \propto \sqrt{k_s/k_n}$ (this proportionality is valid strictly only for $e_n = 1$). For uniform spheres,

$$I = \frac{2}{5} mR^2, \tag{3.16}$$

and the periods of tangential and normal oscillation are equal when $k_s/k_n = 2/7$. The actual value of v_s^f additionally depends on v_s^i. In Fig. 3.4d, ψ^f vs. ψ^i is presented as obtained using force (3.13) for $k_s/k_n = 1,\ 2/7,\ 1/5$. With $k_s/k_n = 2/7$, one obtains a regime of constant negative e_s for small to intermediate ψ^i, caused by the restoring of tangential kinetic energy by the tangential spring. For higher ψ^i, the Coulomb condition governs (3.13), and one enters a regime of sliding friction. The region where reversal of initial tangential velocity is observed extends from normal impacts to $\psi^i \approx 1.6$ ($\vartheta \approx 58°$), in good agreement with the experimental results by Foerster *et al.* [193]. For k_s/k_n smaller or higher than 2/7, the extension of the ($e_s < 0$) region is unchanged, but new subtleties arise. For $k_s/k_n = 1$, there is a slight rise in ψ^f before it falls below the abscissa, just as predicted theoretically by Maw *et al.* [196] for perfectly elastic spheres and $k_s/k_n = 1$, but is not observed in Foerster's data. For $k_s/k_n = 1/5$, the simulation results match the experimental values quite well. The corresponding behaviour of $e(\sin\vartheta)$ is shown in Fig. 3.5d. Here, it does not seem to make much of a difference which value of k_s/k_n is chosen.

Another model that leads to very realistic impact behaviour was used by Walton and Braun [83]. Their scheme is patterned after Mindlin's results for constant normal force and varying tangential force [195], assuming that in each time step, the normal force changes only by a small amount that will not influence the tangential force significantly. It introduces a force dependent k_s, such that for each time step

$$F_s = F_s' + k_s \cdot |\zeta - \zeta'|, \tag{3.17}$$

where a prime refers to the respective values in the previous time step and

$$k_s = \begin{cases} k_s^0 \left(1 - \dfrac{F_s - F_s^*}{\mu F_n - F_s^*}\right)^{1/3} & \text{if } v_s \text{ in initial direction} \\ \\ -\ k_s^0 \left(1 - \dfrac{F_s^* - F_s}{\mu F_n + F_s^*}\right)^{1/3} & \text{if } v_s \text{ in opposite direction.} \end{cases} \tag{3.18}$$

Here, k_s^0 denotes the *initial* tangential stiffness. F_s^* is initially equal to 0 and set to the value of F_s whenever v_s reverses its direction. The change in the normal force that inevitably occurs during impact is accounted for by using the instantaneous value of F_n in the evaluation of k_s. In Mindlin's elastic theory [195], the initial tangential stiffness k_s^0 is related to the normal stiffness by $k_s^0 = k_n(1-\nu)/(1-\nu/2)$. The Poisson ratio ν is

of order 1/3 for most materials, such that $k_s^0/k_n \approx 2/3$. Fig. 3.4e and Fig. 3.5e show ψ^f vs. ψ^i and $e(\sin\vartheta)$ obtained for (3.17) with k_s^0/k_n =1, 2/3, 1/3. The results look quite similar to those of force (3.13), though they seem to match the experimental values a bit better for $k_s^0/k_n = 2/3$.

Brilliantov *et al.* [235] formulated a force assuming that the tangential moment transmission (thus, the apparent tangential force) is mediated by microscopic asperities on the contacting surfaces which yield if the local stress exceeds a certain threshold. With their model, they derive

$$F_s = -\mu F_n \left(\frac{\zeta}{\zeta_0} - \left\lfloor \frac{\zeta}{\zeta_0} \right\rfloor \right) \tag{3.19}$$

where $\lfloor x \rfloor$ means the integer truncation of x, ζ_0 is a length connected to material constants and surface roughness, and μ is expressed in terms of microscopic parameters. Force (3.19) is a saw-tooth function in ζ with period ζ_0. Clearly, ζ_0 should be much smaller than ζ^f, the final tangential displacement immediately before the contact ends. ζ^f lies in a range from about 10^{-7} to 10^{-5} m (from nearly normal to nearly grazing) for the impact angles and normal stiffness used in our simulations. The properties of force (3.19) are shown in Fig. 3.4f and Fig. 3.5f for $\zeta_0 = 10^{-8}$ m and $\mu = 0.25$. Changing ζ_0 to 10^{-7} m or 10^{-9} m does not alter the curve visibly. One obtains reversion of initial tangential velocity for small impact angles, but the extension of this region is smaller than with forces (3.13) and (3.17). On the other hand, the coefficient of total restitution e seems to be overestimated with regard to the forces (3.13) and (3.17) especially in the region $\sin\vartheta \approx 0.7$.

3.1.2.2 Influence of the normal force on oblique impacts

Finally, I want to discuss the changes in collisional behaviour when normal force laws different from (3.1) are applied. The coefficient of tangential restitution e_s and ψ^f vs. ψ^i depend on the normal force indirectly through $F_s = f(F_n)$ and through t_n, the normal oscillation half period:

$$v_s^f - v_s^i = \Delta v \propto \int_0^{t_n} F_s \, dt. \tag{3.20}$$

Therefore, if one replaces force (3.1) by other normal forces, some changes in the behaviour of oblique impacts must be expected. Those changes are discussed here for the dynamic friction force (3.10) and the elastic tangential force (3.13).

The non-elastic force (3.10) is not likely to be very sensitive to the normal force chosen, because it essentially leads either to rolling or slipping. Of course, by choosing a non-linear normal force, t_n becomes velocity-dependent, and the same must be true for Δv. In practice, however, the velocity dependence in (1.28) is so weak that for a large range of v_n^i, the changes in ψ^f vs. ψ^i are too small to be represented here.

For the elastic tangential force (3.13), the situation is different. Here, as pointed out before, the impact results depend on the ratio of the half period of tangential oscillation t_s and the normal collision time t_n. In order to get meaningful results, k_s must be set such that for one particular impact velocity, $t_s/t_n = c \approx 1$. According to (3.15) and (3.16), this leads to the condition

$$k_s = \frac{2}{7} m_{\text{eff}} \left(\frac{\pi}{t_n c} \right)^2 \tag{3.21}$$

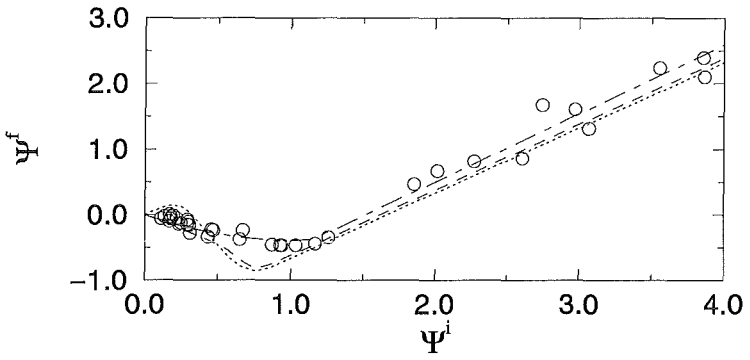

Figure 3.6: ψ^f *vs.* ψ^i *for combination of Hertz-Kuwabara-Kono normal force (3.6) with linear tangential elasticity (3.13) for* $v^i_{\text{rel}} = 0.1$ *m/s (dotted line), 1.0 m/s (dashed line), 15.0 m/s (dot-dashed line). The circles denote the experimental values for the impact of acetate spheres [193].*

In Fig. 3.6, ψ^f vs. ψ^i is shown for impacts obeying the Hertz-Kuwabara-Kono force (3.6) in combination with the tangential force (3.13) with varying impact velocities $v^i_{\text{rel}} = |\vec{v}^i_2 - \vec{v}^i_1|$. Here $k_s = 9.43 \times 10^4$ N/m in order to achieve $t_s/t_n = 1$ for $v^i_{\text{rel}} = 1$ m/s. It is clearly seen how the different impact velocities affect t_n and therefore the collision behaviour. On the other hand, the results of Fig. 3.6 look very similar to those of Fig. 3.4d (obtained with force (3.1) and varying k_s/k_n) and also fit the experimental results – as long as the tangential spring constant k_s is selected with care and as long as the range of v^i_n occurring in the simulations is not too broad. Note that with force (3.6), the numerical value of k_s is nearly 1000 times smaller than that of k_n, whereas with the linear normal force (3.1), both spring constants have to be of the same order of magnitude to achieve $c \approx 1$.

There is, however, a way to circumvent this problem. The relation $k_s = k_n(1-\nu)/(1-\nu/2)$ given by Mindlin in fact holds for elastic Hertz theory and for a given contact radius [239], i.e. according to Mindlin, $k_n \propto a$, where a is the contact radius. Therefore, also k_s has to be proportional to the contact radius, or, according to eq. (1.21), $k_s \propto \xi^{1/2}$. Thus, it is to be expected that the use of the shear force

$$F_s = -\min(|k_s \xi^{1/2} \zeta|, |\mu F_n|) \cdot \text{sign}(\zeta) \tag{3.22}$$

in combination with a Hertz law for the normal force would solve the problem of different time scales in the normal and tangential period of oscillation. Figure 3.7 shows the results obtained with the tangential force law (3.22) for the same cases and parameters as in Fig. 3.6, but $k_s/k_n = 2/3$ as expected from the Mindlin relation. Note that now k_s is of the *same* order of magnitude as k_n. In addition, for $v^i_n = 1$m/s the case $k_s/k_n = 1/5$ is shown. It is obvious from Fig. 3.7 that the dependence of the tangential coefficient of restitution on v^i_n has disappeared nearly completely. The little variation with v^i_n is probably due to the dependence of t_n on v_n in inelastic collisions, which deviates from eq. (1.28). As in the case of the linear tangential spring (3.13), good agreement with the experimental data is found for $k_s/k_n = 1/5$. Surprisingly, the tangential force (3.22) has never been used in TD simulations so far.

Since the coefficient of *total* restitution is a direct function of both the normal and the

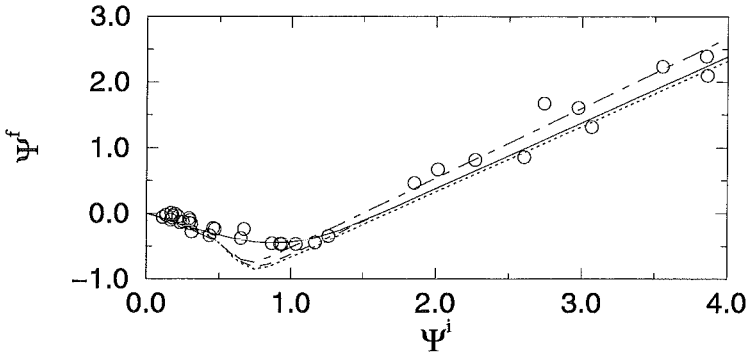

Figure 3.7: ψ^f *vs.* ψ^i *for the combination of Hertz-Kuwabara-Kono normal force (3.6) with force (3.22) for the same initial velocities as in Fig. 3.6. Besides, the curve for* $v_n^i = 1m/s$ *and* $k_s = k_n/5$ *is shown (full line). The circles denote the experimental values for the impact of acetate spheres [193].*

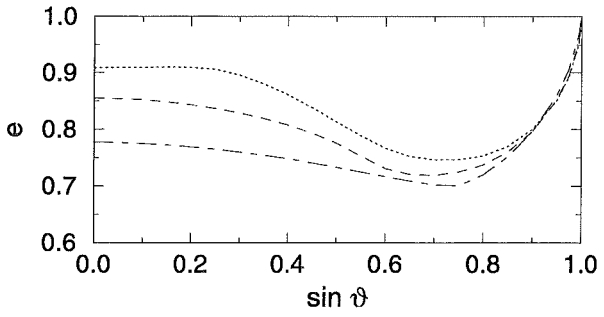

Figure 3.8: *Dependence of the coefficient of total restitution e on the impact offset* $\sin\vartheta$ *for the same forces and parameters as Fig. 3.6.*

tangential dissipation, the normal force has a strong influence on the behaviour of the $e(\sin\vartheta)$ curve, especially for small impact angles. With non-linear normal forces that lead to a velocity-dependent coefficient of normal restitution, $e(\sin\vartheta)$ becomes also velocity-dependent. This is true for non-elastic and elastic tangential forces alike. Figure 3.8 shows how $e(\sin\vartheta)$ is influenced by the velocity dependence of e_n using the same forces and parameters as in Fig. 3.6. This problem does not disappear when the tangential force (3.22) is used, since it is entirely due to the normal force.

3.2 Lasting contacts

The previous discussion of force laws pertained only to collisions, i.e. to contacts obeying a very well-defined evolution of forces and velocities. Besides, the duration of a collision is restricted to a relatively short time, usually shorter than the times between collisions in granular flows. For the case of long-lasting contacts, the evolution of contact forces

can be arbitrary, because it is essentially due to outer forces acting on the system. For comparison with experiments, contact forces and dissipation in the contact would have to be measured – a difficult task in experiments.

If the contacts in the system remain closed, one may dispense with dissipation, and the Hertz law (1.18) and appropriate tangential forces (like the approximation to Mindlin's theory used by Thornton and Randall [240]) can be used. In a system where all contacts remain closed, the property of interest is the dispersion of waves propagating through the medium. As Falcon [241] showed, the nonlinearity of the contact law is important to model the dispersion in sound propagation in a granular medium realistically.

Sadd *et al.* [242] conducted an investigation on the properties of several contact laws for the case of dense systems with long-lasting contacts. They studied the influence of the force law on wave propagation in the system. They partly used quite unusual contact laws not presented here so far, e.g. a normal force $F_n = -k_n \xi^\alpha$ with an arbitrary exponent α that was fitted so that the right value for the speed of sound as measured in experiments could be found (in their case this was fulfilled for $\alpha = 1.4$, i.e. close the the Hertz contact law). They then added a linear velocity dependent damping to this law, however, found that this led to too strong dissipation. This comes as no surprise, as for this law e_n decreases with v_n^i. Sadd *et al.* also tested a non-linear version of the hysteretic normal force (3.7), which gave the best comparison with experimental data. For the tangential force laws tested, no experimental data were available, and Sadd *et al.* obtained no conclusive results.

In a lasting contact, besides the influence of the normal force law on properties like wave propagation, the quantity of major interest is the tangential force. Probably the best (because most robust) choice for a combination of normal and tangential force is the linear spring-dashpot force (3.1) with either of the regularized Coulomb laws (3.12) or (3.13) in the tangential direction, as shown in the previous section. These forces are simple and give good agreement with experimental data. As pointed out in Section 2.2 in the discussion of the CD simulation method, Coulomb's friction law is a relation, but not a function of the shear velocity v_s. Both forces (3.12) and (3.13) are regularizations of Coulomb's law around $v_s = 0$. Therefore, they should find the right reaction force F_s as a function of some auxiliary variable. In the case of the viscous force (3.12) this is a small shear velocity v_s in "sticking" contacts, in the case of the elastic force (3.13), this is a small shear displacement with respect to the relative positions of the particles at the onset of the contact.

A suitable system for comparison of tangential force laws in lasting contacts is a single cylinder that is pushed along a flat frictional plane by a block, which may be frictional as well (see Fig. 3.9). It has the advantage of being analytically solvable, i.e. for a given weight of the particle, given pushing force F_p and given friction coefficients μ_b and μ_p all forces in the system can be calculated [243]. Besides, both contacts cannot be sticking (although that would be favourable energetically), so in the system usually a sticking and a sliding contact coexist. In this situation it is checked whether the different tangential force laws find the right forces in the two contacts and the right translational and rotational accelerations for the particle in the steady state. A similar test was already performed for the tangential force (3.12) for a whole array of particles [244]. Though there, no analytical solution exists, a comparison can be effected between TD and CD simulations. For force (3.12) the agreement with CD simulations was found to be remarkably good. The only

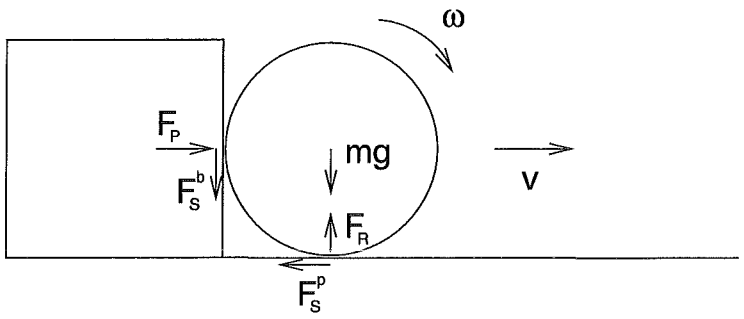

Figure 3.9: *Definition sketch for the parameters in the problem of a cylinder pushed along a flat plane. The friction coefficients block-cylinder and cylinder-plane are denoted by μ_b and μ_p respectively.*

situations in which TD simulations did not find exactly the right behaviour was in cases where there was indeterminacy also in the CD simulation, i.e. in situations where it is not clear if there is a unique solution.

The analytical treatment of the system depicted in Fig. 3.9 [243] shows that there exist two critical pushing forces

$$F_p^1 = \frac{\mu_p(1+I)}{\mu_b(1-\mu_p)+I(1-\mu_b\mu_p)} \tag{3.23}$$

and

$$F_p^2 = \frac{\mu_p}{\mu_b(1-\mu_p)}, \tag{3.24}$$

such that for $F_p < F_p^1$ the cylinder-plane contact is sticking and the cylinder-block contact is sliding (the cylinder rolls on the plane), while for $F_p > F_p^2$ the cylinder-plane contact is sliding and the cylinder-block contact is sticking (the cylinder slides on the plane). In the intermediate region $F_p^1 < F_p < F_p^2$, both contacts are sliding.

The test that will be performed on the force laws (3.12) and (3.13) is the following. The block pushes the cylinder with a force $F_p > F_p^2$. As soon as the steady state is reached (in the kinematic sense, i.e. the accelerations $\dot{v}$ and $\dot{\omega}$ are constant and $\dot{v} \cdot v > 0$), the force is reduced to a value $F_p < F_p^1$ and again the system is allowed to evolve towards the steady state. The values for the shear forces F_s^p and F_s^b and the accelerations $\dot{v}$ and $\dot{\omega}$ in the steady state can then be compared to the analytical results. In such a test situation, i.e. a situation where a previously sliding contact changes back into a sticking contact, force (3.13) is expected to exhibit problems. Since in a sliding contact $v_s \neq 0$, the shear displacement $\zeta = \int_{t_0}^{t} v_s(t')dt'$ keeps growing during the contact as long as v_s does not change its sign. Therefore, the tangential spring is stretched far beyond the elongation corresponding to the Coulomb friction limit μF_n, so that even if the outer force applied to the system changes, the friction force may remain at $F_s = \mu F_n$.

There is, however, a way to circumvent this problem. If in each time step, ζ is adjusted according to

$$\zeta = \min\left(|\zeta|, \mu|F_n|/k_s\right) \cdot \mathrm{sign}(\zeta), \tag{3.25}$$

the elongation of the tangential spring is kept at the value corresponding to μF_n, which seems realistic. It is not clear from the literature if this procedure was used in the works

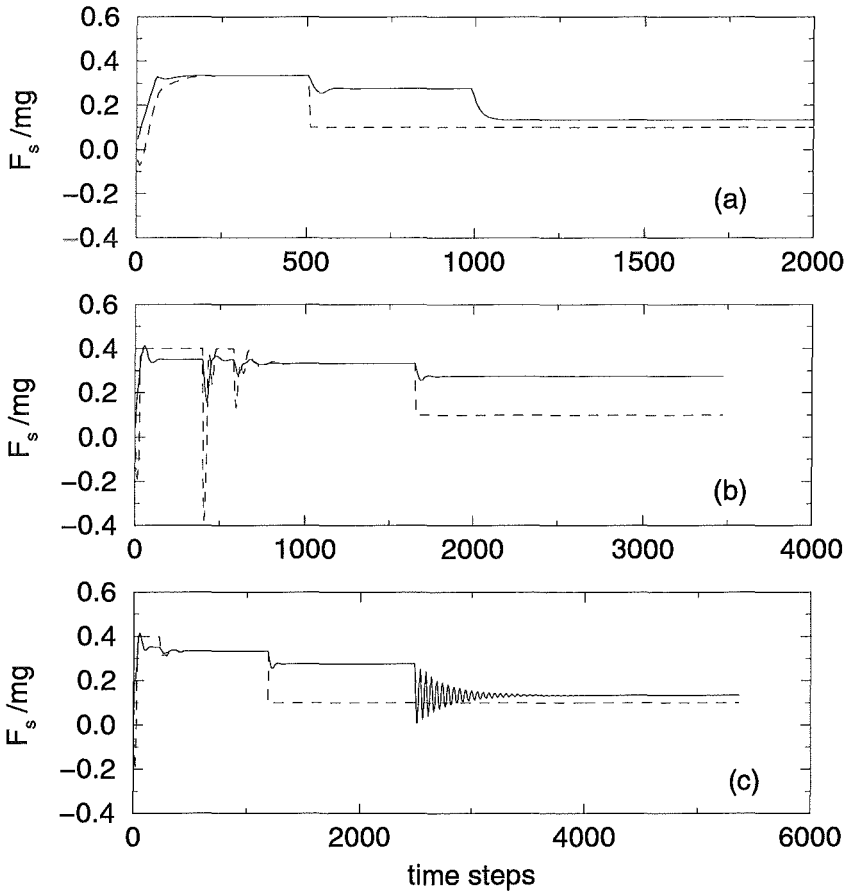

Figure 3.10: *Comparison of the approach of the steady state for different force laws. The dashed line denotes F_s^b, the solid line F_s^p. (a) Tangential force (3.12) with $\gamma_s = 1000$. (b) Tangential force (3.13) with $k_s = k_n$. (c) Same as (b), but with the additional condition (3.25).*

using the tangential force law (3.13) or not. Therefore, here the results of both (3.13) and (3.13) with the additional condition (3.25) will be discussed.

Figure 3.10 shows the evolution of the tangential forces in the two contacts for three different tangential force laws. In the corresponding simulation, $\mu_b = 0.5$ and $\mu_p = 0.25$ were chosen. With mass m, gravitational acceleration g and radius r set to 1, the moment of inertia is $I = 1/2$ and thus $F_p^1 = 6/13$ and $F_p^2 = 2/3$. Therefore, $F_p = 0.8$ was chosen as the starting value, and after the system reached a steady state, it was reduced to $F_p = 0.2$. In the simulation, the linear force (3.1) was used as a normal force with $e_n = 0.2$ and $k_n = 2 \cdot 10^7$. The details of the normal force are not so important in this situation. However, strong damping ensures faster approach to equlibrium, which motivates the choice of a small coefficient of restitution.

The values calculated analytically for the quantitites in question are for $F_p < F_p^1$

$$F_s^p = \frac{I + \mu^b}{1 + I} \cdot F_p \tag{3.26}$$

$F_p = 0.8$	Theory	Force (a)	Force (b)	Force (c)
F_s^p	1/3	0.333333	0.333334	0.333333
F_s^b	1/3	0.333333	0.333333	0.333332
$\dot{v}$	0.466667	0.466667	0.466667	0.466667
$\dot{\omega}$	0	$6.15 \cdot 10^{-6}$	$-4.22 \cdot 10^{-7}$	$1.47 \cdot 10^{-6}$
$F_p = 0.2$	Theory	Force (a)	Force (b)	Force (c)
F_s^p	0.133333	0.133333	0.275000	0.133333
F_s^b	0.1	0.100000	0.100000	0.100000
$\dot{v}$	0.066667	0.066667	-0.075000	0.066667
$\dot{\omega}$	0.066667	0.066667	0.350000	0.066667

Table 3.1: *Values of the forces and accelerations in the steady state for the simulation runs shown in 3.10.*

$$F_s^b = \mu_b F_p \tag{3.27}$$

and

$$\dot{\omega} = \dot{v} = \frac{1-\mu^b}{1+I} \cdot F_p. \tag{3.28}$$

In the case $F_p^2 < F_p$, we have

$$F_s^p = F_s^b = \frac{\mu^p}{1-\mu_p} \tag{3.29}$$

and

$$\dot{\omega} = 0 \tag{3.30}$$

$$\dot{v} = F_p - \frac{\mu^p}{1-\mu_p}. \tag{3.31}$$

In Table 3.1 these theoretical values are compared to the results obtained in the simulation.

From Table 3.1 it is obvious that for the first driving force, all tangential forces seem to find the right friction forces and corresponding accelerations equally well. However, when the force is changed to a different value to change the states of the contacts, only force (a) and (c) find the right corresponding new values. For the simple tangential spring (b), instead, the particle-plane contact exhibits a sliding friction force, which gives rise to a $\dot{v} < 0$, i.e. a braking instead of an accelerating force. Besides, already in the first contact relatively strong oscillations appear in the tangential force (b). The reason for these oscillations is the fact that in the beginning of the simulation, both contacts are sliding, so that by the time the tangential velocity in the contact that is to become sticking changes direction, the tangential spring is elongated very strongly, and therefore oscillates quite violently before finding its equilibrium state when $v_s \to 0$.

Comparing the evolution towards equilibrium for the only forces that give the right steady state, i.e. for force (a) and (c), it is obvious that the viscous force (3.12) goes towards the steady state most smoothly, while for force (3.13) with condition (3.25) oscillations occur for the transition from a sticking to a sliding contact. There is essentially only one disadvantage to force (3.12). In the case of a small shear velocity, there is dissipation in the

"sticking contact." This deviation from a true sticking contact increases with the normal force and the coefficient of friction, since the Coulomb range $[-\mu F_n, \mu F_n]$ increases then. The maximum possible deviation from $v_s = 0$ in a contact therefore is $|v_s| \leq \mu F_n/\gamma_s$. This error also gives rise to an error in dissipation. Whereas a true sticking contact is non-dissipative, the tangential force (3.12) gives a dissipation rate equal to $\gamma_s v_s^2$ at a sticking contact.

3.3 Concluding remarks

From this discussion of specific and generic properties of force schemes used in TD simulations of granular materials it should have become clear that great care has to be taken in the choice of a particular force scheme. Some of the forces exhibit a quite realistic behaviour in normal and oblique impacts, others less so. Which of the force schemes is the most appropriate for simulations cannot be answered in general; this depends very much on the specific geometry, particle density, mean flow velocity, etc. A good example for this dependence was shown in the previous section. The force law that seems to model experimental results best in binary collisions of spheres may not be the best in the simulation of a dense packing of spheres with a number of lasting contacts. Therefore, in any simulation various force schemes should be tested out, and special attention paid to the influence of the corresponding free parameters on the flow properties to find the force that is right for the specific situation.

Chapter 4

Dynamics of a single particle on a rough incline

> *All difficult things in the world are sure to arise from a previous state in which they were easy, and all great things from one in which they were small. Therefore the sage, while he never does what is great, is able on that account to accomplish the greatest things.*
> — Lao Tze, "Tao Teh King"

As mentioned briefly in Section 1.3.3, free surface flow is one of the more complicated forms of flow of granular matter, even if it takes place in a simple geometry. Because this geometry is so simple, it is a very common one, and occurs in inclined chutes [100] and all kinds of avalanche processes, such as rockslides [245], rotating drums [172–176, 178–181] or avalanches on a sandpile. The reason surface flows of granular materials are so hard to handle is that they can get unstable. By this I do not mean the development of instabilities like density waves etc. as described in Section 1.3.1, but the question of whether a steady state can exist at all, where the flow is neither stopped nor accelerated on average.

Whether or not a flow can be stable does not only depend on particle properties like shape, coefficient of restitution, coefficient of friction, but it also depends strongly on the roughness of the plane (and, clearly, on its slope). Contrary to intuition, macroscopic roughness of a plane can even help to sustain flow at angles of inclination where material on a macroscopically smooth plane comes to rest [74]. Segregation in surface flows is also related to the problem of stability of the flow on a rough surface, as discussed in Section 1.5. Besides, the question of appropriate boundary conditions for the interaction between the flowing grains and a rough boundary is not solved completely.

To gain a better understanding of such surface flows, in this chapter the simplest of such flows will be examined, namely the motion of a single ball of radius R moving down an inclined plane onto which other balls of radius r are glued. Figure 4.1 shows a schematic drawing of the set-up. The two dimensional case of a sphere moving down a line of spheres and the three dimensional case of a sphere moving on an inclined plane are discussed separately, to clarify similarities and differences in the bahaviour due to the presence or

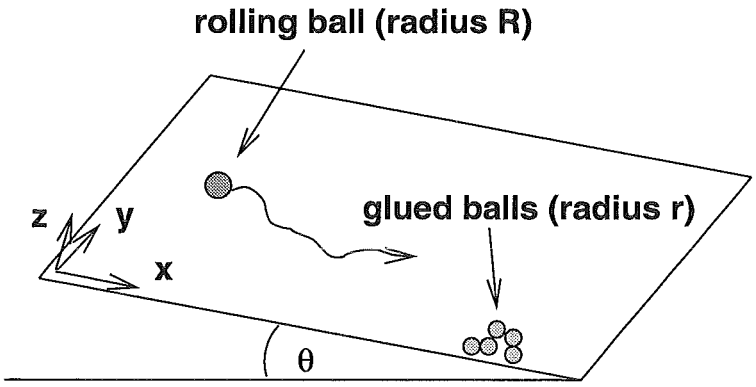

Figure 4.1: *Sketch of the set-up discussed in this chapter.*

absence of transverse motion. Most results presented in this chapter are published in a series of original papers [246–248] and conference proceedings [249–254].

The advantage of having only a single particle move in an otherwise fixed environment is the nearly perfect control of all important parameters - the slope of the plane can be fixed (and does not vary in time as in an avalanching sand heap or a rotating drum), as well as the roughness of the plane by choosing the radius R of the moving particle and the radius r of the particles on the plane. The particle can be introduced on the plane with a well-defined starting velocity, which is important since this may affect its motion. For many-particle flow in inclined chutes it is still unclear, how the flow is affected by the way particles are introduced into the system [99]. The main questions this system poses are the following: Given a size ratio $\Phi = R/r$ of the particles, i.e. the roughness of the plane, and an inclination angle θ, will the particle reach a steady state, and if so, is it independent of the initial conditions? How does the friction force exerted on the particle by the bumps on the plane scale with these parameters, and how does it depend on material properties like the coefficient of restitution and the friction coefficient of the particles?

4.1 Previous results

The motion of a single particle on a rough inclined plane has already been investigated in a number of studies, but still, many open questions remain. Before describing these previous works in more detail, I will first sum up the results common to all of them. In all studies dealing with the motion of a single particle on a rough incline, three different types of motion could be observed, depending on the angle of inclination θ of the plane and on the roughness seen by the moving particle. Characterizing the roughness of a particular plane by the size ratio $\Phi = R/r$, one can illustrate these different types of motion by a "phase diagram" as shown in Fig. 4.2.

The three different "phases" of the motion, denoted by A, B and C, have the following characteristics:

- Phase A: When the ball is launched onto the plane with some initial velocity, its velocity decreases continuously, and the ball stops on the plane. This stopping takes

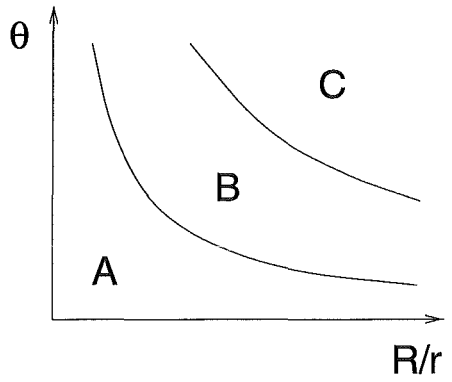

Figure 4.2: *Schematic drawing of the phase diagram.*

place independently of the initial velocity, which only influences the distance covered before stopping takes place.

- Phase B: The ball reaches a mean velocity which is independent of the initial velocity. This mean velocity increases with increasing inclination angle, i.e. the particle experiences a velocity dependent friction force. Here, the ball may sometimes be stopped, but this stopping is very different from that in phase A – it is very abrupt, and seems to happen when the ball encounters an unusually large hole on the surface. Otherwise, the ball moves with a constant average velocity, and is not decelerated continuously as in region A.

- Phase C: This phase is the one least investigated. The reason for this lack of information is that here the ball starts to move in larger jumps and accelerates throughout the whole length of the plane. This makes measurements in this region difficult. The question whether this acceleration is only a transient state, or if it persists until other mechanisms of dissipation, like air resistance, take over, will be discussed in a bit more detail in the present work. In any case, this regime is again very clearly distinguishable from regime B, since the ball very quickly reaches velocities considerably larger than those stable in region B.

The "phase boundaries" indicated by the lines in Fig. 4.2 will be denoted by θ_{AB} and θ_{BC} respectively in the following.

From these qualitative features of the motion essentially two questions arise: What determines the "phase boundaries"? What determines the mean velocity in phase B? The same questions can be asked for many particle flow on an inclined plane if *mean velocity* is substituted by *velocity profile in the steady state.* However, they amount to essentially one question, which is equally valid for the single particle and the many particle case: How does the global dissipation in the system arise from the local dissipative properties? It is this question which will be addressed in detail in the analysis of the numerical simulations of the system.

Before addressing these questions from the point of view of simulations of the system, I will now summarize briefly the details of previous experimental, numerical and theoretical work on this subject. Some of these studies were performed parallel to the work presented

in this thesis, partly in close collaboration. Their results will not be discussed in much detail in this introduction, but rather in the appropriate section dealing with the simulation results.

4.1.1 Experiments

A number of experiments has been performed on the motion of a single sphere on a rough inclined plane. The first experiment was conducted by Jan *et al.* for a quasi two dimensional system [255]. They used a channel just 1 particle diameter wide, and let a sphere roll down a bed of identical spheres, i.e. in their case, the size ratio $\Phi = R/r$ was always 1. Assuming that the energy losses are made up of both frictional and collisional losses, they deduced that the mean velocity should depend on the inclination angle as

$$\bar{v}_x = \sqrt{\frac{2gr(\sin\theta - \mu\cos\theta)}{f}}, \tag{4.1}$$

where f is a fitting parameter. Their experimental curves could be fitted by this expression very well.

F.-X. Riguidel *et al.* conceived the original experimental set-up to study this problem in 3D [256–258]. The rough plane consists of a glass plate, onto which a sheet of contact paper is placed. Glass beads (in the experiments, their mean diameter was typically 0.5 to 1 mm) were then spread uniformly on the self-adhesive paper, thus forming the rough surface. Riguidel explored in detail the phase diagrams for steel beads rolling down this surface. While in all that follows, particles are always introduced onto the plane with some starting velocity, Riguidel also investigated the static angle of repose, i.e. the angle of inclination where beads placed onto the inclined plane lose their static equilibrium. Both this static angle of repose θ_s and the phase boundary $\theta_{AB}(\Phi)$ could roughly be fitted by a power law $\theta(\Phi) \propto \Phi^{\beta}$, with an exponent $\beta = -0.8$ for θ_s, and $\beta = -1.7$ for θ_{AB}. Similar power laws were found as well by Aguirre *et al.* [259] for steel, glass and plastic balls moving on a rough surface consisting of sifted sand or glass beads. They remarked as well that the material used for the rolling balls obviously had no influence on the mean velocity.

Riguidel also found that the mean distance L covered by a ball in region B before being abruptly stopped as described above strongly depends on the size ratio Φ, i.e.

$$L \propto e^{A\Phi^3 \sin^2\theta}, \tag{4.2}$$

where A is a constant independent of Φ and θ. He also measured the mean velocity $\bar{v}_x$ in region B and came to the conclusion that

$$\bar{v}_x \propto \Phi^{1.5} \sin\theta. \tag{4.3}$$

This result was hardly to be expected, since from Bagnold's argument discussed in Subsection 1.3.2, which should be valid for a single particle as well, one gets $\bar{v}_x^2 \propto \sin\theta$. For a ball moving down a line of discs (confined to a V-shaped groove, which allows variation of R, contrary to [255]), Riguidel indeed found such a relation [256]. These findings raise the

question whether there is a fundamental difference between the two dimensional and three dimensional system. Since Bagnold's argument takes only two dimensions into account, as well as neglecting fluctuations of the motion, which should be expected to be stronger in 3D than in 2D, it might not be valid in 3D any more. However, no premature conclusions should be drawn from the results, since they are far less clear than suggested above. Though the velocity curves collapse quite nicely on the curve given by eq. (4.3), most of the *single* velocity curves exhibit some definite curvature – the reason for the relatively good fit might simply be the fact that most curves cover only a very narrow range of angles, and hardly overlap.

Far cleaner velocity measurements were performed by Samson *et al.* [260,261], who refined Riguidel's experimental set-up by placing a number of lasers (spaced 5 cm apart from each other) on the plane. This allowed to measure the velocity on different sections of the plane, and thus enables a better check of the velocity being really constant. The velocity curves extracted from these measurements and from filmed trajectories of the moving ball again seemed to be linear in $\sin\theta$, and scaled with $\Phi^{1.05}$ [254]. However, in an effort to reconcile her results and those of Riguidel, Samson found that it was possible to collapse all results (hers and Riguidel's) onto one curve by scaling the velocities by a factor $\Phi^{1.25}\sqrt{r}$ [260]. Though it is trivial that the velocity scales by a factor $\sqrt{r}$, as $\sqrt{rg}$ is the appropriate factor to nondimensionalize the velocity, the fact that all these scalings work (by visual inspection of the results) equally well shows that maybe the range over which data can be obtained is too small to decide definitely on a scaling exponent. I will return to this question later when discussing simulation results.

Besides these measurements of the global properties of the motion, Samson performed a detailed analysis of the diffusive motion of the particles on the plane. This was done by analyzing both filmed trajectories of the ball, as well as results obtained by measuring the dispersion of passage times between lasers (for the longitudinal dispersion) and by collecting large numbers of particles at the bottom of the plane in small bins for the transverse dispersion.[1] The results of these diffusion measurements will be discussed later, together with the simulation results, since their interpretation is not straightforward and to a large extent still unclear.

Henrique *et al.*, already mentioned above in the context of the global features of the motion, also performed more detailed measurements of the particle motions [254, 262]. With the help of a microphone attached to the glass plate below the rough plane, they measured the noise emitted in collisions of the moving steel ball with the glass beads on the plane. These noise measurements show very distinct differences between regions A, B and C of the phase diagram [254], thus providing another possibility to assess the phase boundaries. Another important result of these measurements was the fact that the distribution of times between successive collisions corresponded roughly to the distribution of distances between balls on the plane, i.e. the ball seemed to collide roughly once per ball on the plane it passed.

Henrique *et al.* also investigated the dependence of stopping distances in region A as a function of the initial energy provided to the ball when launched onto the plane [263]. The objective in these experiments was to understand better the details of the dissipation

[1] The set-up to measure the transverse dispersion is the same as used to demonstrate that a Galtonian board produces a gaussian distribution.

mechanism in region A. They found that the mean stopping distance for relatively high starting velocity (so that the ball first bounced visibly) varied linearly with the kinetic energy with which the ball was launched on the plane. This behaviour could be explained by the observation (which was confirmed in simulations) that the ball, when it was jumping, experienced a constant friction force, while when it started to jump and roll on the plane, the friction force dropped and exhibited a similar velocity dependece as in region C. However, the distance covered in this rolling motion was much smaller than that travelled during the jumping, therefore the stopping distance was mainly determined by this jumping motion.

It should maybe be mentioned at this point that while Riguidel's results were the starting point of the simulations presented in this thesis, the experiments by Samson *et al.* and Henrique *et al.* paralleled the simulation work, i.e. evolved at the same time and in close collaboration with the theoretical efforts presented in this chapter. They should thus not be viewed as completely detached from the work presented in this thesis, or as known a priori before this work was started. For these reasons, some details of the experimental results will be discussed later, at the appropriate point in the discussion of the simulation results.

4.1.2 Simulations and theoretical approaches

Since some of these experimental results are quite startling, considerable effort has been put into theoretical models of the motion. Besides, some computer simulations were performed of this system, which I will briefly summarize here as well.

Riguidel *et al.*, in an effort to understand the Φ-dependence of the static angle of repose θ_s, investigated the static limit of stability of spheres placed on a rough plane with a very simple algorithm [257]. They simply produced a rough plane with the random sequential absorption (RSA) model, randomly placed particles onto it and calculated at which inclination angle these positions ceased to be statically stable. They found a similar power law for the dependence of θ_s on Φ as the experiments, however, they could not explain this law or the exponent from theoretical considerations, either. Riguidel *et al.* also modeled the motion in region B [258]. They proposed a Langevin equation to describe the motion, where, however, the proportionality of $\bar{v}_x$ with $\sin\theta$ is put in from the start. Thus, the analysis gives no explanation for the surprising linearity.

Ristow *et al.* performed TD simulations of the two dimensional sytem (i.e. a ball moving down a line of balls) [264]. They found velocity curves comparable to the experimental ones, however, the value for θ_{AB} found in simulations was slightly too high, while the one for θ_{BC} was slightly too low. They also performed simulations for balls moving along a line with a random spacing of balls, and found that increasing the disorder (i.e. the maximum spacing between balls) led to a decrease in the width of region B. Ristow *et al.* also claimed that in region C, the ball eventually reaches a steady state, though with a steady state velocity which is two orders of magnitude larger than that in region B. I will later show, when discussing motion in region C, that this was probably due to the brake failure effect, or rather the corresponding emergency brake phenomenon discussed in Section 2.1.2. Another observation made by Ristow *et al* was that in region B, the ball collides with every ball it passes on the line approximately once. Again, as we will see

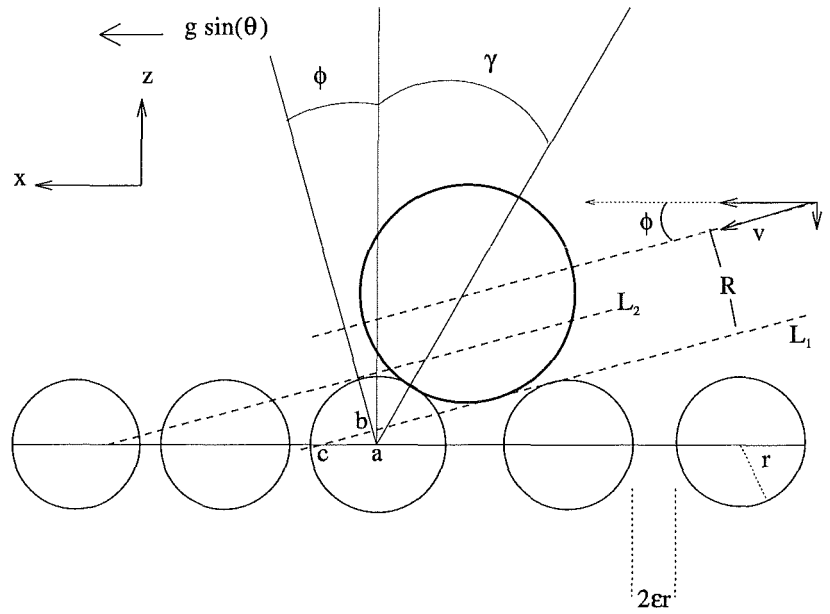

Figure 4.3: *Definition sketch for the inclined line of discs, r, on which the disc R is released. The collision depicted is that for the largest negative value of γ, the contact angle, i.e. γ is taken negative on the up-hill facing side of balls on the plane, and positive on the down-hill facing side.*

later, this was probably an artifact of the choice of the force law, namely the Hertzian normal force with viscous damping (3.5), which artificially increases dissipation for *small* impact velocities (see Section 3.1.1).

4.1.3 A stochastic model for the motion

Batrouni *et al.* proposed a two dimensional stochastic model that a priori makes no assumption about the statistics of collisions [246]. This model is discussed here in more detail than the other models presented so far, since some parts of the calculation will be used later on in the discussion of the simulation results. The model attempts to mimic the motion on the inclined plane by randomly placing balls on a line (which could be viewed as an approximation to a section through the plane). Figure 4.3 gives a definition of most of the quantities used in the following. The vertical direction is denoted by z to be consistent throughout this chapter, since in the three dimensional case, the y coordinate will denote the transverse direction.

Stochasticity enters into the model solely in the way the contact angle γ for each collision is determined. Collisions are treated as hard sphere collisions, with the Walton model explained in Section 2.1.3. However, the rotational degree of freedom is neglected, so that all changes in the tangential velocity of the contact point change the velocity of the center of mass of the particle, and not the rotational velocity. To distinguish the tangential velocity of the center of mass from the shear velocity v_s in the contact point (which, without rotation, are equal), in the following the tangential velocity of the center of mass

will be denoted by v_t. The tangential and normal velocities in the kth collision $v_t(k)$ and $v_n(k)$ can be expressed in terms of the contact angle as

$$\begin{aligned} v_n(k) &= v_x(k)\sin\gamma + v_z(k)\cos\gamma & (4.4)\\ v_t(k) &= v_x(k)\cos\gamma - v_z(k)\sin\gamma. & (4.5)\end{aligned}$$

The velocities $v_t'(k)$ and $v_n'(k)$ after the collision are given by

$$\begin{aligned} v_n'(k) &= -e_n v_n(k) & (4.6)\\ v_t'(k) &= e_t v_t(k), & (4.7)\end{aligned}$$

with

$$e_t = 1 - \frac{7}{2}(1+e_n)\mu/\psi_i. \tag{4.8}$$

Except for a factor $\mathrm{sign}(v_t(k))$ in the second term on the right-hand side this is identical with Eq. (2.28). Since in the system in question only $v_t \geq 0$ can occur, this factor is redundant here. However, this treatment of a collision is very unphysical. In the derivation of Eq. (2.28) explicit use is made of the fact that *rotational* velocity contributes to v_s. Therefore it cannot simply be used for v_t as done in the stochastic model. The correct treatment of the collision of two frictional spheres that cannot rotate leads to

$$e_t = 1 - (1+e_n)\mu/\psi_i, \tag{4.9}$$

i.e. to a larger coefficient of tangential restitution. In [246], however, eq. (4.8) was used. Independently of the details of e_t, this model yields for the postcollisional x- and z-velocities

$$\begin{aligned} v_x'(k) &= v_n'(k)\sin\gamma + v_t'(k)\cos\gamma\\ &= -e_n\left(v_x(k)\sin\gamma + v_z(k)\cos\gamma\right)\sin\gamma\\ &\quad +e_t\left(v_x(k)\cos\gamma - v_z(k)\sin\gamma\right)\cos\gamma & (4.10)\\ v_z'(k) &= v_n'(k)\cos\gamma - v_t'(k)\sin\gamma\\ &= -e_n\left(v_x(k)\sin\gamma + v_z(k)\cos\gamma\right)\cos\gamma\\ &\quad -e_t\left(v_x(k)\cos\gamma - v_z(k)\sin\gamma\right)\sin\gamma & (4.11)\end{aligned}$$

The collision can thus be described by a collision operator $K(\gamma)$, defined as

$$K(\gamma) = \begin{pmatrix} e_t\cos^2\gamma - e_n\sin^2\gamma & -(e_t+e_n)\sin\gamma\cos\gamma \\ -(e_t+e_n)\sin\gamma\cos\gamma & -e_n\cos^2\gamma + e_n\sin^2\gamma \end{pmatrix} \tag{4.12}$$

acting on $\vec{v}(k)$. Right before the next collision, the sphere has the velocity $\vec{v}(k+1)$ with

$$\vec{v}(k+1) = K(\gamma)\,\vec{v}(k) + \vec{g}\,\tau, \tag{4.13}$$

where τ denotes the time of flight. In principle, one might thus simply iterate eq. (4.13) to determine the motion of the sphere. But, since the exact calculation of τ involves the solution of a fourth-order polynomial, this would get very involved.

The stochastic model thus introduces a simplification for the determination of τ. It is assumed that for impacts with the collision angle $\gamma(k) < 0$ in the kth collision, $v_z'(k)$

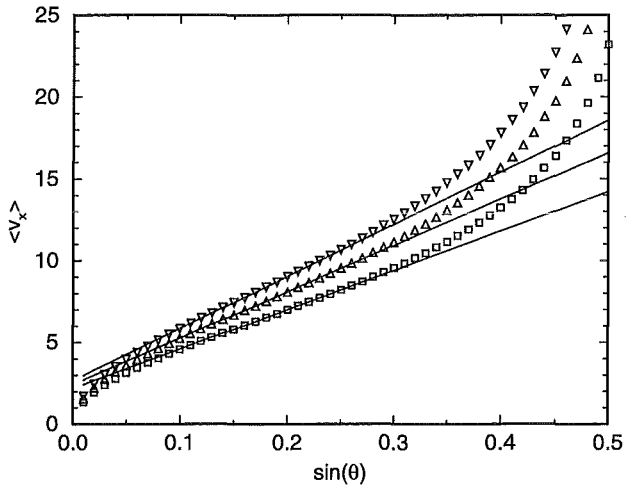

Figure 4.4: *Dependence of* $\langle v_x \rangle$ *(in* cm/sec*) on* $\sin\theta$ *as obtained from the stochastic model. The line indicates a linear fit to the central region.* $R = 3, 4, 5$mm *for* $\square, \triangle, \triangledown$, $\mu = 0.142$, $e_n = 0.9$, $\beta = 0.45$, $r = 0.5$mm.

determines the time of flight, where it is assumed that the sphere collides again at the same height with the spheres on the plane, i.e. $v_z(k+1) = v_z'(k)$ and

$$\tau = \frac{2v_z(k+1)}{g\cos\theta}, \tag{4.14}$$

whereas for $\gamma(k) \geq 0$, the sphere will directly move over to the next sphere on the plane, i.e.

$$\tau = \frac{2(r+\epsilon)}{v_x'(k)}. \tag{4.15}$$

All that remains now is to determine $\gamma(k+1)$. As illustrated in Fig. 4.3, not all points on a sphere are accessible if the large sphere is approaching the line with velocity $\vec{v}$. From Fig. 4.3 it can be deduced that all angles between

$$\gamma_{\min} = \phi - \arccos\left(1 - 2\frac{1+\epsilon}{1+\Phi}\sin\phi\right), \tag{4.16}$$

and

$$\phi = \arcsin\frac{v_z}{|\vec{v}|} \tag{4.17}$$

are accessible. Here $2\epsilon r$ is the gap between the disc under collision and that to its right. Assuming that all angles in the interval $[\gamma_{\min}, \phi]$ are equally likely to be hit by the sphere, it follows after some manipulations that $\gamma(k)$ is given by

$$\sin\gamma(k) = \sin\phi(k)\frac{R+\delta\sin\phi(k)}{r+R} - \cos\phi(k)\left[1 - \left(\frac{R+\delta\sin\phi(k)}{r+R}\right)^2\right]^{1/2}, \tag{4.18}$$

where δ is a uniform random number with

$$\delta \in \left[\frac{r}{\sin\theta} - 2r(1+\epsilon), \frac{r}{\sin\theta}\right]. \tag{4.19}$$

Equation (4.13) can now be iterated. The ball is assumed to be trapped on the plane if a collision occurs which results in $v_x'(k) \leq 0$.

The stochastic process described gives rise to a θ- and R-dependent mean velocity in a range of inclination angles (see Fig. 4.4). The curves can be fitted very well by straight lines in an intermediate angle region and give the same range of stable mean velocities as experiments. The size ratios Φ for which a steady state is obtained rather correspond to those stable in three dimensional systems, and are generally larger than those found to be stable in two dimensional systems. Besides, the range of inclination angles for which a steady state is found is far larger than in both 2D and 3D experiments. Reasons for these discrepancies will be discussed after presenting the numerical simulations of both the two and three dimensional systems.

4.2 The 2D case

In this Section, numerical simulations of the two dimensional case of a sphere moving down a line onto which spheres are glued are presented. Special attention is paid to the details of the motion, which suggest a simplified theoretical model for the motion.

4.2.1 Set-up

The motion of a sphere on an inclined line consisting of spheres was simulated using TD simulations as discussed in Chapter 2. The force laws used in the simulations are the linear spring-dashpot model in the normal direction (3.1), and viscous damping with a cut-off at the Coulomb friction limit in the tangential direction (3.12). Since, as we will see, both collisions and lasting rolling contacts dominate the motion, this force seems to be a reasonable choice in this particular case.

Throughout the simulations the parameters $k_n = 2 \cdot 10^6$ N/m, $\gamma_s = 100$ kg/s, $\mu = 0.13$, $r = 5$ mm and $M = \frac{4}{3}\pi R^3 \rho$ for the mass of the rolling ball with $\rho = 7.8$ g/cm^3 were used. The values of these parameters were chosen to match the steel balls used in [256,264]; the choice of k_n leads to a collision time of the order of 10^{-5} s, which is a typical value for steel balls of this size. The reason for using the moment of inertia of spheres even in this completely two dimensional system for the moving particle is that all quasi two dimensional experiments were performed with spheres. Therefore, even in the two dimensional system the particle will be called sphere instead of disc. The value of γ_s is high enough such that F_s is reasonably close to the exact Coulomb friction law in the sense explained in Section 3.1.2. The damping γ_n is determined by fixing the normal coefficient of restitution e_n. Unless stated otherwise, the results presented in the following were obtained using $e_n = 0.7$ and the above mentioned parameters. The influence of the material parameters e_n and μ on the behaviour of the system will be discussed later. The only external force acting on the ball is gravity, the gravitational acceleration in the x (z) direction is given by $g \sin\theta$ ($-g\cos\theta$). The geometry is essentially the same as in Fig. 4.3. The spacing between two balls fixed on the line is $2\epsilon r$, where ϵ is a number which in the disordered case is chosen uniformly distributed in the interval $[0, \epsilon_{\max}]$.

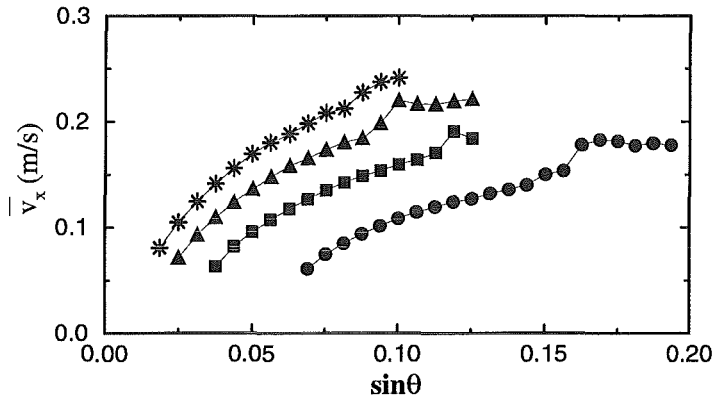

Figure 4.5: *Dependence of the mean velocity $\bar{v}_x$ on the inclination of the line for various size ratios Φ: $\Phi = 1.5$ (circles), $\Phi = 2.0$ (squares), $\Phi = 2.5$ (triangles), $\Phi = 3.0$ (stars).*

4.2.2 Global features of the motion in the steady state

In all simulations presented here, the ball was launched onto the line with a rather high starting velocity v_x and quite low v_z. If inclination angle θ and size ratio $\Phi = R/r$ are in a suitable range, the moving ball very quickly, usually after passing only a few balls on the line, reaches a steady state with well-defined mean velocities in the x– and z–directions. Clearly, the average over v_z is zero here, so the only interesting *mean* velocity is the average over v_x, denoted by $\bar{v}_x$. To obtain this mean velocity, v_x is first averaged over a certain number of timesteps (usually 500). This value is large enough to average out the comparably large fluctuations occurring during collisions, while it is still so small that the ball moves only a very short distance (much less than the radius of the balls on the line) during this time. This averaged value clearly still gives a fluctuating velocity, but the fluctuations are very small, and $\bar{v}_x$, the mean value of these averaged velocities, is well-defined.

In the following, results for the motion of the ball both on lines with equally spaced balls and on lines with randomly spaced balls will be discussed. The essential features of the motion are alike in both cases, i.e. do not depend on the random arrangement of balls on the line. Fig. 4.5 shows the velocity of the rolling ball for various Φ and equal spacing of balls on the line with spacing $\epsilon = 0$ as obtained from simulations using the above mentioned parameters. ϵ is defined as in Fig. 4.3. For the case $\epsilon = 0$, experimental data is available (though only for size ratios $\Phi \leq 2.0$) [256, 264]. The stable mean velocities in the simulations are of the same order of magnitude, but the range of inclination angles for which $\bar{v}$ is well–defined, i.e. a steady state is reached, is a bit narrower than in the experiments, although the simulated system is even more dissipative than the steel spheres used in the experiments.[2] This might be due to the difference in the experimental setup. There, a ball moved down a line of balls sitting in a V-shaped groove, and it is to be expected that contact with the groove walls influenced the motion as an additional source of dissipation due to friction and collisions with the walls, but it is unclear how strong this

[2]The value $e_n = 0.7$ is significantly smaller than the appropriate value $e_n = 0.95$ for polished steel spheres.

influence was. For a direct comparison of simulation and experiment, it would be desirable that a "more" 2–dimensional experiment be done, like for example a ball moving down a row of cylinders, to rule out these boundary effects.

Fig. 4.5 shows that there is a lower limiting angle θ_{AB} for the steady state region as described in Section 4.1. For $\theta < \theta_{AB}$, the ball loses all velocity it had in the beginning and very quickly stops, usually after passing only very few balls on the line. All velocity curves in Fig. 4.5 exhibit a sudden increase of $\bar{v}_x$ to a value where it remains roughly constant. This sudden increase has also been observed in experiments [264]. For angles smaller than the one where this happens, the velocity of the ball shows only very small fluctuations and the steady state velocity $\bar{v}_x$ does not depend on the initial velocity of the ball. At the inclination angle where the velocity suddenly shoots up, the behaviour changes qualitatively. The fluctuations of v_x increase significantly, and the behaviour of the ball now depends on the initial velocity. Depending on the starting velocity, the ball can accelerate (usually if the starting velocity is larger than the stable mean velocity) and start to jump visibly, or it can reach a constant velocity (if released with an initial velocity smaller than the stable $\bar{v}_x$ in this region). However, even when the ball does not accelerate, in this region $\bar{v}_x$ can depend somewhat on the initial velocity. This dependence on the initial velocity leaves some ambiguity as to how exactly the phase boundary θ_{BC} should be defined. In the following, the angle at which the sudden increase takes place will thus be taken to define $\theta_{BC}(\Phi)$, since this definition of region B is independent of the initial velocity of the ball.

If θ increases even more, the ball accelerates and starts to jump significantly (the length and height of the jumps reaches a few ball diameters). This jumping regime will be discussed in more detail later. For the moment, the discussion will be restricted to the steady state and its limits.

The velocity curves obtained for the steady state from experiments as well as from simulations suggest the functional form

$$\bar{v}_x = v_0(\Phi) + f(\Phi)\sqrt{\sin\theta - \sin\theta_{AB}(\Phi)} \tag{4.20}$$

for a fixed value of r in region B. All curves start at a certain offset velocity v_0, which seems to depend slightly on Φ. $f(\Phi)$ denotes a (still unknown) scaling function, which, unlike in 3D, does not seem to be a simple power law. Thus, $(\bar{v}_x - v_0(\Phi))^2$ is plotted in Fig. 4.6, where $v_0(\Phi)$ is obtained by fitting a square root to $\bar{v}_x(\sin\theta)$. $v_0(\Phi)$ typically is of the order of 4 cm/s. The error bars give the variance of the averaged velocities, averaged (as the plotted value of $\bar{v}_x$ itself) over a number of simulation runs with different starting velocities. Fig. 4.6a shows velocities in the case $\epsilon = 0$ for various size ratios, Fig. 4.6b illustrates the influence of disorder on the velocity of a ball of size ratio $\Phi = 2.25$.

Figure 4.6b demonstrates how the velocity of the ball is affected by the introduction of disorder to the line. It shows that $\bar{v}_x$ on the disordered line with $\epsilon_{\max} = 0.2$ can be approximated by the velocity on a line with equally spaced balls and a spacing $\epsilon = 0.1$, corresponding to the mean value of the disordered case. It also shows that $\theta_{BC}(\Phi)$ depends on both Φ and the arrangement of the balls on the line, whereas the maximum $\bar{v}_x$ only seems to depend on Φ.

In Fig. 4.7 the corresponding phase diagram is plotted for three cases: two cases for a line

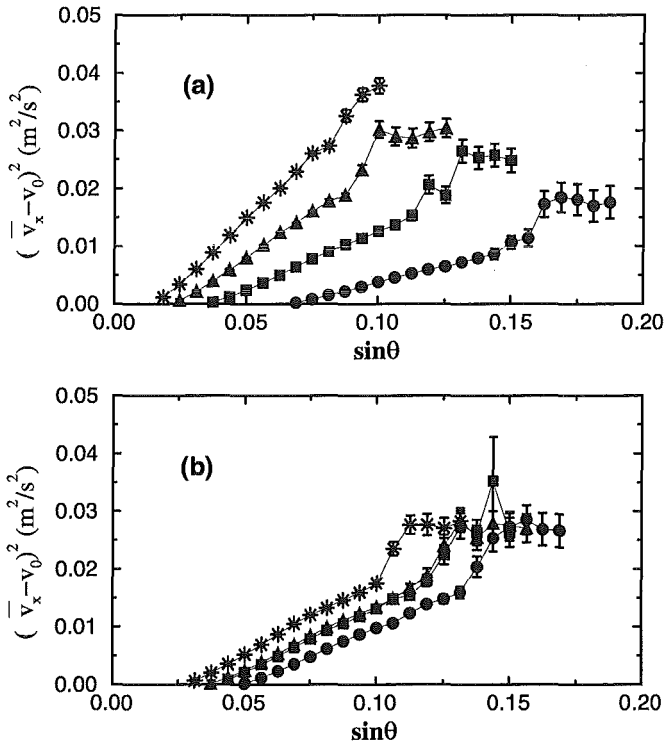

Figure 4.6: *Dependence of the mean velocity $\bar{v}_x$ on the inclination of the line (a) for the same parameters as Fig. 4.6; (b) for various spacings of the balls on the line ($\Phi = 2.25$): balls equally spaced with $\epsilon = 0$ (stars), $\epsilon = 0.1$ (triangles), $\epsilon = 0.2$ (circles); balls disordered with $\epsilon_{\max} = 0.2$ (squares).*

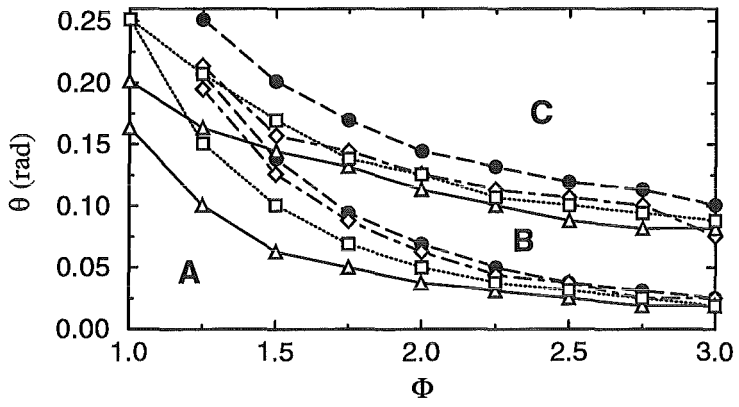

Figure 4.7: *Phase diagram for $e_n = 0.7$ and various spacings of the balls on the line: balls equally spaced with $\epsilon = 0$ ($\triangle$, solid line), $\epsilon = 0.1$ ($\square$, dotted line) and $\epsilon = 0.2$ ($\bullet$, dashed line); balls disordered with $\epsilon_{\max} = 0.2$ ($\diamond$, dot–dashed line).*

with balls equally spaced, with $\epsilon = 0$ and $\epsilon = 0.2$, the third for a disordered line with $\epsilon_{\max} = 0.2$. The lines denote the phase boundaries given by the angles $\theta_{AB}(\Phi)$ and $\theta_{BC}(\Phi)$ defined previously. Obviously, the introduction of disorder has the same effect on θ_{AB} as the introduction of an equal spacing of balls with $\epsilon = \epsilon_{\max}$. This is understandable; the stopping of a ball should be ruled by the deepest "traps" into which it might fall. By contrast, θ_{BC} rather seems to be determined by the mean spacing of balls, since in the disordered case it falls essentially on the same curve as θ_{BC} for an ordered array with $\epsilon = 0.1$.

4.2.3 Details of the motion

In order to investigate the mechanism by which the ball maintains a constant velocity in region B, the details of the motion have to be considered. Certainly, distributions of the impact angle γ, of times of flight between impacts or of the impact velocity $\vec{v}^{\,i}$ would be of interest. The main interest in considering these in detail is that while the time of flight between impacts (together with the velocity) controls the amount of potential energy gained during the flight, the impact velocity determines the dissipation in the collisions. Thus, these quantities should be crucial in determining the mean velocity, since they control the balance of energy gain and energy loss. Another point of interest is the question whether there are correlations between impacts at certain angles and the corresponding impact velocities or between the time of flight after an impact and the corresponding impact angle. Actually, these correlations provide even more detailed information; for this reason they are examined here first. I will first discuss the ordered case of a line with no spacing between the balls, i.e. with $\epsilon = 0$.

In Fig. 4.8 the velocity of the ball right before an impact is plotted as a function of the corresponding impact angle γ. Each dot corresponds to a collision. The normal velocity v_n and the tangential *translational* velocity $v_t = \vec{v} \cdot \vec{s}$ rather than v_x and v_z are plotted, as they provide more information on the mechanisms involved. Since dissipation takes place only through the normal velocity (dissipation due to F_s is negligible, as we will see later), the evolution of this quantity may explain the mechanism by which energy loss maintains the steady state. Since v_t is the velocity component of the motion of the center of mass of the ball along the bumps of the surface, it reflects how this bumpyness is felt. It is obvious that there is a strong correlation between the impact angles and the corresponding impact velocities. The times of flight between impacts and corresponding previous impact angles are equally strongly correlated (see Fig. 4.9).

From both Fig. 4.8 and 4.9 it is obvious that the ball moves down the line in a series of bounces. There is even a certain range of impact angles that are never hit. In addition, one can deduce from Fig. 4.9 that the typical times of flight between impacts correspond to a distance of less than 3 mm, which is smaller than the radius of the balls constituting the line. So the bounces the ball undergoes cannot be very high or far, and the bouncing ball collides with every ball on the line several times. This means that very strong correlations develop between successive collisions. The observation that there are in fact many collisions with each ball on the line is in contrast with previous results by Ristow *et al.* [264], who claim that there is approximately one collision with each ball on the line. The reason is that they used a Hertz law in the normal direction combined with viscous

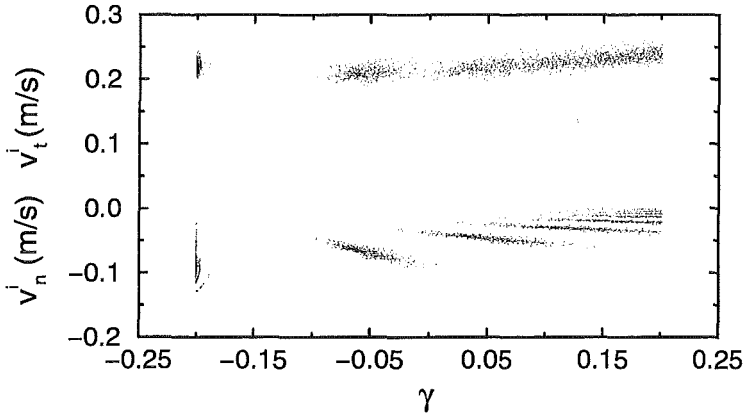

Figure 4.8: *Correlation of impact velocities with impact angles for* $\Phi = 4$, $\sin\theta = 0.05$, $\epsilon = 0$. *The upper points correspond to the relative translational tangential velocity* $v_t = \vec{v} \cdot \vec{s}$, *the lower ones to the relative normal velocity* v_n.

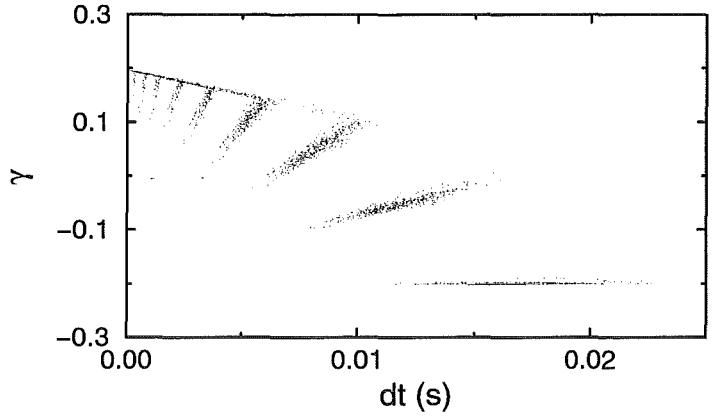

Figure 4.9: *Correlation of time of flight after an impact at angle* γ *and corresponding previous impact angles (parameters as in Fig. 4.8).*

damping, i.e. force (3.5), which leads to very strong dissipation for impact velocities approaching zero. Therefore, it is to be expected that for the small velocities occurring in most collisions, e_n was quite low and therefore "collapse" of the moving ball on the balls forming the line occurred after a significantly smaller number of collisions than in my simulations.[3]

How can these results be understood? From Fig. 4.8 two important points can be extracted. First we see that at certain impact angles γ, the moving ball is likely to hit the ball on the line with a well-defined corresponding normal velocity v_n, which leads to an equally well-defined time of flight (see Fig. 4.9). Second, the normal velocities are largest for negative impact angles (*i.e.* hitting on the uphill side of a ball on the line) and get

[3]It is not even clear where the value $e_n = 0.7$ stated in [264] comes from, since the way the damping is used there, the coefficient of restitution depends strongly on the mass of the particle.

smaller (and eventually very close to zero) with increasing impact angles. The second observation helps to explain the correlations and reveals the reasons for the regularity of the motion.

Consider a ball that has just arrived at the maximum possible positive impact angle $\gamma_{\max}$ on a certain ball on the line, say ball number k. The value of $\gamma_{\max}$ is given by the geometry and defined as

$$\gamma_{\max} = \arcsin \frac{1+\epsilon}{1+\Phi}. \tag{4.21}$$

From Fig. 4.8 it is obvious that at $\gamma_{\max}$ the moving ball has lost nearly all normal velocity with respect to ball k, *i.e.* it is rolling or sliding down the lower part of the "downhill side" of the corresponding ball on the line. Even though the total shear velocity v_s at the point of contact is quite small (the ball rolls, thus rotational velocity is opposed to the translational tangential velocity and nearly compensates it), the translational tangential velocity v_t plotted in Fig. 4.8 is quite large (close to $\bar{v}_x$ for larger Φ). Immediately after having reached $\gamma_{\max}$ on ball k, the moving ball impacts the next ball, $k+1$, at $-\gamma_{\max}$, where a large part of this previously tangential velocity is now normal velocity, as the direction of the vector $\vec{n}$ connecting the centers of the impacting balls with respect to $\vec{v}$ has changed. The ball thus gets thrown up again, and manages to reach the downhill side of ball $k+1$ after a few jumps. The comparably high normal velocity of the ball at $-\gamma_{\max}$ is lost in two ways in crossing a fixed ball: most is lost by dissipation due to impacts, but partly it is converted into tangential velocity by the increasing obliqueness of successive impacts at positive γ.[4] In the process of bouncing over the top of ball $k+1$ on the line, the moving ball loses nearly all of its normal velocity, so that it again reaches $\gamma_{\max}$ with nearly only tangential velocity. These steps repeat themselves over and over again while the ball moves down the plane, thus retaining a constant mean velocity. Note that strong geometrical constraints prevent the ball from rolling down the line without ever bouncing. Whenever the moving ball rolls down the downhill side of a ball k, it is thrown onto the uphill side of ball $k+1$ with considerable normal velocity with respect to ball $k+1$ as a result of the change in the geometry. To remain in contact with ball $k+1$, the moving ball would have to lose a very substantial amount of this normal velocity in a single impact, or it would jump up. Persistent rolling thus is only possible in the case of vanishing normal restitution. Rolling on a part of each ball is possible, however, as will be shown in a moment.

In order to describe things more quantitatively, one should take a look at the distribution of impact angles. Figure 4.10a gives an example for an angle of inclination in the middle of region B of the phase diagram for $\Phi = 2.5$. The distribution exhibits clear peaks for $\gamma < 0$. As γ increases, the peaks broaden somewhat and approach each other until they are nearly indistinguishable in the histogram, although there still is structure in the correlation plots. For plane inclinations closer to θ_{AB} than θ_{BC}, the distribution, like in Fig. 4.10a, even breaks off at a value $\gamma < \gamma_{\max}$, indicating the start of a long-lasting contact. Here, the ball has lost so much of its normal velocity in impacts it suffered on crossing over the top of a ball on the line, that it finally starts to roll over part of this ball. This rolling motion can even start while the moving ball is still on the uphill facing side of the fixed ball, though this only takes place very close to θ_{AB} for $e_n = 0.7$. All these impacts *end* at $\gamma_{\max}$, which leads to the very pronounced peak at $-\gamma_{\max}$. Integrating the distribution over negative

[4] For $\gamma < 0$, v_x gained during the free flight in fact partially adds to v_n.

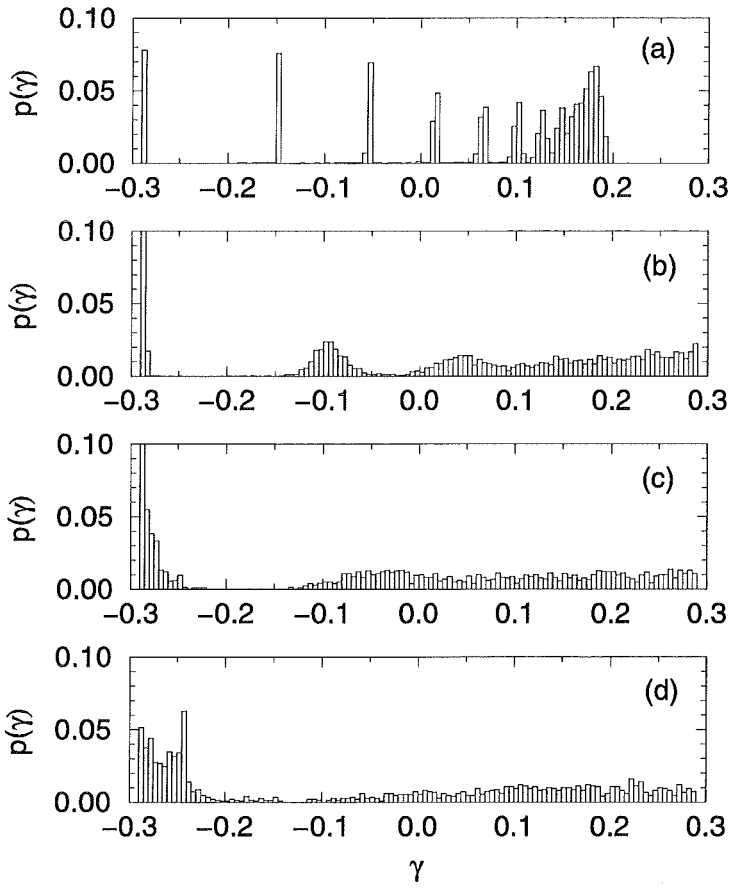

Figure 4.10: *Distribution of impact angles for* $\Phi = 2.5$, $\epsilon = 0$ *and (a)* $\sin\theta = 0.057$ *(b)* $\sin\theta = 0.075$ *(c)* $\sin\theta = 0.091$ *(d)* $\sin\theta = 0.103$.

and positive angles respectively yields the result that there are actually more impacts for positive than for negative γ.

When θ is increased, the peaks for negative γ, except the one at $-\gamma_{\max}$, move towards zero, finally disappearing into the continuous distribution for positive γ (see Fig. 4.11). At a large enough inclination, they get visibly broader, showing that the velocity at $\gamma_{\max}$ is now no longer as sharply defined as before, probably due to the fact that not all the normal velocity can be lost on only one ball. Still, the ball does not accelerate as long as its starting velocity is only a little higher than its stable mean velocity (this is the region beyond the transition from linear to more irregular behaviour in Fig. 4.5).

Figure 4.10(b-d) shows how the motion of the ball changes qualitatively at θ_{BC}. The θ-values are taken a little below (b), as close as possible to (c) and a little above θ_{BC} (d). The heretofor clearly defined peak at $-\gamma_{\max}$ broadens considerably and even seems to develop a small side peak as θ reaches θ_{BC}. The qualitative change of the behaviour of the ball can also be observed in the velocities. In particular in the angle region where the velocity curve flattens out again, an intermittent behaviour of the ball can be observed – it will accelerate a little, even start to jump a little, but then suddenly get braked again. The mean velocity in this case is determined by how fast the ball is accelerated and

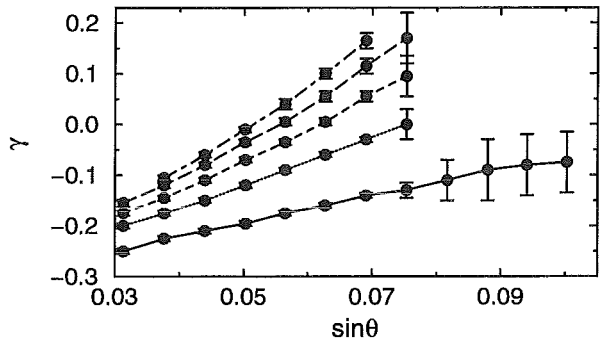

Figure 4.11: *Location of the peaks in the distribution of impact angles for* $\Phi = 2.25$. *The error bars denote the width of the peak. The solid, dotted, dashed, long-dashed and dot-dashed lines denote respectively the 1st, 2nd,..., 5th distinguishable peak, excluding the one at* $-\gamma_{\max}$.

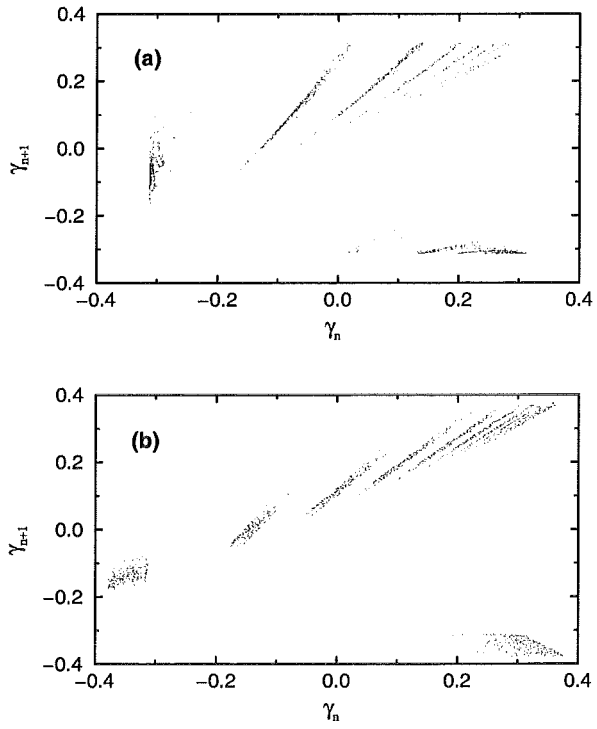

Figure 4.12: *First return map of impact angles for* $\Phi = 2.25$, $\sin\theta = 0.094$. *(a) Balls on the line regularly spaced* ($\epsilon = 0$), *(b) balls on the line disordered with* $\epsilon_{\max} = 0.2$.

braked respectively. The same intermittent behaviour of the ball shortly before passing from motion with a mean constant velocity to a jumping regime has been observed in 3D experiments [256] and in the stochastic model described in Section 4.1.3 [246].

While the intermittent behaviour marks the transition from region B to region C in the phase diagram, stopping of the ball takes place when the typical tangential velocity at

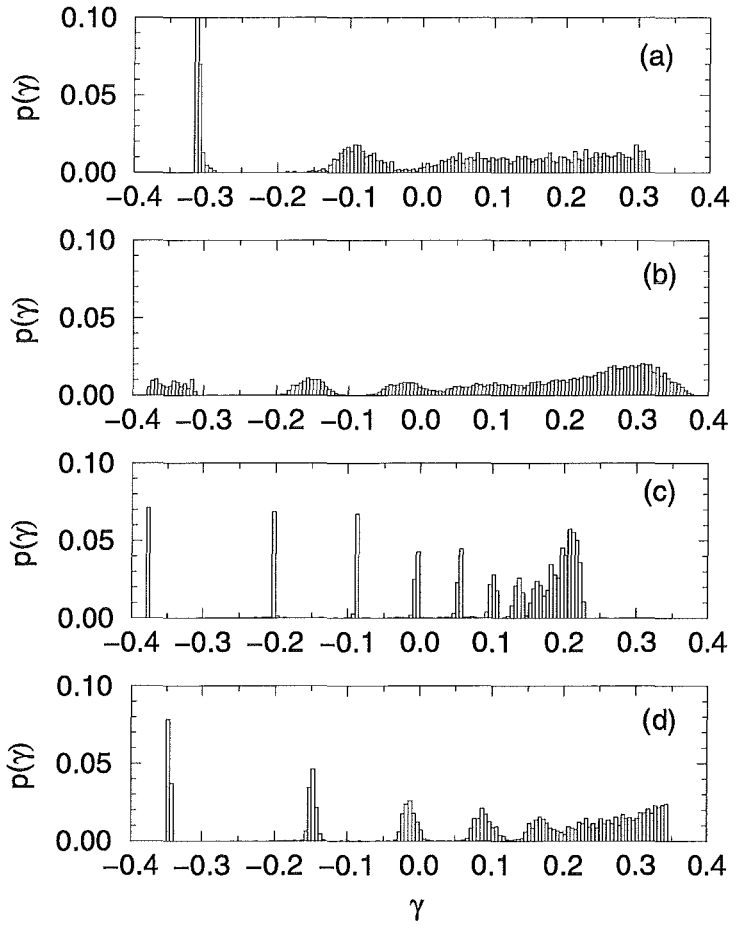

Figure 4.13: *Distribution of impact angles for* $\Phi = 2.25$, $\sin\theta = 0.088$ *and various spacings of the balls on the line. (a) regular spacing,* $\epsilon = 0$ *(b) disordered line,* $\epsilon_{\max} = 0.2$ *(c) regular spacing,* $\epsilon = 0.2$ *(d) regular spacing,* $\epsilon = 0.1$

$\gamma_{\max}$ does not convert into enough normal velocity at $-\gamma_{\max}$ to carry the ball over the top of the next ball in the line in a few jumps, or at least up to a point where the remaining tangential velocity suffices to make it roll over the top of this ball.

In regime B, the motion is not only characterized by typical impact angles γ, but also by a very strong correlation of successive impact angles. Figure 4.12 shows γ_{n+1}, the impact angle for impact $n+1$, as a function of the previous impact angle γ_n. Even when a random spacing of balls on the line is introduced, the strong correlation remains. This observation directly leads to the discussion of the behaviour of the moving ball on a disordered line. The phase diagram already suggests that introducing disorder has a similar influence on the motion of the ball as the introduction of an appropriate regular spacing. In both cases, the region of stable motion in the phase diagram shifts to larger Φ and θ. Plotting the distribution of impact angles for the cases displayed in Fig. 4.6b shows the effect of disorder (see Fig. 4.13).

It was checked that this regularity in the case of a disordered line is not a finite size effect. The angle distributions do not change when the size of the system is increased. From

Fig. 4.13 it can be seen that the distributions for the impact angles in the disordered case lie between the limiting cases $\epsilon = 0$ and $\epsilon = 0.2$ of an ordered line. In addition, the peaks for $\epsilon = 0.1$ correspond to the center of the peaks in the disordered case. The reason for the large width of the peaks in the case $\epsilon = 0$ lies in the fact that here the velocity is already quite high (see Fig. 4.6b). The results of the disordered case are interpreted in the following way. The motion of the ball is influenced mainly by two factors - the minimum and maximum spacing of balls on the line. If the ball is to keep its mean velocity, without being stopped and without being accelerated, the velocity has to have a value that enables it to get out of the "deepest valleys" existing between two balls (given by $\epsilon_{\max}$), but still is low enough that in all cases (even in those where $\epsilon = 0$) most of the normal velocity is dissipated on crossing over the corresponding ball, so that at $\gamma_{\max}$ of this ball essentially tangential velocity is left. The variations in this tangential velocity are so small that they only broaden the peaks for the impact angles, but do not lead to a *qualitative* change of the motion of the ball.

4.2.4 Influence of material properties on the motion

4.2.4.1 Influence of the coefficient of restituion

Having explained the mechanism by which the ball moves down the line and keeps a constant average velocity, the question is now how much this mechanism and the global results like $\bar{v}_x$ are influenced by material properties. The material properties incorporated in the simulation are the coefficient of normal restitution e_n and the friction coefficient μ. Here, it will be shown that their influence on $\bar{v}_x$ and the mean rotational velocity $\bar{\omega}$ is very small.

As mentioned before in discussing experimental results, experiments in 3D already indicate that the characteristics of the motion are hardly influenced by material properties [259, 260]. Rolling steel, glass and plastic balls down the plane gives nearly the same velocity, though for plastic (which has the lowest e_n and largest μ) the B region of the phase diagram is found to be somewhat extended. The simulations in 2D indeed show that the mean velocity $\bar{v}_x$ is nearly independent of both e_n and μ. Fig. 4.14 demonstrates this for the case of a ball of size ratio $\Phi = 2.25$. There, the velocities for varying normal coefficient of restitution e_n are shown. It can clearly be seen that e_n influences the phase diagram, *i.e.* the extension of region B, but has only a very small influence on $\bar{v}_x$ (The value of v_0 that was subtracted was the same in all cases). Though θ_{AB} is hardly affected by e_n (except for very small Φ), θ_{BC} moves to larger inclination angles θ with decreasing e_n. But e_n influences $\bar{v}_x$ slightly in a direction that is contrary to what one would expect intuitively. Increasing the dissipation leads to a slight increase in the velocity.

The reason for the small influence of e_n is the fact that there are a number of collisions with the same ball, and therefore strong correlations between successive collisions. Since the ball moves over each ball on the line in a succession of bounces, in the course of which it loses all or most of its relative normal velocity with respect to this ball on the line, e_n mainly determines how many bounces are necessary to achieve this. As long as the moving ball has only a negligible amount of normal velocity left as it reaches $\gamma_{\max}$, it seems to be unimportant for the tangential velocity at this point how many impacts were needed to

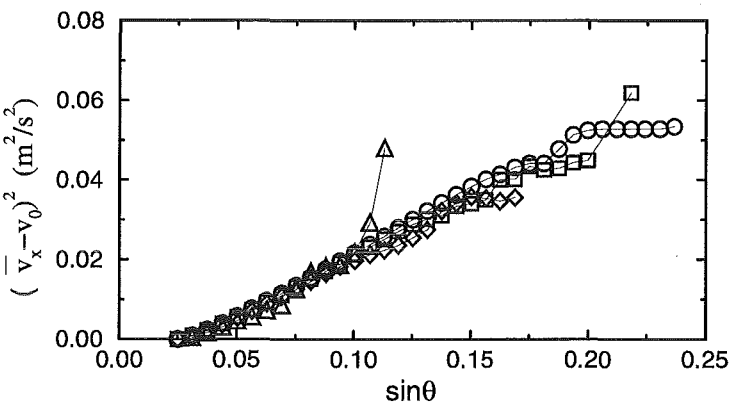

Figure 4.14: *Dependence of $\bar{v}$ on the dissipation for $\Phi = 2.25$ and $\epsilon = 0$: $e_n = 0.4(\bigcirc)$, $0.5(\square)$, $0.6(\diamond)$, $0.8(\triangle)$.*

lose the normal velocity the ball had at $-\gamma_{\max}$. The reason for the slight decrease of $\bar{v}_x$ with increasing e_n is the fact that it is energetically more advantageous to lose all v_n with respect to a certain sphere on the line early on, and then only gain v_t. The reason is that in collisions part of the v_x gained in free flight adds to the normal velocity (at least for $\gamma < 0$), which leads to slightly increased dissipation with respect to the case of immediate loss of all v_n at $-\gamma_{\max}$. This increase of dissipation due to a larger number of impacts gets stronger for $\Phi \to 1$.

For θ_{BC}, the value of e_n is important. Since the motion of the ball starts to get unstable when the motion is no longer regular, one would expect the destabilization to start when the normal velocity at $-\gamma_{\max}$ with respect to one ball cannot be lost by the time $\gamma_{\max}$ is reached. But e_n, which determines the energy loss in a collision and thus the height (and thereby the length) of the next jump, together with $\bar{v}_x$ determines how many jumps are made on each ball on the line. It thus gives an upper limit to the maximum amount of energy that can be dissipated on a single ball on the line. The smaller e_n, the more energy is dissipated in each jump, and the more jumps are possible, as their length decreases. Thus, θ_{BC} shifts to larger θ for a given Φ with decreasing e_n and approaches the static angle of stability, which in the 2D case is given by $\gamma_{\max}$.

4.2.4.2 Influence of the friction coefficient and rotation on the motion

If the ball is allowed to rotate, as in all the simulations presented so far, the value of the friction coefficient μ is even less important for the behaviour of the ball than e_n (see Fig. 4.15). μ influences neither $\bar{v}_x$ nor the mean rotational velocity $\bar{\omega}$ significantly. It also does not change the phase boundaries. The reason for this is that for the range of θ considered here, the ball can be expected to roll without slipping most of the time independently of μ if the implementation of the tangential force law correctly reproduces Coulomb's law for sliding friction. Let us assume for a moment that the ball, while moving down the line, is always in contact with the balls on this line, which is only possible if $e_n = 0$. It would then roll without slipping if at all γ the condition $|F_s| \leq \mu |F_n|$ were

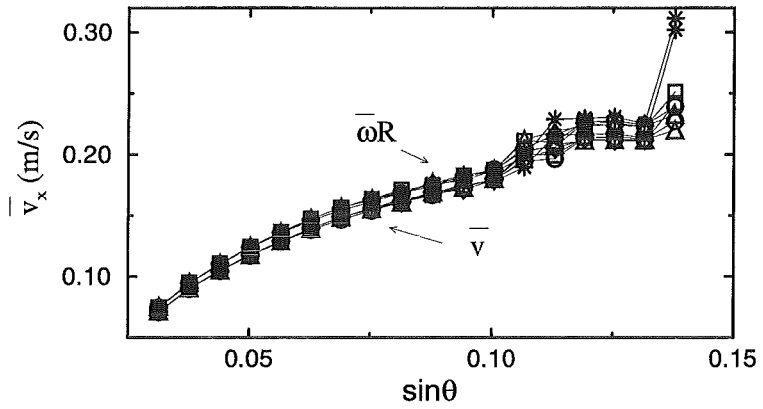

Figure 4.15: *Dependence of $\bar{v}$ and $\bar{\omega}R$ on the friction coefficient μ: μ = 0.1(○), 0.3(□), 0.5(◇), 0.7(△), 1.0(⋆).*

fulfilled. For a rolling sphere under the action of gravity [243],

$$|F_s| = \frac{2}{7}|\vec{g} \cdot \vec{s}| \tag{4.22}$$

so that the criterion for μ for the ball to roll without slipping according to eq. (3.23) reads

$$\mu > \frac{2}{7}|\tan(\theta + \gamma)|. \tag{4.23}$$

Though close to $\gamma_{\max}$ this condition is usually not fulfilled (the smaller Φ, the larger the region of γ for which slip can occur), it holds on the largest part of a ball on the line even for small μ. It is thus to be assumed that the ball on average rolls without slipping in the case of $e_n = 0$, even for small values of the friction coefficient μ.

In the simulations, however, larger values for e_n were used, like $e_n = 0.7$ in Fig. 4.15, so there the ball rather bounced than rolled down the line. But the distances the ball covers between bounces in the steady state are very small. In the simulations it is found that the ball, which is launched onto the plane without rotational velocity, soon picks up rotation during impacts, such that when the steady state is reached, the rotational velocity has adjusted itself to a value which on average leads to zero relative velocity of the surfaces of the moving ball and the fixed balls (except close to $\gamma_{\max}$, just as would be expected from eq. (4.23)). In the free flight between collisions, the ball picks up translational velocity while the rotational velocity remains unchanged. The moving ball has thus gained excess shear velocity, which is converted nearly completely into rotation in the next impact, if it was small enough. This is usually the case in the steady state, where distances covered between bounces are small.

If the ball is prevented from rotating (by applying the tangential force not as an angular momentum at the contact point, but as a force at the center of mass), but the same friction force maintained (as in the stochastic model [246]), the picture changes. Obviously, as is to be expected, the tangential friction force implemented in the simulation now has a strong influence on the total friction force, as is shown in Fig. 4.16. If friction is included, but rotation suppressed, the velocity curves shift towards larger θ. The solid friction force arising from the tangential force implemented in the simulation thus provides a velocity-independent background, on top of which the velocity-dependent friction force due to the

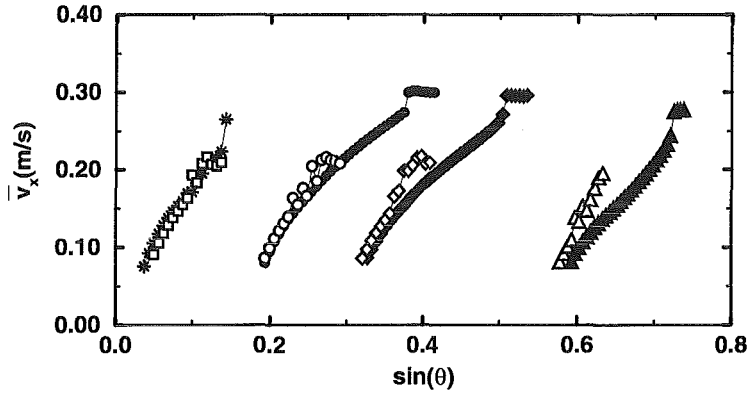

Figure 4.16: *Mean velocity of the sphere without rotation for motion on an inclined line (distances between balls on the line randomly distributed in the interval [2r,2.2r], $\Phi = 2.25$) for $\mu = 0$ (squares), $\mu = 0.13$ (circles), $\mu = 0.25$ (diamonds) and $\mu = 0.53$ (triangles); open symbols correspond to $e_n = 0.7$, full symbols to $e_n = 0.3$. For comparison, also a simulation including rotation for $e_n = 0.7$ and $\mu = 0.13$ is shown as well ($\star$).*

normal dissipation is added. For small μ, e_n again only influences the size of the steady state region, but not the mean velocity. For higher μ, $\bar{v}_x$ has a small dependence on e_n, but it is not clear if this is directly due to the Coulomb friction force or only indirectly, because the solid friction force shifts the steady state region to quite high inclination angles (for $\mu = 0.53$ even close to 45°).

The independence of $\bar{v}_x$ of e_n even when the ball cannot rotate and therefore experiences an additional friction force is somewhat surprising. In a collision, the dissipated kinetic energy ΔE_t related to frictional loss in v_t according to eq. (4.9) is given by

$$\Delta E_t = \frac{1}{2} m \Delta v_t^2 = \frac{1}{2} m \mu^2 (1 + e_n)^2 v_n^2, \tag{4.24}$$

which is independent of v_t. By contrast, in a lasting contact the dissipation rate due to friction dE_t/dt is

$$dE_t/dt = \mu F_n v_t = \mu g \cos(\gamma + \theta) v_t \tag{4.25}$$

in the case of a sphere sliding on a ball on the plane. Though it is clear qualitatively that the lower collisional losses due to eq. (4.24) for smaller e_n are made up for by the earlier onset of rolling, and therefore by a larger contribution from eq. (4.25), it is not clear why these differences should balance to give the same amount of dissipation for different e_n.

4.2.5 A theoretical model for the steady state velocity

4.2.5.1 Exact calculation of the mean velocity for $e_n = 0$

Since $\bar{v}_x$ hardly depends on e_n, it is tempting to investigate the limiting case $e_n = 0$. As in the case where the ball is allowed to rotate, due to friction the ball is able to sustain

$v_s = 0$ on average (*i.e.* the ball would roll without slipping in the case $e_n = 0$ for large μ), in the following the limiting case $e_n = 0$, $\mu \to \infty$ is investigated. From these assumptions, a very accurate result for $\bar{v}_x$ can be deduced.

It is assumed that the moving ball is always in contact with the fixed balls, i.e. rolls down the line without slipping. Thus at all times,

$$|\vec{v}| = v_t = \vec{v} \cdot \vec{s}, \tag{4.26}$$

$$v_n = 0, \tag{4.27}$$

$$\omega R = v_t. \tag{4.28}$$

From these conditions the equation of motion of the ball on a single ball on the line from $-\gamma_{\max}$ to $\gamma_{\max}$ can be derived. The kinetic energy of the ball is

$$E_{\text{kin}} = \frac{1}{2} m v_t^2 + \frac{1}{2} I \omega^2 \tag{4.29}$$

where I denotes the moment of inertia of the moving particle. Using condition (4.28) and defining an effective mass $m_{\text{eff}} = m(1 + I/(m\,R^2))$, this gives

$$E_{\text{kin}} = \frac{1}{2} m_{\text{eff}} v_t^2. \tag{4.30}$$

For a solid sphere, $m_{\text{eff}} = \frac{7}{5} m$. The potential energy depends on the location of the moving ball on the line ball:

$$E_{\text{pot}} = mg(R + r)\cos(\gamma + \theta). \tag{4.31}$$

Since $v_t = (R + r)\dot{\gamma}$, the energy balance reads (denoting the energies at the start of the motion by E^0_{kin} and E^0_{pot})

$$E^0_{\text{kin}} - \frac{1}{2} m_{\text{eff}} (R + r)^2 \dot{\gamma}^2 = mg(R + r)\cos(\gamma + \theta) - E^0_{\text{pot}}. \tag{4.32}$$

Differentiating with respect to time yields the equation of motion for $\gamma(t)$

$$\ddot{\gamma} = \frac{m}{m_{\text{eff}}} \frac{g}{R + r} \sin(\gamma + \theta). \tag{4.33}$$

The completely inelastic collision at $-\gamma_{\max}$ that occurs when the moving ball passes from one ball on the line to the next one defines the boundary conditions for the problem. The velocity of the ball at $\gamma_{\max}$ is denoted by $v_t(\gamma_{\max}) = v_i$. Since rolling without slipping is assumed, on this ball on the line

$$v_i = \omega_i R \tag{4.34}$$

with $\omega_i = \omega(\gamma_{\max})$. In the next instant, the moving ball hits the next ball on the line at $-\gamma_{\max}$, with the tangential velocity $v_t(-\gamma_{\max})$, which with respect to this ball is (due to the change in geometry)

$$v_t(-\gamma_{\max}) = v_i \cos(2\gamma_{\max}). \tag{4.35}$$

In the collision that is now about to take place, the normal component

$$v_n(-\gamma_{\max}) = v_i \sin(2\gamma_{\max}) \tag{4.36}$$

is reduced to zero, but this is not the whole effect of the collision. Since v_t dropped *before* the impact due to the change in geometry, but ω was left unaffected, at $-\gamma_{\max}$, there is excess rotational velocity and thus excess shear velocity v_s. If the frictional force is high enough (which is assumed in this treatment), then the shear velocity at the point of contact should again be reduced to zero during the impact, such that tangential and rotational velocity *after* the impact at $-\gamma_{\max}$, which are denoted by v_f and ω_f respectively, fulfill the condition

$$v_f = \omega_f R. \tag{4.37}$$

During the impact at $-\gamma_{\max}$ the rotational and translational velocities thus adjust themselves, with only negligible energy loss (friction here mainly helps to distribute the excess rotational velocity to the translational degree of freedom, but, as the ball can rotate freely, dissipates only very little energy during the adjustment). Before the adjustment of rotational and translational velocities, the kinetic energy of the system was

$$E_{\text{kin}} = \frac{1}{2} m v_i^2 \cos^2(2\gamma_{\max}) + \frac{1}{2} I \omega_i^2 \tag{4.38}$$

With eqs. (4.30) and (4.37) one thus obtains from the energy balance the condition for v_f

$$\frac{1}{2} m v_i^2 \cos^2(2\gamma_{\max}) + \frac{1}{2} I \omega_i^2 = \frac{1}{2} m_{\text{eff}} v_f^2. \tag{4.39}$$

Substituting ω_i according to eq. (4.34) gives

$$v_f = v_i \sqrt{1 - \frac{m}{m_{\text{eff}}} \sin^2(2\gamma_{\max})} \tag{4.40}$$

for the tangential velocity after the collision at $-\gamma_{\max}$. Since $v_t = (R + r)\dot{\gamma}$, this provides the boundary condition for eq. (4.33).

There are now two possibilities to obtain $\bar{v}_x$. One consists in numerically integrating the equation of motion eq. (4.33) with the boundary condition (4.40), as done in [247], the other makes use of the energy balance eq. (4.32) [253]. The second possibility actually provides an analytic expression for $\bar{v}_x$, though in terms of an elliptic integral. This second possibility will be discussed in the following. To this end, let us turn back to the energy balance eq. (4.32). By setting

$$E_{\text{kin}}^0 = \frac{1}{2} m_{\text{eff}} (R + r)^2 \dot{\gamma}^2(\gamma_{\max}) \tag{4.41}$$

and

$$E_{\text{pot}}^0 = mg(R + r)\cos(\theta + \gamma_{\max}), \tag{4.42}$$

the values right before the impact with the next ball in the line, and by using the fact that in the steady state

$$\dot{\gamma}(-\gamma_{\max}) = e_t \dot{\gamma}(\gamma_{\max}) \tag{4.43}$$

with

$$e_t = \sqrt{1 - \frac{m}{m_{\text{eff}}} \sin^2(2\gamma_{\max})}, \tag{4.44}$$

from eq. (4.32) the velocity right before the collision with the next ball $\dot{\gamma}(\gamma_{\max})$ in the steady state

$$\dot{\gamma}^2(\gamma_{\max}) = \frac{g}{R + r} \frac{\sqrt{c}}{c(1 - c)} \sin\theta \tag{4.45}$$

is obtained, where $c = \sin^2\gamma_{\max}$. Substituting this into eq. (4.32), the instantaneous velocity $\dot{\gamma}$ is given by

$$\dot{\gamma}^2(\gamma) = 2\frac{m}{m_{\text{eff}}}\frac{g}{R+r}\left[\frac{m_{\text{eff}}}{2m}\frac{\sin\theta}{\sqrt{c}(1-c)} - \cos(\theta+\gamma) + \cos(\theta+\gamma_{\max})\right]. \tag{4.46}$$

The mean velocity in the steady state is

$$\bar{v}_x = \frac{2(R+r)\gamma_{\max}}{T}, \tag{4.47}$$

where T is the time needed to pass a ball on the line, i.e.

$$T = \int_{-\gamma_{\max}}^{\gamma_{\max}} \dot{\gamma}^{-1} d\gamma. \tag{4.48}$$

With the use of eq. (4.46), this yields

$$T = a\int_{\theta-\gamma_{\max}}^{\theta+\gamma_{\max}} \frac{d\gamma}{\sqrt{b-\cos\gamma}} \tag{4.49}$$

with the characteristic time

$$a = \left(\frac{2m}{m_{\text{eff}}}\frac{g}{R+r}\right)^{-1/2} \tag{4.50}$$

and the dimensionless constant

$$b = \frac{m_{\text{eff}}}{2m}\frac{\sin\theta}{\sqrt{c}(1-c)} + \cos(\theta+\gamma_{\max}). \tag{4.51}$$

The integral in eq. (4.49) is an elliptic integral of the first kind and cannot be solved in closed form. Figure 4.17 shows a comparison of the numerical solution of eq. (4.49) with simulation data for various coefficients of restitution and various size ratios Φ. Clearly, the simulation for small e_n is closest to the theoretical curve (which assumes $e_n = 0$), but also for higher e_n the approximation is still good.

For the case $\epsilon > 0$ eq. (4.47) yields equally good results as in the case $\epsilon = 0$ presented in Fig. 4.17. In the case of a disordered line, an estimation of $\bar{v}_x$ with the value of $\gamma_{\max}$ chosen according to the mean value $\bar{\epsilon}$ of the spacings ϵ, i.e.

$$\bar{\gamma}_{\max} = \arcsin\left(\frac{1+\bar{\epsilon}}{1+\Phi}\right), \tag{4.52}$$

fits the simulation results equally well. This is illustrated in Fig. 4.18 for $\Phi = 3$.

Ancey *et al.* [265] at the same time approached the problem in a similar way as discussed here. They, however, neglect the effect of the rotational velocity in the impact at $-\gamma_{\max}$, though rotation is explicitly included in their equation of motion. They thus have to introduce a fitting parameter to match their curves to experimental data. This is not necessary if the influence of rotation is included in the boundary conditions of the problem, as was shown here. They even go so far as to postulate that the necessity of introducing this fitting parameter shows that the usual treatment of collisions must be wrong. It has to be emphasized that eqs. (4.33) and (4.40) hold for the *instantaneous* velocity only in the case of vanishing normal restitution and perfectly rough surfaces, conditions which are not likely to be fulfilled by any commonly used material. However, as shown here, the *mean* velocity of the ball is not influenced by the coefficients of restitution and friction and thus is correctly described.

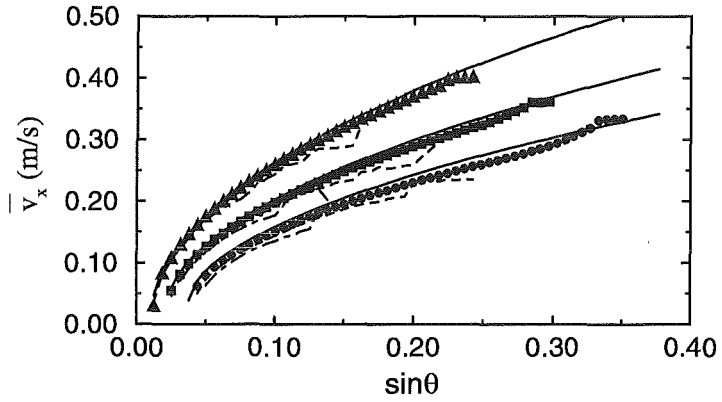

Figure 4.17: *Theoretical prediction of $\bar{v}_x$ (solid lines) for $\epsilon = 0$ under assumption of $e_n = 0$ and simulation data for $e_n = 0.1$ and size ratios Φ =1.75 (circles), 2.25 (squares), 3.0 (triangles). The dashed and dot-dashed lines also show the corresponding simulation data for $e_n = 0.5$ and 0.7 respectively.*

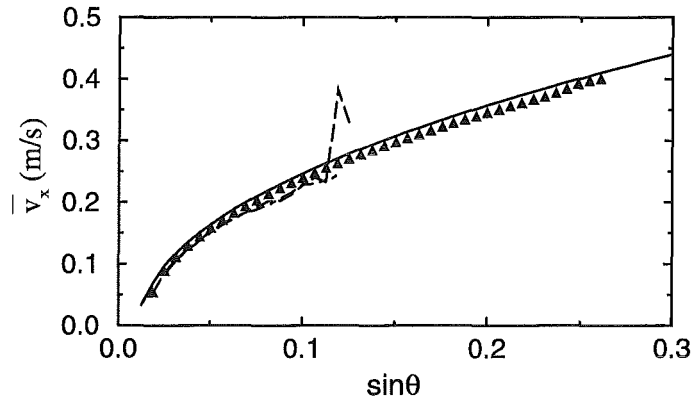

Figure 4.18: *Comparison of the analytical results for $\bar{\epsilon} = 0.1$ with simulation results for $e_n = 0.1$ (triangles) and $e_n = 0.7$ (dot-dashed line) on a disordered line with $\epsilon_{\max} = 0.2$ and simulation results for $e_n = 0.7$ and an ordered line with $\epsilon = 0.1$ (dashed line).*

4.2.5.2 Linearization of the full calculation

At the beginning of this Section, when presenting simulation results, it was shown that $\bar{v}_x^2$ seemed to depend linearly on $\sin\theta$. Though, as is clear from eq. (4.49), this is not the exact result, it can be found from the first order approximation of the elliptic integral in eq. (4.49).

To this end, first the constant b [eq. (4.51)] is expanded in $c = \sin^2\gamma_{\max}$ for fixed inclination angle θ:

$$b - \cos\theta = \sin\theta\left(\frac{m_{\text{eff}}}{2m}\frac{1}{\sqrt{c}\,(1-c)} - \sqrt{c}\right) + \cos\theta(\sqrt{1-c} - 1)$$

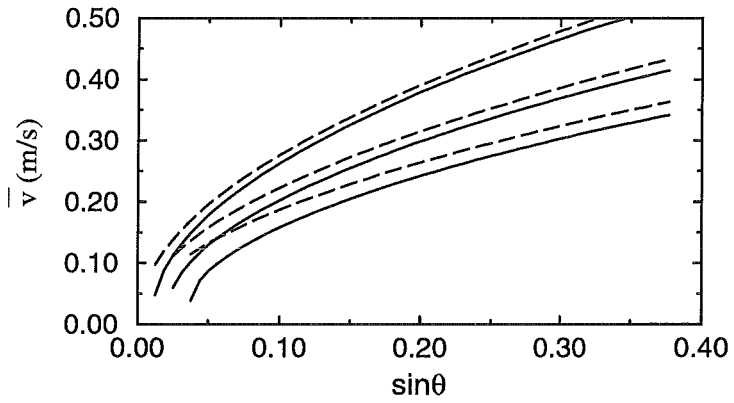

Figure 4.19: *Comparison of eq. (4.55) (dashed lines) to the exact results (full lines) for $\Phi = 3$, 2.25 and 1.75 (from top to bottom).*

$$= \sin\theta \left(\frac{m_{\text{eff}}}{2m} \frac{1}{\sqrt{c}} + \left(\frac{m_{\text{eff}}}{2m} - 1 \right) \sqrt{c} \right) + \mathrm{O}(c). \tag{4.53}$$

In leading order the passage time T [eq. (4.49)] can be approximated by

$$T = 2a\gamma_{\max}/\sqrt{b - \cos\theta}\,(1 + \mathrm{O}(c^{3/2})), \tag{4.54}$$

which, inserting the result (4.53), yields for the mean velocity

$$\bar{v}_x \approx \sqrt{rg \left(\frac{1}{\sin^2 \gamma_{\max}} + 1 - \frac{2m}{m_{\text{eff}}} \right) \sqrt{\sin\theta}} + \mathrm{O}(\sqrt{c}). \tag{4.55}$$

This gives the desired linear dependence of $\bar{v}_x^2$ on $\sin\theta$. The offset vanishes for $\Phi \to \infty$. In Fig. 4.19 eq. (4.55) is compared to the exact result obtained from eq. (4.49). It is obvious that the larger Φ, the better the approximation. The vanishing of the offset in eq. (4.55) for increasing Φ is also clearly visible.

4.2.5.3 Calculation of θ_{AB}

Another result that can be obtained from this theoretical treatment is the phase boundary θ_{AB}. One may assume that the phase boundary θ_{AB} is reached when the moving ball arrives at the angle $\gamma = -\theta$ with zero velocity, since from there it can roll down simply by the action of gravity, even with zero starting velocity. For smaller inclination angles, the ball would roll back before reaching this point and thus stop, for larger inclination angles it would pass this point with some velocity and move on.

As a matter of fact, this angle is the one for which the integral in eq. (4.49) diverges, i.e. for which $b = 1$. However, this only holds for a line with equally spaced balls. For a line with disorder, both the mean and the maximum spacing determine θ_{AB}. While the mean spacing determines the mean velocity, the maximum spacing determines whether this velocity suffices to help the ball out of even the largest "traps" into which it might fall. To give a general derivation of θ_{AB} both for lines with ordered and disordered arrays

of particles, a different road than in [253] will be taken here. The following treatment is a generalization of the argument presented in [247].

Assume that the particle is moving at its steady state velocity and encountering the largest spacing between two balls. Its velocity at $\gamma_{\max}$ is, according to eq. (4.46), given by

$$\dot{\gamma}^2(\gamma_{\max}) = 2\frac{m}{m_{\text{eff}}}\frac{g}{R+r}\left[\frac{m_{\text{eff}}}{2m}\frac{\sin\theta}{\sqrt{\bar{c}}\,(1-\bar{c})} - \cos(\theta+\gamma_{\max}) + \cos(\theta+\bar{\gamma}_{\max})\right] \tag{4.56}$$

with $\bar{c} = \sin^2\bar{\gamma}_{\max}$. Inserting the conditions $\gamma = -\theta_{AB}$ and $\dot{\gamma}(-\theta_{AB}) = 0$ in eq. (4.32) gives

$$e_m^2\dot{\gamma}^2(\gamma_{\max}) = \frac{2m}{m_{\text{eff}}}\frac{g}{R+r}\left(1-\cos(\theta_{AB}-\gamma_{\max})\right), \tag{4.57}$$

with $e_m^2 = 1 - 4\frac{m}{m_{\text{eff}}}c\,(1-c)$, where $c = \sin^2\gamma_{\max}$.

Substituting eq. (4.56) in eq. (4.57), this gives after some manipulation

$$\begin{aligned}\left(\frac{m_{\text{eff}}}{2m}\frac{e_m^2}{\sqrt{\bar{c}}\,(1-\bar{c})} + e_m^2(\sqrt{c}-\sqrt{\bar{c}}) + \sqrt{c}\right)\sin\theta_{AB} \\ + \left(e_m^2(\sqrt{1-\bar{c}}-\sqrt{1-c}) + \sqrt{1-c}\right)\cos\theta_{AB} \;=\; 1.\end{aligned} \tag{4.58}$$

This equation for θ_{AB} can be solved using the fact that

$$a\sin\theta + b\cos\theta = \sqrt{a^2+b^2}\sin\left(\theta + \arctan\frac{b}{a}\right). \tag{4.59}$$

With

$$a = \frac{m_{\text{eff}}}{2m}\frac{e_m^2}{\sqrt{\bar{c}}\,(1-\bar{c})} + e_m^2(\sqrt{c}-\sqrt{\bar{c}}) + \sqrt{c} \tag{4.60}$$

and

$$b = e_m^2(\sqrt{1-\bar{c}}-\sqrt{1-c}) + \sqrt{1-c} \tag{4.61}$$

this yields

$$\theta_{AB} = \arcsin\frac{1}{\sqrt{a^2+b^2}} - \arctan\frac{b}{a}. \tag{4.62}$$

In the case $\bar{\gamma}_{\max} \neq \gamma_{\max}$, i.e. for a line with disorder, this is a very cumbersome expression, however, in the case of a line with equally spaced balls, i.e. $\bar{c} = c$, it reduces to

$$\theta_{AB} = \arcsin\left(\frac{1}{\sqrt{a^2+1-c}}\right) - \arctan\left(\frac{\sqrt{1-c}}{a}\right) \tag{4.63}$$

with

$$a = \left(\frac{m_{\text{eff}}}{2m}\frac{1}{c\,(1-c)} - 1\right)\sqrt{c}. \tag{4.64}$$

This is the same result as derived in [253] with the assumption that θ_{AB} is determined by the inclination angle where the integral in eq. (4.49) diverges.

Fig. 4.20 shows a comparison of this result to simulation data, both for a simulation on a line with spheres touching and for a simulation with disorder and $\epsilon_{\max} = 0.2$. Obviously, the theoretical result approximates the simulation results best for larger Φ. For Φ close to 1 the deviations get quite large. The reason might be that here, a number of successive impacts are more dissipative than a single impact for $e_n = 0$, even for $e_n = 0.1$, due to the strong curvature of the surface. In any case, eq. (4.62) provides a lower limit for the value of θ_{AB}.

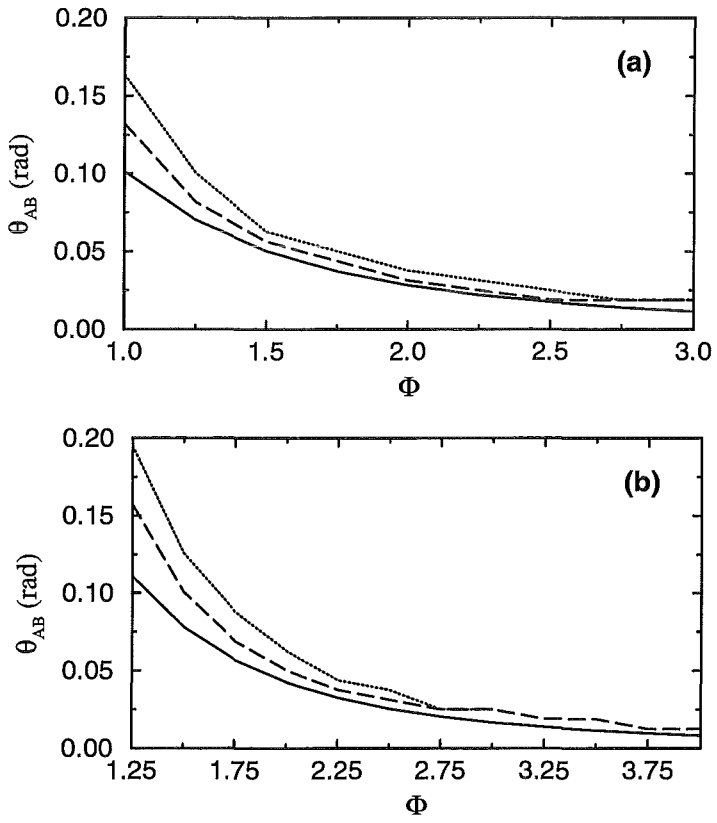

Figure 4.20: *The phase boundary* θ_{AB} *for* $e_n = 0.7$ *(dotted line),* $e_n = 0.1$ *(dashed line) and the theoretical result from eq. (4.62) for* $e_n = 0$ *(solid line). (a) ordered array,* $\epsilon = 0$*, (b) disordered array,* $\epsilon_{\max} = 0.2$*.*

4.2.6 Transients and motion far from the steady state

Though it has become very clear by now what happens in the steady state, i.e. when the motion of the particle is ruled by correlations between successive bounces, nothing has been said so far about the characteristics of the motion during the transient towards the steady state (or stopping in region A), or about the motion in region C. Here, I only want to outline briefly some characteristics of this motion, though mainly on a heuristic and very qualitative level.

Imagine a sphere dropped on the plane with a relatively high starting velocity. Let us further assume that the tangential coefficient of restitution $e_t = 1$, i.e. that all dissipation comes from the normal component of the velocity (though this might not be fulfilled as well as in the steady state). Since $v_n = v_x \sin\gamma + v_z \cos\gamma$, most of the velocity loss comes about through v_z and not through v_x. Though certainly according to the collision matrix (4.12) collisions at $\gamma < 0$ transfer part of v_x to v_z, while those at $\gamma > 0$ transfer part of v_z to v_x, on average this effect should cancel if successive bounces are uncorrelated and if all γ are equally likely to be hit.[5] So the effect of a collision is on average a larger loss of v_z

[5] Certainly this can only hold if there is no large change in v_x during the time of flight between successive collisions – a condition that for very large plane inclinations is not likely to be fulfilled.

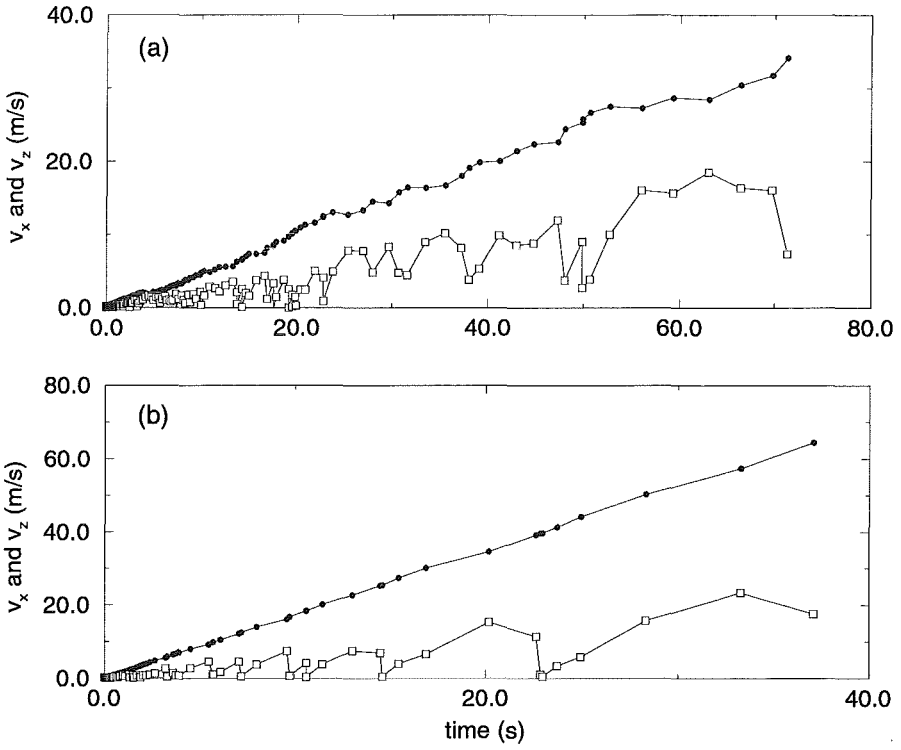

Figure 4.21: *Impact velocities v_x (●) and v_z (□) as a function of time in regime C for $\Phi = 3$, $\epsilon = 0$, $e_n = 0.7$, $\mu = 0.13$, $\beta = 0.34$ (Walton collision model) and (a) $\sin\theta = 0.15$ (b) $\sin\theta = 0.3$.*

than v_x. If successive collisions are uncorrelated, and distances flown between collisions are reasonably large, so that the roughness of the plane can be neglected, the time of flight τ can be approximated by $\tau = 2v_z/g\cos\theta$ as in the stochastic model for impacts with $\gamma < 0$. At the end of this time of flight, v_z is back at the value it had when the free flight started, while v_x has grown by an amount $\Delta v_x = 2v_z \tan\theta$.

The net effect of a number of uncorrelated collisions of the ball with the plane is thus a decrease in v_z, while v_x may decrease or increase, but in any case will decrease more slowly than v_z. One might also say that the bouncing sphere on average sees the general direction of the plane, and loses velocity normal to it, while it loses far less in the direction tangential to the plane. Energetically, it would be most advantageous for the particle to move parallel to the plane, as it might on a macroscopically smooth plane, because in this case it would not collide with the plane and therefore lose no energy. On the bumpy plane, this is impossible. In the scenario described above, at some point $v_z/v_x \leq \tan\gamma_{\max}$, i.e. some angles of the interval $[-\gamma_{\max}, \gamma_{\max}]$ are not accessible to the ball in collisions any more. The consequences are that the geometry of the system now favours impacts for $\gamma < 0$ and closer to the top of balls, and that the time of flight may depend on the starting point of the free flight, because a ball on the plane might get in the way of the flight trajectory.

Now, depending on whether we are in regime A, B or C, different things may happen. In regime B, as we have seen, the ball enters into a very regular motion, and instead of

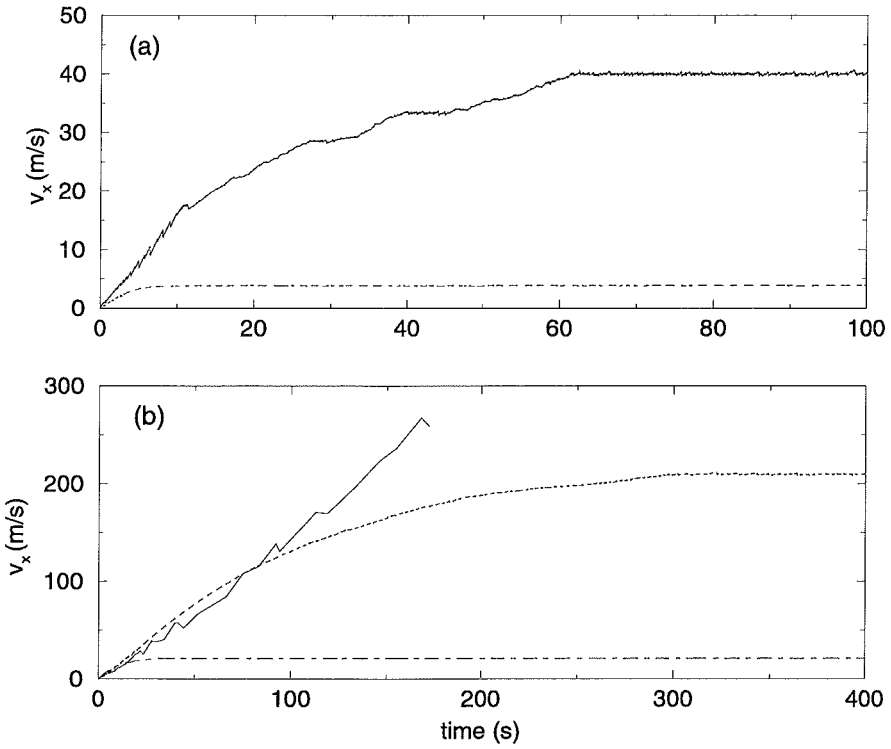

Figure 4.22: *Evolution of v_x for different force laws and spring constants for $\Phi = 2.25$ and $\sin\theta = 0.3$. (a) Forces as used by Ristow et al. [264], same parameters as in [264], but for $k_n = 10^6 kg\, m^{1/2}/s^2$ (dashed line) and $k_n = 10^7 kg\, m^{1/2}/s^2$ (solid line). (b) Linear force as used throughout my simulations for $e_n = 0.7$, with $k_n = 10^4 Nm$ (dot-dashed line) and $k_n = 10^6 Nm$ (solid line). For comparison, a result from ED simulations for the same material parameters as in Fig. 4.21 is shown as well (solid line).*

adjusting its velocity to the direction of the plane in general, adjusts the direction of its velocity to the surface of each bump it crosses. In regime A, the behaviour is very similar, however, the dissipation in crossing over the surface asperities is too strong to be made up for by the gain in potential energy, so the ball finally stops when its velocity is too small to cross over another asperity [263]. In regime C, things are different. Figure 4.21 shows the evolution of v_x and v_z in region C in successive collisions as obtained with ED simulations (the reason for using ED in this case will be discussed in a moment). The symbols denote the velocity at the time of each collision. The starting velocities were very low, in the range of typical steady state velocities. It is obvious from this figure that though both v_x and v_z increase on average, there is a repeated increase and decrease of v_z. v_z decreases in the way described above until collisions get so oblique that in an impact at some $\gamma < 0$ a transfer of a significant amount of v_x to v_z is accomplished. The main difference between a transient in regime A or B and the acceleration regime C is that during the following time of flight the gained v_x in regime C is larger than the previous loss in the collision, while in regime A or B it is smaller than this loss.

As mentioned in Section 4.1.2., Ristow *et al.* [264] claim that the accelerating regime is

only a transient state, and that finally, a steady state is reached in region C as well, though with a mean velocity two orders of magnitude higher than in region B. This observation is entirely due to the brake failure effect described in Section 2.1.2 and the resulting "emergency brake". Changing the spring constant in the simulations also changes the terminal velocity in this region, i.e. the existence of a steady state in region C is a numerical artifact. Figure 4.22 shows this effect for the linear force law used in my simulations and for the force law used in the simulations performed by Ristow *et al.* for different spring constants. The reason for the use of the ED method for the simulation of the motion in region C now becomes clear as well. Though certainly ED is far more economic as far as computing time is concerned if the motion consists mainly of large bounces, its most important advantage is the absence of the brake failure effect. However, it is not suitable for simulating the motion in region A or B if no measures are taken to deal with the inelastic collapse inevitably occurring in these regimes using traditional ED.

4.2.7 Summary of the 2D case

Before entering into the discussion of the three dimensional case of a sphere moving down a plane, it seems appropriate to sum up the numerous results of the two dimensional case. The most important finding is certainly that the motion of the ball in the steady state is very regular and consists of a series of small bounces on *each* ball on the line, contrary to what so far had been assumed [246, 264]. In the course of these bounces the moving ball loses all relative normal velocity with respect to this ball. This dissipation mechanism holds both for lines with equally spaced balls and for lines with a random distribution of balls. Furthermore, the location of these bounces is the same on each ball in the case of a constant spacing between balls on the line. A random spacing of the balls on the line only smears out these locations a bit, but does not alter the motion significantly. Thus, the velocity of the ball in the case of a random spacing of balls on the line can be approximated by the motion of the ball on an ordered line with appropriate spacing. The main reason for this regularity of the motion is that the moving ball has to climb over the top of every ball forming the line by a few bounces in the steady state. Since disorder only slightly changes the height to be climbed, it has only a small influence on the motion.

Another important result, which is due to the fact that there are always a number of collisions of the moving sphere with each ball on the line that it passes, is that material properties like the normal coefficient of restitution e_n and the Coulomb friction coefficient μ hardly influence the mean velocity $\bar{v}_x$ in the steady state. This result and the knowledge of the mechanism stabilizing the motion of the ball allows to predict $\bar{v}_x$ theoretically under the assumption of completely inelastic collisions. Only geometrical considerations suffice for this treatment and give a very good approximation to the simulation results. The results in this extreme case also allow the calculation of a lower limit for the phase boundary θ_{AB}, which for large Φ gives a good approximation of θ_{AB} regardless of the value of the coefficient of restitution. This result can be relevant to the problem of segregation in the flow on inclined planes or in rotating drums.

Still, some open questions remain, even in the 2D case. Since the phase boundary θ_{BC}, which separates steady motion of the ball from the accelerating regime, depends on e_n, it cannot be derived directly from the theoretical treatment for $e_n = 0$. Besides, for size ratios

$\Phi \to 1$, or rather $\gamma_{\max} \to 0.5$, e_n starts to have an influence on $\bar{v}_x$ and θ_{AB}. This is due to the fact that the more curved the surface over which the particle moves, the less valid the approximation that all normal velocity is lost in the first collision with a bead. Instead, a number of collisions on the uphill facing side of a bead is more dissipative, since some of the velocity gained during the free flight is normal velocity in the ensuing collisions and therefore dissipated additionally. Another question that remains unanswered is why in the angle region where the behaviour of the ball depends on the starting velocity (i.e. where the starting velocity decides whether the ball reaches a steady state or accelerates), the mean velocity remains at a constant level independently of the inclination angle.

The central question to be addressed in the three dimensional simulation is whether this mechanism for keeping a constant velocity still holds in 3D, where there is a number of ways for the ball to choose to go down the plane. In the 3D case one would expect the motion to be ruled by a competition between static equilibrium (or non-equilibrium) of the ball on the plane and the preferential direction given by the plane inclination and inertia of the moving ball. One might argue that introducing stronger disorder in the 2D case, for example by using polydisperse balls on the line, would model a longitudinal section of the plane much closer. But this will not eliminate the strong dimensional difference between the 2D and 3D cases. In 3D, the moving ball, hitting a ball on the plane a little on the side (which would be one of the smaller balls in the 2D section), would be deflected towards the side, which in 2D is impossible. In the constant velocity regime in 2D on a line with size polydispersity, the moving ball will again lock into some kind of quasiperiodic behaviour for the same reasons as explained above. The problem of having to overcome some maximum threshold (to get out of the deepest valley between two balls on the line) to keep moving is even stronger, contrary to the 3D case. There a ball, having suffered a large impact which brakes it a lot, might still find some way around the bump that braked it and accelerate until the next impact via some statically unstable path. Thus, the motion in 3D is expected to be more irregular than can be modeled in 2D.

The regularity of the motion in 2D is incompatible with the two dimensional stochastic model presented in Section 4.1.3. However, since it gives a linear dependence of $\bar{v}_x$ in $\sin\theta$, as was observed in 3D experiments, the question remains to be addressed whether it describes the stronger randomness in 3D accurately.

4.3 The 3D case

As we have seen, the two dimensional case shows a number of properties which seem to be strongly related to the dimensionality of the system. In addition, the simulations showed no indications of a mean velocity *linear* in $\sin\theta$, as was to be expected from the 2D experiments. Therefore, the three dimensional case also has to be investigated to check if the simulations will yield $\bar{v}_x \propto \sin\theta$ and to find possible reasons. The main difference between the two dimensional and three dimensional cases is the fact that in 3D the ball has an additional degree of freedom. It can (and does) move into the direction perpendicular to the inclination of the plane, due to oblique impacts with balls on the plane. This leads to increased dissipation of energy compared to 2D, since transverse motion "drains" the particle of a part of v_x, as transverse motion is only dissipative. Though certainly v_y can be transferred back to v_x, this only means giving back part of what previously had been

lost, so there is only net dissipation due to the additional degree of freedom. But why this increase should lead to $\bar{v}_x \propto \sin\theta$ is still unclear.

It is thus necessary to investigate the fluctuations of the motion more closely, since they seem to be the key difference between 2D and 3D. Indeed, the argument leading to $\bar{v}_x \sim \sqrt{\sin\theta}$ disregards fluctuations. These can be neglected in 2D, due to the regularity of the motion. In 3D, they should be of greater importance. Recent experimental efforts have thus concentrated on the measurement of the dispersion properties of the plane, i.e., on the measurement of diffusion coefficients and their dependence on Φ and θ [261], as briefly described in Section 4.1.1. The simulation results obtained in the 3D case will be compared to the experimental results of Samson *et al.* [260, 261].

4.3.1 Simulation method and preparation of the plane

The system is modeled by TD simulations, the forces are the same as in the 2D case, but in the general three dimensional geometry described in Section 2.1.1. In all simulations of the 3D case presented here the parameters $k_n = 2 \times 10^5$ N/m, $\gamma_s = 1000$ kg/s, $\mu = 0.13$, $r = 0.5$ mm and $M = \frac{4}{3}\pi R^3 \rho$ for the mass of the rolling ball with $\rho = 7.8$ g/cm^3 were used. The values of these parameters were chosen to match the steel balls used in [256, 260, 261, 264] and the size of the glass beads glued onto the inclined plane [261]; the choice of k_n leads to a collision time of the order of 10^{-5} s. For the choice of γ_s, which is mainly a technical parameter, see Chapter 3. The coefficient of restitution was varied in the range $0.4 \leq e_n \leq 0.8$.

The main problem in the 3D simulation, if it is to be compared with experiments, lies in producing a plane with similar density *and* disorder as in experiments, especially as *disorder* cannot be easily quantified. In the experiments the rough plane was produced by placing a sheet of contact paper on a glass plate, and then spreading glass beads onto it slowly moving from one edge of the plane to the other. This gave area fractions of glued beads in a range from 0.68 to 0.74. Algorithms designed to produce random 2-dimensional packings, like for example the random sequential adsorption (RSA) model [258] or more refined versions of it, cannot reach such a high density. Attempts to create a packing of higher compactivity by compressing a granular "gas" to the right density produced very ordered assemblies of particles. Simulations of the motion of a ball on these planes resulted in far too narrow parameter ranges for the existence of a steady state.

It was thus decided to use a scanned configuration of the "real" plane in the simulations. The section of the plane used contained 4085 particles, the size was 11.25 cm by 4.35 cm. As the data received contained only the positions, but not the sizes of the beads, $r = 0.5$ mm is taken for all balls on the plane, though in reality there is a certain size distribution with a mean value of 0.5 mm. Though this leads to overlap of particles in some cases, the radii of overlapping particles are not adjusted, since this does not disturb the simulation, and reducing *all* particle sizes by 10% to check the effect this has on the motion showed only a very small influence. Periodic boundaries in both directions were achieved in a similar way by simply attaching a copy of the system at the boundary and removing particles with too much overlap, carefully avoiding the creation of big holes. Figure 4.23 shows the distribution of balls on the plane. Both the distance between centers of neighbouring spheres and between centers of spheres and the corresponding vertex in

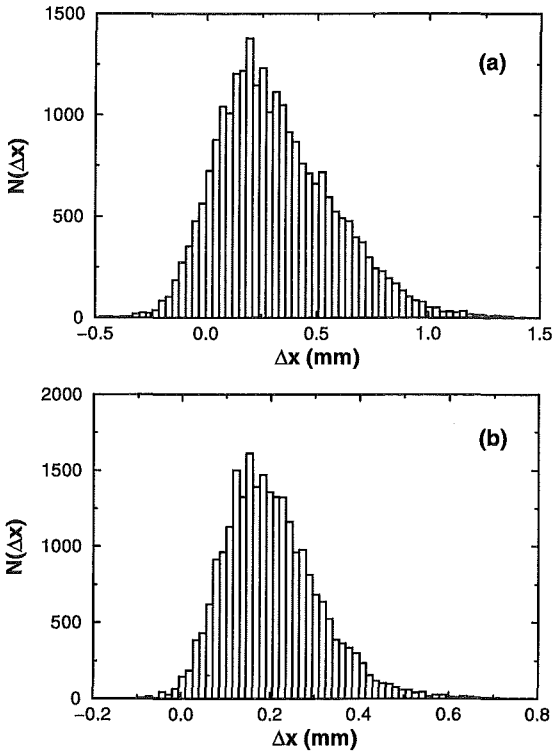

Figure 4.23: *Distribution of distances between balls on the plane. (a) Shows the distribution of distances between centers of spheres, where* $\Delta x = |\vec{r}_i - \vec{r}_j| - 2r$ *(b) Shows the same for the distances between centers of spheres and the corresponding vertex in the Voronoi tesselation of the plane, i.e.* $\Delta x = |\vec{r}_i - \vec{r}_j^V| - r$*, where* $\vec{r}_j^V$ *is the coordinate of the corresponding vertex.*

the Voronoi tesselation of the plane is shown, since the latter is a better estimate for the size of "holes" in which particles might get stuck. Approximately 75% of the values for $\Delta x < 0$ correspond to particles on the boundaries, there is very little overlap of particles inside the sample.

4.3.2 Simulation results

4.3.2.1 Average properties

In the simulations presented here, the ball was launched onto the plane with a rather high starting velocity v_x and $v_y = 0$. When the ball reached a steady state with $\bar{v}_x \neq 0$ for a certain combination of Φ and θ, an average over several runs with different starting velocities and starting positions was taken. In each run, the velocity fluctuated somewhat, and also the mean velocity varied a bit more from run to run than in 2D. Figure 4.24 shows typical velocity distributions. The tail towards smaller x-velocities corresponds to larger y-velocities (see Fig. 4.25), i.e., to parts of the motion where a large amount of x-velocity could be transferred to the y-direction. Very similar distributions and correlations of v_x

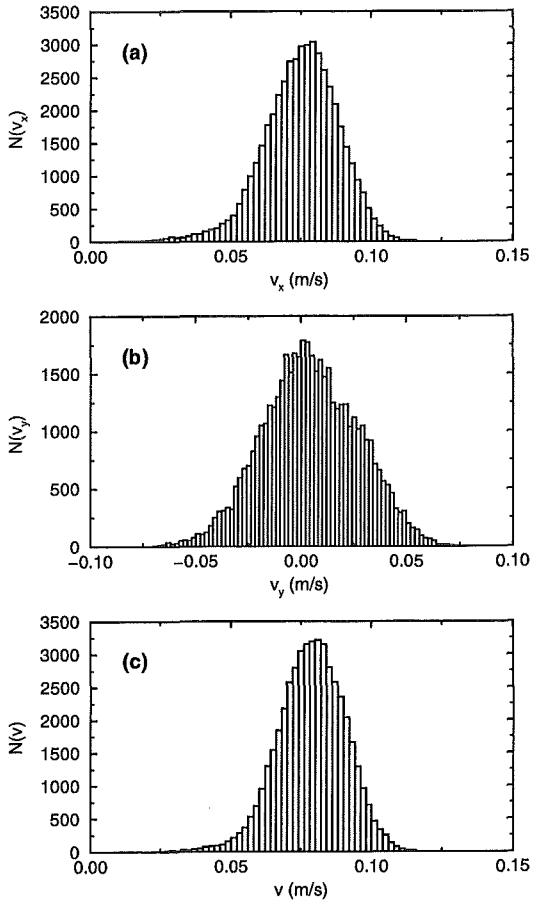

Figure 4.24: *Histograms of the velocity distributions for* $\Phi = 5$ *and* $\theta = 0.05$.

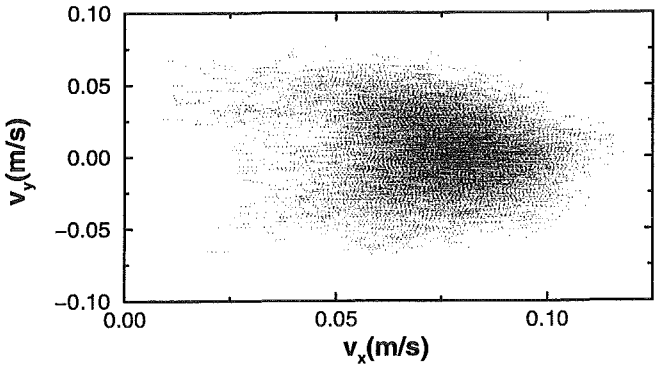

Figure 4.25: *Correlation of* v_x *and* v_y *for the same parameters as in Fig. 4.24.*

and v_y were found in experiments [261].

In Fig. 4.26 the velocity $\bar{v}_x$ for various size ratios Φ is plotted as a function of $\sin\theta$ for $e_n = 0.8$ and $e_n = 0.4$. As in the two dimensional case, there is only a very small influence of e_n on $\bar{v}_x$. Obviously for very large Φ the velocity curves look more like $\sqrt{\sin\theta}$ (though

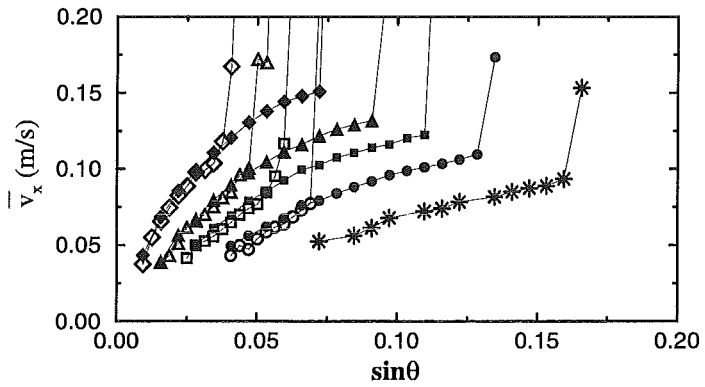

Figure 4.26: *Mean velocities for $e_n = 0.8$ (open symbols) and $e_n = 0.4$ (closed symbols) and $\Phi = 3$ (stars), $\Phi = 4$ (circles), $\Phi = 5$ (squares), $\Phi = 6$ (triangles), $\Phi = 8$ (diamonds).*

it is hard to decide if the exponent is really 1/2), whereas for smaller Φ the curvature seems to decrease. Besides, for intermediate Φ, some curves look more linear for $e_n = 0.8$ than for $e_n = 0.4$, however, the difference is very small. The sudden rise of the velocity curves corresponds to a similar intermittent motion as observed in the 2D simulations and 3D experiments [256], where the ball still maintains a mean constant velocity, but with stronger fluctuations and short accelerating and decelerating phases. It was checked that like in the 2D case, the coefficient of friction μ does not influence the mean velocity.

At this point, some remarks about the "scaling" of $\bar{v}_x$ with Φ seem appropriate. Figure 4.27 shows the scaling of the simulation curves for $e_n = 0.4$ with $\Phi^{-1.25}$. The scaling is slightly worse than in experiments [260], but some collapse of the data is clearly achieved. In [248] it was shown that for $e_n = 0.8$ a good collapse (slightly better than that in Fig. 4.27) could be achieved by scaling the velocity with $\Phi^{-1.5}$. The fact that a number of "scaling laws" work reasonably well is probably due to the small range of inclination angles over which data exists. As we have seen in the theoretical treatment of the 2D case, the Φ-dependence of the velocity comes both from the prefactor in the equation of motion and the boundary conditions. Thus, in fact no simple scaling is to be expected. Since in 3D the situation is even more complicated, it is questionable if any of the "scaling laws" found has a deeper meaning.

Figure 4.28 shows the phase diagram obtained from these velocity curves for both $e_n = 0.4$ and $e_n = 0.8$. Contrary to the 2D case, in region B sometimes the ball comes to a sudden stop after having previously travelled with constant velocity, because it is trapped by a large hole on the plane, as observed in experiments [256, 258]. The steady state region B for $e_n = 0.8$ is much smaller than in experiments, and shifted towards smaller θ, even though $e_n = 0.8$ is appropriate (and even a bit too small) for steel on glass. But it is unclear how strong the effect of the combined setup (glass beads on contact paper on glass plate) is. The glued glass beads are not immoveably stuck, and might shift slightly during impacts. A test performed on the real plane by dropping a steel ball on the horizontal plane resulted in only very little rebound. Still, this does not help in measuring the coefficient of restitution, since it cannot be controlled under what angle the ball hit a ball on the plane, so pre- and post-collisional normal velocities are simply not known.

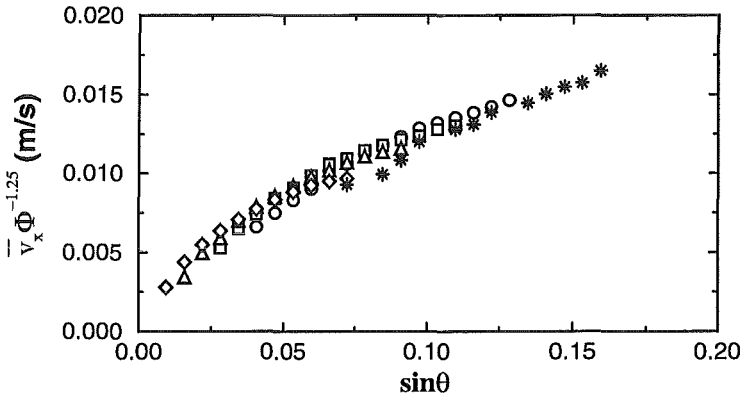

Figure 4.27: *Scaling of the velocity with Φ for $e_n = 0.4$ and the velocity curves from Fig. 4.26.*

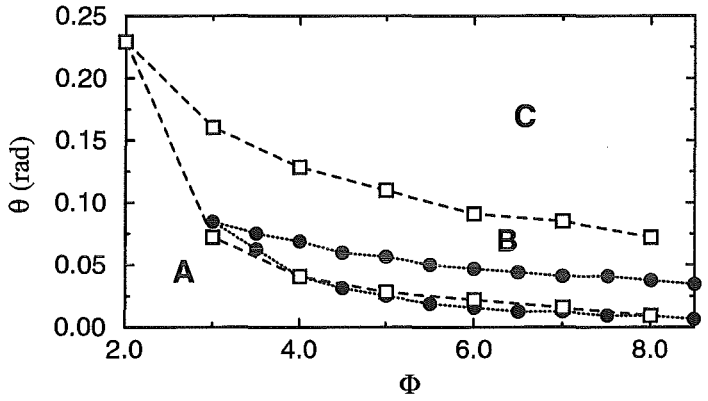

Figure 4.28: *Phase diagram for the same parameters as in Fig. 4.26 and $e_n = 0.4$ (□) and $e_n = 0.8$ (•).*

It is not completely clear what conclusions should be drawn from these results on the mean velocities. There might be a passage from linear behaviour to a square root, for which the critical Φ depends on the coefficient of restitution. But the seemingly linear curves might as well just be part of a square root, and the curves too short to decide this. It is also not completely clear if there might be a fundamental difference between experiment and simulation. The experimental values look linear, but the range of angles over which a steady state could be found in experiments is so small that they are fitted equally well by a line and a square root. However, if there is a fundamental difference between the two dimensional and three dimensional cases, it must arise from the fluctuations of the motion.

4.3.2.2 Fluctuations

As stated before, the velocity of the particle fluctuates around the mean velocity depicted in Fig. 4.26. Besides being a possible source for differences between the 2D and 3D cases, these fluctuations should be interesting for the ability of the plane to promote segregation

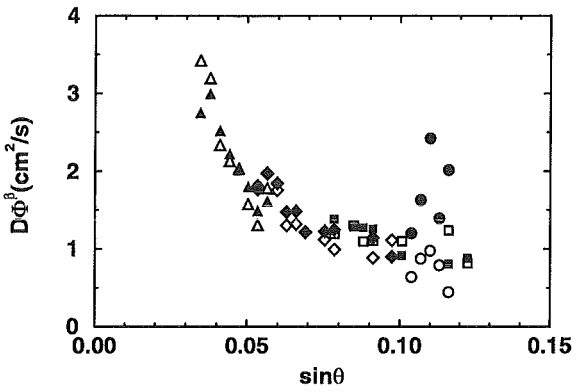

Figure 4.29: *Diffusion coefficient for* $e_n = 0.4$ *and various size ratios.* $\Phi = 3$ *(circles),* $\Phi = 4$ *(squares),* $\Phi = 5$ *(diamonds) and* $\Phi = 6$ *(triangles). Open symbols:* D_y, $\beta = 0$. *Full symbols:* D_x, $\beta = 1.5$.

in the transverse direction. In addition, it should be expected that fluctuations affect the phase boundaries (the stronger the fluctuations in the longitudinal direction, the higher the probability that close to θ_{AB} the ball may be trapped and that close to θ_{BC} the ball may achieve a velocity that cannot be braked any more). In the direction transverse to the main direction of motion, the particle undergoes a diffusive motion [251, 261], and in a reference frame moving with $\bar{v}_x$ with the particle, the same is true for the longitudinal direction. Though the corresponding velocity distributions are not perfectly gaussian, as is obvious from Fig. 4.24, transverse and longitudinal diffusion coefficients are defined by

$$D_x = \lim_{t\to\infty} < (x(t) - x(0) - \bar{v}_x t)^2 > /2t \tag{4.65}$$

$$D_y = \lim_{t\to\infty} < (y(t) - y(0))^2 > /2t. \tag{4.66}$$

In Fig. 4.29 the diffusion coefficients obtained in the simulations for various size ratios and $e_n = 0.4$ are shown. They were obtained by performing several long runs (100 seconds each) with different initial conditions and then cutting these down to pieces of different length, up to 3 seconds each to perform the ensemble average. Because of the anisotropy in the system introduced by gravity, anisotropy is to be expected in the diffusion coefficients as well and thus they are computed separately. Unlike in [251], where D_x and D_y were plotted as functions of the mean velocity $\bar{v}_x$, here they are shown as functions of $\sin\theta$. This is the quantity which in any practical application, where segregation might play a role, will be important, since the inclination will usually be at some fixed value while the velocity may evolve freely. In Fig. 4.29, $D_x\Phi^{1.5}$ instead of D_x is plotted, since this makes D_x and D_y fall approximately on the same curve.

The diffusion coefficients found in the simulations are in good agreement with experimental values [251, 261] and obviously decrease with increasing angle of inclination. This decrease can be fitted reasonably well by $(\sin\theta)^{-1}$, but again the range of inclination angles over which the scaling is obtained is too small to decide whether a different exponent would fit the data better. When D_x is scaled by $\Phi^{1.5}$, the values for D_x and D_y are of approximately the same magnitude, i.e. there is a Φ-dependent anisotropy in the diffusion coefficients. A similar anisotropy is found in sedimentation, where, however, the diffusion coefficient

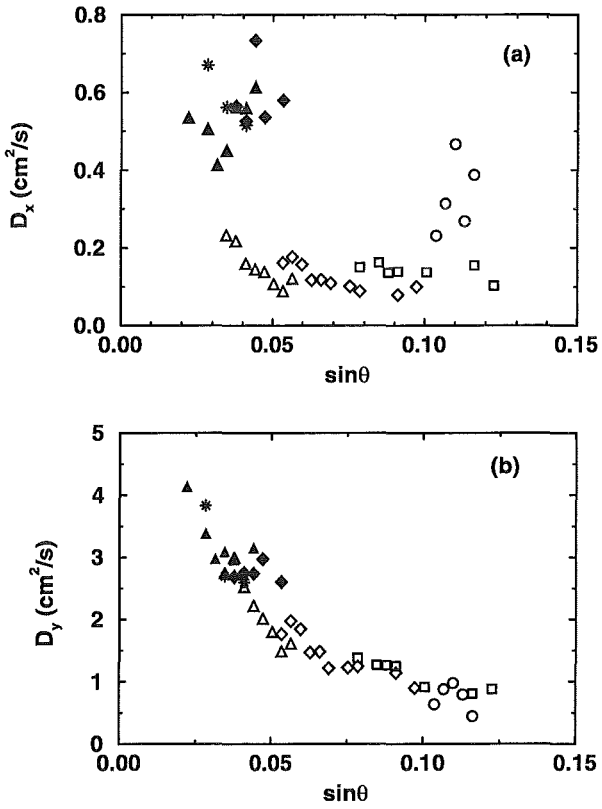

Figure 4.30: *Dependence of diffusion coefficients on e_n. Full symbols: $e_n = 0.8$, open symbols: $e_n = 0.4$. For the various Φ values, symbols are the same as in Fig. 4.29. The stars correspond to $\Phi = 5.5$, $e_n = 0.8$.*

corresponding to the mean direction of motion is larger than the one corresponding to the transverse direction [266]. Here, the reverse is true.

In Fig. 4.30 the diffusion coefficients are shown for two different values of e_n, this time without any scaling. Though for D_y the data for $e_n = 0.8$ fall more or less on the same curve as those for $e_n = 0.4$, for D_x they seem to be larger by approximately a factor of 2 for $e_n = 0.8$ as compared to $e_n = 0.4$. They thus cannot be scaled by the same factor Φ^β to make them collapse on the D_y curve. I will come back to this later and discuss possible reasons, after having presented results about the details of the motion. It should also be noted that even though for fixed Φ, the values of D_x decrease with increasing θ, they all fall in approximately the same narrow range even for different Φ. The circles in Fig. 4.30a that fall out of this range correpond to $\Phi = 3$, where $\bar{v}_x$ fluctuates quite strongly, which can lead to errors in the estimation of D_x.

4.3.3 Details of the motion

To see how the transverse motion and the increased disorder in three dimensions affect the motion, similar quantities as in the two dimensional case are investigated here. The most important quantities there were the times of flight between successive collisions, the

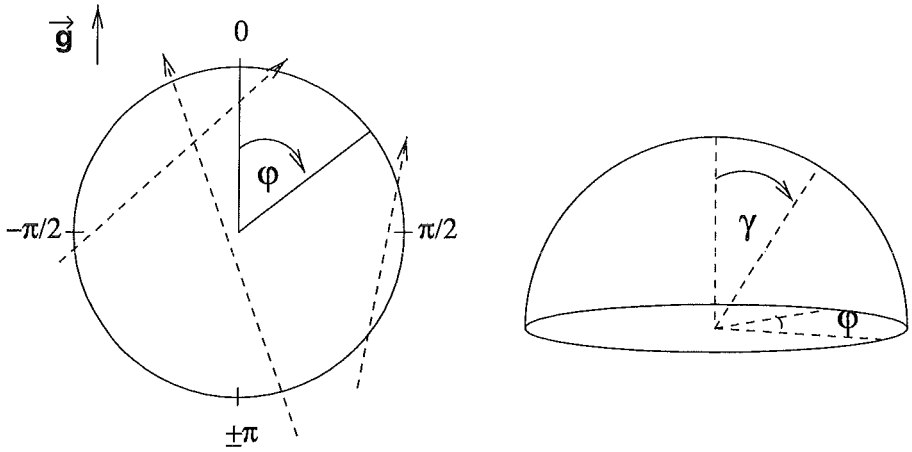

Figure 4.31: *Definition of the impact angles. Left: View of a ball on the plane from top and definition of the azimuthal angle φ. The dashed arrows show possible paths the moving ball may take. Right: View of a ball on the plane from the side and definition of γ.*

exact locations on balls on the line where the collisions take place, and the velocities in these collisions. The regularity of the motion in 2D was revealed especially by correlations between these quantities. In 3D, one would expect this strong regularity to disappear, since in 3D there are many influences that suppress it. When the ball collides with a ball on the plane slightly sideways, it is deflected towards the side. Thus the direction of motion changes at this point. Also the distance travelled over this ball before hitting the next one may be much smaller than the diameter of a ball on the plane. Some of these possibilities are shown on the left-hand side of Fig. 4.31, assuming that the direction of motion is hardly affected by interaction with the curved surface of the ball. The ball might also roll down the plane without going over the tops of the balls on the plane, moving mainly in the valleys formed by the bumps of the surface. Or, a completely different possibility, it might be deflected by the first impact with a ball on the plane so strongly that it could jump over to another ball immediately. Considering these possibilities, it has to be kept in mind that the area on the balls on the plane which is accessible to the moving ball is very small and only very slightly curved, due to the large values of Φ.

Figure 4.32 shows distributions of times between two successive collisions for two different inclination angles θ and two strongly different coefficients of restitution. As it turns out, in 3D similar correlation plots as those of Figs. 4.8 and 4.9 give very little information, since they are very blurred clouds where an internal structure may only be guessed. Thus, I have chosen to plot distributions of the different quantities. The values of θ were chosen such that they lie close to the lower and upper boundary of the region B respectively for the coefficient of restitution in question (see Fig. 4.26). Impacts on the up-hill facing side of the balls on the plane ($|\varphi| \geq \pi/2$, see Fig. 4.31) were separated from those on the down-hill facing side ($|\varphi| < \pi/2$). As a matter of fact, this is quite an arbitrary way of separating the distributions, as we will see, but I adopt it here to enable later comparison with results from the stochastic model described in section 4.1.3. The most important difference between collisions at $|\varphi| \geq \pi/2$ and $|\varphi| < \pi/2$ is that in a collision at $|\varphi| \geq \pi/2$, v_x is transferred to v_z, while for $|\varphi| < \pi/2$, v_z is transferred to v_x. This

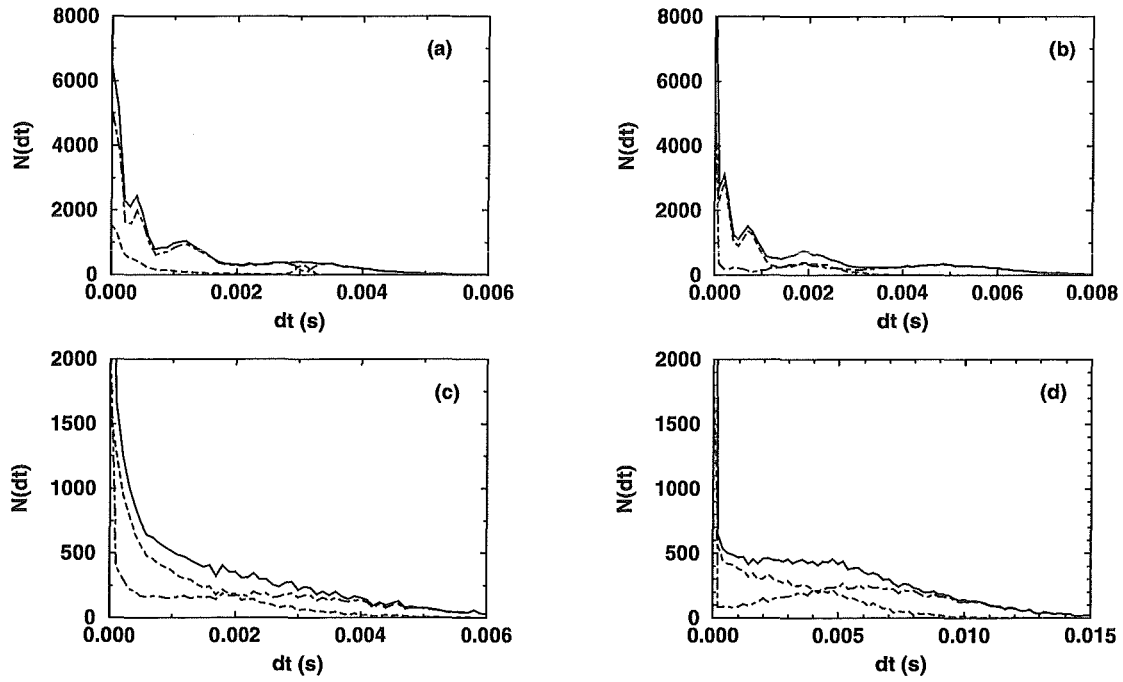

Figure 4.32: *Histograms of times of flight for* $\Phi = 5$ *and (a)* $e_n = 0.4$, $\theta = 0.05$, $\bar{v}_x = 8.2$ *cm/s (b)* $e_n = 0.4$, $\theta = 0.08$, $\bar{v}_x = 10.7$ *cm/s (c)* $e_n = 0.8$, $\theta = 0.03$, $\bar{v}_x = 5.1$ *cm/s (d)* $e_n = 0.8$, $\theta = 0.05$, $\bar{v}_x = 7.8$ *cm/s. Full line: total distribution, dashed line: previous impact at* $|\varphi| < \pi/2$, *dot-dashed line: previous impact at* $|\varphi| \geq \pi/2$.

means, that collisions on the up-hill facing side of the bumps drive the particle away from the plane, while collisions on the down-hill facing side drive it towards the plane. As in 2D, the times between collisions are on average smaller (and some very close to zero) for $|\varphi| < \pi/2$ than for $|\varphi| \geq \pi/2$, in contradiction to [246]. When the inclination angle increases, both distributions get broader, but the pronounced decay of the distribution for $|\varphi| < \pi/2$ remains, whereas the peaks of the distribution for $|\varphi| \geq \pi/2$ move towards larger times. Multiplying the times between collisions by the mean velocity, we find that the corresponding distances passed between impacts are much smaller than a particle radius.

Obviously, the overall shapes of the distributions depend far stronger on the coefficient of restitution than on the inclination angle. While the total distribution for $e_n = 0.8$ is essentially a decaying function, the distribution for $e_n = 0.4$ rather consists of multiple peaks, getting narrower with smaller times of flight. Besides, the form of the distributions corresponding to $|\varphi| < \pi/2$ and $|\varphi| \geq \pi/2$ respectively changes, losing some peaks for $|\varphi| \geq \pi/2$ and gaining some for $|\varphi| < \pi/2$. While the shape of the distributions is largely unaffected by θ, they generally extend towards larger times with increasing θ, and for $e_n = 0.8$, a shoulder develops for higher θ.

A quantity that has not been measured experimentally yet, and would indeed be very hard to measure, is the distribution of impact angles, i.e. *where* exactly impacts take place on the ball on the plane. The definition of the angles is given in Fig. 4.31. Figures 4.33

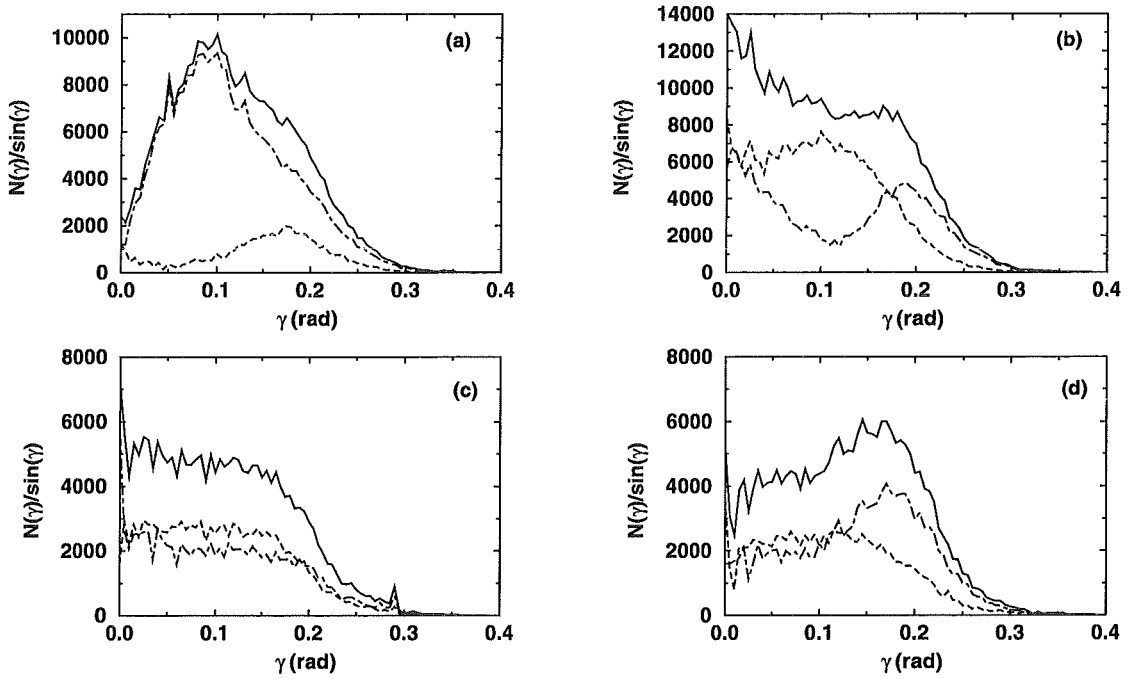

Figure 4.33: *Histograms of impact angles γ, same parameters as in Fig. 4.32.*

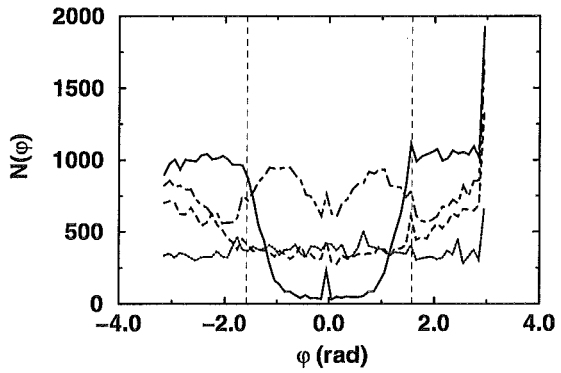

Figure 4.34: *Histograms of impact angles φ. The vertical dashed lines indicate $\pm\pi/2$. $\Phi = 5$, $e_n = 0.4$ and $\theta = 0.05$ (full line), $\theta = 0.08$ (dot-dashed line), $e_n = 0.8$ and $\theta = 0.03$ (dotted line), $\theta = 0.05$ (dashed line).*

and 4.34 show these angle distributions for the same cases as the distributions of times of flight in Fig. 4.32. In the case of γ, $N(\gamma)/\sin(\gamma)$ is plotted to normalize the distributions by the size of the corresponding volume element.

Unfortunately, even though for $e_n = 0.4$ some structure seems to be evident, it is not at all as clear from these distributions as in the 2-dimensional case, what exactly is happening as the ball moves down the plane. As in the case of the times of flight distributions, for $e_n = 0.8$ the shape of the distributions does not change very much with increasing θ, though the one corresponding to $|\varphi| \geq \pi/2$ develops a pronounced peak. Figure 4.33(c)

corresponds to a run where the ball, after having moved a distance of 2 m on the plane with constant mean velocity, suddenly stops because it gets trapped by a large hole – hence the small peak at $\gamma = 0.3$, which corresponds to the depth of the hole where the ball got trapped. For $e_n = 0.4$, the distributions again change quite significantly in form with changing θ, just like those for the times between collisions. Another point that might be noted is that for $e_n = 0.4$ the distribution shows more collisions towards the top of balls on the plane with increasing θ, while for $e_n = 0.8$ the number of collisions at the top of balls on the plane decreases with increasing θ. This increase and decrease respectively is entirely due to the change in the distribution corresponding to $|\varphi| < \pi/2$.

Though the distributions for times of flight and impact angles γ were already separated according to the side of the ball on which the impact takes place, it is quite instructive to have a more detailed look at the azimuthal angles φ where impacts take place. Figure 4.34 shows these distributions for the same cases as depicted in Figs. 4.32 and 4.33. Again, there are quite strong differences between the different coefficients of restitution. While for $e_n = 0.8$ the distribution for smaller θ is uniform, for larger θ it starts to develop a peak on the up-hill side, which clearly corresponds to the peak for γ in Fig. 4.33d. For $e_n = 0.4$, most impacts are on the up-hill side of balls on the plane, and only very few on the downhill side (with a uniform distribution on the uphill side) for small θ. For larger θ, this uniform distribution forms a peak similar to the one for $e_n = 0.8$ and two additional peaks develop symmetrically on the down-hill side.

All these details taken separately give a somewhat confusing picture. But adding one more detail that can be extracted from the simulation, the mechanism providing the friction force that maintains the steady state velocity becomes clear. The quantity that reveals what happens in detail on each ball on the plane is the loss of normal velocity per particle passed, i.e. how the normal velocity *after* the last impact with a certain ball relates to the normal velocity *before* the first impact with the same ball on the plane. Figure 4.35 shows the relation of these velocities for two different coefficients of restitution at the same angle of inclination of the plane.

Obviously, all points cluster around integer powers of e_n, for $e_n = 0.4$ most of the time all normal velocity with respect to the ball passed is lost, i.e. most points concide with the x-axis. In both cases, only the points where $v_n^f \neq 0$ are shown. This is the reason for the small number of points in Fig. 4.35b, because here most of the time all v_n^i can be dissipated on each ball passed. In Fig. 4.35b 98 % of the points coincide with the x-axis, versus only 7 % in Fig. 4.35a. Since in the tangential direction nearly no velocity is dissipated, this means that the amount of dissipation on passing a ball is simply determined by the normal velocity in the first impact and the number of collisions with this particular ball (which can be read off from Fig. 4.35 for each point). In fact, this is very similar to the two dimensional system, the only difference consists of the larger variation of the number of collisions per ball in the three dimensional case. The results obtained and their implications for the mean properties of the motion will be discussed in the following.

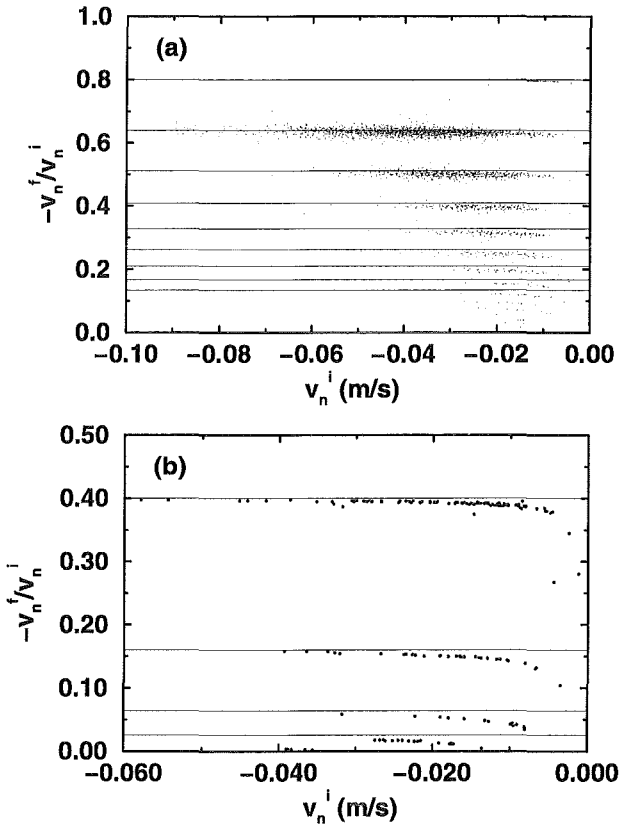

Figure 4.35: *Relation of normal velocity directly after the last impact with a ball on the plane to normal velocity directly before the first impact with the same ball for* $\Phi = 5$, $\theta = 0.05$ *and (a)* $e_n = 0.8$, *(b)* $e_n = 0.4$. *The lines denote integer powers of the corresponding restitution coefficient.*

4.3.4 Discussion of the results

4.3.4.1 Discussion of the simulation results

The results described above for the details of the motion show that in the three dimensional case, the motion of the ball is very similar to the motion in the two dimensional case. Obviously, the ball does not move down the plane by randomly hopping from particle to particle, but rather, when it arrives at a bead, it collides with it several times. Since we are dealing with a single ball, it can roll freely, and thus most dissipation comes from the part of the normal component of the velocity lost in collisions, and *not* from frictional contacts, where the tangential velocity might play a role.

As Fig. 4.35 shows, there are usually a number of impacts with each ball on the plane. In this succession of impacts, the velocity of the moving ball aligns with the tangent to the surface of the ball it is passing, since it gains velocity in the tangential direction and loses velocity in the normal direction. If this alignment succeeded for the whole surface of the plane, as it would on a perfectly smooth plane, the ball would go on accelerating.

However, the plane used here is too rough to allow this. Whenever this alignment succeeds, the rolling ball will roll onto another ball on the plane from which it rebounds. This collision transfers velocity tangential to the local plane surface to velocity normal to the local plane surface, which can then be dissipated. This mechanism is the same as in the two dimensional case – the only difference here is that there is a much larger variation in the distances available for the ball to adjust to the surface of a ball it is passing in 3D (see Fig. 4.31). This larger variation is also obvious from Fig. 4.35a – in a very large number of cases, especially close to θ_{BC}, there are only one or two impacts with each ball on the plane, because very often a ball on the plane is passed close to the side. Thus quite often, the adjustment succeeds only imperfectly for high e_n. However, this does not seem to be too important, as long as once in a while, all v_n is lost. Already in the 2D case, such behaviour was observed for high coefficients of restitution. Such "leftover" v_n (or rather the largest part of it, since some transfers back into v_t) is added to the freshly gained v_n and partially dissipated on the next bump. The main effect of leftover v_n, which tends to destabilize the motion, is the fact that this leads to a first collision with the next bump at smaller γ, which leads to less efficient transfer of v_t to v_n.

Another reason for the larger variation in the number of collisions with the balls passed is due to the fact that this first impact, besides transferring tangential velocity to normal velocity, may also change the direction of the tangential velocity with respect to the plane. This change should be the main source of the diffusive motion the particle performs in the transverse direction. When the particle rolls, the curvature of the ball surface on which the particle moves is so small that it has only a minor influence on the motion (recall the typical range of γ accessed by the ball as shown in Fig. 4.33).

This understanding of the mechanism by which the steady state is maintained also helps to comprehend better the details of the motion presented in the previous section. Let us first take a look at the distributions of γ in Fig. 4.33. For $e_n = 0.4$, dissipation is so strong that already after the first impact, balls have lost so much normal velocity that they do not jump very far. The drop of the distribution towards $\gamma = 0$ is not an indication that the ball does not pass over the top of the bumps, but is rather due to the fact that it does not manage to jump over the top, but rolls. This is exactly the same behaviour as found in the 2D case at small inclination angles. The decay of the distribution towards larger γ and partly the small peak for impacts on the down-hill side corresponds to the distribution of distances between balls on the line. Note that whenever a peak appears in the distributions shown, it is at approximately the same point and has approximately the same form. For $e_n = 0.8$, especially close to θ_{AB}, there are so many collisions on each ball that the number of collisions remains high close to $\gamma = 0$, while for higher inclination angles, the peak is quite prominent. This is probably due to the fact that the first jump on each ball carries the ball far enough away from the first impact, so the peak does not get smeared out so strongly as for lower inclination angles. The same reason might hold for the partly emerging second peak for impacts on the up-hill side in Fig. 4.33b.

The distributions of impact angles φ in Fig. 4.34 confirm this. Whereas for $e_n = 0.4$ at lower angles of inclination nearly all impacts are on the up-hill side, we find two new peaks emerging for higher angles of inclination, obviously corresponding to the second peak close to $\gamma = 0$ and the third one close to $\gamma = 0.1$ in Fig. 4.33b, i.e. balls now manage to *jump* over to the down-hill side. For $e_n = 0.8$, the same characteristics are found, i.e. with increasing θ there seem to be more impacts on the up-hill side than on the down-hill side.

The main reason is that the first impact in most cases takes place on the up-hill side, but this first impact may either remain the only one, or the following ones will occur in its vicinity. The distributions of the times between collisions (Fig. 4.32) show these multiple collisions quite clearly for $e_n = 0.4$, while for $e_n = 0.8$, the distributions for the single collisions are smeared out too much to be distinguished.

All these details help to understand some of the global properties of the motion discussed in Section 4.3.2. The fact that the steady state velocity $\bar{v}_x$, and thus the effective friction force felt by the particle, hardly depends on the coefficient of restitution can be explained in the same way as in the two dimensional case. Since the amount of energy dissipated mainly depends on how much tangential velocity is converted into normal velocity in the first collision with a ball on the plane, which in turn is determined only by the geometry of the impact, but not by e_n, it is not surprising that the steady state velocity does not depend on e_n. The same is valid for the lower boundary θ_{AB} of the steady state region, just like in the two dimensional case. The ball only gets stuck when it cannot roll out of the deepest valleys any more. The upper boundary θ_{BC}, however, does depend on e_n, because e_n determines how many bounces on each ball are necessary to lose a large part of the normal velocity with respect to each ball before the next one on the plane is hit – if this is not possible, the ball accelerates.

Since the explanations I have just given are the same as in the two dimensional case, the question arises as to whether the mean velocity can be calculated in the same way as in the 2D case by treating the ball as completely inelastic and perfectly rough. In the two dimensional case, the disorder of the plane can simply be incorporated into the calculation by assuming the balls on the plane to be equally spaced, with a spacing corresponding to the mean value of the distribution of distances. Here, this does not suffice. In the three dimensional case, it is also important to estimate the amount by which the ball will be deflected in the transverse direction. When moving at an angle δ with respect to the x-direction, the ball suffers the same number of impacts as if it were moving in the x-direction, since the number of collisions it suffers in crossing a certain length does not change. But it is moving *down* the plane more slowly, thus gains energy more slowly. Obviously, this additional dissipation has a strong influence on the motion, since in 3D the average Φ where the motion of a ball can be stable is significantly larger than in 2D. So far, I have not found a reasonable assumption which would incorporate this scattering in the transverse direction in a simple calculation, since unfortunately this amount of scattering changes with increasing plane inclination.

This leads to a completely new feature in the three dimensional case, the fluctuations of the motion. They are measured by calculating the diffusion coefficients corresponding to the longitudinal and transverse directions of motion (separately, because the system is highly anisotropic). Again, the possible reasons for their θ and Φ dependence can only be discussed qualitatively. As was just explained, the very first impact of the moving ball on each ball on the plane with which it interacts seems to be crucial in determining its motion over this single ball. One might thus expect that this is true as well for the direction into which the ball is scattered in this single impact. Though the changes Δv_x and Δv_y in a single impact depend on e_n, this dependence falls out of the quotient $\Delta v_x / \Delta v_y$ that determines the change of direction in this impact.[6] Since the diffusion in the transverse

[6]This is very easily seen when rotation is neglected and the collision written down in spherical coor-

direction is mainly due to such changes in the direction of the motion, this is the reason for the insensitivity of D_y to e_n. D_x should be composed of two components - one resulting from scattering in the y-direction, and thus related to D_y, and another one resulting from variations in the number of collisons per ball (i.e. variations in the loss of normal velocity per ball). These variations get stronger with increasing e_n and exist in the two dimensional case as well, which could be the reason for the dependence of D_x on e_n.

Far more puzzling is the dependence of the diffusion coefficients on Φ, namely that D_x is independent of Φ, while $D_y \approx \Phi^\beta D_x$, with an exponent β that seems to depend on the coefficient of restitution. So far, I have not found an explanation for the observation that the transverse coefficient of diffusion depends on the size ratio Φ, while the longitudinal one does not.

The slight tendency of the diffusion coefficients to decrease with increasing θ is easier to explain. Supposing that the diffusion is largely due to the scattering of the ball in the first impact with each ball on the plane it interacts with, it should depend on the distribution of these impacts. The more head-on the impact, the smaller the scattering to the transverse direction, the more oblique, the stronger this scattering. Figure 4.33 shows that with increasing θ, these impacts get less oblique, so scattering should be reduced and thus reduce diffusion.

4.3.4.2 Comparison with experimental results and the stochastic model

As mentioned in Section 4.3.2.1., the agreement of simulations with experiments is not perfect. The mean velocities found in simulations are slightly too high, θ_{AB} is lower than the values found in experiments, and for e_n values corresponding to steel on glass collisions θ_{BC} is significantly smaller than in experiments. The fluctuations (diffusion coefficients, etc.) are on average smaller in the simulations than in the experiments. The reason why the mean quantities are larger might be that in granular materials dissipation usually increases with increasing fluctuations (e.g. granular temperature) [61]. However, the simulation is not a perfect duplicate of the experimental setup. Some points that differ are the following: The particles in the simulation are rigidly fixed to the plane. They are perfectly spherical and monodisperse. These conditions are not given in that rigor in the experimental situation, and it is not clear how important this might be especially for angles of inclination where a large part of the motion consists of rolling. The adhesion of balls on self-adhesive tape is probably not as perfect as one would wish for, which could lead to strongly reduced and maybe even angle-dependent coefficients of restitution. Even nearly perfect adhesion of a bead to a plate can reduce the coefficient of restitution by approximately 10 % [267].

Also in the details of the motion, namely in the times between collisions, there is some disagreement between experimental results [262] and the simulation results. This discrepancy between experiment and simulation may be explained by the lower resolution of the experimental measurement techniques. The times between collisions extracted from noise measurements in experiments are (translated into distances) of the order of the radii of

dinates in a coordinate system located in the sphere with which the mobile bead collides (see Fig. 4.31). This calculation yields $\Delta v_y / \Delta v_x = \tan\varphi$.

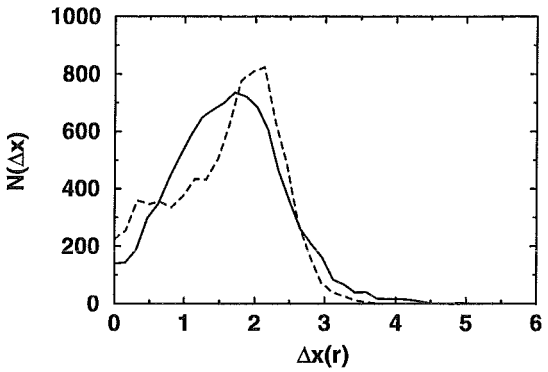

Figure 4.36: *Total time spent interacting with the same ball on the plane, translated into distances in units of particle radius of the small particles. Both curves for* $\Phi = 5$, $\theta = 0.05$; *full line for* $e_n = 0.8$, *dashed line for* $e_n = 0.4$.

the balls on the plane, i.e. much larger than in the simulations. As mentioned above, best agreement of the simulation data with experimental results is found for lower coefficients of restitution, like $e_n = 0.4$. If e_n is that low in the experiments, already the second and third collision on the same ball take place with strongly reduced normal velocity, and thus with far less noise than the first one. Besides, the resolution of the noise measurements is far smaller than in our simulations, so in the experiments times between collisions as small as those in the simulations may not be resolved any more. But if only the first collision with each ball on the plane is loud enough to be recorded, this means that not the time between single collisions, but rather the time spent interacting with each ball on the plane is measured. This time can also be extracted from the simulations and is shown for two different e_n in Fig. 4.36. There, $\bar{v}_x dt/r$ is plotted on the x-axis to give an idea about the corresponding distances. These distributions agree nicely with the times between collisions measured in experiments.

In the stochastic model, a clear double peak structure is found, which disagrees both with simulation and experiment. The times between collisions are of the same order of magnitude as in the simulations for $|\varphi| \geq \pi/2$ for small θ, while for $|\varphi| < \pi/2$ they are of the same order of magnitude as in experiments. The experimental data show no evidence of a double peak. In the stochastic model, these peaks are clearly separated from each other and the peak at smaller times corresponds to $|\varphi| \geq \pi/2$, i.e. to times after collisions at the up-hill side of balls on the plane. Even if the decaying distribution and the very broad peak in Fig. 4.32(c) and (d) were interpreted as two peaks, they disagree with the stochastic model, since then on average smaller times between collisions would correspond to the downhill side, and not the uphill side.

With the results of Section 4.3.3., this discrepancy can easily be explained. It arises from the way these times are determined in the stochastic model. There, the time of flight depends on whether the previous impact occured at the up-hill or down-hill side of a ball on the plane. If it was on the up-hill side, the time of flight is assumed to be $2v_z/g$, disregarding the details of the plane surface, if it was on the down-hill side, it is assumed that the time of flight is $2r/v_x$. The next impact angle is chosen at random, though according to eqs. (4.18) and (4.19), which reflects the angles actually accessible to the

particle due to the obliqueness of the impact.

By contrast, in the simulation it does not depend on the exact location of an impact whether the time until the next one is determined by v_x or v_z, but rather on whether the ball is rolling or jumping. If it is rolling, the time until the next collision is mainly determined by v_t and the distance between the point of onset of rolling and the next ball on the plane. Though the probability of the ball already rolling is higher towards the down-hill than the up-hill side, no distinction can be made a priori. The typical distance moved by a rolling ball before colliding with the next one is usually (especially for higher e_n) much smaller than r, which gives a much smaller time between collisions than the estimate in the stochastic model, where this distance is always $2r$. If the ball is jumping, the time of flight will be determined by v_z, or rather by a combination of v_x, v_z and the exact location on a surface bump where the last impact took place. The random choice of impact angles in the stochastic model, even if it takes place under certain geometrical restrictions, is another important difference. In the simulations, one finds that that in the steady state, if the ball is jumping, successive impacts are highly correlated, since the ball is moving in a preferred direction and there are a few impacts on the same ball on the plane. Especially on the up-hill side, the ball may be prematurely stopped (compared to the time of flight calculated by disregarding the details of the surface). In the stochastic model, this is only taken into account in calculating the possible impact angles, but not in the calculation of the time of flight. Therefore, the stochastic model on average overestimates the time of flight.

Besides these differences in the details of the motion, there is also a quite significant discrepancy between some global experimental and simulation results and the stochastic model. In the stochastic model, a linear dependence of $\bar{v}_x$ on $\sin\theta$ is found for $6 \leq \Phi \leq 10$ at angles of inclination $0.1 \leq \sin\theta \leq 0.3$, and the whole steady state region extends over a range $0.02 \leq \sin\theta \leq 0.45$ for these Φ. These angles of inclination are far too high compared to the range found for the steady state in experiments and simulations. The reason probably is that the randomness introduced in the stochastic model leads to much higher dissipation than experienced by the particle in experiments or simulations. In the simulations one finds as well that the more random the particle motion gets (like for high e_n as compared to low e_n), the higher dissipation gets. In the steady state, it seems to be more advantageous for the particle to keep as closely to the plane as possible, i.e. to dissipate all the normal velocity gained in moving from one particle to the next as soon as possible, and then move parallel to the surface until the next abrupt change in the surface direction takes place. However, especially when the motion starts to get more irregular, i.e. in region C, the stochastic model should be appropriate for describing the motion. However, it still gives a steady state for such irregular motion.

The reason for the existence of a steady state for very large θ results from the absence of rotation in the stochastic model. If the particle cannot rotate, but experiences friction, the angle region for which a steady state exists shifts towards significantly larger θ, compared to a rotating particle, as we have seen in Section 4.2.4.2. Figure 4.16 shows that if particle rotation is excluded, the steady state region lies in the range $0.2 \leq \sin\theta \leq 0.4$ for $\Phi = 2.25$ and a friction coefficient $\mu = 0.13$ (the same μ as used in the stochastic model). Since there is friction present in the stochastic model, but the particle cannot rotate, friction is an additional source of dissipation which obviously extends region B to significantly higher θ.

4.3.5 Summary of the results in 3D

The simulations of the three dimensional system have shown that the origin of the friction force experienced by the moving sphere in a certain range of inclination angles is essentially the same as in the two dimensional case discussed in [247]. In the steady state, the moving ball tries to adjust its velocity to each particle on the plane it passes, i.e. it strives to move parallel to the surface. Adjustment of the velocity occurs in a series of small bounces on each ball that is passed, since in each collision velocity normal to the surface is lost. If this adjustment could be achieved permanently, as it would for a ball dropped on a perfectly smooth (though maybe microscopically rough) plane, the ball would never reach a steady state. But, since the direction of the plane surface (i.e. the tangent to the plane) changes abruptly every time the moving sphere passes from one surface asperity to the next, this adjustment can never succeed completely. In this first collision with each ball on the plane part of the previously tangential velocity is transferred to normal velocity due to the change in the direction of the surface. This new normal velocity is subsequently dissipated in the same way.

Just as in 2D, the coefficient of restitution mainly determines how many collisions with each ball on the plane are necessary to dissipate all or a large amount of this velocity. The main importance of the roughness of the plane is the continuous conversion of energy gained (in moving parallel to the surface) to energy that can be dissipated. This is achieved by transferring velocity from the tangential direction to the normal direction. The plane thus prevents the particle from "collapsing" on the plane permanently. A steady state can only be reached if this "collapse" or at least a substantial reduction of v_n is achieved on most balls on the plane that are passed. If it can be achieved, it is unimportant in how many collisions this happened, hence the insensitivity of $\bar{v}_x$ to e_n. This means that in the steady state, the friction force exerted on the particle by the rough plane in unaffected by the velocity loss in a single collision, and only determined by the geometrical roughness of the surface.

As far as a possible linear dependence of $\bar{v}_x$ on $\sin\theta$ is concerned, the three dimensional simulations show no conclusive results; however, there are very strong indications that the experimental results simply look linear because the range of inclination angles over which measurements were obtained was so limited that the curvature was not noticed. Unfortunately, the steady state region in the experiments was smaller than that in the simulations of small e_n. Especially, in experiments θ_{AB} is higher, therefore the curves lack the angle region where in simulations the velocity curves exhibit clear curvature. Thus, it seems futile at this point to continue the search for reasons of the linear dependence of $\bar{v}_x$ on the driving force in this particular geometry.

With the understanding of the mechanism that maintains the steady state velocity the details of the motion like distributions of impact angles and distributions of times between collisions can be explained as well. The diffusion coefficients in the transverse and longitudinal direction were found to collapse on a decreasing function of $\sin\theta$ if D_x was scaled by Φ^β. The exponent β slightly depends on e_n, since D_x does so, and for $e_n = 0.4$ $\beta \approx 1.5$ was found. By contrast, D_y hardly seems to be affected by either Φ or e_n. A qualitative explanation could be given for some of these properties with the help of the details of the motion.

4.4 Summary of results for the single particle

To sum up the most important results for the motion of a single particle, I want to recall the objectives in examining this problem stated in the beginning of this chapter. The main goal was to determine the properties of the steady state motion as well as the limiting conditions for steady state of "flow" of a single particle on a rough plane as a function of control parameters like roughness r/R of the plane, angle of inclination, and material properties like coefficient of restitution and coefficient of friction. Another important question to be addressed was the influence of disorder and of the dimensionality of the system.

Simulations showed that the effect of disorder on the motion of the particle is relatively small, at least in the two dimensional case, where the effect of disorder can be assessed by a relatively simple mean field approximation. As far as the influence of dimensionality of the plane is concerned, the main effect of the additional transverse direction is increased dissipation, since in the transverse direction, the ball is only braked, but not accelerated. Therefore, the size ratios Φ for which the motion can be stable over a reasonable range of inclination angles are on average larger in 3D than in 2D. Unfortunately, the disorder in 3D is harder to describe mathematically than in 2D, therefore no such simple model as for the motion in 2D could be derived.

The derivation of a simplified model for the motion in 2D by assuming perfectly inelastic collisions was made possible by the observation that the steady state can only be maintained if the particle collides with every ball on the plane or line several times, once in a while losing all its normal velocity relative to a bead on the plane. If the jumps get farther on average, the velocity loss in the collisions can no longer make up for the gain during this free flight. One question that will be addressed in the following chapter discussing many particle flow is in how far similar behaviour can be observed in the case of many particles flowing down an incline. There, another contribution comes from collisions among particles, not only from the interaction with the boundary. However, also in this case, the fact remains valid that the system is open at the top, i.e. that it may reach so dilute a state that also the collisions between particles are too rare to dissipate enough energy. This is completely different from any closed system – it is entirely due to the fact that the time of flight between collisions can get longer with increasing velocity, therefore allowing more efficient gain of kinetic energy, as compared to a system where some mean free path can be fixed via the packing fraction.

For the single particle, the tendency of the particle to stay very close to the plane and the multiple collisions with each bead on the plane passed arising from it, leads to insensitivity of the steady state velocity and the lower boundary θ_{AB} to μ and e_n. It is in fact this insensitivity that allows the simplified theoretical treatment in 2D. The question to be addressed in the case of many-particle flow is therefore in how far similar insensitivity to material parameters might be seen there – for the flow in general, or at least for the boundary conditions, i.e. for the interaction with the rough plane.

Chapter 5

Flow on a rough inclined plane

> *Some people – and I am one of them – hate happy ends. We feel cheated. Harm is the norm. Doom should not jam. The avalanche stopping in its tracks a few feet above the cowering village behaves not only unnaturally but unethically.*
> — Vladimir Nabokov, "Pnin"

One objective in examining the motion of the single particle in detail was to gain some insight into more complicated flows, where many particles are involved. The natural extension of this work is therefore the simulation of many particle flow on a rough inclined plane to see if properties of the single particle system survive. The simulations of the many particle system presented in this chapter will be restricted to two dimensions, partly to reduce the computational effort, and partly because in the single particle case it could be shown that there are no fundamental differences between the 2D and 3D case, while the simulation results in 2D were far more lucid than in 3D.

One important difference between the single particle and the many particle system is the fact that the parameter space grows considerably. For the single particle, there are already five parameters determining the motion – the size ratio Φ, the distribution of particles on the line (given by the distribution of particle spacings ϵ), the angle of inclination θ, and the material parameters μ and e_n. In the many particle case, there is additionally the number N of particles, which together with the number of wall grains N_w determines the number of layers in the chute. Besides, it is possible to have a different coefficient of friction μ^w and restitution e_n^w for particle-wall collisions than for particle-particle collisions. In addition, there may be a size distribution for the moving particles. Since a complete scan of the parameter space is beyond the scope of this work, simulations will be perfomed in a restricted parameter space.

The main interest lies in checking if the most salient features of the single particle case are conserved, namely the development of strong correlations between successive collisions or the ensuing insensitivity to material parameters μ and e_n. For the sake of simplicity, these are taken to be the same for particle-particle and particle-wall collisions, even though this is a relatively strong restriction. The particles on the line are taken as equally sized and touching each other. Besides, in all cases presented in the following, the diameter

of the wall particles equals the mean diameter of the particles in the flow. The particles are taken as slightly polydisperse to avoid the strong cristallization that occurs in two dimensional systems of monodisperse particles. Though it is clear that especially a change of the boundary conditions can affect the flow quite strongly, the basic properties of the flow should become clear in the cases studied here as well. This chapter by no means provides a discussion of flow on an inclined plane that is as complete as that of the motion of a single sphere presented in the previous chapter. The aim is essentially to show that some of the single particle results are relevant to many particle flow, and to indicate some directions for future work.

Before discussing previous work on the subject of flow in inclined chutes and finally my own simulation results, I would like to make some remarks about the specific problems and particular features of this special kind of flow. As we have seen for the single particle, there exists a large region of parameter space where the particle keeps accelerating, and does not reach a steady state, because it is driven away from the plane by collisions with the surface asperities. Therefore it may gain more kinetic energy during the increasing time of flight than can be dissipated in the rare collisions (note that not only the energy loss is proportional to the square of the velocity, but also the energy gain during free flight, since the time of flight is proportional to the velocity). The same should hold true for the flow of many particles. Though in this case dissipation comes about not only through collisions with the boundary, but also to a large extent through particle-particle collisions, the flow may as well dilate, since the uppermost particles have the same freedom to move up as the single particle. But, with the dilation of the flow, the mean free path of the particles increases, and it is to be doubted if this can be counteracted by the possible accompanying increase of granular temperature which might increase the dissipation in the system.

Another important feature to note is that, unlike in a granular gas or in a pipe, where contact with other particles or with the wall mainly arises from the fluctuations of the particle velocities, on an inclined plane there is also an applied outer force, namely the component of gravity normal to the plane surface that forces the particles towards the dissipative bottom boundary. It also forces them together, since all particles tend to move in this direction.[1] Therefore, it would be expected that the influence of the coefficient of restitution on the mean properties of the flow should be either small or opposite to that in a geometry like a pipe. There, fluctuations (which strongly depend on e_n) rule the dissipation, since they promote contact with the wall, thereby increasing dissipation with increasing e_n [61], i.e. there global dissipation is increased by decreasing local dissipation.

5.1 Overview of previous work

Since flow of granular material in an inclined chute is of such great practical importance and one of the simpler forms of granular flow, a large amount of experimental and theoretical work on this system exists already, as well as some simulations. Before discussing my own

[1] In this respect, the inclined plane is very similar to a shaken container filled with granular material, where gravity as well forces the particles towards the bottom. Note, however, that the analogy ends here, since in the vibrated box, particles may gain energy directly through collisions with the bottom, but not during free flight.

simulation results, I will thus first give an overview of existing work on flow in inclined chutes. In each subsection, the previous works are presented in chronological order.

5.1.1 Experiments

Most experiments on flow in inclined chutes were carried out in three dimensions. Only recently, quasi two dimensional experiments were performed [100, 101, 268]. A very good overview of experiments before 1983 is given by Savage [50]; the contents of this review paper will be summed up here briefly. The main problem in the early works is that the quantitative data was gathered in a very crude way. Besides, in many experiments it was not checked (and seemed to be of no particular interest) if the flow reached a steady state, or if there were velocity gradients along the chute. Some of the experiments were performed in chutes closed at the top, but with such low filling levels that for smaller angles of inclination the flow might be unaffected by the top wall. Obviously, all these results are therefore very hard to compare.

Takahashi [88] measured the mean distance flown by sand grains flowing out from an inclined rectangular funnel and deduced the mean outflow velocity from this. He found two flow regimes – one very dense, where there was a steep increase in the mean outflow velocity with the inclination angle, and, for higher angles of inclination, a very dilute one where the increase of outflow velocity with θ was much slower. The transition occurred at decreasing θ with increasing channel width. It was not checked if the flows were steady or accelerating down the chute.

Roberts [89] measured the evolution of the flow profiles for grains flowing out of an orifice leading into a curved pipe. He found that the flow developed a thinning region somewhere in the middle of the pipe, where flow was fastest. He proposed a simple model for the flow, assuming it to consist of layers gliding on each other with an effective friction coefficient. In later work, Roberts and Scott [90] applied this simple analysis to various flow geometries and compared it to experimental results obtained in such chutes. The agreement with experimental results is quite remarkable, however, it has to be kept in mind that some of the constants entering the theoretical model, like the effective coefficient of friction μ_E, are extracted from the experiments themselves.

Ridgway and Rupp [91] measured outflow rates of sand from a rectangular chute made of polished brass. Profiles were obtained by splitting the flow with a knife edge at the desired height and determining the mass flow rate of material extracted from below the knife. With the help of a window in the side wall, the flow was filmed with a high-speed camera. The top layer was found to move at approximately the same speed as the material near the bottom of the chute, which is quite surprising, and might only be explained by the very smooth chute bottom or possible interference of the blade used for separating the flow. Since the velocity was constant throughout the whole height of the chute, the mass flow profiles directly translate into density profiles, which exhibited a clear maximum approximately in the middle of the flow. The inclination angles ranged from 30 to 60°, but only for $\theta = 30°$ a steady state seems to have been reached towards the lower end of the chute; in all other cases, the flow accelerated.

Augenstein and Hogg [92] used a similar device as Takahashi [88] to measure the outflow

velocity, but collected the material in little boxes, as to obtain velocity profiles. They used both a stainless steel surface and a rough surface to which the same particles as used in the flow were glued. The thickness of the flowing layer was higher in the case of the rough bed than for the smooth bed, and on the smooth bed the flow thinned out considerably towards the lower end of the chute. The inclination angles ranged around 40°, and the flow always accelerated down the chute. In the case of the stainless steel surface, the velocity profiles were very narrow, with significant slip at the chute bottom, similar to the results obtained by Ridgway and Rupp [91]. On the rough surface, no slip was observed, and the velocity increased linearly, with a crossover to slower increase towards the top, from the bottom of the chute. Similar velocity profiles with some slip at the bottom could be obtained by using finer sand than that used in the flow for roughening the bottom. Along the chute, the mean velocity was found to be proportional to the square root of the distance from the inflow point, as one would expect from energy considerations in an accelerating flow.

Savage [93] measured surface velocity profiles in a rough-walled rectangular chute as well as the depth of the flow and velocity profiles in a glass-walled chute with a rough rubber bottom with large cylindrical asperities. The flow depths were compared with Roberts' simple theory [89]. However, agreement with these theoretical profiles was not very good, since the theory predicted accelerating flows where in the experiments steady flow was found. The velocity profiles have a similar form as those measured by Augenstein and Hogg [92] with a rough bottom. Savage also reports for the first time the observation of so-called "granular jumps" in chute flow experiments, where, just as in the case of hydraulic jumps in liquids, where a supercritical flow transforms into a subcritical one, a relatively shallow flow suddenly transforms into a flow of a few times the initial depth. The jumps were generated by adding a small down-stream obstruction to the channel.

Ishida and Shirai [94] measured the velocity of the uppermost layer in an inclined rectangular chute for different flow depths. They found that the velocity increased with layer thickness, slowly for very thin layers, but faster and almost linearly for thicker layers. In a later work, Ishida *et al.* [95] used an aerated chute (i.e. with a porous bottom through which air was introduced into the chute) to perform similar measurements. They found a similar dependence of the velocity gradient on the inclination angle as Takahashi [88] and identified the different velocity gradients with different flow regimes.

Brennen *et al.* [96] investigated granular jumps in inclined chutes by placing small obstructions into the flow near the chute end. They found that the height ratio of the "sub-" and "supercritical" flows was larger than in typical liquids, i.e. the jump is more pronounced in granular materials.

Campbell *et al.* [97] investigated the differences in the mass flow rates in dense ("subcritical") and dilute ("supercritical") flows. The different flow regimes could be achieved by regulating the inflow with a gate. For small gate openings, flows were usually "supercritical," while above a critical gate opening the flow becomes subcritical. The mass flow rates first increased with increasing gate opening, but at some point became roughly constant. The angles of inclination ranged from 20 to 38°.

Patton *et al.* [98] measured average densities, gradients of these along the chute and outflow rates in a rectangular open chute with a smooth bottom. The average density at a given

point in the chute was measured in a very crude way, namely by jamming a box into the flowing material and weighing the contents in the box. They found that their results were in qualitative agreement with Bagnold's result for the shear stress on flow in an inclined chute.

Johnson *et al.* [99] measured the relation between mass hold-up and mass flow rate in a chute with both a smooth aluminum base and a rough sandpaper base. The mass hold-up is defined as the amount of material over some unit area, and in their case was determined in the same way as in the experiments by Patton *et al.* [98]. The mass hold-up is a combined measure of density and height. Johnson *et al.* found that for mass flow rates above some critical value, there was a bistability in the flow, depending on the entry conditions. For loose entry conditions (material entering the chute directly from the hopper) relatively small mass flow rates (low mass hold-up) were obtained, with a diffuse upper boundary and low density, whereas for dense entry conditions (material entering the chute via a gate, behind which material from the hopper is collected before being released) very dense flows (with volume fractions up to 0.6 and a well-defined upper surface) were observed. This bears some resemblance to the granular jumps mentioned earlier on. The values for mass flow rate and mass hold-up measured in the experiments were compared to their theory, which will be sketched in section 5.1.3, and which matched their results at least qualitatively for dense flows and a smooth bottom, and for dilute flows and a rough bottom.

Ahn *et al.* [102] performed detailed measurements of velocity, velocity fluctuation and density profiles, as well as of the shear stress at the base. The chute was a rectangular 3 m long aluminum chute, the same as used by Patton *et al.* [98]. The bottom was flat, and for some experiments was coated with a thin film of rubber. Two different sizes of glass beads were used, and the velocities measured by fiber-optic probes. The measured velocity profiles were nearly linear, with significant slip at the bottom (even for the rubber surface). For the smooth aluminum surface, the velocity gradient was very small. The fluctuation velocity increased linearly with height for the rubber surface and was nearly constant with height for the aluminium surface. The density profile was quite blunt for the rubber surface, with a slight decrease towards the free surface; for the smooth aluminum surface, the decrease set in closer to the bottom. The flows observed were quite shallow, only up to 6 particle diameters deep. The measured stresses were compared to the theoretical results of Lun *et al.* [68], which could be fit only qualitatively. On average, measured stresses were smaller than the theoretical values.

Nishimura *et al.* [103] measured velocity and density profiles for the flow of small ($d \approx 3$ mm) ice spheres in an inclined chute with a sandpaper bottom for angles of inclination between 30° and 40°. The flow was filmed with a high speed video camera at 200 frames/second through a sidewall of the chute. The density profiles were blunt, with a small thinning region near the bed, and nearly linear velocity profiles were found. The velocity profiles exhibited significant slip at the bottom. The slip velocity increased slightly with increasing temperature, indicating that it was both due to the relatively large size ratio of the ice spheres and the sandpaper roughness and to the friction of the ice spheres themselves, since their coefficient of friction should decrease with increasing temperature. The velocity profiles are also strongly affected by the temperature, the flow getting faster with increasing temperature. Unfortunately, temperature influences two material properties at once: both the friction and restitution coefficient decrease with increasing

temperature. It was not checked whether the flows were steady.

Pouliquen and Renaut [104] investigated the onset of flow on a rough inclined surface in a quasi 2-dimensional geometry, i.e. using cylindrical aluminum rods. They found that flow set in at lower angles of inclination the larger the bed height. They compared this with time-step driven MD simulations, where similar behaviour was found. The same analysis was repeated in a fully 3-dimensional experiment, where the static and dynamic angles of repose were measured using glass beads and crushed walnut shells. Also in this setup, the same dependence of θ_c on the bed height was observed, both in the static and dynamic case.

Drake [100, 101] performed the first quasi 2-dimensional experiments on inclined chute flow. He used a glass-walled chute, 6.7 mm wide, 0.5 m deep, 3.7 m long and open at the top, which was filled with cellulose acetate spheres of diameter 6 mm. Small dots were imprinted on these spheres to enable measurement of particle spins. Different smooth (polished aluminum and high-friction rubber) and rough beds (6 mm cellulose acetate spheres glued to the bed with random spacing and 4 mm cellulose acetate sphere glued to the bed touching each other) were used. The flow was then filmed with a high-speed camera operating at rates of 240 - 2880 frames per second. The influence of air drag, side wall friction and possible eloctrostatic charging was examined very carefully. Typical inclination angles ranged around 40°.

The flows were nearly steady and uniform, characterized by large block gliding zones. In the case of a smooth bed, the flow was supported by a rolling-particle layer at the bottom, on top of which a block of several particle layers moved, with nearly constant velocity in the whole layer. In the case of the rough beds, velocity profiles were linear in the lower part, sometimes with a cross-over to a different slope in the higher regions, sometimes with a smooth transition towards a constant velocity near the top. The density profiles in all cases tended either to be constant, with a thinning region towards the top, or decreasing monotonously (sometimes linearly) from bottom to top.

One intention of these experiments was to test the validity of kinetic theories, thus besides velocity and density profiles, rotational velocity and temperature profiles were measured. The granular temperature was more or less constant over the flow depth; the same holds for the rotational part of the temperature, which is smaller than the translational part by approximately a factor of 2.

Recently, very similar experiments to those of Drake were performed by Azanza *et al.* [268]. They used steel and aluminum spheres, and found dense flows similar to Drake's for aluminum, while the flows for steel spheres were far more dilute. They compared the results obtained with steel spheres with the kinetic theory of Jenkins and Richman [269] for plane shear flows, but the agreement is poor. Only for the velocity, there is some agreement at least for the lowest 6-8 layers. All other profiles compare badly with theory.

5.1.2 Simulations

Most simulations of granular chute flow reported in the literature were carried out in 2 dimensions, all were performed with molecular dynamics methods, most of them with

time-step driven MD.

The first simulations of granular chute flow were done by Campbell and Brennen [105], using the ED method. The system was very small, consisting of only 40 particles, with a system width of 4 particle diameters, periodic boundary conditions and a flat bottom. They found a steady state for a plane inclination of 30°; for inclinations of 20° and 40° it was not clear whether the steady state was really reached. The velocity profile had a slightly parabolic shape, with significant slip at the bottom; the density was lower at the bottom, reached a maximum and then decreased again towards the top; the temperature was very large at the bottom and decreased strongly towards the top. This is a very surprising results, since in none of the experiments with a flat bottom anything similar was observed, and such density and temperature profiles would be expected rather for chutes with a rough bottom. The only possible reasons are that in the simulations, a higher coefficient of restitution was used for the wall-grain collisions than for grain-grain collisions ($e_n = 0.6$, $e_n^w = 0.8$), or that maybe the steady state was not reached yet.

Thompson and Grest [87] performed TD simulations of flow in an inclined chute where the diameter of the touching wall grains was twice the diameter of the monodisperse grains in the flow. However, they measured no flow quantities, but only the angle of repose θ_r and the angle of marginal stability θ_m. For a system with $e_n = 0.92$ and $\mu = 0.5$, they found the values $\theta_m = 32°$ and $\theta_r = 15°$.

Pöschel [106] simulated flow in a rough inclined chute, where the roughness mimicked the beds used by Drake [100, 101]. Unfortunately, as a normal force in his TD simulations he used a Hertzian spring with linear damping, which, as discussed in Chapter 3, gives unrealistic dissipation behaviour. He investigated mainly the flow properties in the accelerating regime and found a kink in the evolution of the kinetic energy with time. He attributes the "low energy regime" to relatively dense flow with large block gliding zones, whereas in the "high energy regime" the flow is far more disordered. However, the change in dissipation might well be due to the anomalous property of the normal contact law, which leads to less dissipation with higher impact velocities. For $\theta = 10°$ he finds a steady state, but does not discuss the velocity and density profiles in this region.

Walton [107] performed 3-dimensional TD simulations in a chute with a flat frictional bottom at an inclination of 17°. He found that the condition $\mu > \tan\theta$ had to be fulfilled to reach a steady state. He also found that the mean flow velocity increased with the number of particles in the system (i.e. the flow depth), but decreased with increasing e_n. At small flow depths the flow exhibited a linearly decreasing velocity profile, which with larger flow depths started to develop a blunt region, and finally showed some sort of plug over a narrow shearing region at the bottom. At the higher flow depths, a crystalline structure was supported by a narrow shear layer. The crystalline structure, however, may have been an artifact of the narrow cell size used for the larger flow depths.

Drake and Walton [108] duplicated the experimental situtation from [100,101] by means of TD simulations. They found that in order to achieve a steady state at the same angles of inclination as in the experiments, fluid drag has to be taken into account in the simulations. Neglecting the drag force, which in the simulations was taken to be a simple Stokes drag force, could lead the material to accelerate down the chute. Though not mentioned in [108], they noticed that it was of utter importance to use the correct spacing of the chute side-

walls in the simulations, since their braking influence on the flow was quite strong [270]. This strong influence of the wall spacing was also seen experimentally in the experiments by Azanza and Chevoir [271]. Drake and Walton showed that also in a smaller system with periodic boundary conditions and random starting conditions the flow converged to the same steady state as in the full simulation including the realistic filling procedure and allowing the material to flow out at the lower end of the chute.

Finally, Zheng and Hill [109] simulated two dimensional flow on an inclined plane with a TD algorithm. Like Pöschel [106], they used a Hertz contact law combined with linear damping in the normal direction. The contact time was quite long. The plane was bumpy, with two different roughnesses; one with discs of the same size as those in the flow touching each other, and one where every ninth discs had twice the size of the particles in the flow. The depth of the flows was approximately 8 layers of particles, the inclination angles for which a steady state was observed ranged from 10 to 30°. At the lower inclination angles, the profiles of the flow quantities were similar to those of previous simulation studies. At higher inclination angles, quite disperse flows were found, but even in the disperse case, the density of the material increased towards the bottom for the smoother boundary. For the rougher boundary, there was a very small low-density zone near the bottom. For the higher inclination angles (30°), it is not completely clear if really a steady state was evaluated. The time over which a steady state was observed was shorter than the time needed by the system to evolve towards this steady state, and Zheng and Hill state that only the kinetic energy at this point was constant, while other flow properties were still evolving. This strongly indicates that the steady state was not reached yet.

5.1.3 Theory

The earliest approach to a theoretical description of granular chute flow is due to Bagnold [65]. He applied the result obtained for the shear stress in gravity-free shearing of spheres to the inclined plane. On the inclined plane, the applied shear stress τ_{xy} on a plane at distance y below the upper free surface is $\sigma g \sin\theta \int_y^0 C dy$, where $C(y)$ is the volume fraction of the grains.[2] With the expression stated previously for the shear stress [eq. (1.5)], this gives

$$a_i \sigma \lambda^2 D^2 \left|\frac{\partial v_x}{\partial y}\right| \frac{\partial v_x}{\partial y} \sin\alpha = -\sigma g \sin\theta \int_y^0 C dy, \tag{5.1}$$

with λ, a_i, σ and α defined as in Section 1.3.2. Assuming C to be constant, and summing up all constants in one constant k, this leads to the differential equation

$$\frac{dv_x}{dy} = k\,(g\sin\theta)^{1/2}\, y^{1/2}, \tag{5.2}$$

which can be solved to yield

$$v_x = \frac{2}{3} k\,(g\sin\theta)^{1/2} \left(y_0^{3/2} - y^{3/2}\right). \tag{5.3}$$

Bagnold also performed experiments to test this result [65]. Qualitatively, his experimental results followed this trend, however, they were obtained by measuring the surface velocity in flows of different depth, i.e. velocities *in* the flow were not measured.

[2] In the following, y will denote the direction vertical to the plane.

Bagnolds treatment neglects two important features: the fluctuations of the motion, and the weight of the grains. The latter may be quite important, since each layer in the flow feels the weight of the layers on top of it. Besides, Bagnolds calculation holds for a system at constant volume, which in an open chute is only fulfilled in the steady state, but cannot be taken for granted generally.

However, for nearly 20 years, no progress beyond these results was achieved. Only when strong activity in developing kinetic or contiuum theories for granular flows started in the 70's and 80's, the interest in flow on an inclined plane was revived, since this system seemed to be treatable in the context of these theories due to its simple geometry. Unfortunately, the system is not as simple as it may seem, since it poses the problem of specifying appropriate boundary conditions for a free surface. Thus, most treatments of the flow on an inclined plane by means of continuum or kinetic theories differ in the boundary condtions imposed on the flow – at the bottom as well as on the free surface – and in the constitutive relations used to close eqs. (1.7) - (1.9).

In 1971, Goodman and Cowin [272] developed a continuum theory for the stresses occurring during flow of granular materials which was applied to open-channel flow and to flow in a vertical pipe. They assume the stress tensor to be a combination of a (non-dissipative) part arising from density gradients and a (dissipative) Newtonian term. Due to the Newtonian assumption, they find that a steady state is always possible for angles of inclination larger than the angle of repose. The profiles of the important quantities, like density, velocity and stresses depend on a quite complicated dimensionless length ratio (where it does not become evident what the physical meaning of these lengths is). The shape of the profiles is strongly dependent on this length ratio, and it is not clear how to relate it to material parameters.

A slightly simpler theory was introduced by Cowin and Savage in 1979 [93]. However, it is only slightly simpler in the sense that some of the variables can be discarded for a vanishing strain rate. Savage applied it to the same flow geometries as Goodman and Cowin [272], and recovers Bagnold's result as a special case for a certain chute inclination where the density is uniform [93].

Richman and Marciniec [273] employ the constitutive relations derived by Jenkins and Richman [274] for fully collisional flow of smooth particles to solve eqs. (1.7) - (1.9). The constitutive relations obtained by Jenkins and Richman [274] include both collisional and translational momentum and energy transport and therefore hold for all volume fractions below the dilatancy threshold. As boundary conditions Richman and Marciniec assume that the stresses and the energy flux vanish at the free surface, and that balance of momentum and energy are satisfied at the base, which is assumed to consist of spherical particles.

They find an analytical expression for the granular temperature, an algebraic one for the solid fraction, and solve numerically for the velocity profile. They also calculate lower and upper limiting angles for the steady state, which lie in the range $15° \leq \theta \leq 25°$ for a flow with $e_n = 0.8$ and $e_n^w = 0.95$ and are only very slightly affected by the mass flow rate. They also find that for given mass flow rate, it is possible to have two solutions with different height and density, just as observed by Johnson *et al.* in their experiments [99]. In addition, Richman and Marciniec find density profiles where the density decreases monotonously

with increasing height, while the reverse holds true for the temperature for $e_n = 0.95$ and $e_n^w = 0.8$. By contrast, for $e_n = 0.8$ and $e_n^w = 0.95$, the temperature decreases from bottom to top, and the solids fraction may exhibit a local maximum at an intermediate height in the flow. The velocity profiles in both cases are very similar. Though the form of all profiles is not too strongly affected by the inclination angle, the absolute values are, and the solids fractions for these steady flows are very low (maximum values in a range $0.1 \leq \eta \leq 0.4$).

Johnson *et al.* [99] assume that the stresses and dissipative terms can be decomposed in a collisional and a frictional part, where in the collisional part they take the expressions valid over the whole density range into account. For the frictional term, they simply assume that the stresses are given by the Coulomb relation $S_f = N_f \tan\phi$ where S_f and N_f are the shear and normal stresses and ϕ the so-called internal friction angle. They compare the results of their theory to their experimental results, however, find only qualitative agreement.

Anderson and Jackson [275] compare the results from this theory to those for theories taking only collisions into account for various boundary conditions at the bottom. Surprisingly, they find e.g. for the temperature profiles that in the frictional-collisional theory the temperature decreases from bottom to top for a smooth chute, but increases from bottom to top for a rough chute. However, they also use a smaller coefficient of restitution for particle-wall collisions in the case of the rough bottom ($e_n^w = 0.8$ and $e_n = 0.91$, while for the smooth bottom $e_n = e_n^w = 0.91$), which may as well have caused the effect.

Jenkins [110] performs a very similar analysis as that of Richman and Marciniec [273], but restricts the treatment to dense flows, which simplifies the calculation. For $e_n = e_n^w = 0.7$ and a boundary bumpyness corresponding to $\gamma_{\max} = \pi/5$ for spheres in the flow and on the boundaries of equal size, he finds temperature profiles that decrease from bottom to top, nearly linear velocity profiles and density profiles with a clear maximum in the upper half of the flow, some way below the free surface.

Unfortunately, none of the treatments discussed above can directly be related to the two dimensional simulations that will be presented in the following section. Application of these theories to the two dimensional case would entail a new calculation solving the two dimensional versions of eqs. (1.7) - (1.9), as well as a two dimensional derivation of the appropriate boundary conditions.

5.1.4 Summary of previous results

The experimental, theoretical and simulation results presented here show that despite the enormous amount of work performed on this system, the essential features of the motion especially in the steady state are far from clear. The different experimental and simulation results are hard to reconcile, because many of them operate in widely different parts of the parameter space. Therefore, it is very hard to say if differences between experiment, simulation and theory come about from conceptual differences or deficiencies, or simply from the difference in the regions of parameter space probed. The theoretical treatment partly shows how strongly little changes in the system can affect density and temperature profiles (while the velocity profiles are quite robust in general), but still there are very few

comparisons with experiments, and, when available, results agree only qualitatively.

It should be noted here that there are many reasons why it cannot be said whether this indicates a general lack of the theories or is simply a sign that differences between the experimental set-up and the theories are too large.[3] It is therefore necessary to do a more systematic scan of at least part of the parameter space to allow a better comparison of results and to assess the importance of the different parameters.

5.2 Simulation of the many particle system

The simulations of the many particle system are performed in the same way as those of the two dimensional single particle system presented in the previous chapter. However, since the simulation results are not to be compared with any specific experiment, for the sake of simplicity here dimensionless units will be used, i.e. $m = g = d = 1$, where $d = 2r$ is the diameter of the wall particles. Thus, velocities are measured in units of $\sqrt{dg}$, lengths in units of d, and forces in units of mg. The force parameters are set to $k_n = 5 \cdot 10^6$ and $\gamma_s = 1000$. The relatively high value for k_n was chosen to shift the onset of brake failure to very high velocities, since especially in such a system it is very likely to occur. The damping γ_n is fixed according to the coefficient of restitution e_n specified. Forces are the same as in Section 4.2. The system is typically $30d$ in length with periodic boundary conditions in the x-direction. The number of particles N is fixed according to the desired number of layers in the system. In all simulations discussed here, the particles have a gaussian size distribution with mean diameter $d = 1$ and a standard deviation of the diameter $\sigma_d = 0.05$. In the beginning of the simulation, particles are arranged on a square lattice, starting one particle diameter above the bed, with a typical distance of $2.5r$ between centers of neighboring particles. The particles are supplied with random velocities at the start of the simulation.

5.2.1 Influence of the coefficient of restitution for frictionless particles

In view of the single particle results, the most interesting question concerning the many particle system is certainly in how far the coefficient of restitution influences the properties and stability of the flow. It is clear that, unlike for a single particle that can rotate freely, μ should have a very large influence on the motion. To separate this influence from that of collisions, I first discuss the flow properties of frictionless particles. In the simulations presented here, the system (of length $L = 30d$) contained 300 particles, amounting to a flow height of approximately $10d$. This is the typical width of a shear zone in a granular material [45–48], therefore it should be expected to be a flow height where all material will flow. For thicker layers, the danger exists that only a shear zone at the top of the flow is actually fluidized, while for thinner layers, there would be less data than desirable to decide on the form of velocity profiles etc. Though certainly also for larger filling heights a fully developed flow may be expected, there is some risk that this will only occur at

[3] Hanes reports simulation results showing a significant difference between the temperature profiles near the walls and towards the middle of the chute – indicating that side-wall effects may have significant influence on the flow [276].

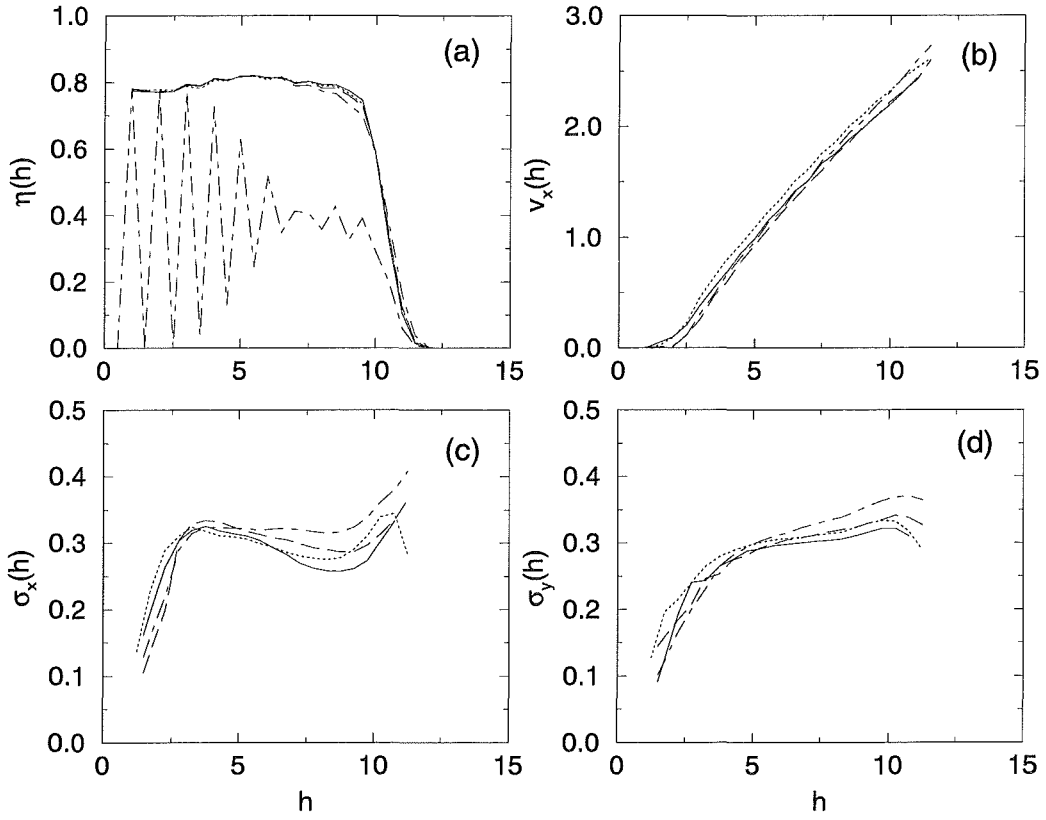

Figure 5.1: *Profiles of various flow quantities for $\mu = 0$, $\theta = 14.4°$ and $e_n = 0.4$ (full line), $e_n = 0.6$ (dotted line), $e_n = 0.7$ (dashed line), $e_n = 0.8$ (dot-dashed line). For $e_n = 0.8$, the results obtained by using smaller bins is shown as well (though scaled by a factor $1/2$) to give an idea of the strong layering in the system. The profiles are averages from a number of simulations runs (typically 5) of a few million timesteps with different initial conditions. The initial conditions had no influence on the steady state properties.*

inclination angles where no steady flow is possible any more.

Figure 5.1 shows the profiles of various quantities (area fraction η, mean x-velocity v_x, mean deviatoric x- and y velocity σ_x and σ_y defined according to $\sigma_x = \sqrt{T_x} = \sqrt{\langle {v_x}^2 \rangle - \bar{v}_x^2}$ as functions of the height h above the bed, measured from the centers of the glued particles) for a flow at an inclination angle of $\theta = 14.4°$. This is in the middle of the range of stable θ, which, for the case of frictionless particles and this particular roughness of the plane, was $12.6° \leq \theta \leq 16.2°$ for $0.4 \leq e_n \leq 0.8$ in the simulations. For higher inclination angles, a steady state may still be possible for smaller e_n, however, since the influence of a larger range of e_n on the flow is to be tested, here I focus on a particular inclination angle in this range. In the case of frictionless particles, for $e_n = 0.9$ no steady state could be found for this filling height of the system.

Only very dense flows could be found for these material parameters, with a strongly layered

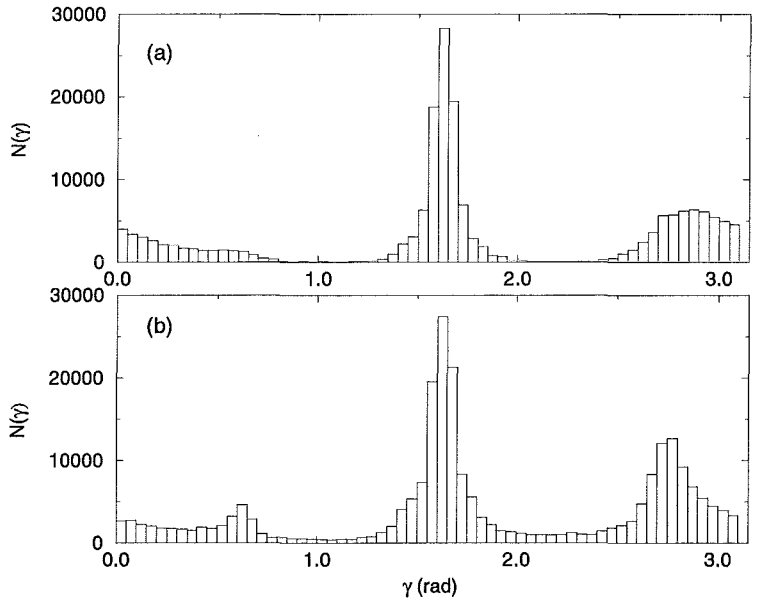

Figure 5.2: *Distributions of impact angle γ (mod π) in the steady state for (a) $N = 160$, $N_w = 40$, $\theta = 13.5°$ and $e_n = 0.6$ and (b) $N = 200$, $N_w = 20$, $\theta = 14.4°$ and $e_n = 0.8$.*

structure as indicated in Fig. 5.1a.[4] As far as the "temperature" profiles are concerned, some influence of the coefficient of restitution is evident, though mostly towards the upper layers of the flow. Probably most striking is the fact that just as for the single particle, the velocity profile is independent of e_n. This is not to be expected at first sight from the predictions of kinetic theories, where both the collisional energy loss γ [see eq. (1.9)] and the dissipation at the boundaries are proportional to $(1 - e_n)$.[5] It is also different from the situation in a vertical pipe, where e_n has a strong influence on mean flow velocity and velocity profiles [61]. However, also in a pipe, at very high packing fraction the influence of e_n on the temperature is quite small [61].

Visualizations of the flow show that the motion of each single particle in the flow very much resembles that of the single particle on the inclined plane. Particles move in quite ordered layers, and seem to climb over the particles in the layer below in a number of collisions. Especially at lower angles of inclination particles remain "stuck" for a short time in the local minimum between two lower particles before they manage to make it over to the next minimum. Particles move around in the whole system and do not remain in a certain layer for a long time.

Figure 5.2 shows the distributions of impact angles γ averaged over all particles in the flow for two simulation runs with different e_n, number of layers in the system and slightly different inclination angle. γ is defined as in the two dimensional single particle case, i.e. $\gamma = 0$ corresponds to the positive y-direction, $\gamma = \pm\pi$ to the negative y-direction and

[4]The profiles were obtained by counting each particle as occupying a bin containing its center with its whole area. Therefore, distributions obtained with bins smaller than the particle diameter tend to overemphasize the layering that occurs in the system.

[5]However, since the dissipative terms are also proportional to the granular temperature T in some form, which should increase with increasing e_n, these effects might cancel.

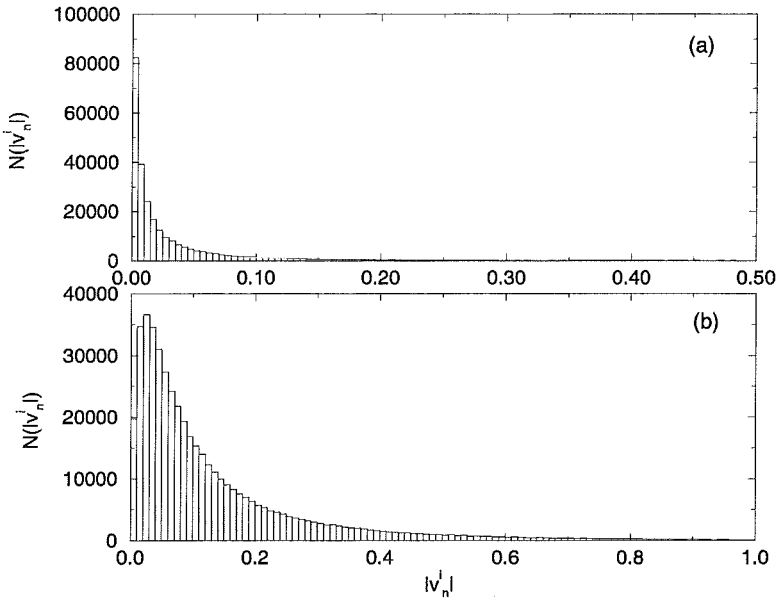

Figure 5.3: *Distributions of impact velocity* $|v_n^i|$ *for the same parameters as in Fig. 5.2*

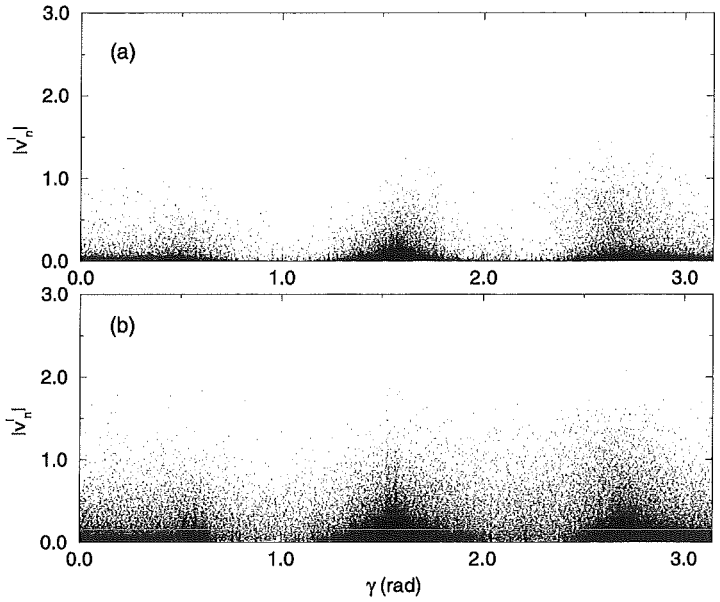

Figure 5.4: *Correlation between impact angle* γ *(mod* π*) and impact velocity* $|v_n^i|$ *for the same parameters as in Fig. 5.2.*

$\gamma = \pm\pi/2$ to the positive and negative x-direction respectively. Since for each collision of a particle at some angle $\gamma > 0$, the other particle in this collision sees it as a collision at $\gamma - \pi$, in the following all angles γ are evaluated modulo π. In Fig. 5.3 distribution of the corresponding impact velocities v_n^i are plotted for the same cases, and Fig. 5.4 shows how these quantities are correlated.

As observations of the visualizations of the simulation results show, particles usually climb

over the particle below them in a series of collisions. Between successive collisions with the same neighbouring particle, each particle also undergoes collisions with other neighbouring particles. Therefore, the correlation plots relating v_n^i and the impact angle γ in such flows reveal no such strong regularity of the motion as for the single particle, but are rather blurred. Nevertheless, there seems to be an indication that highest impact velocities v_n are reached for collisions around $\gamma_{\max}$, $(\pi - \gamma_{\max})$, and $\pi/2$. At least for smaller e_n, there are quite prominent peaks at these γ, however, they wash out for larger e_n. A similar effect was remarked by Zhang and Campbell [49] in simulations of plane shearing in two dimensions.

In the cases depicted in Figs. 5.2 – 5.4 the most prominent peak is certainly that at $\pi/2$, i.e. that corresponding to collisions between neighbouring particles in the same layer, followed by the one at $\pi - \gamma_{\max}$ and, a bit less pronounced, at $\gamma_{\max}$. One might therefore argue that most of the collisions occur through sterical constraints imposed on the particles, and not that many through random motion, therefore emphasizing the role of geometry in the dissipation far more than one might expect at first sight. In this case, it is not too surprising that the coefficient of restitution plays a minor role in such dense flows, since there, smaller energy loss in a single collision might be counteracted by a larger number of collisions in this particular position. Still, this is only a tentative explanation, but a quite likely one considering as well the single particle results.

Another question of interest is how far the profiles of the different flow quantities change when the inclination angle changes. Figure 5.5 shows velocity, density and temperature profiles for a coefficient of restitution $e_n = 0.6$ in the range $12.6° \leq \theta \leq 18.0°$. The value of e_n was chosen such that a reasonably large region of stable inclination angles exists. Obviously, the density changes only very little, while there are significant changes in the velocity and temperature profiles.

At this point, I would like to comment on some problems in the simulations. Very often the results reported in the literature on simulations of flow on an inclined plane are not averaged over several runs with different starting conditions, as is done here, but instead flow profiles were taken from only a single run. Though this may not be too much of a problem in the middle of the steady state region, misinterpretation may arise close to the upper boundary of the steady state. Figure 5.6 shows how 3 different runs evolved for $e_n = 0.6$ at $\theta = 18.0°$. The starting conditions differed only in the choice of the mean velocity $\bar{v}_x$ of the particles.

While two runs quickly evolved to the same steady state, the third one (actually the one with the lowest mean starting velocities) reached a state which at first seemed to be steady, though with a higher mean velocity $\bar{v}_x$ and comparably strong fluctuations. Finally, it even accelerated more and did not reach the steady state at all. Flow profiles obtained in the case of this simulation run, while the flow still seemed steady, exhibited a maximum of the temperature near the bottom, as predicted by some kinetic theories for steady flows. This uncharacteristic behaviour was not due to any artifacts caused by too small stiffness of the particles, since it was reproducible with exactly the same starting conditions, but a normal stiffness k_n increased by a factor of 10. Unlike "usual" accelerating runs, where acceleration was accompanied by a dilution of the system, here the system stayed quite dense, and the flow evolved into a state where a relatively static mass was supported by a strongly agitated thin shear layer. However, in all simulations presented in this chapter,

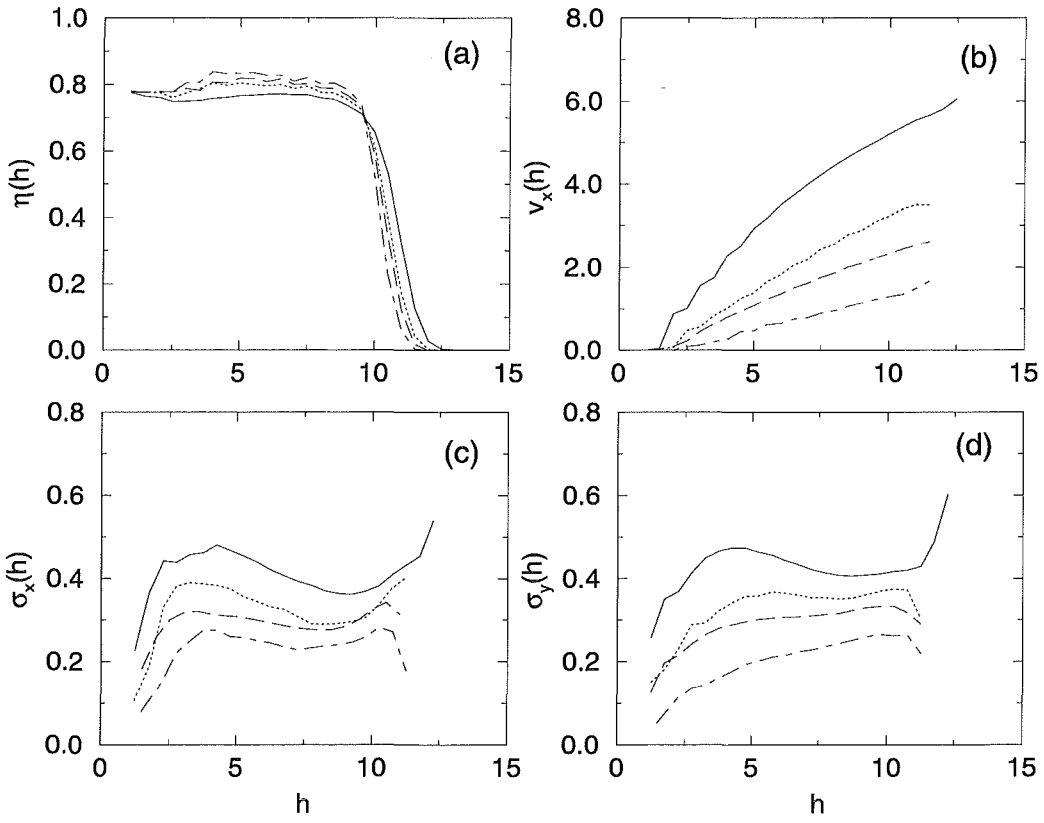

Figure 5.5: *Various flow profiles for* $e_n = 0.6$, $\mu = 0$ *and* $\theta = 12.6°$ *(dot-dashed line),* $\theta = 14.4°$ *(dashed line),* $\theta = 16.2°$ *(dotted line),* $\theta = 18.0°$ *(solid line). Averages were obtained in the same way as for Fig. 5.1.*

this effect occurred only once, namely in the case presented here. This example shows how much care has to be taken in evaluating simulations of flow on an inclined plane. One reason for discrepancies between different simulation results reported in the literature might be that sometimes, "steady states" were evaluated which were not steady at all, but rather transient states.

5.2.2 Influence of the coefficient of friction

As a matter of fact, meaningful comparison of simulation results for various coefficients of friction is not such a simple task. The coefficient of friction influences the range of inclination angles for which a steady state is possible quite strongly, just as in the case of a single particle. Therefore, it is hard to find an inclination angle for which a steady state exists for a reasonably large range of μ. Nevertheless, to give an idea of the influence of friction, in Fig. 5.7 the profiles for various flow quantitities are shown for different values of μ at an inclination angle of $\theta = 18°$. Obviously, friction has a relatively strong influence on the values of velocity and temperature profiles, though in the lowest 1-2 layers, its influence is rather weak. It should be noted that although the flows are so dense and friction seems to play such an important role in the dissipation, there are essentially no

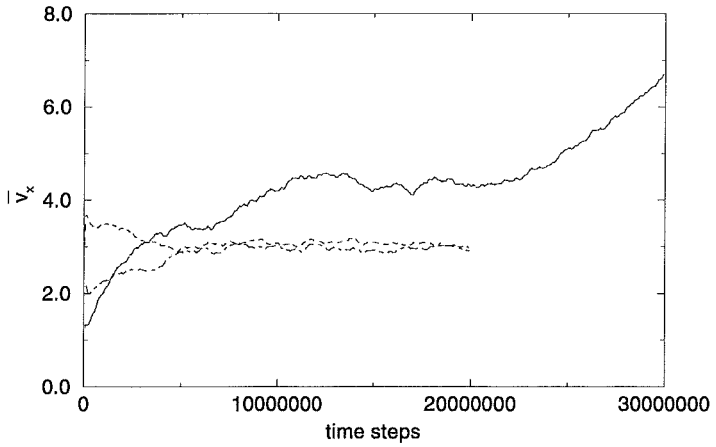

Figure 5.6: *Evolution of the mean velocity $\bar{v}_x$, averaged over all particles in the systems, for various starting conditions for $e_n = 0.6$ and $\mu = 0$ at $\theta = 18.0°$. In all cases, the initial values for the temperature were $\sigma_x = \sigma_y = 2$, but the initial velocity was varied from $\bar{v}_x = 1$ (solid line), $\bar{v}_x = 2$ (dot-dashed line) and $\bar{v}_x = 3.5$ (dashed line).*

lasting contacts, and binary collisions are the predominant source of energy loss. Another observation is the fact that the shift of the steady state region due to friction is not as strong as in the case of the single particle without rotation. Generally, this region is found at lower angles than for the single particle without rotation.

In the case of frictional particles, the rotational velocity profile is of interest as well. In Fig. 5.8, it is shown for the same cases as in Fig. 5.7, i.e. for $\mu = 0.25$ and $\mu = 0.5$. The kinetic theory by Lun and Savage [69] for frictional particles predicts that in simple shear, $\vec{\omega} = \frac{1}{2}\nabla \times \vec{v}$, which in our simple geometry reduces to $\omega = \frac{1}{2}\partial v_x(h)/\partial h$. This dependence was also seen experimentally by Drake [101] and is fulfilled quite well in our simulations, except for the uppermost layers. It therefore seems that ω is influenced by μ mostly indirectly, i.e. by the influence of the increased dissipation in the system on the velocity profile.

5.2.3 Influence of the coefficient of restitution for frictional particles

The next question to be addressed is in how far the coefficient of restitution influences the flow properties in the presence of friction. As it turns out, the damping effect of friction can be strong enough that it allows stable flow to exist for coefficients of restitution for which no stable flow could be found for $\mu = 0$. Figure 5.9 shows simulation results for $\mu = 0.5$ and restitution coefficients in the range $0.6 \leq e_n \leq 0.9$. Obviously, the situation is very similar to that of the case $\mu = 0$. Only for $e_n = 0.9$ is there a visible difference in the mean velocity and especially in σ_y in the upper half of the system. There, the velocity and the temperature are higher, though the stronger agitation of the particles obviously does not produce a visible expansion of the system (see Fig. 5.9a). There is even less difference in the temperature for $e_n \leq 0.8$ than in the frictionless case. However, for $e_n \to 1$, for which in the absence of friction no steady state could be found, differences start to show.

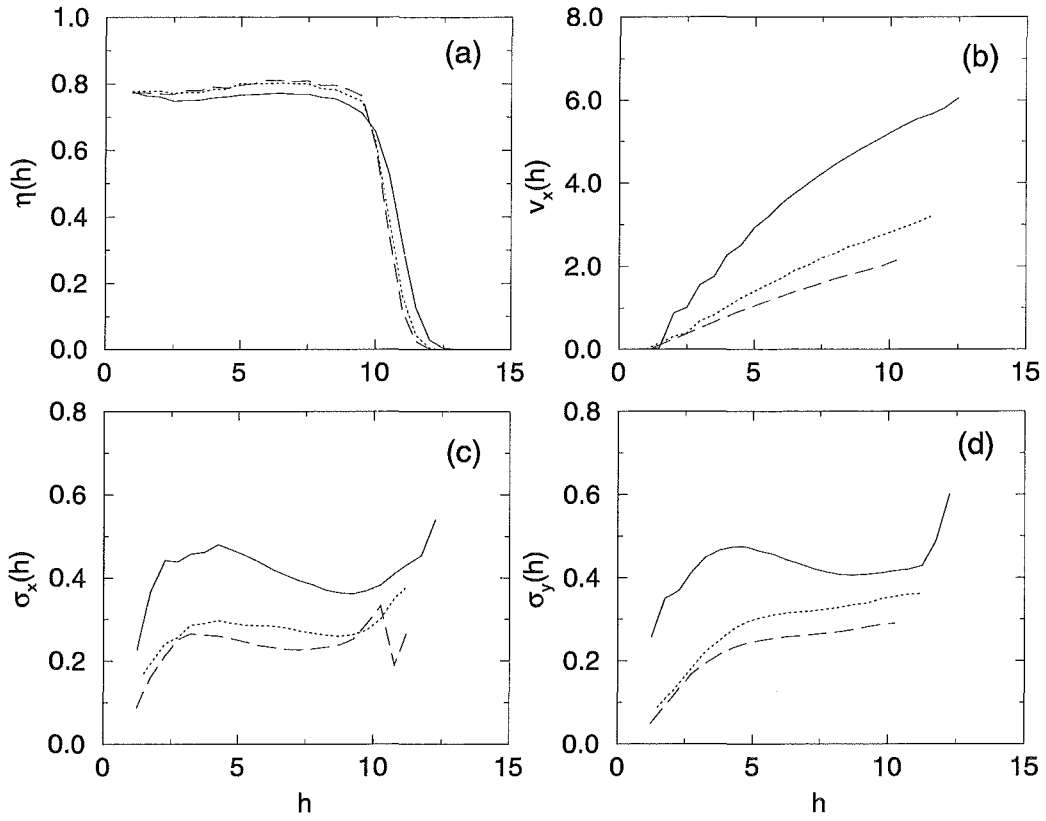

Figure 5.7: *Steady state profiles for density, velocity and temperature, for* $e_n = 0.6$, $\theta = 18°$ *and* $\mu = 0$ *(solid line),* $\mu = 0.25$ *(dotted line) and* $\mu = 0.5$ *(dashed line).*

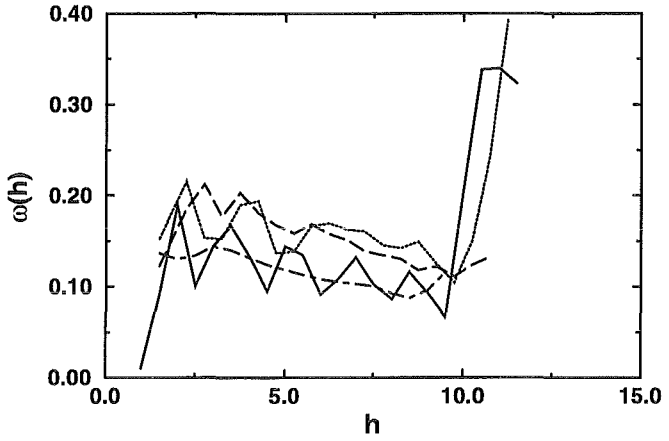

Figure 5.8: *Rotational velocity profiles for* $e_n = 0.6$, $\theta = 18°$, $\mu = 0.25$ *(dotted line) and* $\mu = 0.5$ *(solid line).* $\partial v_x(h)/2\partial h$ *is shown as well. The dashed line corresponds to* $\mu = 0.25$, *the dot-dashed line to* $\mu = 0.5$.

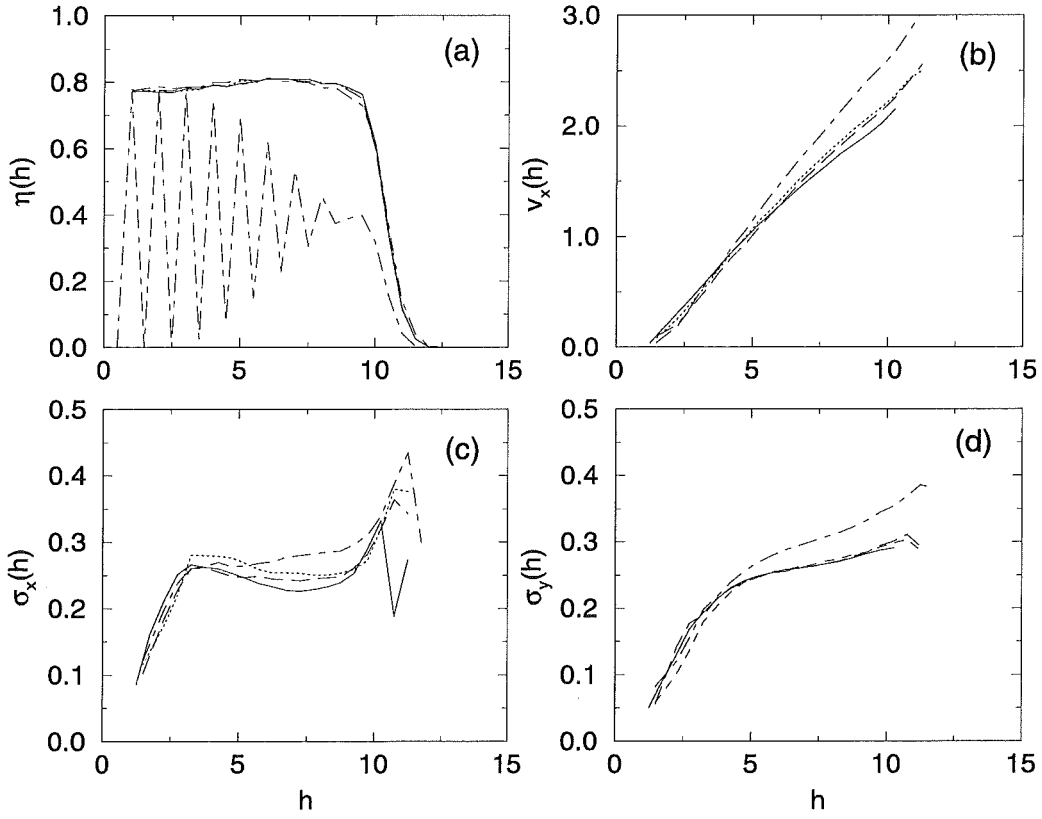

Figure 5.9: *Profiles of various flow quantities for $\mu = 0.5$, $\theta = 18°$ and $e_n = 0.6$ (full line), $e_n = 0.7$ (dotted line), $e_n = 0.8$ (dashed line), $e_n = 0.9$ (dot-dashed line). For $e_n = 0.8$, the results obtained by using smaller bins (scaled by a factor 1/2) is shown as well to give an idea of the strong layering in the system. Averages were obtained as for Fig. 5.1.*

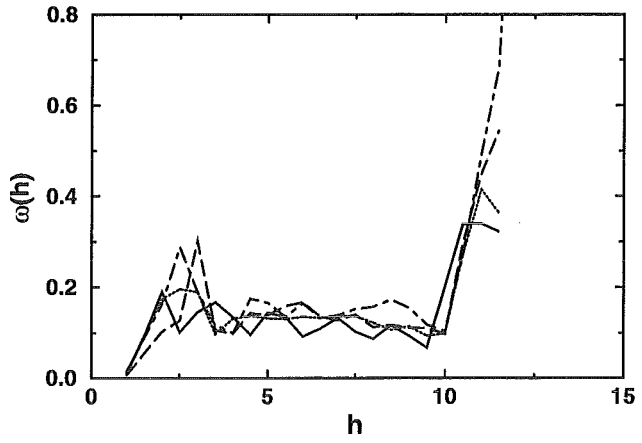

Figure 5.10: *Rotational velocity profiles for the same cases as in Fig. 5.9.*

For the rotational velocity ω, there is just as little influence of e_n as for v_x (see Fig. 5.10). Only for $e_n = 0.9$ it is slightly higher in the upper layers – in accordance with the fact that there $\partial v_x/\partial h$ is higher there as well.

An interesting question to ask is certainly what happens when $e_n \to 1$. I performed some simulation runs on a system with $\mu = 0.5$ and $e_n = 0.99$, and could only find a steady state for $\theta = 16.2°$ (i.e. for $16.2° \pm 1°$ no steady state could be found – for the lower angles of inclination the particles got stuck on the plane, for the higher ones they accelerated). One might even speculate that for $e_n = 1$ *exactly* one inclination angle would lead to a steady state, just like in the case of a solid body on a rough inclined plane. However, since this angle is not simply given by $\mu = \tan\theta$ (as for a block on an inclined plane), it is to be expected that it would be quite hard to get close enough in simulations to find such a steady state. Besides, unlike for a solid block, it may not exist at arbitrarily high velocities, even though the dissipation in such a system is in principle independent of the velocity. Velocities that are too high might lead to too strong an expansion of the system, which would reduce friction.

Figures 5.11 and 5.12 show a comparison of the simulation results for $e_n = 0.99$ with those for $e_n = 0.6$ at this inclination angle. This figure shows very clearly that the main difference between the flows in the two cases is the higher σ_y for the higher e_n (besides, certainly, the difference in the velocity profiles). Obviously, this higher temperature arises from the high elasticity of the system, and the expected gain in dissipation through higher temperature seems to be too weak to make up for the low dissipation in the collisions themselves.

5.3 Summary and discussion of the simulation results

In this chapter, simulations of flow on an inclined plane in two dimensions were discussed. The main emphasis was on the influence of material properties, i.e. the coefficient of restitution and the coefficient of friction, on the flow properties, while the geometry of the system remained fixed (except, of course, the inclination angle θ). The most important result is certainly the fact that, both in the presence or absence of friction, the coefficient of restitution has only a minor influence on the steady state properties of the flow for $e_n \leq 0.8$. It does, however, just like in the case of the single particle, influence the limits for the existence of a steady state. For frictionless particles, no steady state could be found for higher coefficients of restitution. For frictional particles, flows were stable for higher e_n as well; for $\mu = 0.5$, even for $e_n = 0.99$ a steady state could be found, though only in an extremely narrow region of inclination angles. When friction helps to stabilize the motion, also for higher e_n the flows are very dense. They differ from those at smaller e_n mainly in the upper layers, where v_x and the deviatoric velocity σ_y are higher for larger e_n.

The independence of the flow properties of e_n seems to come about because in such dense flows the particles move in a relatively ordered layered structure, where each particle undergoes most collisions while being trapped in the local minima of these layers. Therefore, though in a slightly different way than in the case of a single particle, the energy loss seems to be determined far more by geometry than by the energy loss in a single collision.

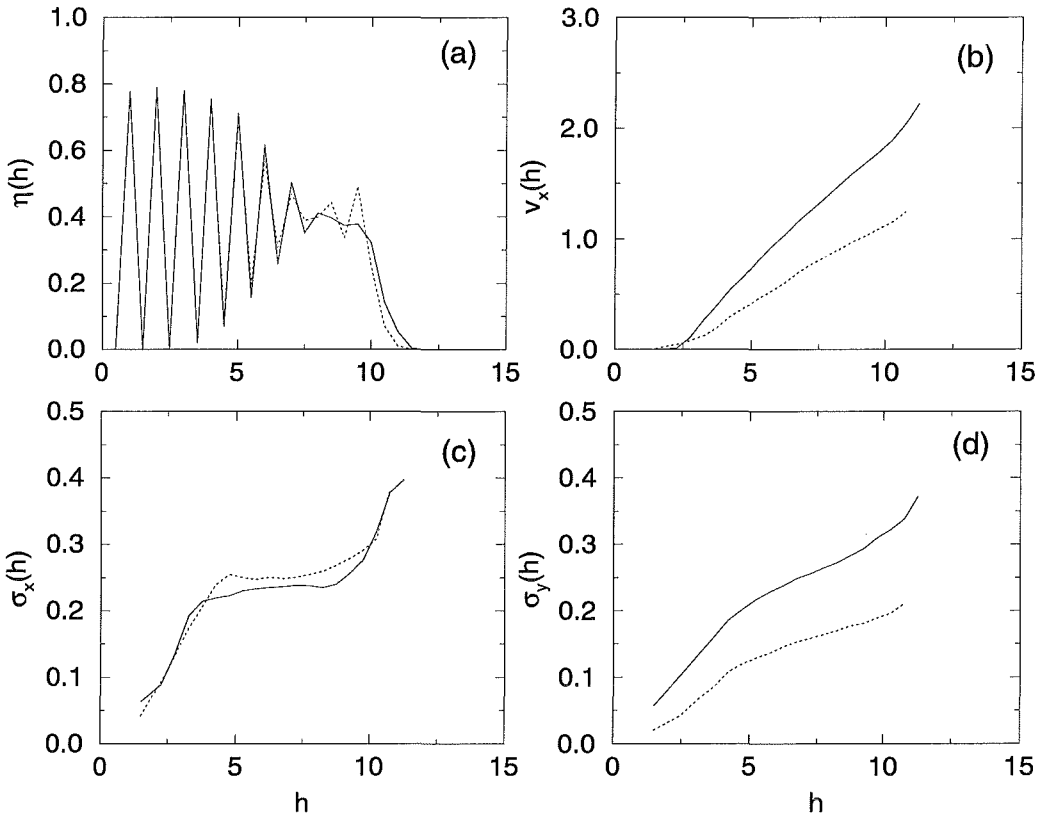

Figure 5.11: *Profiles of various flow quantitites for* $\mu = 0.5$, $\theta = 16.2°$, $e_n = 0.99$ *(solid line) and* $e_n = 0.6$ *(dotted line). A relatively small bin size was used for the density profiles to show that also for* $e_n = 0.99$, *there is still quite strong order in the largest part of the system.*

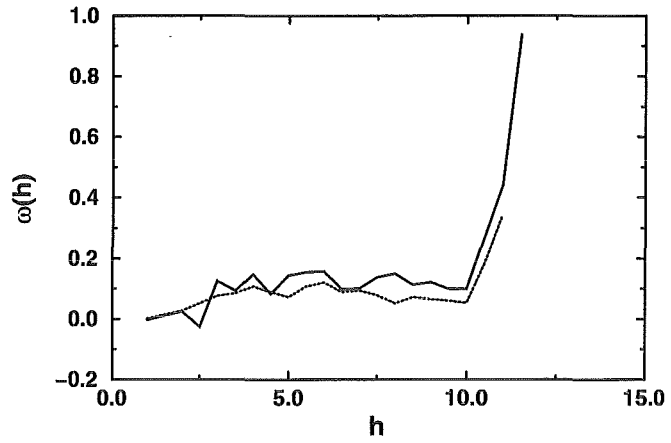

Figure 5.12: *Rotational velocities corresponding to the profiles in Fig. 5.11.*

No steady states could be found where the granular temperature decreased from bottom to top, or where the density had a maximum at an intermediate height, as predicted by some kinetic theories. It should be mentioned that more dilute steady states than in the simulations were found in quasi two dimensional experiments of granular chute flow [268]. However, since there it was also shown that the spacing of the side walls has significant influence on the flow, it is possible that these flows were partially stabilized through the (frictional) influence of the side walls. Besides, it is not clear how far the periodic boundaries in the x-direction, used in the simulations, reinforced small velocity gradients along the chute, thereby accelerating flows that might be nearly stable in systems where material flows out at the bottom.

The main result obtained in this chapter, namely the independence of many flow properties of the coefficient of restitution for $e_n \leq 0.8$, has far-reaching consequences, since it applies especially to that range of e_n for which kinetic theories do not apply. Therefore, it is complementary to kinetic theories and might help to develop a simpler theoretical description for flows of more inelastic particles. Since many materials in nature are rather inelastic, this would allow a description of a far wider range of materials than kinetic theories can provide so far. As a matter of fact, it seems as if the appropriate approach would be very similar to the route take by Bagnold.

5.4 Directions for future research

The simulation results presented in this chapter are certainly far from complete. A very important question which was not addressed here is that of the influence of boundary roughness on the flow. Besides, the influence of different coefficients of restitution and friction $e_n \neq e_n^w$ and $\mu \neq \mu^w$ on the motion have to be investigated. Especially flows with high e_n^w and low e_n would be of interest, since there it might be possible to achieve higher temperature near the bed than in the bulk.

The next question that would have to be addressed is that of the influence of an additional spatial dimension. It should be checked if the independence of the flow properties of e_n for a wide range of e_n prevails in three dimensions as well. Besides, experiments indicate a strong influence of the side walls on the flow in "real" chutes [276], therefore the influence of different boundary conditions in the transverse direction (presence of side walls, their spacing, and also periodic boundary conditions in this direction) should be investigated.

In addition, it is certainly an important and interesting question in how far non-spherical particles behave differently from spherical particles, since in nature, many particles cannot be approximated very well by a spherical shape. Since, as we have seen, sterical constraints seem to be extremely important in determining the flow properties, a different geometry of the particles may be expected to affect the flow properties significantly.

Summary and outlook

Er suchte vor dem versammelten Hof, der damals in Gießen residierte, und vielen Gelehrten aus Wetzlar und Marburg nachzuweisen, daß unser Verstand nicht ausreiche, irgend etwas zu erkennen.
— "Allgemeine Deutsche Biographie" über Johann Konrad Dippel (1673-1734)

In this thesis, the flow of granular material on a rough inclined plane was discussed, where specific attention was drawn to the flow behaviour of a single particle. Computer simulations were used as a tool to assess details of the motion inaccessible to experimental observations.

After a general discussion of the properties of granular materials in Chapter 1, in Chapter 2 the simulation methods used in this work are presented in some detail, as well as a brief outline of other simulation techniques commonly used for granular materials. Most of the results presented in this thesis were obtained by means of time-step driven molecular dynamics simulations (TD). This requires specification of the forces acting between grains. Since there is no generally accepted force model for this interaction, Chapter 3 is devoted to a careful comparison of the most commonly used force laws. It was shown that some forces show such unrealistic behaviour that they can be discarded immediately on the grounds of being unphysical, while others have advantages and disadvantages which make them appropriate for the use in specific flow situations. For two tangential force laws, modifications were proposed that can remedy their most obvious deficiencies.

In Chapter 4, the properties of the motion of a sphere on a rough inclined plane are investigated in detail. After a discussion of previous experimental, theoretical and numerical work, simulation results for both the two dimensional case of a sphere moving down a line of spheres and the three dimensional case of a sphere moving down a plane onto which spheres were glued randomly are discussed. In the two dimensional case, it could be shown that the motion of the particle in the steady state is very regular, consisting of a number of bounces on each ball passed. Therefore, strong correlations between successive bounces develop, which lead to an insensitivity of the steady state mean velocity to material properties like the coefficient of restitution e_n and the coefficient of friction μ. This observation allowed the calculation of the steady state velocity and the lower boundary for the existence of a steady state. Due to the regularity of the motion, disorder in the arrangement of the particles constituting the line has no important influence, and simply taking into account mean and maximum spacing in the calculation suffices to get a very good estimate for mean velocity and lower boundary of the steady state even in the disordered case.

The motion in the three dimensional case was shown to exhibit the same development of correlations between successive collisions as the two dimensional case, leading to the same insensitivity of the mean velocity to material properties as in the two dimensional case. The most important effect of the additional degree of freedom is increased dissipation. This is a result of scattering in the transverse direction, where there is only energy loss and no energy gain. The longitudinal and transverse diffusion coefficients were computed and showed remarkable agreement with recent experimental results obtained by Samson [260]. However, no simple explanation for their dependence on the geometry of the system, like size ratio Φ and inclination angle θ, could be found. Nevertheless, a relatively simple explanation was found for the independence of the transverse diffusion coefficient of e_n.

In Chapter 5, the flow of many particles on an inclined plane in two dimensions was discussed. The main focus in the simulations of the many particle system was on the influence of material properties like e_n and μ. The natural question arising from the single particle results is whether the insensitivity to these parameters is also observed if additionally to the boundary effects the interaction of particles in the flow comes into play. It could be shown that for the systems investigated (i.e. typically 10 layers of particles deep) the coefficient of restitution had practically no influence on the flow properties in the steady state if $e_n \leq 0.8$. In the case of frictionless particles, there is a slight influence of e_n on the temperature in the upper layers; however, these small differences obviously are damped away in the case of frictional particles. Friction clearly has a strong influence on the motion, and increasing μ shifts the range of inclination angles for which a steady state exists towards larger θ.

These results, especially the independence of the velocity profiles and, to a certain extent, also the independence of the temperature profiles of e_n (for coefficients of restitution not too close to unity) have far-reaching consequences. Since kinetic theories of granular flow apply only to nearly elastic particles, i.e. for coefficients of restitution close to unity, the results presented here provide the basis for an alternative approach suited for more inelastic particles by showing that in these cases, geometrical constraints are far more important than the energy loss in a single collision. This is quite important, since many materials occurring in nature (sand, rocks, etc.) are quite inelastic. Besides, even in the cases where there were discrepancies between the results for lower and higher e_n, there was still a strong agreement of all results in the lowest layers, close to the bottom, i.e. the results are valid for the boundary conditions at the bottom.

Future work in the case of many-particle flow on a rough incline should focus on the influence of boundary roughness on the flow, a question not addressed here, though certainly very important, since geometry plays such a predominant role in determining the flow properties as could be shown here. Another question of interest is that of the influence of different coefficients of restitution and friction for particle-particle and particle-wall collisions. A possibly even more important point is the behaviour of the system beyond the steady state. Since the steady state exists only in a quite narrow range of inclination angles, the estimation of the properties in the accelerating and decelerating state would probably be even more important for practical applications. The same question is also of interest for the single particle moving on a rough incline. Another point to be addressed in future work is that of differences between flow on an inclined plane in two and three dimensional systems. Besides, differences between three dimensional systems having open boundaries, periodic boundaries or side walls should be investigated.

Bibliography

[1] B. J. Ennis, J. Green, R. Davies, The legacy of neglect in the U.S., Chem. Eng. Prog., April 1994, 32.

[2] A. E. Scheidegger, On the prediction of the reach and velocity of catastrophic landslides, Rock Mech. **5**, 231 (1973).

[3] H. M. Jaeger, S. R. Nagel, R. P. Behringer, Granular solids, liquids and gases, Rev. Mod. Phys. **68**, 1259 (1996).

[4] K. Pye, H. Tsoar, *Aeolian sand and desert dunes*, London 1990 (Unwin Hyman).

[5] R. A. Bagnold, *The Physics of Blown Sand and Desert Dunes*, London 1956 (Chapman and Hall).

[6] O. Reynolds, On the dilatancy of media composed of rigid particles in contact, Philos. Mag. Ser. 5 **20**, 469 (1885).

[7] C. F. Jenkin, The pressure exerted by granular material: an application of the principle of dilatancy, Proc. Roy. Soc. A **131**, 53 (1931).

[8] V. K. Horvàth, I. M. Jànosi, P. Vella, Anomalous density dependence of static frction in sand, Phys. Rev. E **54**, 2005 (1996).

[9] G. D. Scott, D. M. Kilgour, The density of random close packing of spheres, Brit. J. Appl. Phys. (J. Phys. D) **2**, 863 (1969).

[10] G. Y. Onoda, E. G. Liniger, Random loose packings of uniform spheres and the dilatancy onset, Phys. Rev. Lett. **64**, 2727 (1990).

[11] J. G. Berryman, Random close packing of hard spheres and disks, Phys. Rev. A **27**, 1053 (1986).

[12] C. A. Coulomb, Théorie des machines simples, Acad. R. Sci. Mem. Math. Phys. **10**, 161 (1785).

[13] M. Barquins, La tribologie – la science pour comprendre et maîtriser le frottement et l'usure, Bull. Assoc. Phys. **88**, 793–822, 949–972 (1994).

[14] F. P. Bowden, D. Tabor, *The friction and lubrication of solids. Part I*, Oxford 1954 (Clarendon).

[15] E. Rabinowicz, *Friction and wear of materials*, New York 1965 (Wiley).

[16] R. M. Nedderman, *Statics and kinematics of granular materials*, Cambridge 1992 (Cambridge University Press).

[17] C.-h. Liu, S. R. Nagel, Sound in sand, Phys. Rev. Lett. **68**, 2301 (1992).

[18] S. B. Savage, Problems in the statics and dynamics of granular materials, in: *Powders & Grains 97*, R. P. Behringer and J. T. Jenkins (eds.), Rotterdam 1997 (Balkema).

[19] A. Drescher, G. De Josselin De Jong, Photoelastic verification of a mechanical model for the flow of a granular material, J. Mech. Phys. solids **20**, 337 (1972).

[20] T. Travers, M. Ammi, D. Bideau, A. Gervois, J. C. Messager, J. P. Troadec, J. Phys. (France) **49**, 939 (1988).

[21] C.-h. Liu, D. A. Schecter, S. N. Coppersmith, S. Majumdar, O. Narayan, T. A. Witten, Force Fluctuations in Bead Packs, Science **260**, 513 (1995).

[22] D. Howell, R. P. Behringer, Fluctuations and dynamics for a two-dimensional sheared granular material, in: *Powders & Grains 97*, R. P. Behringer and J. T. Jenkins (eds.), Rotterdam 1997 (Balkema).

[23] F. Radjai, M. Jean, J. J. Moreau, S. Roux, Force distribution in dense two-dimensional granular systems, Phys. Rev. Lett. **77**, 274 (1996).

[24] F. Radjai, D. E. Wolf, S. Roux, M. Jean, J. J. Moreau, Force networks in dense granular media, in: *Powders & Grains 97*, R. P. Behringer and J. T. Jenkins (eds.), Rotterdam 1997 (Balkema).

[25] F. Radjai, Dynamique des rotations et frottement collectif dans les systèmes granulaires, PhD thesis, Université de Paris-Sud (1995).

[26] D. M. Mueth, H. M. Jaeger, S. R. Nagel, Force distribution in a granular medium, Preprint, 1997.

[27] J. Smid, J. Novosad, Pressure distribution under heaped bulk solids, Proc. of 1981 Powtech Conference, Ind. Chem. Eng. Symp. **63**, D3/V/1 (1981).

[28] S. Luding, J. Duran, E. Clément, J. Rajchenbach, Simulations of dense granular flow: dynamic arches and spin organization, J. Phys. I (France) **6**, 823 (1996).

[29] S. C. Cowin, A theory for static loads in bins, J. Appl. Mech. **44**, 409 (1977).

[30] J. Eibl, Design of silos – pressures and explosions, The Structural Engineer **62A**, 169 (1984).

[31] H. A. Janssen, Versuche über Getreidedruck in Silozellen, Zeitschr. VDI **39**, 1045 (1895).

[32] G. Hagen, Über den Druck und die Bewegung des trocknen Sandes, Berlin Monatsber. Akad. Wiss. 1852, 35 (1852).

[33] J. P. Wittmer, P. Claudin, M. E. Cates, J.-P. Bouchaud, An explanation for the central stress minimum in sand piles, Nature **382**, 336 (1996); J. P. Wittmer, M. E. Cates, P. Claudin, Stress propagation and arching in static sandpiles, J. Phys. I (France) **7**, 39 (1997).

[34] D. H. Trollope, The systematic arching theory applied to the stability analysis of embankments. Proc. 4th Intn. Conf. Soil Mech. and Found. Eng., London 1957, p. 382; D. H. Trollope, The mechanics of discontinua or elastic mechanics in rock problems, in: *Rock mechanics in Engineering Practice*, New York 1968 (Wiley).

[35] S. N. Coppersmith, C.-h. Liu, S. Majumdar, O. Narayan, T. A. Witten, Model for force fluctuations in bead packs, Phys. Rev. E **53**, 4673 (1996).

[36] P. Claudin, J.-P. Bouchaud, Static avalanches and giant stress fluctuations in silos, Preprint 1996.

[37] J. Hemmingsson, A sandpile model with dip, Physica A **230**, 329 (1996); J. Hemmingsson, H. J. Herrmann, S. Roux, Vectorial cellular automaton for the stress in granular media, J. Phys. I (France) **7**, 291 (1997).

[38] S. Luding, Stress distribution in static two dimensional granular model media in the absence of friction, Phys. Rev. E **55**, 4720 (1997).

[39] P. Bak, C. Tang, K. Wiesenfeld, Self-organized criticality: An explanation of 1/f noise, Phys. Rev. Lett. **59**, 381 (1987); P. Bak, C. Tang, K. Wiesenfeld, Self-organized criticality, Phys. Rev. A **38**, 364 (1988).

[40] V. Buchholtz, T. Pöschel, Avalanche statistics of sand heaps, J. Stat. Phys. **84**, 1373 (1996).

[41] V. Frette, K. Christensen, A. Malthe-Sørenssen, J. Feder, T. Jøssang, P. Meakin, Avalanche Dynamics in a pile of rice, Nature **379**, 49 (1996).

[42] G. Baumann, D. E. Wolf, Self-organized criticality in a two-dimensional rotating drum model, Phys. Rev. E **54**, R4504 (1996).

[43] J. Rajchenbach, Flow in powders: from discrete avalanches to continuous regime, Phys. Rev. Lett. **65**, 2221 (1990).

[44] H. M. Jaeger, C.-H. Liu, S. R. Nagel, T. A. Witten, Friction in granular flows, Europhys. Lett. **11**, 619 (1990).

[45] R. M. Nedderman, C. Laohakul, The thickness of the shear zone in flowing granular materials, Powder Technol. **25**, 91 (1980).

[46] J. Bridgwater, On the width of failure zones, Géotechnique **30**, 533 (1980).

[47] D. M. Hanes, D. L. Inman, Observations of rapidly flowing granular-fluid materials, J. Fluid Mech. **150**, 357 (1985).

[48] D. M. Hanes, J. T. Jenkins, M. W. Richman, The thickness of steady plane shear flows of circular disks driven by identical boundaries, J. Appl. Mech. **55**, 969 (1988).

[49] Y. Zhang, C. S. Campbell, The interface between fluid-like and solid-like behaviour in two-dimensional granular flows, J. Fluid Mech. **237**, 541 (1992).

[50] S. B. Savage, The mechanics of rapid granular flows, Adv. Appl. Mech. **24**, 289 (1984).

[51] S. Ogawa, Multitemperature theory of granular materials, in: *Proc. US-Japan Seminar on Continuum-Mechanical and Statistical Approaches in the Mechanics of Granular Materials*, S. C. Cowin u. M. Satake (eds.), Tokyo 1978 (Gakujutsu Bunken Fukyukai).

[52] S. Ogawa, A. Umemura, N. Oshima, On the equations of fully fluidized granular materials, J. Appl. Math. Phys. **31**, 483 (1980).

[53] P. K. Haff, Grain flow as a fluid-mechanical phenomenon, J. Fluid Mech. **134**, 401 (1983).

[54] I. Goldhirsch, G. Zanetti, Clustering instability in dissipative gases, Phys. Rev. Lett. **70**, 1619 (1993).

[55] I. Goldhirsch, Microstructures and kinetics in rapid granular flows, in: *Proceedings of "HLRZ Workshop on Traffic and Granular Flow"*, D. E. Wolf, M. Schreckenberg, A. Bachem (eds.), Singapore 1996 (World Scientific).

[56] M. Babić, Gravity-driven flows of smooth, inelastic disks between parallel bumpy boundaries, J. Appl. Mech. **60**, 59 (1993).

[57] S. E. Esipov, T. Pöschel, The granular phase diagram, J. Stat. Phys. **86**, 1385 (1997).

[58] S. McNamara, W. R. Young, Dynamics of a freely evolving, two-dimensional granular medium, Phys. Rev. E **53**, 5089 (1996).

[59] T. Pöschel, Recurrent clogging and density waves in granular material flowing through a narrow pipe, J. Phys. I (France) **4**, 499 (1994).

[60] J. Lee, Density waves in the flows of granular media, Phys. Rev. E **49**, 281 (1994).

[61] J. Schäfer, Rohrfluß granularer Materie: Theorie und Simulationen, PhD thesis, Universität Duisburg, 1996.

[62] M. A. Hopkins, M. Y. Louge, Inelastic microstructure in rapid granular flows of smooth disks, Phys. Fluids A **3**, 47 (1991).

[63] C.-H. Wang, R. Jackson, S. Sundaresan, Stability of bounded rapid shear flows of a granular material, J. Fluid Mech. **308**, 31 (1996).

[64] S. B. Savage, Instability of unbounded uniform granular shear flow, J. Fluid Mech. **241**, 109 (1992).

[65] R. A. Bagnold, Experiments on a gravity-free dispersion of large solid spheres in a newtonian fluid under shear, Proc. Roy. Soc. A **225**, 49 (1954).

[66] S. B. Savage, D. J. Jeffrey, The stress tensor in a granular flow at high shear rates, J. Fluid Mech. **110**, 255 (1981).

[67] J. T. Jenkins, S. B. Savage, A theory for the rapid flow of identical, smooth, nearly elastic, spherical particles, J. Fluid Mech. **130**, 187 (1983).

[68] C. K. K. Lun, S. B. Savage, D. J. Jeffrey, N. Chepurniy, Kinetic theories for granular flow: Inelastic particles in Couette flow and slightly inelastic particles in a a general flow field, J. Fluid Mech. **140**, 223 (1984).

[69] C. K. K. Lun, S. B. Savage, A simple kinetic theory for granular flow of rough, inelastic, spherical particles, J. Appl. Mech. **54**, 47 (1987).

[70] B. Miller, C. O'Hern, R. P. Behringer, Stress fluctuations for continuously sheared granular materials, Phys. Rev. Lett. **77**, 3110 (1996).

[71] R. A. Bagnold, The flow of cohesionless grains in fluids, Phil. Transactions A **249**, 235 (1956).

[72] S. B. Savage, S. McKeown, Shear stresses developed during rapid shear of dense concentrations of large spherical particles between concentric cylinders, J. Fluid Mech. **127**, 453 (1983).

[73] S. B. Savage, M. Sayed, Stresses developed by dry cohesionless granular materials sheared in an annular shear cell, J. Fluid Mech. **142**, 391 (1984).

[74] O. Hungr, N. R. Morgenstern, High velocity ring shear tests on sand, Géotechnique **34**, 4125 (1984).

[75] S. Chapman, T. G. Cowling, *The Mathematical Theory of Non-Uniform Gases*, Cambridge 1970[3] (Cambridge Univ. Press).

[76] K. Hui, P. K. Haff, J. E. Ungar, R. Jackson, Boundary conditions for high-shear grain flows, J. Fluid Mech. **145**, 223 (1984).

[77] M. W. Richman, C. S. Chou, Boundary effects on granular shear flows of smooth disks, J. Appl. Math. Phys. (ZAMP) **39**, 885 (1988).

[78] J. T. Jenkins, Boundary conditions for rapid granular flow: Flat, frictional walls, J. Appl. Mech. **59**, 120 (1992).

[79] M. W. Richman, Boundary conditions for granular flows at randomly fluctuating bumpy boundaries, in: *Advances in Micromechanics of Granular Materials*, H. H. Shen et al. (Hrsg.), Amsterdam 1992 (Elsevier).

[80] M. W. Richman, Boundary conditions for granular flows at randomly fluctuating bumpy boundaries, Mech. Materials **16**, 211 (1993).

[81] T. Raafat, J. P. Hulin, H. J. Herrman, Density waves of dry granular media falling through a vertical pipe, Phys. Rev. E **53**, 4345 (1996).

[82] C. S. Campbell, C. E. Brennen, Computer simulation of granular shear flows, J. Fluid Mech. **151**, 167 (1985).

[83] O. R. Walton, R. L. Braun, Viscosity, granular-temperature, and stress calculations for shearing assemblies of inelastic, frictional discs, J. Rheol. **30**, 949 (1986).

[84] M. Y. Louge, J. T. Jenkins, M. A. Hopkins, Computer simulations of rapid granular shear flows between parallel bumpy boundaries, Phys. Fluids A **2**, 1042 (1990).

[85] J. Cao, G. Ahmadi, Numerical simulation of granular Couette flows between two rough parallel plates, Part. Sci. and Technol. **13**, 133 (1995).

[86] S. Nasuno, A. Kudrolli, J. P. Gollub, Friction in granular layers: hysteresis and precursors, Phys. Rev. Lett. **79**, 949, 1997.

[87] P. A. Thompson, G. S. Grest, Granular flow: friction and the dilatancy transition, Phys. Rev. Lett. **67**, 1751 (1991).

[88] K. Takahasi, On the dynamical properties of granular mass, Geophys. Mag. (Jpn.) **11**, 165 (1937).

[89] A. W. Roberts, An investigation of the gravity flow of noncohesive granular materials through discharge chutes, J. Eng. Ind. **91**, 373 (1969).

[90] A. W. Roberts, O. J. Scott, Flow of bulk solids through transfer chutes of variable geometry and profile, Bulk Solids Handling **1**, 715 (1981).

[91] K. Ridgway, R. Rupp, Flow of granular material down chutes, Chem. Proc. Eng. **51**, 82 (1970).

[92] D. A. Augenstein, R. Hogg, An experimental study of the flow of dry powders over inclined surfaces, Powder Technol. **19**, 205 (1978).

[93] S. B. Savage, Gravity flow of cohesionless granular materials in chutes and channels, J. Fluid Mech. **92**, 53 (1979).

[94] M. Ishida, T. Shirai, Velocity distributions in the flow of solid particles in an inclined open channel, J. Chem. Eng. Jpn. **12**, 46 (1979).

[95] M. Ishida, H. Hatano, T. Shirai, The flow of solid particles in an aerated inclined channel, Powder Technol. **27**, 7 (1980).

[96] C. E. Brennen, K. Sieck, and J. Paslaski, Hydraulic jumps in granular material flow, Powder Technol. **35**, 31 (1982).

[97] C. S. Campbell, C. E. Brennen, R. H. Sabersky, Flow regimes in inclined open-channel flow of granular materials, Powder Technol. **41**, 77 (1985).

[98] J. S. Patton, C. E. Brennen, R. H. Sabersky, Shear flows of rapidly flowing granular materials, J. Appl. Mech. **554**, 801 (1987).

[99] P. C. Johnson, P. Nott, R. Jackson, Frictional-collisional equations of motion for particulate flows and their application to chutes, J. Fluid Mech. **210**, 501 (1990).

[100] T. G. Drake, Structural features in granular flows, J. Geophysical Reserch **95**, 8681 (1990).

[101] T. G. Drake, Granular flow: physical experiments and their implications for microstructural theories, J. Fluid Mech. **225**, 121 (1991).

[102] H. Ahn, C. E. Brennen, R. H. Sabersky, Measurements of velocity, velocity fluctuation, density, and stresses in chute flow of granular materials, J. Appl. Mech. **58**, 792 (1991).

[103] K. Nishimura, K. Kosugi, M. Nakagawa, Experiments on ice-sphere flows along an inclined chute, in: *Advances in Micromechanics of Granular Materials*, ed. by H. H. Shen *et al.*, Amsterdam 1992 (Elsevier).

[104] O. Pouliquen, N. Renaut, Onset of granular flows on an inclined rough surface: dilatancy effects, J. Phys. II (France) **6**, 923 (1996).

[105] C. S. Campbell, C. E. Brennen, Chute flows of granular material: some computer simulations, J. Appl. Mech. **52**, 172 (1985).

[106] T. Pöschel, Granular material flowing down an inclined chute: a molecular dynamics simulation, J. Phys. II (France) **3**, 27 (1993).

[107] O. R. Walton, Numerical simulation of inclined chute flows of monodisperse, inelastic, frictional spheres, Mech. of Mater. **16**, 239 (1993).

[108] T. G. Drake, O. R. Walton, Comparison of experimental and simulated grain flows, J. Appl. Mech. **62**, 131 (1995).

[109] X. M. Zheng, J. M. Hill, Molecular dynamics modelling of granular chute flow: density and velocity profiles, Powder Technol. **86**, 219 (1996).

[110] J. T. Jenkins, Rapid granular flow down inclines, Appl. Mech. Rev. **47**, S240 (1994).

[111] S. McNamara, J.-L. Barrat, The energy flux into a fluidized granular medium at a vibrating wall, Phys. Rev. E **55**, 7767 (1997).

[112] S. Luding, Die Physik kohäsionsloser granularer Medien, Habilitationsschrift, Universität Stuttgart, 1997.

[113] K. Liffman, G. Metcalfe, P. Cleary, Convection due to horizontal shaking, in: *Powders & Grains 97*, R. P. Behringer and J. T. Jenkins (eds.), Rotterdam 1997 (Balkema).

[114] M. Medved, personal communication.

[115] J. B. Knight, C. G. Fandrich, Ch. N. Lau, H. M. Jaeger, S. R. Nagel, Density relaxation in a vibrated granular material, Phys. Rev. E **51**, 3957 (1995).

[116] E. Ben-Naim, J. B. Knight, E. R. Nowak, Slow relaxation in granular compaction, J. Chem. Phys. **100**, 6778 (1996).

[117] D. C. Hong, S. Yue, J. K. Rudra, M. Y. Choi, Y. W. Kim, Granular relaxation under tapping and the traffic equation, Phys. Rev. E **50**, 4123 (1994).

[118] S. J. Linz, Phenomenological modeling of the compaction dynamics of shaken granular systems, Phys. Rev. E **54**, 2925 (1996).

[119] M. Nicodemi, A. Coniglio, H. J. Herrmann, Frustration and slow dynamics of granular packings, Phys. Rev. E **55**, 3962 (1997).

[120] M. Nicodemi, A. Coniglio, H. J. Herrmann, The compaction in granular media and frustrated Ising models, J. Phys. A **30**, L379 (1997).

[121] P. Evesque, J. Rajchenbach, Instability in a sand heap, Phys. Rev. Lett. **62**, 44 (1989).

[122] E. Clément, J. Duran, J. Rajchenbach, Experimental study of heaping in a two-dimensional "sandpile," Phys. Rev. Lett. **69**, 1189 (1992).

[123] M. Faraday, On a peculiar class of acoustical figures, Philos. Trans. R. Soc. London **52**, 299 (1831).

[124] C. Laroche, S. Douady, S. Fauve, Convective flow of granular masses under vertical vibrations, J. Phys. France **50**, 679 (1989).

[125] H. K. Pak, E. van Doorn, R.P. Behringer, Effects of ambient gases on granular materials under vertical vibration, Phys. Rev. Lett. **74**, 4643 (1995).

[126] J. B. Knight, E. E. Ehrichs, V. Y. Kuperman, J. K. Flint, H. M. Jaeger, S. R. Nagel, Experimental study of granular convection, Phys. Rev. E **54**, 5726 (1996).

[127] K. M. Aoki, T. Akiyama, Y. Maki, T. Watanabe, Convective roll patterns in vertically vibrated beds of granules, Phys. Rev. E **54**, 874 (1996).

[128] E. E. Ehrichs, H. M. Jaeger, G. S. Karczmar, J. B. Knight, V. Yu. Kuperman, S. R. Nagel, Granular convection observed by magnetic resonance imaging, Science **267**, 1632 (1995).

[129] V. Yu. Kuperman, Nuclear magnetic resonance measurements of diffusion in granular media, Phys. Rev. Lett. **77**, 1178 (1996).

[130] S. Luding, E. Clément, A. Blumen, J. Rajchenbach, J. Duran, Onset of convection in molecular dynamics simulations of grains, Phys. Rev. E **50**, R1762 (1994).

[131] Y.-H. Taguchi, New origin of a convective motion: elastically induced convection in granular materials, Phys. Rev. Lett. **69**, 1367 (1992).

[132] J. A. C. Gallas, H. J. Herrmann, S. Sokołowski, Convection cells in vibrating granular media, Phys. Rev. Lett. **69**, 1371 (1992).

[133] E. L. Grossmann, The effects of container geometry on granular convection, to appear in Phys. Rev. E (1997).

[134] J. B. Knight, External boundaries and internal shear bands in granular convection, Phys. Rev. E **55**, 6016 (1997).

[135] M. Bourzutschky, J. Miller, "Granular" convection in a vibrated fluid, Phys. Rev. Lett. **74**, 2216 (1995).

[136] E. Clément, L. Vanel, J. Rajchenbach, J. Duran, Pattern formation in a vibrated 2D granular layer, Phys. Rev. E **53**, 2972 (1996).

[137] S. Luding, E. Clément, J. Rajchenbach, J. Duran, Simulations of pattern formation in vibrated granular media, Europhys. Lett. **36**, 247 (1996).

[138] M. D. Shattuck, C. Bizon, P. B. Umbanhowar, J. B. Swift, H. L. Swinney, 2d vertically vibrated granular media: Experiment and simulation, in: *Powders & Grains 97*, R. P. Behringer and J. T. Jenkins (eds.), Rotterdam 1997 (Balkema).

[139] H. K. Pak, R. P. Behringer, Surface waves in vertically vibrated granular materials, Phys. Rev. Lett. **71**, 1832 (1993).

[140] F. Melo, P. Umbanhowar, H. L. Swinney, Transition to parametric wave patters in a vertically oscillated granular layer, Phys. Rev. Lett. **72**, 172 (1994).

[141] P. B. Umbanhowar, F. Melo, H. L. Swinney, Localized excitations in a vertiacally vibrated granular layer, Nature **382**, 793 (1996).

[142] T. Shinbrot, Granular patterns: a competition between randomizing impacts and inelastic collisions?, preprint, 1997.

[143] S. Luding, Models and simulations of granular materials, PhD thesis, Universität Freiburg, 1994.

[144] J. A. C. Gallas, H. J. Herrmann, S. Sokołowski, Molecular dynamics simulation of powder fluidization in two dimensions, Physica A **189**, 437 (1992).

[145] E. Clément, S. Luding, A. Blumen, J. Rajchenbach, J. Duran, Fluidization, condensation and clusterization of a vibrating column of beads, Int. J. Mod. Phys. B **7**, 1807 (1993).

[146] S. Luding, Granular materials under vibration: Simulations of rotating spheres, Phys. Rev. E **52**, 4442 (1995).

[147] Y. Lan, A. D. Rosato, Macroscopic behavior of vibrating beds of smooth inelastic spheres, Phys. Fluids **7**, 1818 (1997).

[148] S. Warr, J. M. Huntley, G. T. H. Jacques, Fluidization of a two-dimensional granular system: Experimental study and scaling behavior, Phys. Rev. E **52**, 5583 (1995).

[149] J. Lee, Scaling behavior of granular particles in a vibrating box, Physica A **219**, 305 (1995).

[150] S. Luding, H. J. Herrmann, A. Blumen, J. Rajchenbach, J. Duran, Simulations of two-dimensional arrays of beads under external vibrations: Scaling behavior, Phys. Rev. E **50**, 3100 (1994).

[151] M. Müller, S. Luding, H. J. Herrmann, Simulations of vibrated granular media in 2d and 3d, in: *Proceedings of "HLRZ Workshop on Friction, Arching, Contact Dynamics"*, D. E. Wolf, P. Grassberger (eds.), Singapore 1997 (World Scientific).

[152] S. Luding, E. Clément, A. Blumen, J. Rajchenbach, J. Duran, Studies of columns of beads under external vibrations, Phys. Rev. E **49**, 1634 (1994).

[153] J. C. Williams, The segregation of particulate materials. A review, Powder Technol. **15**, 245 (1976).

[154] M. H. Cooke, D. J. Stephens, J. Bridgwater, Powder mixing – a literature survey, Powder Technol. **15**, 1 (1976).

[155] K. Ahmad, I. J. Smalley, Observation of particle segregation in vibrated granular systems, Powder Technol. **8**, 69 (1973).

[156] A. Rosato, K. J. Strandburg, F. Prinz, R. H. Swendsen, Why the brazil nuts are on top: size segregation of particulate matter by shaking, Phys. Rev. Lett. **58**, 1038 (1987).

[157] A. D. Rosato, T. Vreeland, F. B. Prinz, Manufacture of powder compacts, Int. Mat. Rev. **36**, 45 (1991).

[158] R. Jullien, P. Meakin, A. Pavlovitch, Three-dimensional model for particle-size segregation by shaking, Phys. Rev. Lett. **69**, 640 (1992).

[159] J. Duran, J. Rajchenbach, E. Clément, Arching effect model for particle size segregation, Phys. Rev. Lett. **70**, 2431 (1993).

[160] S. Dippel, S. Luding, Simulations on size segregation: Geometrical effects in the absence of convection, J. Phys. I (France) **5**, 1527 (1995).

[161] J. B. Knight, H. M. Jaeger, S. R. Nagel, Vibration-induced size separation in granular media: The convection connection, Phys. Rev. Lett. **70**, 3728 (1993).

[162] T. Pöschel, H. J. Herrmann, Size segregation and convection, Europhys. Lett. **29**, 123 (1995).

[163] W. Cooke, S. Warr, J. M. Huntley, R. C. Ball, Particle size segregation in a two-dimensional bed undergoing vertical vibration, Phys. Rev. E **53**, 2812 (1996).

[164] J. A. C. Gallas, H. J. Herrmann, T. Pöschel, S. Sokolowski, Molecular dynamics simulation of size segregation in three dimensions, J. Stat. Phys. **82**, 443 (1996).

[165] L. Vanel, A. D. Rosato, R. N. Dave, Rise-time regimes of a large sphere in vibrated bulk solids, Phys. Rev. Lett. **78**, 1255 (1997).

[166] J. A. Drahun, J. Bridgwater, The mechanisms of free surface segregation, Powder Tech. **36**, 39 (1983).

[167] S. B. Savage, Flows of granular materials with applications to geophysical problems, Lecture notes of the IUTAM International Summer School on Mechanics, International Centre of Mechanical Sciences (CISM), Udine, Italy, 22-26 June 1992.

[168] S. B. Savage, Disorder, diffusion and structure formation in granular flows, in: *Disorder and Granular Media*, D. Bideau and A. Hansen (eds.), Amsterdam, 1993 (Elsevier).

[169] O. Pouliquen, J. Delour, S. B. Savage, Fingering in granular flows, Nature **386**, 816 (1997); O. Pouliquen, Fingering instability in granular flows, in: *Powders & Grains 97*, R. P. Behringer and J. T. Jenkins (eds.), Rotterdam 1997 (Balkema).

[170] H. A. Makse, S. Havlin, P. R. King, H. E. Stanley, Spontaneous stratification in granular mixtures, Nature **386**, 379 (1997); H. A. Makse, P. Cizeau, H. E. Stanley, Possible stratification mechanism in granular mixtures, Phys. Rev. Lett. **78**, 3298 (1997).

[171] J. Koeppe, M. Enz, J. Kakalios, Avalanche segregation in granular media, in: *Powders & Grains 97*, R. P. Behringer and J. T. Jenkins (eds.), Rotterdam 1997 (Balkema).

[172] F. Cantelaube, D. Bideau, Radial segregation in a 2d drum: an experimental analysis, Europhys. Lett. **30**, 133 (1995).

[173] G. Baumann, I. M. Jánosi, D. E. Wolf, Surface properties and flow of granular material in a two-dimensional rotating-drum model, Phys. Rev. E **51**, 1879 (1995).

[174] C. M. Dury, G. H. Ristow, Radial segregation in a two-dimensional rotating drum, J. Phys. I (France) **7**, 737 (1997).

[175] K. M. Hill, A. Caprihan, J. Kakalios, Bulk segregation in rotated granular material measured by magnetic resonance imaging, Phys. Rev. Lett. **78**, 50 (1997).

[176] D. V. Khakhar, J. J. McCarthy, J. M. Ottino, Radial segregation of granular mixtures in rotating cylinders, submitted to Phys. Fluids, 1997.

[177] G. H. Ristow, Particle mass segregation in a two-dimensional rotating drum, Europhys. Lett. **28**, 97 (1994).

[178] O. Zik, D. Levine, S. G. Lipson, S. Strikman, J. Stavans, Rotationally induced segregation of granular materials, Phys. Rev. Lett. **73**, 644 (1994).

[179] K. M. Hill, J. Kakalios, Reversible axial segregation of binary mixtures of granular materials, Phys. Rev. E **49**, R3610 (1994).

[180] K. M. Hill, J. Kakalios, Reversible axial segregation of rotating granular media, Phys. Rev. E **52**, 4393 (1995).

[181] R. Chicharro, R. Peralta-Fabi, R. M. Velasco, Segregation in dry granular systems, in: *Powders & Grains 97*, R. P. Behringer and J. T. Jenkins (eds.), Rotterdam 1997 (Balkema).

[182] K. L. Johnson, *Contact Mechanics*, Cambridge 1989 (Cambridge Univ. Press).

[183] H. Hertz, Über die Berührung fester elastischer Körper, Journal f. d. reine u. angew. Math. **92**, 156 (1882).

[184] L. D. Landau, E. M. Lifschitz, *Lehrbuch der Theoretischen Physik Bd. VII (Elastizitätstheorie)*, Berlin 1987 (Akademie Verlag).

[185] W. Goldsmith, *Impact - The Theory and Physical Behaviour of Colliding Solids*, London 1960 (Edward Arnold Publ.).

[186] J. M. Lifshitz, H. Kolsky, Some experiments on anelastic rebound, J. Mech. Phys. Solids **12**, 35 (1964).

[187] K. L. Johnson, K. Kendall, A. D. Roberts, Surface energy and the contact of elastic solids, Proc. Roy. Soc. Lond. A **324**, 301 (1971).

[188] G. Giese, A. Zippelius, Collision properties of one-dimensional granular particles with internal degrees of freedom, Phys. Rev. E **54**, 4828 (1996).

[189] G. Kuwabara, K. Kono, Restitution coefficient in a collision between two spheres, Jpn. J. Appl. Phys. **26**, 1230 (1987).

[190] F. G. Bridges, A. Hatzes, D. N. C. Lin, Structure, stability and evolution of Saturn's rings, Nature **309**, 333 (1984).

[191] R. Sondergaard, K. Chaney, C. E. Brennen, Measurements of solid spheres bouncing off flat plates, J. Appl. Mech. **57**, 694 (1990).

[192] T. G. Drake, R. L. Shreve, High-speed motion pictures of nearly steady, uniform, two-dimensional, inertial flows of granular material, J. Rheol. **30**, 981 (1986).

[193] S. F. Foerster, M. Y. Louge, H. Chang, K. Allia, Measurements of the collision properties of small spheres, Phys. Fluids **6**, 1108 (1994).

[194] M. J. Adams, B. J. Briscoe, Deterministic Micromechanical Modelling of Failure or Flow in Discrete Planes of Densely Packed Particle Assemblies: Introductory Principles, in: A. Mehta, *Granular Matter*, New York 1994 (Springer).

[195] R. D. Mindlin, H. Deresiewicz, Elastic spheres in contact under varying oblique forces, J. Appl. Mech. **20**, 327 (1953).

[196] N. Maw, J. R. Barber, J. N. Fawcett, The oblique impact of elastic spheres, Wear **38**, 101 (1976).

[197] N. Maw, J. R. Barber, J. N. Fawcett, The role of elastic tangential compliance in oblique impact, J. Lubr. Technol. **103**, 74 (1981).

[198] K. Walton, The oblique compression of two elastic spheres, J. Mech. Phys. Solids **26**, 139 (1978).

[199] O. R. Walton, Numerical simulation of inelastic, frictional particle-particle interactions, in: *Particulate Two-Phase Flow*, M.C. Roco (ed.), Boston, 1993 (Butterworth-Heinemann).

[200] D. E. Wolf, Modelling and computer simulation of granular media, in: *Computational Physics: Selected Methods - Simple Exercises - Serious Applications*, K. H. Hoffmann, M. Schreiber (eds.), Heidelberg, 1996 (Springer).

[201] W. M. Visscher, M. Bolsterli, Random packing of equal and unequals sphere in two and three dimensions, Natuer **239**, 504 (1972).

[202] M. P. Allen, D. J. Tildesley, *Computer Simulation of Liquids*, Oxford, 1987 (Clarendon Press).

[203] P. A. Cundall, O. D. L. Strack, A discrete numerical model for granular assemblies, Géotechnique **29**, 47 (1979).

[204] O. R. Walton, Particle-dynamics calculations of shear flow in: *Mechanics of Granular Media*, ed. by J. T. Jenkins and M. Satake, Amsterdam 1983 (Elsevier).

[205] P. K. Haff, B. T. Werner, Computer simulation of the mechanical sorting of grains, Powder Technol. **48**, 239 (1986).

[206] G. H. Ristow, Simulating granular flow with molecular dynamics, J. Phys. I (France) **2**, 649 (1992).

[207] Y. Tsuji, T. Tanaka, T. Ishida, Lagrangian numerical simulation of plug flow of cohesionless particles in a horizontal pipe, Powder Technol. **71**, 239 (1992).

[208] J. Lee, H. J. Herrmann, Angle of repose and angle of marginal stability: molecular dynamics of granular particles, J. Phys. A **26**, 373 (1993).

[209] S. Melin, Wave propagation in granular assemblies, Phys. Rev. E **49**, 2353 (1994).

[210] W. H. Press, S. A. Teukolsky, W. T. Vetterling, B. P. Flannery, *Numerical Recipes in FORTRAN - The Art of Scientific Computing*, Cambridge 1992[2] (Cambridge Univ. Press).

[211] S. Luding, E. Clément, A. Blumen, J. Rajchenbach, J. Duran, Anomalous energy dissipation in molecular-dynamics simulations of grains: The "detachment" effect, Phys. Rev. E **50**, 4113 (1994).

[212] J. Schäfer, D. E. Wolf, Bistability in simulated granular flow along corrugated walls, Phys. Rev. E **51**, 6154 (1995).

[213] B. Bernu, R. Mazighi, One-dimensional bounce of inelastically colliding marbles on a wall, J. Phys. A **23**, 5745 (1990).

[214] S. McNamara, W. R. Young, Inelastic collapse and clumping in a one-dimensional granular medium, Phys. Fluids A **4**, 496 (1992).

[215] S. McNamara, W. R. Young, Inelastic collapse in two dimensions, Phys. Rev. E **50**, R28 (1994).

[216] T. Zhou, L. P. Kadanoff, Inelastic collapse of three particles, Phys. Rev. E **54**, 623 (1996).

[217] N. Schörghofer, T. Zhou, Inelastic collapse of rotating spheres, Phys. Rev. E **54**, 5511 (1996).

[218] S. Luding, Surface waves and pattern formation in vibrated granular beds, in: *Powders & Grains 97*, R. P. Behringer and J. T. Jenkins (eds.), Rotterdam 1997 (Balkema).

[219] M. Y. Louge, Computer simulations of rapid granular flows of spheres interacting with a flat, frictional boundary, Phys. Fluids A **6** 2253 (1994).

[220] J. J. Moreau, New computation methods in granular dynamics, in: *Powders and Grains 93*, C. Thornton (Hrsg.), Rotterdam 1993 (Balkema).

[221] F. Radjai, L. Brendel, S. Roux, Non-smoothness, indeterminacy and friction in granular systems, Phys. Rev. E **54**, 861 (1996).

[222] P. Devillard, Scaling behaviour in size segregation ("Brazil Nuts"), J. Phys. France **53**, 369 (1990).

[223] G. A. Bird, Molecular gas dynamics and the direct simulation of gas flows, Oxford 1994 (Clarendon).

[224] R. Jullien, P. Meakin, Mechanism for particle size segregation in three dimensions, Nature **344**, 425 (1990).

[225] R. Jullien, P. Meakin, A. Pavlovitch, Particle size segregation by shaking in two-dimensional disc packings, Europhys. Lett. **22**, 523 (1993).

[226] G. Baumann, E. Jobs, D. E. Wolf, Granular cocktail rotated and shaken, Fractals **1**, 767 (1993).

[227] G. Baumann, Modelle und Computersimulationen granularer Materie, PhD thesis, Universität Duisburg, 1997.

[228] A. Mehta, G. C. Barker, Vibrated powders: a microscopic approach, Phys. Rev. Lett. **67**, 394 (1991).

[229] G. W. Baxter, R. P. Behringer, Cellular automata models of granular flow, Phys. Rev. A **42**, 1017 (1990)

[230] G. Peng, H. J. Herrmann, Density waves of granular flow in a pipe using lattice-gas automata, Phys. Rev. E **49**, R1796 (1994).

[231] A. Károlyi, J. Kertész, Hydrodynamic cellular automata for granular media, in: *Proceedings of the 6th EPS-APS International Conference on Physics Computing*, Lugano 1994 (CSCS).

[232] A. Károlyi, J. Kertész, Lattice gas simulations of granular media, in: *Proceedings of "HLRZ Workshop on Traffic and Granular Flow"*, D. E. Wolf, M. Schreckenberg, A. Bachem (eds.), Singapore 1996 (World Scientific).

[233] J. Schäfer, S. Dippel, D. E. Wolf, Force schemes in simulations of granular materials, J. Phys. I (France) **6**, 5 (1996).

[234] Y.-h. Taguchi, Powder turbulence: direct onset of turbulent flow, J. Phys. II **2**, 2103 (1992).

[235] N. V. Brillantov, F. Spahn, J. M. Hertzsch, T. Pöschel, The collision of particles in granular systems, Physica A **231**, 417 (1996).

[236] S. Melin, Simulation of sound propagation in granular media on the Connection Machine, Int. J. Mod. Phys. C **4**, 1103 (1993).

[237] G. H. Ristow, H. J. Herrmann, Density patterns in two-dimensional hoppers, Phys. Rev. E **50**, R5 (1994).

[238] O. R. Walton, Force models for particle-dynamics simulations of granular materials, in: *Mobile Particulate Systems*, E. Guazzelli, L. Oger (Hrsg.), Dordrecht 1995 (Kluwer).

[239] R. D. Mindlin, Compliance of elastic bodies in contact, J. Appl. Mech. **16**, 259 (1949).

[240] C. Thornton, C. W. Randall, Applications of theoretical contact mechanics to solid particle system simulation, in: *Micromechanics of Granular Materials*, M. Satake and J. T. Jenkins (ed.), Amsterdam 1988 (Elsevier).

[241] E. Falcon, Comportements dynamiques associés au contact de Hertz: processus collectifs de collision et propagation d'ondes solitaires dans les milieux granulaires, PhD thesis, Université Claude Bernard – Lyon I (1997).

[242] M. H. Sadd, Q. Tai, A. Shukla, Contact law effects on wave propagation in particulate materials using distinct element modeling, Int. J. Non-Linear Mechanics **28**, 251 (1993).

[243] F. Radjai, S. Roux, Friction-induced self-organization of a one-dimensional array of particles, Phys. Rev. E **51**, 6177 (1995).

[244] F. Radjai, J. Schäfer, S. Dippel, D. Wolf, Collective friction of an array of particles: a crucial test for numerical algorithms, J. Phys. II (France) **7**, 1053 (1997).

[245] S. B. Savage, K. Hutter, The motion of a finite mass of granular material down a rough incline, J. Fluid Mech. **199**, 177 (1989).

[246] G. G. Batrouni, S. Dippel, L. Samson, Stochastic Model for the motion of a particle on an inclined rough plane and the onset of viscous friction, Phys. Rev. E **53**, 6496 (1996).

[247] S. Dippel, G. G. Batrouni, D. E. Wolf, Collision-induced friction in the motion of a single particle on a bumpy inclined line, Phys. Rev. E **54**, 6845 (1996).

[248] S. Dippel, G. G. Batrouni, D. E. Wolf, How transversal fluctuations affect the friction of a particle on a rough incline, Phys. Rev. E **56**, 3645 (1997).

[249] S. Dippel, L. Samson, G. G. Batrouni, Motion of a Ball on a Rough Inclined Plane, in: *Proceedings of "HLRZ Workshop on Traffic and Granular Flow"*, D. E. Wolf, M. Schreckenberg, A. Bachem (eds.), Singapore 1996 (World Scientific).

[250] S. Dippel, G. G. Batrouni, D. E. Wolf, Motion of a particle on a rough inclined plane: Comparison of 2 and 3 dimensions, in: *Powders & Grains 97*, R. P. Behringer and J. T. Jenkins (eds.), Rotterdam 1997 (Balkema).

[251] L. Samson, I. Ippolito, S. Dippel, G. G. Batrouni, Diffusive motion of single particles on an inclined bumpy plane, in: *Powders & Grains 97*, R. P. Behringer and J. T. Jenkins (eds.), Rotterdam 1997 (Balkema).

[252] S. Dippel, G. G. Batrouni, D. E. Wolf, Friction experienced by a particle moving on a rough inclined plane, in: *Proceedings of "HLRZ Workshop on Friction, Arching, Contact Dynamics"*, D. E. Wolf, P. Grassberger (eds.), Singapore 1997 (World Scientific).

[253] D. E. Wolf, F. Radjai, S. Dippel, Dissipation in granular flows, to appear in Phil Mag.

[254] D. Bideau, I. Ippolito, L. Samson, G. G. Batrouni, S. Dippel, A. Aguirre, A. Calvo, C. Henrique, Gravity Driven Motion of a Single Sphere on a Rough Inclined Surface, in: *Proceedings of "HLRZ Workshop on Traffic and Granular Flow"*, D. E. Wolf, M. Schreckenberg, A. Bachem (eds.), Singapore 1996 (World Scientific).

[255] C. D. Jan, H. W. Shen, C. H. Ling, and C. I. Chen, A sphere moving down an inclined bumpy surface, in: *Proceedings of the 9th Conference on Engineering Mechanics, College Station, Texas*, L. D. Lutes and J. M. Niedzwecki (eds.), New York, 1992 (American Society of Civil Engineers).

[256] F.-X. Riguidel, Écoulements de particules sur un plan rugueux incliné, PhD thesis, Université de Rennes I (1994).

[257] F.-X. Riguidel, R. Jullien, G. H. Ristow, A. Hansen, D. Bideau, Behaviour of a sphere on a rough inclined plane, J. Phys. I (France) **4**, 261 (1994).

[258] F.-X. Riguidel, A. Hansen, D. Bideau, Gravity-driven motion of a particle on an inclined plane with controlled roughness, Europhys. Lett. **28**, 13 (1994).

[259] A. Aguirre, I. Ippolito, A. Calvo, C. Henrique, D. Bideau, Effects of geometry on the characteristics of the motion of a particle rolling down a rough surface, Powder Tech. **92**, 75 (1997).

[260] L. Samson, Analyse de l'écoulement d'un grain dans des systèmes désordonnés bi et tridimensionnels, PhD thesis, Université de Rennes I (1997).

[261] L. Samson, I. Ippolito, G. G. Batrouni, and J. Lemaître, Diffusive Properties of motion on a rough surface, submitted to J. Phys. I.

[262] C. Henrique, M. A. Aguirre, A. Calvo, I. Ippolito, and D. Bideau, Sound experimental technique in granular flows, Powder Tech. **94**, 85 (1997).

[263] C. Henrique, M. A. Aguirre, A. Calvo, I. Ippolito, S. Dippel, G. G. Batrouni, and D. Bideau, Energy dissipation and trapping of particles moving on a rough surface, submitted to Phys. Rev. E.

[264] G. H. Ristow, F.-X. Riguidel, D. Bideau, Different characteristics of the motion of a single particle on a bumpy inclined line, J. Phys. I (France) **4**, 1161 (1994).

[265] C. Ancey, P. Evesque, P. Coussot, Motion of a Single Bead on a Bead Row: Theoretical Investigations, J. Phys. I (France) **6**, 725 (1996).

[266] W. Kalthoff, S. Schwarzer, G. Ristow, and H. Herrmann, On the application of a novel algorithm to hydrodynamic diffusion and velocity fluctuations in sedimenting systems, Int. J. Mod. Phys. C **7**, 543 (1996).

[267] A. Lorenz, C. Tuozzolo, M. Y. Louge, Measurements of impact properties of small, nearly spherical particles, Experimental Mechanics, to appear (1997).

[268] E. Azanza, F. Chevoir, P. Moucheront, Experimental study of rapid granular flows in a two-dimensional channel, in: *Powders & Grains 97*, R. P. Behringer and J. T. Jenkins (eds.), Rotterdam 1997 (Balkema).

[269] J. T. Jenkins, M. Richman, Kinetic theory for plane flows of a dense gas of identical, rough, inelastic, circular disks, Phys. Fluids **5**, 781 (1985).

[270] O. Walton, personal communication.

[271] E. Azana, Écoulements granulaires bidimensionnels sur un plan incliné, PhD thesis, École Nationale des Ponts et Chaussées, Paris, 1998.

[272] M. A. Goodman, S. C. Cowin, Two problems in the gravity flow of granular materials, J. Fluid Mech. **45**, 321 (1971).

[273] M. W. Richman, R. P. Marciniec, Gravity-driven granular flows of smooth, inelastic spheres down bumpy inclines, J. Appl. Mech. **57**, 1036 (1990).

[274] J. T. Jenkins, M. Richman, Grad's 13-moment system for a dense gas of inelastic spheres, Arch. Rat. Mech. **87**, 355 (1985).

[275] K. G. Anderson, R. Jackson, A comparison of the solutions of some proposed equations of motion of granular materials for fully developed flow down inclined planes, J. Fluid Mech. **241**, 145 (1992).

[276] D. Hanes, Observations and simulations of nearly-ellipsoidal, inelastic particles down a bumpy incline, talk at conference "Powders & Grains", Durham, NC, May 18-22 (1997).

Acknowledgements

Numerous persons contributed to this work, either directly by being involved in it, or indirectly, by making life and work richer through their presence during the last three years.

First, I would like to thank Prof. Dietrich Wolf, my thesis advisor, for the freedom he gave me in pursuing this work, his kindness and the trust he placed in me. I thank Prof. Peter Grassberger for continuing my position at HLRZ when he took over as director after Prof. Wolf returned to Duisburg.

I am indebted to George Batrouni, who introduced me to the problem of the ball on the inclined plane, and who contributed a lot by being a devil's advocate in numerous discussions, thereby forcing me to get a very clear picture of the details of this system. I also thank him for finding the time to proof-read this thesis.

The central part of this work is concerned with a system that was investigated experimentally by Liliane Samson in her PhD thesis at the Université Rennes I, and by Christian Henrique during his military service in Buenos Aires. I thank them for sharing and discussing their results with me, in Jülich and in Rennes. I am indebted to Daniel Bideau for inviting me to Rennes several times, and giving me the opportunity to see the experiments, and thank him, Irene Ippolito, Liliane and Christian for numerous discussions of the problem of a sphere on an inclined plane. I thank the whole GMCM in Rennes for their hospitality.

François Chevoir invited me to the LCPC in Paris, and I am grateful for extensive discussions with him, Emmanuel Azanza and Yann Limon Duparcmeur about flow on an inclined plane, for the hospitality at LCPC and for helping me to get a feeling for the behaviour of the system by showing me the experiments.

The GdR "Physique des Milieux Hétérogènes Complexes" and the HCM network "Cooperative Structures in Complex Media" are acknowledged for travel support.

A lot of people made the HLRZ a very special place, and I enjoyed my time here immensely. I thank my officemates Jochen Schäfer, Elmar Jobs, Tim Scheffler, Johannes Müller-Gerking and Uwe Müssel for their patience with my sometimes too talkative nature, and especially Elmar Jobs for his valuable help in all computer problems. Lothar Brendel and Harald Kallabis always lent me an open ear when I needed to talk about my latest results. Lothar could always be drawn into discussions about my work and granular materials in general, and suggested eq. (3.25).

Jochen Schäfer, Jason Gallas, Imre Jánosi and Franck Radjai always pushed me towards a better understanding of the physics of granular materials by taking nothing for granted, and were there for me when I needed someone to talk to – be it about physics or personal matters. I thank Gerald Baumann for many discussions we had about granular materials.

I also want to thank all those people who spent some time at HLRZ or in Duisburg, and who made up the inspiring international atmosphere: Jochen Arnhold, Gerard Barkema, Ugo Bastolla, Enrico Carlon, Henrik Flyvbjerg, Helge Frauenkron, Erwin Gerstner, Antal Károlyi, Reinhold Lövenich, Subrangshu Sekhar Manna, Cristian Moukarzel, Walter Nadler, Björn Peters, Heiko Rieger, Alexander Schindler, Pavel Šmilauer, Henk van Beijeren, Ulrich Wenschuh.

I warmly thank our system administrator Martina Kamps for her patience with the amounts of data I produced, and for her quick help with all computer problems. Helga Bongartz helped cheerfully and efficiently in all administrative matters.

I would like to thank Tom Drake, Jim Jenkins, Troy Shinbrot and their families as well as Heinrich Jaeger for their hospitality during my trip through the United States, making it a unique experience personally and scientifically. There, I also finally met Michel Louge, who kindly provided the experimental data on the impact of spheres used in this thesis.

I thank my friends Susi Furrer, Ilka Flegel, Anja Stemmer and Helmut Schießel for being there for me whenever they were needed. Even though they were in Freiburg, Omsk, Hamburg, Munich or Santa Barbara, their friendship and encouragement was always here with me. Joannes and Stephanie van der Linden made me feel at home in Aachen, and Joannes had to suffer all my stories about the exciting life of a ball on an inclined plane in many bus rides from Jülich to Aachen. Stefan Luding, friend and fellow "granular" physicist, managed to find the time to proof-read this thesis and came up with many valuable comments. For this, I thank him, as well as for discussing sand, the universe and everything over a glass of beer many times.

Schließlich gilt mein Dank meinen Eltern, die mich während Studium und Doktorarbeit in jeder erdenklichen Weise unterstützt haben.

Forschungszentrum Jülich

Jül-3510
February 1998
ISSN 0944-2952